LOCAL ORGANIZATION AND THE PIEZOELECTRIC EFFECT IN ROOM TEMPERATURE IONIC LIQUIDS (RTILs)

By

Md Iqbal Hossain

A DISSERTATION

Submitted to
Michigan State University
in partial fulfillment of the requirements
for the degree of

Chemistry – Doctor of Philosophy

2023

ABSTRACT

Room temperature ionic liquids (RTILs) have been used in a variety of fields due to their unique physical and chemical properties which are rooted in their complex molecular arrangements and interactions. It is therefore important to shed light on the organization of RTILs to control the physical and chemical properties to maximize potential. The Blanchard group has previously observed an intriguing phenomenon of surface charge induced free charge density gradients (ρ_f) with a characteristic persistence length of ca. 50 μ m. There is no existing theoretical framework for molecular liquid systems that can explain this unprecedented observation. We hypothesized that there is analogy to the piezoelectric effect with this long-range order. Therefore, the larger goal of this work is to determine if RTILs exhibit the piezoelectric effect and to elucidate the underlying molecular-level mechanism.

The free charge density gradient (ρ_f) is sensed by measuring the induced orientational anisotropy decay of trace amounts of charged chromophores in the RTILs as a function of distance from the charged support (silica or ITO). In Chapter 2, we successfully demonstrated the piezoelectric effect in RTILs by measuring open circuit potential (OCP) as a function of applied pulsed pressure. For this measurement, we devised a cylinder-piston cell system which allows the acquisition of reproducible data over many measurements.

In Chapter 3, we conducted a comprehensive investigation into the structure dependence of the piezoelectric effect with six different imidazolium and four different pyrrolidinium RTILs. Our findings revealed that the piezoelectric effect is influenced by the head group of RTILs. We explored chiral ionic liquids anticipating a stronger piezoelectric response due to their non-centrosymmetric nature, a prerequisite for the piezoelectric effect. We found that chiral ionic liquids exhibit the piezoelectric effect which is slightly larger than that of pyrrolidinium based ILs

but is less than that of HMIMTFSI. The piezoelectric effect exhibited by RTILs is not solely a molecular-level phenomenon but, rather, the characteristic length scale of the relevant structural unit is larger.

In Chapter 4 and Chapter 5, we aimed to investigate the impact of dilution on RTILs and explore the existence of nano-domains within RTILs. Our findings revealed that ρ_f persists up to a certain amount of dilution, maintaining its magnitude and characteristic length. However, beyond this dilution level, the free charge density gradients collapses. The functional form of the magnitude and characteristic length do not resemble that of a homogeneous solution, rather the binary mixtures of RTILs are highly heterogeneous (85% of dilution). We calculated the hydrodynamic volume of the reorienting entity in the bulk RTIL-solvent system at 200 μm from the charged support surface, where there is no active free charge density gradient. We found that RTILs aggregate and form nano-domains. Moreover, the size of the nano-domains (aggregates) increases with increasing dilution.

In Chapter 6, we achieved a significant breakthrough by establishing a connection between the free charge density gradients (ρ_f) and molecular scale organization. We measured the rotational diffusion dynamics of two different chromophores, cresyl violet and perylene to investigate polar and non-polar regions, respectively. Both chromophores exhibited the characteristics of oblate rotors, allowing the extraction of the Cartesian components of their rotational diffusion constants, thereby gathering detailed information on the local environments of the rotating entities. This information revealed depth-dependent changes in the organization of the chromophore local environments that correlated with the existence of ρ_f .

In Chapter 7, we summed up and suggested some future work to enhance our understanding of the piezoelectric of RTILs.

Copyright by MD IQBAL HOSSAIN 2023

This thesis is dedicated to 'tw profound impact all through m companion and without their un	y life. My wife, Manjı	ama Alam, who has be ntless support, and sae	een my unwavering

ACKNOWLEDGEMENTS

First and foremost, I am immensely grateful to Professor Gary Blanchard, my advisor, for introducing me to this amazing class of material, Room Temperature Ionic Liquids (RTILs). While it is impossible to find a literal angel on Earth, even if one were to exist, it would undoubtedly resemble Dr. Gary Blanchard. I am extremely fortunate to have had him by my side throughout my graduate studies. I would like to express my heartfelt appreciation to him not only for helping me to be a critical thinker and independent scientist but also shaping my character. He has profound influence and positive impact on my life. I am incredibly thankful for his invaluable guidance and insights over the past few years. I am grateful for his scientific advice and insightful discussions on my current and future research, as well as future career. I hope to uphold these lessons and values throughout the rest of my life.

I would like to extend my gratitude to the committee members, Dr. Greg Swain, Dr. Marcos Dantus, and Dr. Ruth Smith. Thanks for their valuable suggestions and discussions during the committee meetings. I appreciate their support and guidance, which have played a significant role in shaping my academic journey.

I would like to thank Dr. Kathryn Severin for helping and listening to me during my time as a teaching assistant under her guidance. I really enjoyed working with her in the Analytical-Physical (AP) chemistry labs. She provided me with the opportunity to expand my knowledge and skills in various advanced analytical tools beyond my research area. Additionally, I want to extend a special thanks to Dr. Yufeng Wang for her initial training and support on my research endeavors.

I am grateful to the College of Nature Science for awarding me the Dissertation Completion Fellowship (DCF) for the Summer 2023, as well as the Alfred J. and Ruth Zeits Research Endowment Fellowship for the Fall 2022 semesters. These prestigious fellowships have provided

invaluable support during critical stages of my academic journey. Additionally, I want to express my gratitude to the Graduate School and Lyman Briggs College for giving me the opportunity to actively participate in teaching related research as SUTL fellow to further my professional development.

I would like to express my gratitude to the current members of the Blanchard group, Andrew Wendel, Homa Sadeghzadeh and Neelanjana Mukherjee, Emily Simonis, Alexandra Korabiewski, as well as all the former group members, with a special mention to Dr. Masroor Hossain. I would also like to extend a special thanks to Sheryl Blanchard for setting my research bench on the third floor. Her efforts have made me feel like a part of the family.

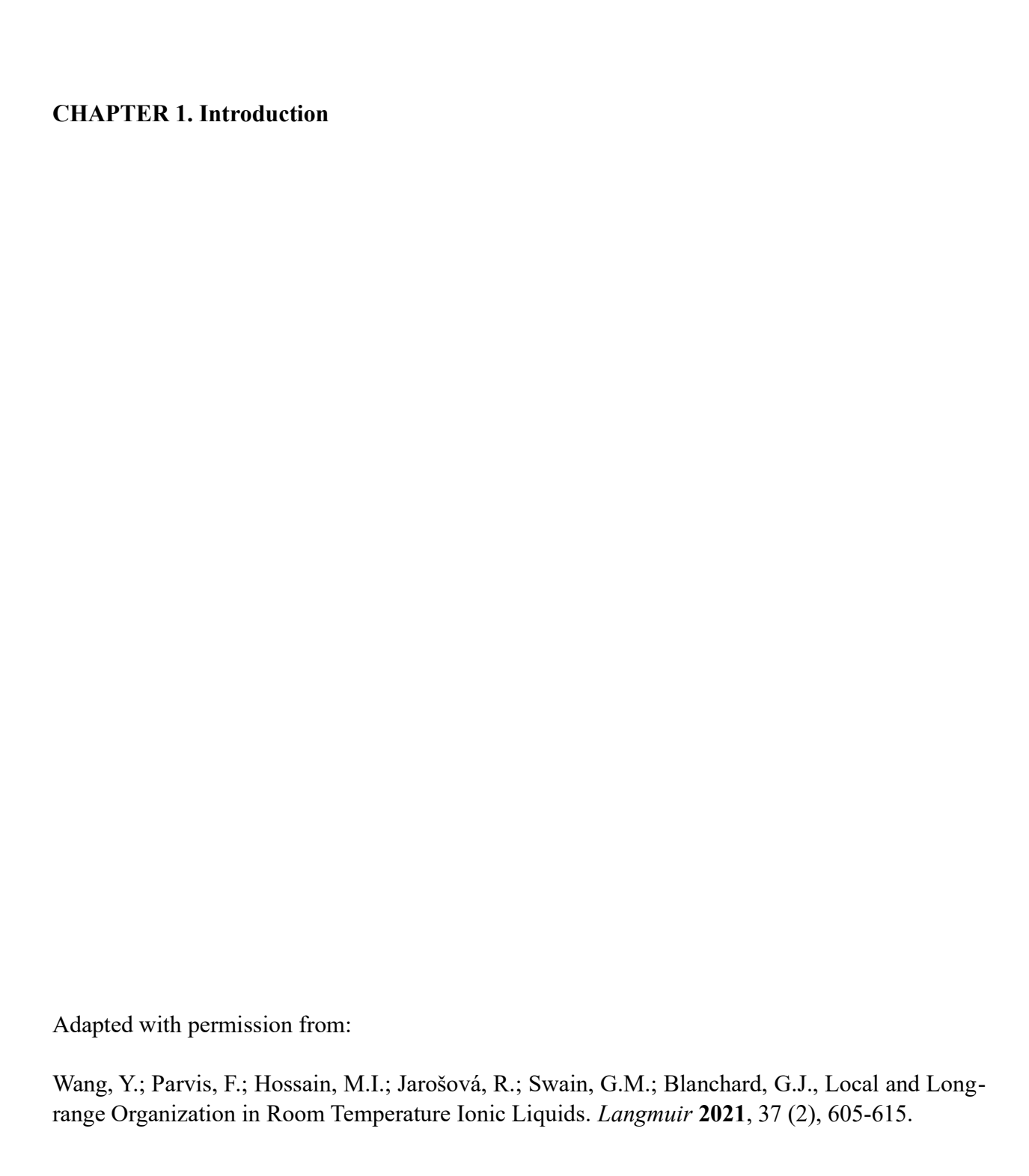
I want to thank my friend Dr. Ehsanul Hoque Apu for our weekly coffee meetings. Through our discussions, I have gained valuable insights into the world research beyond my own field. Additionally, I want to extend my thanks to my friend A. K. M. Atique Ullah. I am going to miss our daily evening conversation and coffee. I am grateful to both for nurturing my interest in biological research. Furthermore, I would like to thank all the chemistry graduate students from Bangladesh.

Last but not least, I would like to extend my heartfelt appreciation to my brother and sisters for their unconditional love and care. Their sacrifices have not gone unnoticed, and I am deeply thankful for them. I want to thank my grandma, who has instilled in me a positive outlook on life. Thank you for consistently believing in me and standing by my side.

TABLE OF CONTENTS

CHAPTER 1. Introduction	1
1.1 Overview of Room Temperature Ionic Liquids	2
1.2 Organization in Room Temperature Ionic Liquids (RTILs)	
1.3 Charge Density Gradients in RTILs	
1.3.1 Measuring the Charge Density Gradient	
1.3.2 Gauging the Magnitude of the Charge Density Gradient	13
1.3.3 Controlling the Charge Density Gradient	15
1.4 Piezoelectric Effects of RTILs	
1.5 The Effect of Dilution on Charge Density Gradient	
1.6 Relating the Charge Density Gradient to Molecular-Scale Organization	
1.7 Summary	
REFERENCES	
CHAPTER 2. Ionic Liquids Exhibit the Piezoelectric Effect	32
2.1 Introduction	
2.2 Methods.	
2.2.1 Materials Used	
2.2.2 Measurement of the Direct Piezoelectric Effect in RTILs	
2.2.3 Open Circuit Potential Measurements	
2.3 Results and Discussion	
2.4 Conclusions.	
REFERENCES	
APPENDIX	
CHAPTER 3. Structure-Dependence of the Piezoelectric Effect in Ionic Liquids. Mechanistic Insights 3.1 Introduction.	49
3.2 Methods	
3.2.1 Materials Used	
3.2.2 Measurement of the Direct Piezoelectric Effect	
3.2.3 Open Circuit Potential Measurements	
3.3 Results and Discussion	
3.4 Conclusions.	
REFERENCES	
REFERENCES	01
CHAPTER 4. The Effect of Dilution on Induced Free Charge Density Gradients Temperature Ionic Liquids	
4.1 Introduction	
4.2 Experimental Section	69
4.2.1 Chemicals	
4.2.2 Purification of ILs	70
4.2.3 Preparation of RTIL-Chromophore Solution	70
4.2.4 Sample Cell Preparation	
4.2.5 Fluorescence Anisotropy Decay Measurements	
 V/111	

4.2.6 Binary Systems Preparation	72
4.3 Results and Discussion	
4.4 Conclusions	
REFERENCES	
APPENDIX	
CHAPTER 5. Dilution-Induced Changes in Room Temperature Ionic Liquids.	Persistent
Compositional Heterogeneity and the Importance of Dipolar Interactions	
5.1 Introduction	
5.2 Experimental Section	
5.2.1 Chemicals and Purification	
5.2.2 Solution Preparation.	
5.2.3 Sample Cell Preparation	
5.2.4 Spatially Resolved Fluorescence Anisotropy Decay Measurements	
5.2.5 Semi-empirical Calculations	
5.3 Results and Discussion	
5.3.1 Gradient Magnitude and Persistence Length as a Function of Dilution	
5.4 Conclusions	
REFERENCES	
CHAPTER 6. Relating the Induced Free Charge Density Gradient in a Room Tempera Liquid to Molecular-Scale Organization	130
6.1 Introduction	
6.2 Experimental Section	
6.2.1 Materials Used	
6.2.2 Preparation of Solutions	
6.2.3 Rotational Diffusion Measurement	
6.2.4 Steady State Spectroscopy	
6.3 Results and Discussion	
6.3.1 Perylene Reorientation	
6.3.2 Cresyl violet Reorientation	
6.4 Conclusions	
REFERENCES	153
CHAPTER 7. Conclusions and Future Directions	150
7.1 Conclusions.	
7.2 Future Directions	
7.2.1 Atomic Force Microscopy (AFM) Measurements	
7.2.1 Atomic Force Microscopy (AFW) Measurements	
7.2.3 Piezoelectric Effect under Nano-confinements	
PEFFRENCES	166



1.1 Overview of Room Temperature Ionic Liquids

Room temperature ionic liquids (RTILs) are organic salts with melting points below room temperature. RTILs have emerged as a very useful class of materials with promising applications in numerous venues, including as electrolytes in energy storage devices such as supercapacitors ¹⁻³ and batteries, ⁴⁻⁵ in biomedical applications such as novel anti-cancer and antimicrobial agents, ⁶⁻⁷ as components in bioink, in the fabrication of wearable electronics, as MRI contrast agents, ⁸⁻¹⁰ and for oral and transdermal drug delivery. ¹¹⁻¹² Despite the utility of these materials in so many venues, there remains a great deal to be understood about ionic liquids. RTILs are liquid phase organic

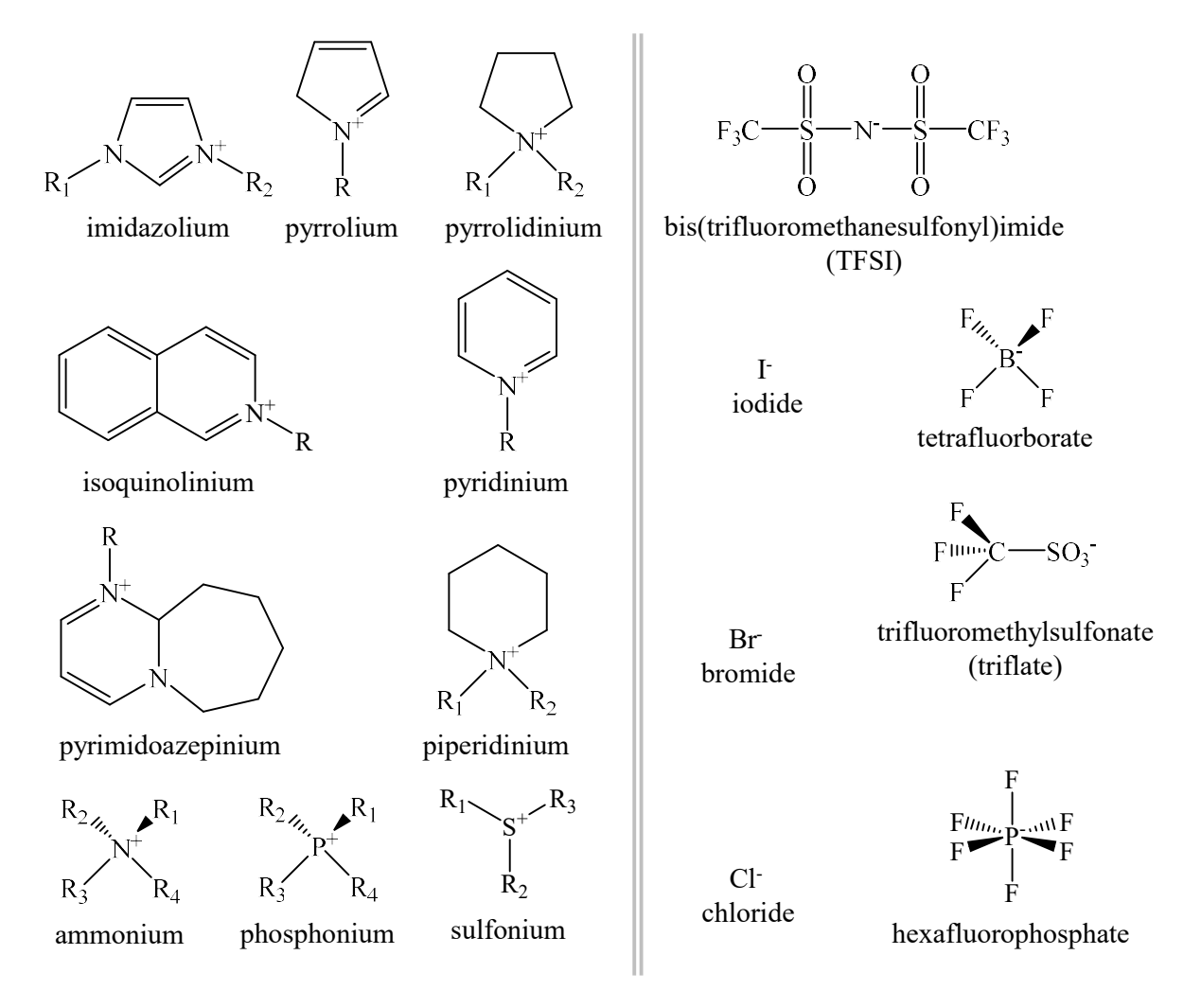


Figure 1.1 Examples of RTIL cation and anion structures.

salts where the constituent cations are typically large, organic and of low symmetry, and the anions are also usually large (examples in Figure 1.1). RTILs are generally characterized by high viscosity, negligible vapor pressure, high thermal stability, and a wide electrochemical window, and for their ability to dissolve both polar and nonpolar compounds. Extensive and significant efforts have been made to develop task-specific ionic liquids. ¹³⁻¹⁸ One example is the incorporation of chirality into RTILs by using chiral cations or the introduction of chiral functionalities in the alkyl chain, ¹³⁻¹⁴ a structural modification that may open the door to applications of RTILs in bio-related and second order nonlinear optical phenomena. Additionally, the careful choice of cation and anion can also be used to tailor viscosity or the formation and size of local heterogeneities in RTILs. ¹⁹⁻²⁰ Ionic liquids also exhibit organization over length scales vastly in excess of that seen in molecular liquid solvents, and it is this property that has posed a significant challenge to our understanding of these materials. In order to harness the maximum utility of these useful materials, we will need to have a fuller understanding of the structural and dynamical heterogeneity that ultimately regulates RTILs physical and chemical properties.

The organization of ionic liquids does not resemble the NaCl lattice where all the ions exist as discrete entities and are arranged in a regular and rigid lattice structure. There is substantial evidence suggesting that ionic liquids exist primarily as ion-paired dipolar species. ²¹⁻²³ However, the degree of dissociation is generally not well characterized due to the difficulties in measuring conductivity and free ion concentrations in the medium, as well as contributions to the apparent conductivity related to the association and dissociation kinetics of the RTIL ions. Drawing comparisons between ionic liquids and (ionic) liquid crystals is appealing, if only to a limited degree. The ability to control molecular orientation by means of templating or applied potential demonstrates that organic systems can exhibit long-range organization. Indeed, some organic ionic

systems go from solid to (ionic) liquid crystalline to ionic liquid phases with increasing temperature and pressure. 24-26 This phenomenon is commonly observed in alkyl imidazolium ionic liquids with long alkyl chains, typically around C₁₄, due to van der Waals interactions. Most imidazolium-based ionic liquids have a C₂-C₈ alkyl chain, with C₄ being the most prevalent. Though a liquid crystalline mesophase has not been reported for these RTILs, it is possible that subtle forms of organization may exist (*vide infra*). There are a number of reports that indicate thin films of imidazolium-based ionic liquids exhibit ordering that is induced by the presence of an interface. 27-32 Additionally, the Brand group in a recent study deposited monolayer of ionic liquids on an Au substrate and demonstrated that the organization of an ionic liquid monolayer can be altered by controlling the surface potential of the gold substate. 33 They found that the orientation of the monolayer imidazolium aliphatic chains exhibited a surface potential-dependent tilt angle. This finding is not only intriguing, but also opens the door to possible control over structural organization in ILs.

Our group has discovered that, apart from induced structural order, macroscopic free charge density gradients can also be induced in ionic liquids. ³⁴⁻³⁶ This finding not only underscores our limited current understanding of RTILs, but also raises the question of the relationship between structural order and the existence of a free charge density gradient in RTILs. There are several bodies of information, some of which are discussed in this dissertation, that point to a connection.

1.2 Organization in Room Temperature Ionic Liquids (RTILs)

Organization in RTILs was first predicted by computer simulations and later established by a range of experimental techniques. To this point, the spatial extent and characteristic length scale of structural order in RTILs appears to depend on the means used to examine the order. There

is a substantial literature on scattering techniques such as X-ray or neutron diffraction by ionic liquids that points collectively to the presence of structural organization of RTIL constituent ions. The specifics of this organization are influenced by factors such as the cation and anion structures, pressure and the temperature of the system. ³⁷⁻⁴¹ Although these findings do not directly indicate the persistence length of molecular-level structural regularity, they have yielded intriguing results, including the concept of extended networks formed by RTIL constituents. These networks encompass a range of structures, from polymeric supramolecular arrangements to aggregates and triple-ion or contact ion pair structures. ⁴¹ The existence of such molecular-scale organization provided a logical basis for anticipating order on longer scales within these materials.

The Israelachvilli group conducted temperature-dependent surface force measurements to investigate the (exponential) Debye decay length of the diffuse double layer forces. $^{21-22}$ Their findings support the notion that ionic liquids (ILs) exhibit long-range electrostatic screening, which is central to understanding the ability of RTILs to support a measurable free charge density gradient. Specifically, Gebbie *et al.* showed a significant temperature-dependence of the effective Debye length using equilibrium force-distance measurements. The Debye length was seen to vary from 6.7 nm at 22 °C to 3.4 nm at 60 °C for RTIL, 1-ethyl-3-methylimidazolium bis(trifluoromethylsulfonyl)imide (EMIM+TFSI) and was measured to be *ca.* 12 nm for 1-butyl-3-methylimidazolium bis(trifluoromethylsulfonyl)imide (BMIM+TFSI). $^{21-22}$ This result indicates either a very low concentration of effective free ions or highly efficient screening of free charge in ILs. From their force-distance data, they determined the charge carrier activation energy to be *ca.* 9.5 k_BT , suggesting that the dissociation of RTILs is very limited. Using the assumption that the chemical potential of RTIL dissociation is given by E_d/ε , where E_d is the dissociation energy and ε is the dielectric constant (relative permittivity) of the RTIL, they estimated the equilibrium

concentration of dissociated ions to be on the order of 10^{-4} M, corresponding to a p K_d of 9.14 for BMIM+TFSI-.²² This finding is not in agreement with other estimates of effective ion concentration in RTILs, based on the concept of 'ionicity,' which evaluates the fraction of ions participating in charge conduction using ion exchange dynamics and diffusion (i.e., kinetic phenomena).^{23, 42} The disparity between these estimates likely arises from the fact that force-distance measurements rely on thermodynamic equilibrium quantities, whereas ionicity measurements focus on kinetic aspects. It is useful to consider that RTIL properties such as temperature-dependent conductivity and viscosity differ from those of simple ionic solutions such as KCl(aq).⁴³ The force-distance measurements reveal an ordering effect in the diffuse double layer that extends further than would be expected if RTILs could be understood in the context of the Gouy-Chapman-Stern or other similar models.

In addition to the organization associated with a Debye length (*ca.* 10 nm), RTILs have exhibited structural order on length scales ranging from 1 nm to 60 nm. ⁴⁴⁻⁴⁶ Much of this structural order is seen within the first several nm of (charged) surfaces, where arrangements such as "herringbone" order and charged layers have been documented. ⁴⁷ RTIL organization on this length scale has also been seen to evolve over time. ⁴⁸ While the details of this organization differ substantially from traditional Gouy-Chapman-Stern or Helmholtz behavior, what is observed is in much closer proximity to the interface than have been reported by several other groups. A recent study by the Brand group has shown that a surface RTIL (C₁₈Im⁺) monolayer formed using Langmuir-Blodgett deposition, significantly alters the electric double layer at a charged electrode. ³³

The Shaw group has found compelling evidence for long-range structural organization in ionic liquids. They employed a dynamic wetting technique to form thin RTIL films and

characterized the long-range order with FTIR, optical ellipsometry and second harmonic generation measurements.²⁷⁻²⁹ By monitoring the polarized infrared reflection absorption (IRRA) spectra of BMIM+TFSI thin films as a function of time (minutes to days), the Shaw group observed gradual band position and intensity changes for several bands in the 1000 cm⁻¹ to 1400 cm⁻¹ region. While some bands remain unchanged, four bands associated with the S-N-S stretch (1069 cm⁻¹), the SO₂ symmetric stretch (1149 cm⁻¹), the CF₃ symmetric stretch (1244 cm⁻¹), and the SO₂ asymmetric stretch (1366 cm⁻¹) of the TFSI anion displayed changes in intensity and/or frequency. The disappearance of these bands from the polarized IRRA spectra suggests that the anion reoriented itself, predominantly aligning these vibrational modes parallel to the film surface and support. The spectral evolution required ca. one hour, and this finding is consistent with the time-dependent second harmonic generation response of the same thin film. For the thin films used, the organization that evolved in time was found to be present through the entire thickness of the film. Thin films of RTILs with different anions, containing cyano groups, have been investigated. Interestingly, RTILs with a B(CN)₄ anion demonstrated ordering that appeared to template from the support surface while RTILs with a N(CN)2 anion demonstrated ordering that was templated from organization of the air-IL interface.²⁹

The Fayer group has utilized surface charge density to control the properties of RTIL thin films ^{30-32, 49-50} and confined environments. ⁵¹ In thin films of RTILs (50 nm to 250 nm thick), they reported the time-resolved band position and shape of the CN stretch of SCN⁻ and SeCN⁻ and CO₂ reorientation to assess the evolution of local environment as a function of surface charge density and RTIL imidazolium aliphatic chain length. ^{30-32, 49-50} They reported that the presence of surface charge slows the dynamics within the RTIL thin films to a distance of *ca*. 250 nm from the surface, and that the influence of interfaces on RTIL dynamics persists up to *ca*. 30 nm. ³⁰ The Fayer group's

work is complementary to that of the Shaw group in the sense that it points to changes in dynamics of the RTIL local environment(s) while the Shaw group's results indicate structural organization. The organization of RTIL films affects the dynamics of the local environments within them and the role of surface charge in mediating these dynamics aligns with the ability to create long-range charge density gradients in RTILs. (*vide infra*).

Various experimental and theoretical methods have revealed the existence of long-range organization in RTILs. This organization cannot be explained by the models appropriate for dilute solution, despite data that suggests very limited dissociation in RTILs. 21-22 Additionally, another body of data indicate the existence of nanoscale heterogeneities in RTILs, which contradicts the notion of RTILs being treated as "normal" liquid phase solvents. 19-20, 52-53 The rationale behind these domains lies in the amphiphilic nature of the cationic constituents of RTILs, where nonpolar moieties, typically found on the cation, are large enough to form nano-domains. Such compositional heterogeneity has been suggested as the basis for the ability of RTILs to solubilize nonpolar species. 20

1.3 Charge Density Gradients in RTILs

There is ample scientific literature in support of surface charge induced structural organization in RTILs. Most of these reports place such organization up to multiple tens of nm,^{21-22, 30-32, 49-51} and in some instances the organization is limited by the thickness of the RTIL films examined.²⁷⁻²⁹ The Blanchard group has found evidence for induced charge density gradients (ρ_f) in RTILs with a spatial extent of tens of μ m.³⁴⁻³⁶ In the following discussion, we consider these findings and their implications, focusing on how the observed free charge density gradients may be influenced by the structural organization within RTILs. It is important to consider that the

structural order observed in thin RTIL films could have longer-range effects in thicker samples, potentially allowing structural organization and free charge density gradients to be reconciled.

1.3.1 Measuring the Charge Density Gradient

The Blanchard group initially observed long range organization in RTILs in the form of a free charge density gradient ρ_F in BMIM⁺BF₄ over a charged surface (silica).²⁸ We measured ρ_F in RTILs through the depth dependent fluorescence anisotropy decay of trace amounts of charged (cationic and anionic) chromophores.⁵⁴ The system used for these measurements is a time correlated single photon counting (TCSPC) detection system coupled with an inverted confocal microscope. The TCSPC data were used to construct induced orientational anisotropy decay functions of an ensemble of chromophores in the confocal imaging plane of the inverted microscope to achieve depth resolution on the order of 900 nm, and precise control over the microscope stage vertical position.

The induced orientational anisotropy decay function, R(t), is the normalized difference of time-resolved plane polarized emission intensities i.e., parallel (vertical) and perpendicular (horizontal) polarization of an ensemble of rotating entities.

$$R(t) = \frac{I_{\parallel}(t) - I_{\perp}(t)}{I_{\parallel}(t) + 2I_{\perp}(t)} = R(0) \exp(-t/\tau_{OR})$$
 [1.1]

$$\tau_{OR} = (6D_{ROT})^{-1} = \frac{\eta V f}{k_{R} T S}$$
 [1.2]

The information content of R(t) has been established and the information of interest is its functional form. The orientational relaxation time constant, τ_{OR} , extracted from fitting R(t) to an exponential decay function, can be related to the rotational diffusion constant, D_{ROT} , the shape of the rotating chromophore, $S_{rotation}^{62-63}$ RTIL viscosity, η , the volume of the rotating chromophore, $V_{rotation}^{57}$

and the frictional boundary condition term f.56,59-60 by the modified Debye-Stokes-Einstein model

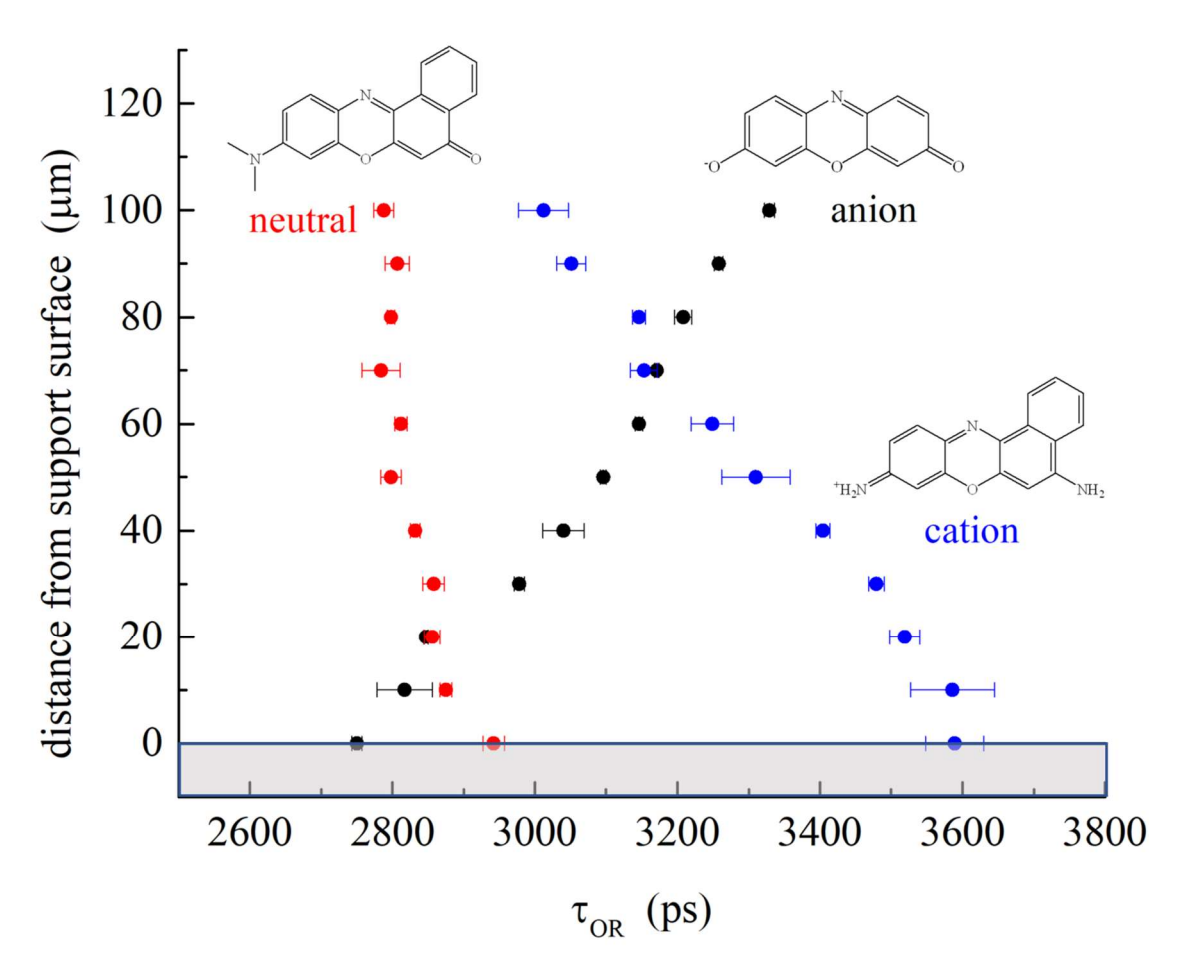


Figure 1.2 Depth-dependent τ_{OR} in BMIM⁺BF₄⁻ supported on a silica surface for anionic (Resorufin), cationic (Cresyl Violet) and neutral (Nile Red) chromophores.

(Eq. 1.2). The τ_{OR} data as a function of distance from the charged surface is shown in Fig. 1.2 for the cationic chromophore cresyl violet (CV⁺), the anionic chromophore resorufin (R⁻), and the neutral chromophore nile red (NR⁰). There are several important features in this data. The first is that for the charged chromophores, there is a clear depth-dependence of τ_{OR} , and the depth-dependencies are different for the cationic and anionic chromophores. The second important feature is that the change in τ_{OR} persists for distances greater than 100 μ m.

The reason for the depth-dependence in τ_{OR} can be determined through examination of Eq. 1.2. The DSE equation contains thermal energy (k_BT), shape (S) and frictional boundary condition (f) terms, and these are all constant or almost constant for all chromophores. The bulk viscosity of the medium, η , is constant, as reflected in the depth-independent τ_{OR} data for NR⁰. The only term that can account for the depth-dependent data for the charged chromophores CV⁺ and R⁻ is the hydrodynamic volume, V, of the reorienting entity. ⁵⁷

Figure 1.3 Schematic of dissociation equilibria of BMIM⁺BF₄⁻(top) and CV⁺BF₄⁻ (bottom).

Depth-dependent changes in V can be accounted for by the fact that the charged chromophores participate in an association equilibrium with free RTIL ions. The dissociation of RTIL (K_{eq} , Fig. 1.3) depends on the identities of the cations and anions. The dissociated RTIL ions form complexes with the chromophore (K_D , Fig 1.3). The chromophore complexation and thus the relative amount of free and complexed species is determined by Le Chatelier's principle. If there is a gradient in the RTIL ions throughout the sample, there will be a corresponding gradient in the relative amounts of free and complexed chromophore, and thus a gradient in V that is reflected by a gradient in τ_{OR} . $\nabla \cdot \tau_{OR}$ (Eq. 1.4) is a consequence of $\nabla \cdot V$ (Eq. 1.3).

$$\nabla \cdot V = V_{free} \nabla \cdot X_{free} + V_{complex} \nabla \cdot X_{complex}$$
 [1.3]

$$\nabla \cdot \tau_{OR} = \frac{\eta f}{k_{\scriptscriptstyle R} TS} \nabla \cdot V \tag{1.4}$$

where the quantities X are mole fractions ($X_{free} + X_{complex} = 1$). V_{free} and $V_{complex}$ can be calculated using the method of van der Waals increments.^{34, 57} The relationship between the measured reorientation time gradient, $\nabla \cdot \tau_{OR}$, and the free charge density gradient, ρ_f , is (Eq. 1.5)

$$\nabla \cdot \tau_{OR} = \frac{\eta f}{k_B T S} \nabla \cdot V = k' \nabla \cdot \mathbf{D} = k' \varepsilon \nabla \cdot E = -k' \varepsilon \nabla^2 \phi = k' \rho_f$$
 [1.5]

The gradient $\nabla \cdot X_{free}$ (Eq. 1.3) is the (normalized) free charge gradient, $\nabla \cdot \mathbf{D}$ (Eq. 1.5), where k' is a collection of constants. In the RTIL, $\nabla \cdot \mathbf{D}$ is related to the surface potential of the silica support through Poisson's equation (Eq. 1.5), where ε is the dielectric constant of the RTIL, ϕ is the scalar electric potential field arising from the surface charge (σ_s). Controlling σ_s thus provides control over the magnitude of ρ_f in the RTIL, which can be seen through $\nabla \cdot \tau_{OR}$. Considering the existence of surface charge induced structural organization in RTILs, it may be tempting to correlate with such order to the ρ_f we observe. However, the slope of the gradient depends on the charge of the chromophore and Nile red (neutral chromophore) shows no depth dependent orientational dynamics (Fig 1.3). Therefore, our reported induced free charge density gradient, ρ_f cannot be explained in the context of a depth-dependent effective viscosity of the RTIL, a quantity that will depend sensitively on structural organization. We note that the change in relaxation dynamics seen by the Fayer group^{30-32, 49-51} must have some effect on the rotational diffusion dynamics of larger chromophores, such as CV+, R- and NR0, but the spatial extent of the slowed dynamics they report is less than the depth of focus of the optics we use for the rotational diffusion measurements and we would not expect to be sensitive to the effect they reported.

The surface charge-induced long-range order that the Blanchard group reported is unprecedented for any liquid system and cannot be explained with the traditional Gouy-Chapman-Stern model. The presence of free charge density gradient in response to surface charge is analogous to the piezoelectric effect in a solid, which can be described by the coupled equations (Eq. 1.6).

$$D = \varepsilon E + \delta T$$

$$S = sT + \delta^t E \tag{1.6}$$

Where, T is the stress applied to a material, S is the resulting strain produced in the material, E is the electric field, s is compliance, δ is the matrix describing piezoelectric effect, and ε is the dielectric constant of the materials. We return to a discussion of the piezoelectric effect in RTILs below.

1.3.2 Gauging the Magnitude of the Charge Density Gradient

The sign and magnitude of ρ_f necessarily depend on the polarity and magnitude of the surface charge density, σ_s , and the extent of RTIL dissociation. There are several points to consider in this regard. A primary consideration is that the RTIL maintains bulk neutrality since no charges are introduced into or removed from the system. In creating ρ_f , the perturbation to the RTIL that produces the charge displacement is determined by σ_s on the support. Quantitation of surface charge density σ_s of silica or ITO can be a challenge because of the complex structures of their surfaces. The surface silanol group density is on the order of 5 μ mol/m² (3×10¹⁴ O⁻/cm²). The silanol groups on silica are characterized by two distinct populations, with p K_a values of ca. 4.5 (20%) and ca. 8.5 (80%). It is not possible to determine the pH of silica surface in contact with RTILs, but if the pH is approximately neutral then the surface charge density is 6×10^{13} O⁻/cm²,

based on the silanols characterized by a p K_a of 4.5 being deprotonated and those with a p K_a of 8.5 are fully protonated.

The magnitude of free charge density gradient ρ_I depends on both the estimation of the equilibrium constants for RTIL dissociation (K_{eq} in Fig. 1.3) and for the chromophore-RTIL counter-ion complex (K_D in Fig. 1.3). It is also necessary to express the reorientation time gradients in a manner that is comparable between different RTILs. We use the normalized change in reorientation time, $\Delta \tau_{OR}/\tau_{OR}$, where the denominator term is the value of τ_{OR} well into the bulk RTIL, where it becomes invariant with depth. From Eq. 1.5, the term of interest is $\nabla \cdot V$ and thus the gradient in the relative concentration of the RTIL counter ion, $\nabla \cdot X_{free}$. Considering this discussion in terms of a cationic chromophore, we have introduced a term, ξ , to relate the concentrations of the free and complexed RTIL counterion (Λ) as a function of distance from the charged support.³⁶

$$\xi = \left| K_{eq}^{-1} \left([A^{-}]_{surface} - [A^{-}]_{bulk} \right) \right| = \left| \frac{1 - X_{free}^{surface}}{X_{free}^{surface}} - \frac{1 - X_{free}^{bulk}}{X_{free}^{bulk}} \right| = \left| \frac{X_{free}^{bulk} - X_{free}^{surface}}{X_{free}^{surface} \cdot X_{free}^{bulk}} \right|$$

$$[1.7]$$

Considering the boundary conditions $\xi = 0$ (no gradient) and $\xi = 10$ (large gradient) where the relative amounts of X_{free} at the surface and bulk can be different by as much as a factor of ~10. For the value of τ_{OR} in the bulk, we use the value at which there is no longer a depth-dependence. We calculate the hydrodynamic volumes of the free and complexed chromophores by the method of van der Waals increments to determine the hydrodynamic volume for the chromophore (CV⁺) and for the RTIL counter-ions we have used, BF₄⁻ and TFSI^{-,57} Using these quantities (V(CV⁺) = 217 Å³, V(BF₄⁻) = 50 Å³, V(TFSI⁻) = 169 Å³) and the concentrations of the RTILs, which will vary according to their molecular weights and densities, $\Delta \tau_{OR}/\tau_{OR}$ will be related to ξ and the specific RTIL system under examination. As the value of ξ ranges from 10 to 0, the corresponding values

of X_{free} will be between 0.91 to 0.09. The normalized change in rotor hydrodynamic volume, $\Delta V/V$, is proportional to ξ according to Eq. 1.7,

$$\frac{\Delta \tau_{OR}}{\tau_{OR}} = \frac{\Delta V}{V} = \xi \left(\frac{X_{free}^{surface} \cdot X_{free}^{bulk} \cdot V_{A^{-}}}{V_{complex} - X_{free}^{bulk} \cdot V_{A^{-}}} \right)$$
[1.8]

 V_A^- is the hydrodynamic volume of the RTIL counter-ion that complexes with the chromophore. The experimentally measured τ_{OR} gradient is thus related to the RTIL counterion concentration gradient in a manner that accounts for the molecular structure of the RTIL counterion. For the imidazolium RTILs, ρ_f ranges from ca. 15 (μ C/cm³)/ μ m for BF4 $^-$ anions to values up to ca. 110 (μ C/cm³)/ μ m for TFSI $^-$ and C₆MIM $^+$.³⁶ To provide some perspective on this magnitude, a charge density gradient of 110 (μ C/cm³)/ μ m corresponds to a concentration gradient of ca. 0.5 ppm/ μ m. To put this gradient in perspective, the K $^+$ gradient across a plasma membrane is on the order of 3.5x10 5 ppm/ μ m, based on [K $^+$] = 10 mM outside the cell, 100 mM inside the cell, and a plasma membrane thickness of 10 nm.

1.3.3 Controlling the Charge Density Gradient

By controlling the sign and magnitude of the surface charge σ_s on the support, the induced free charge density gradient ρ_f can be controlled. (Fig. 1.4). For silica the surface charge density, σ_s is on the order of $6x10^{13}/\text{cm}^2$. The Blanchard group has demonstrated the ability to control the sign and magnitude of ρ_f , in RTILs.³⁵ In that work, a sample cell of sandwich configuration was used in which two ITO- or FTO-coated plates are placed on both side of a spacer of ca. 1 mm thick

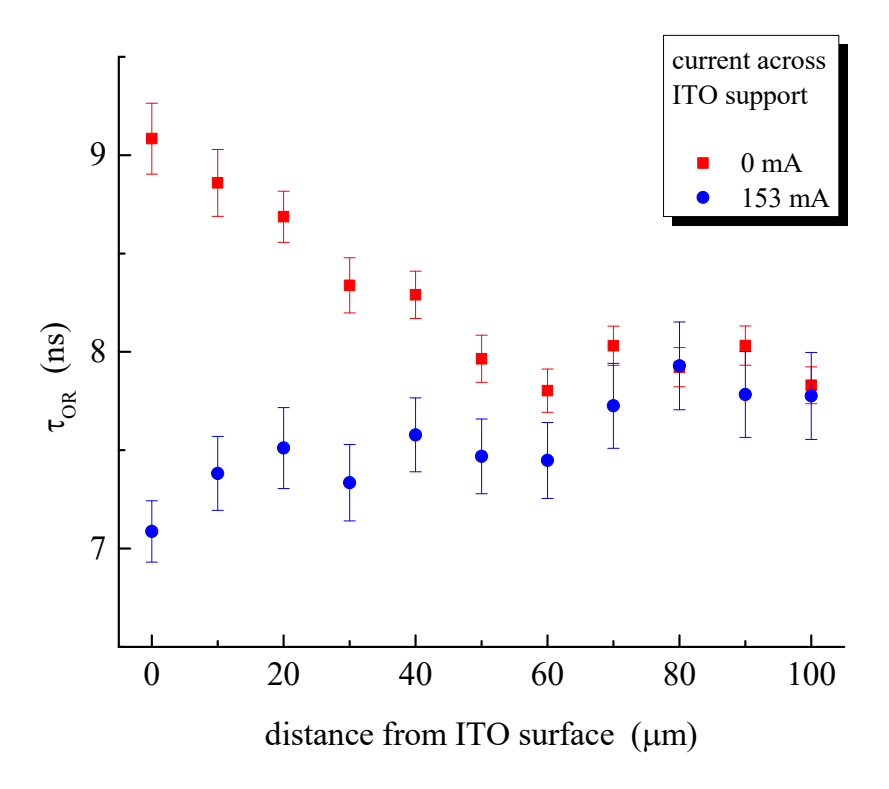


Figure 1.4 Current-dependence of ρ_f measured using CV^+ . The sign of ρ_f changes due to control of σ_s .

with O-ring inside (to confine RTILs) can serve the purpose. Below pH 6, the ITO surface carries a net positive charge. Configuring the sample holder as a capacitor with plate distance of 1 mm does not allow the surface charge density σ_s to be modified beyond a few ppm of the ambient charge, an amount insufficient to make a measurable change in ρ_f . Using one of the support surfaces as a resistor allows for the modulation of σ_s in a charge carrier density range commensurate with the ambient surface charge density of the ITO-coated support. Slow drift velocity of the carriers in the microcrystalline thin film conductor renders current proportional to carrier surface density.

With this configuration, Joule heating of RTIL is a byproduct of operating the ITO surface as resistor. From the modified DSE (Eq. 1.2), the rate at which the chromophore rotates is sensitive to the viscosity and temperature of the surrounding medium. To assess Joule heating, the RTIL

was replaced with ethylene glycol in the sample holder and the rotational diffusion time constant of CV^+ was measured as a function of current applied across the ITO support surface. The relationship between viscosity and temperature is well known for ethylene glycol, providing a facile means to calibrate the temperature of the cell as a function of current. Importantly, no depth-dependence in the CV^+ reorientation is seen for any applied current measured, demonstrating the absence of a temperature gradient within the sample cell. The current required to change the sign of ρ_f gives rise to $\Delta T \sim 6$ °C in the sample. This method of controlling σ_s allows for thermal and free charge density contributions to be readily separable.

1.4 Piezoelectric Effects of RTILs

The known theoretical framework to treat liquids with concentrated charge start from the premise of the Gouy-Chapman-Stern models, $^{69-71}$ where a short-range ion density gradient is expected. The presence of long-range order in the form of a free charge density gradient, with ρ_f up to 100 µm is unprecedented. Therefore, we require an alternative framework for understanding RTILs. The presence of ρ_f in RTILs implies a similarity to piezoelectric materials, as noted earlier, and we have established experimentally that RTILs exhibit the piezoelectric effect. This connection provides a conceptual framework in which to understand and model RTILs. Piezoelectric materials produce surface charge upon experiencing external stress. The direct piezoelectric effect is a mechanically induced charge-displacement, and the converse piezoelectric effect is a charge-induced organizational change in a material, manifested as a dimensional change in solids. We have demonstrated both effects in RTILs. The presence of a charge density gradient ρ_f can be described in the context of the converse piezoelectric effect, which is characterized by a change in the charge distribution within the material resulting from the application of a surface charge. We have demonstrated the direct piezoelectric effect in RTILs in our labs by open circuit

potential measurements using an electrochemical bench (CH Instruments 604B) (Chapter 2). For the measurements, we devised a special cylinder-piston cell system. The body of the cell is made of steel while the piston is made of Delrin® and is equipped with an O-ring to ensure a liquid-tight seal. Two electrodes were attached, one in the center of the piston and the other at the bottom of the cylinder. To our knowledge, this is the first demonstration of the piezoelectric effect in an ionic liquid. We investigated the structure-dependent nature of this effect in RTILs. (Chapter 3) The results indicated that the piezoelectric response in RTILs is not solely governed by the molecular-level arrangement but rather by the organization at the nanometer scale or even larger within the RTILs. This implies that the piezoelectric effect is influenced by the overall structural organization of the RTILs rather than just the individual molecular arrangements. Therefore, it is essential to investigate the molecular processes responsible for the organization in RTILs and it can be done by diluting RTILs with molecular diluents. In the subsequent chapters, we diluted different RTILs with diluents of varying properties.

1.5 The Effect of Dilution on Charge Density Gradient

The ability to establish ρ_f in RTILs rests on two conditions. The first is that there is extensive screening within the RTIL, such that charges are effectively isolated, and the second is that the mobility of dissociated ions within the RTIL matrix is sufficiently low that ρ_f , once established, is not compromised significantly by diffusion. Understanding screening in RTILs and other dielectric media has been treated previously.⁷² It is known that the addition of certain agents (solvents) to RTILs increases constituent mobility.⁷³. To understand the relative importance of

ionic (charge) mobility on the persistence length and magnitude of ρ_f we diluted imidazolium based

Table 1.1 Properties of polar diluents to be used for dilution studies: acetonitrile (ACN), dimethylsulfoxide (DMSO), propylene carbonate (PC), and methanol (MeOH). μ = Dipole moment, η = viscosity, ϵ = dielectric constant and n = refractive index.

Solvent	μ	η	ε	n
	(D)	(cP)		
ACN	3.92	0.33	37	1.344
DMSO	3.96	1.99	48	1.479
PC	4.94	2.50	65	1.419
МеОН	1.69	055	33	1.331

RTILs with diluents of varying properties, such as dielectric constant, viscosity, and dipole moment (Table 1.1). In the work in Chapters 2 and 3, we investigate the molecular-scale processes responsible for compositional heterogeneity in RTIL/solvent binary systems. Since RTIL anions and cations experience different interactions with diluents, we used two different anions (BF₄ and TFSI⁻) with the same cation (BMIM⁺) to investigate the role of anion. These studies are aimed at resolving the role of the RTIL ion structure in mediating ρ_f and persistent long-range organization. We quantify the magnitude and characteristic length scale of ρ_f by fitting the depth-dependence of the reorientation time constant to an exponential decay in distance from the charged support.⁷⁴ Rather than using the rotational diffusion time constant directly (Fig. 1.5a), a quantity that varies

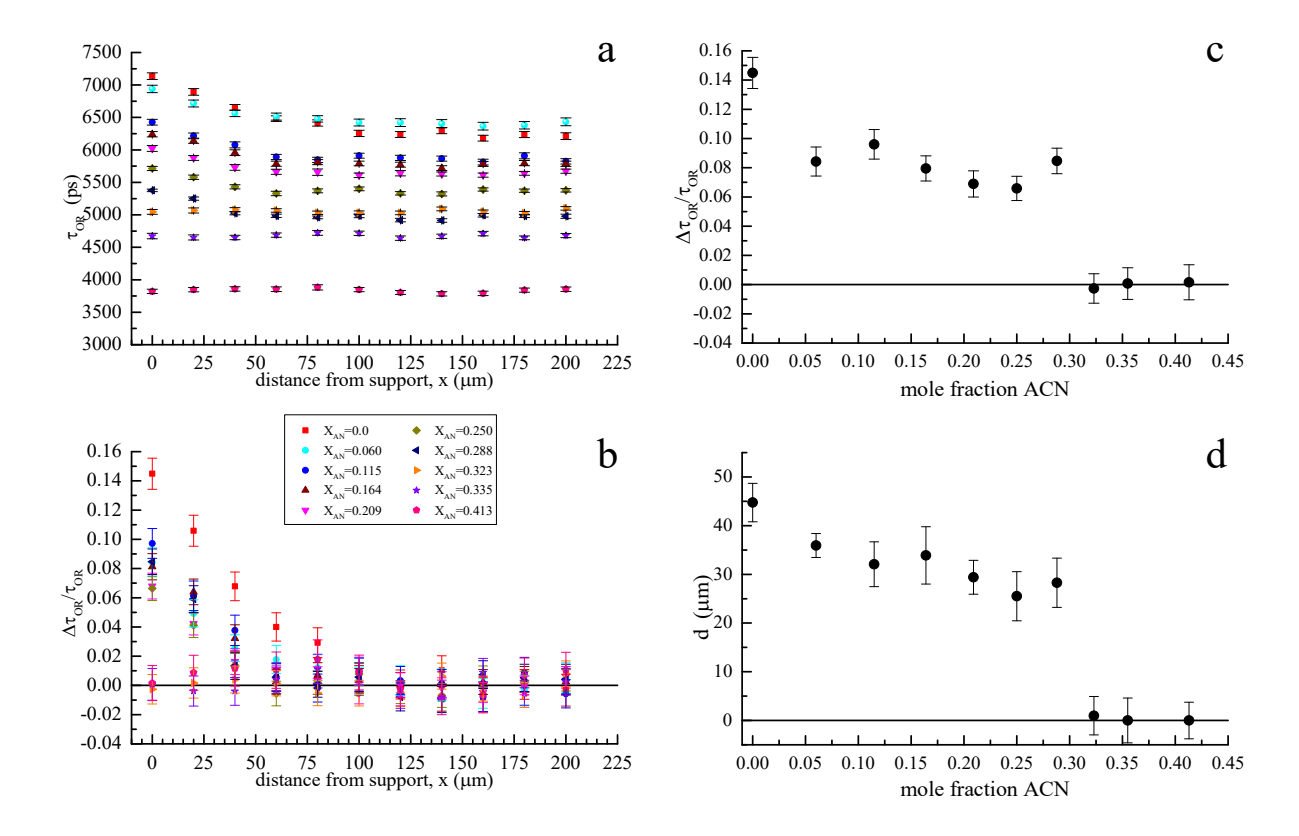


Figure 1.5 (a) Rotational diffusion time constant of CV⁺ in HMIM⁺TFSI⁻ as a function distance from the support surface for a series of acetonitrile diluent concentrations. (b) Normalized τ_{OR} gradient as a function of distance from support surface. (c) Magnitude of $(\Delta \tau_{OR}/\tau_{OR})_{x=0}$ as a function of diluent, and (d) characteristic length scale of ρ_f as a function of diluent.

with the identity of the RTIL constituent species and the chromophore, we use the normalized change in τ_{OR} over the length scale of ρ_f (Fig. 1.5b, Eq. 1.9),

$$\left(\frac{\Delta \tau_{OR}}{\tau_{OR}}\right)(x) = \frac{\left(\tau_{OR}^{x} - \tau_{OR}^{200\,\mu m}\right)}{\tau_{OR}^{200\,\mu m}} = \left(\frac{\Delta \tau_{OR}}{\tau_{OR}}\right)_{x=0} \exp(-x/d) \tag{1.9}$$

where x is the distance from the (charged) support surface and d is the characteristic (e^{-1}) length scale of ρ_f . The measured magnitude of $\Delta \tau_{\rm OR}/\tau_{\rm OR}$ depends on the chemical identity of the RTIL constituents and can be used to quantitate ρ_f . The magnitude of ρ_f is ultimately limited by the surface charge density, σ_s . We extract the quantities ($\Delta \tau_{\rm OR}/\tau_{\rm OR}$)_{x=0} and d from these fits (Fig. 1.5b).

of $10^{-5}\,\mathrm{M\,CV^+}$ (Fig. 1.5c and 1.5d). The data in Figs. 1.5c and 1.5d demonstrate that the magnitude of ρ_f depends on the extent of dilution, but this dependence is not a monotonic trend with increasing dilution. Rather, ρ_l remains at a relative constant level with increasing dilution up to a point and then diminishes to zero with slight additional dilution. The characteristic length scale of ρ_f follows the same functional form with increasing dilution up to the point of collapse. This trend is similar for all the RTILs examined although it varies with the variation of diluents and RTIL identity. Dilution beyond the point of ρ_f disappearing yields anisotropy decay data consistent with aggregates of RTILs rather than isolated chromophores. The aggregates are found to increase in size with increasing dilution (up to 85% of dilution), while aggregate size depending on both RTIL anion and diluent identities. These distinct and complementary findings suggest the existence of persistent compositional heterogeneity in diluted RTIL systems. The magnitude of ρ_f is determined by RTIL dissociation and σ_s , and the length scale over which the gradient persists, d, is expected to diminish in proportion to diluent concentration in a homogeneous system. This is not seen to be a monotonic trend experimentally; RTILs form a compositionally heterogeneous system with the addition of solvent. The raw $\tau_{OR}(x)$ data shown in Fig. 1.5a reveal further information regarding the heterogeneity of the RTIL medium.

For the data presented here, we have used acetonitrile (ACN) and HMIM⁺TFSI, with the addition

As noted above, the Debye–Stokes–Einstein equation (Eq. (1.2)) relates the induced orientational anisotropy decay time constant to the thermal energy of the system (k_BT) parameters that relate to the volume and shape of the rotating entity (V and S) and the interactions between the rotating entity and the surrounding medium (Z and f). Eq. 1.2 relates the rotational diffusion time constant to the volume of the rotating entity. ^{55-56, 59-60} Low viscosity solvents are expected to alter the (diluted) RTIL η significantly. The effective viscosity, as sensed by CV⁺, is calculated to vary

between ca. 75 cP in the neat RTIL to ca. 40 cP for $X_{ACN} = 0.42$, well beyond the collapse of ρ_f . Ethylene glycol (15 cP) and glycerol (1400 cP)⁷⁵⁻⁷⁶ do not support free charge density gradients. Ion mobility thus appears not to be the primary factor leading to the loss of ρ_f with dilution. This finding is consistent with CV^+ residing within RTIL-rich regions of the (heterogeneous) medium. These results are consistent with other studies where RTILs are mixed with water⁷⁷⁻⁷⁸ and acetonitrile.⁷⁹

1.6 Relating the Charge Densigy Gradient to Molecular-Scale Organization

The long-range order we have reported is in the form of free charge density gradient induced by the surface charge of the support (silica or ITO). It is instructive to see if there is any relationship between the induced free charge density gradient and molecular scale-organization. It is well established that RTILs with imidazolium cations exhibit mesoscopic structures when the side chain (alkyl chain) lengths are C₄ or longer. The non-polar domains become larger and interconnected without disrupting the polar/ionic network formed by the polar head groups separated in increments of nonpolar aliphatic regions. 52, 80-82 The use of 1-Decyl-1-methylpyrrolidinium bis(trifluoromethylsulfonyl)imide (DMPyrr+TFSI-) as the RTIL and 1-decanol as the diluent make diluent RTIL cation aliphatic chain lengths equal. Dilution of RTILs with molecular solvents has revealed persistent aggregation of RTIL ion pairs to relatively high dilution, indicating nanoscale compositional heterogeneity (Chapters 2 and 3). The goal of matching the aliphatic functionalities of the RTIL and the molecular solvent was to optimize nanoscale phase segregation to produce a system with comparatively isolated polar and nonpolar regions, which we probe selectively with polar (CV⁺) and nonpolar (perylene) chromophores. We used spatially-resolved and time-resolved fluorescence anisotropy decay measurements to characterize the rotational diffusion dynamics of the two chromophores in the binary RTIL-decanol system. We used Eq. 1.9 to quantify the

magnitude and characteristic length scale of ρ_f by fitting the depth-dependence of the reorientation time constant to an exponential decay in distance from the charged support. The information of interest is the functional form of anisotropy decay R(t). The relationship between the functional form of R(t) and rotational diffusion constant D_{ROT} , and its Cartesian components, has been reported by Chuang and Eisenthal. The anisotropy decay function can contain up to five exponential decays, but with the appropriate assignment of the Cartesian axes to be coincident with transition moment axis or axes, reduces R(t) to either single or bi-exponential anisotropy decay functionalities. The rotating entity can be described by ellipsoidal shapes, with either the unique axis being longer (prolate ellipsoid) or shorter (oblate ellipsoid) than the remaining two axes. For the chromophore absorption transition dipole moment assigned as the x-axis, prolate and oblate ellipsoids result in the functional forms of R(t) given in Eq. 1.10.

Prolate rotor:
$$R(t)=0.4\exp(-6D_z t)$$
 [1.10]
Oblate rotor: $R(t)=0.1\exp(-(2D_x+4D_z)t)+0.3\exp(-6D_x t)$

$$D_{ROT} = \frac{1}{3}(D_x + D_y + D_z) = \frac{k_B TS}{6\eta V f}$$
 [1.11]

For both chromophores in neat DMPyrr⁺TFSI⁻, reorientation as oblate rotors is seen. Perylene maintains a two-component anisotropy decay from neat DMPyrr⁺TFSI⁻ through neat diluent, and CV⁺ exhibits a biexponential decay up to 75 mole% of 1-decanol, and single exponential decay R(t) data for higher fractions of 1-decanol. These data demonstrate long-range order in this binary system, consistent with non-polar regions of quasi-lamellar structure and substantial clustering of RTILs dominated by the polar headgroups. The order seen in this system is more extensive and dilution-resistant than what has been seen in other RTIL-molecular liquid binary systems.

The chromophore reorienting as an oblate rotor allows extraction of the Cartesian components of the rotational diffusion constants and these data provide insight into dilution-dependent changes in the chromophore local environment (Chapter 4). Significantly, these data provide the first direct connection between RTIL local organization and the ability of these materials to support induced free charge density gradients over macroscopic distances.

1.7 Summary

Room temperature ionic liquids have found wide application, in large part because of properties that are anomalous when compared to "normal" molecular solvents. Understanding the molecular-scale dynamics and interactions that are responsible for these properties is central to utilizing this family of materials to their fullest extent. Among the manifestations of the unusual effects is the existence of organization in RTILs on length scales ranging from nanometers to tens of micrometers. To date, both structural organization and induced charge density gradients have been reported in RTILs, with the characteristic length scale of each effect depending significantly on the design of the experiment and the means by which the effect was measured. Our focus has been on understanding free charge density gradients and the direct piezoelectric effect in ionic liquids. We continue to work to identify the mechanism(s) by which the piezoelectric effect operates in RTILs and the commonality and connection between the various long-range phenomena seen in RTILs. Making such connections will lead to novel applications for these materials.

REFERENCES

- 1. Arbizzani, C.; Biso, M.; Cericola, D.; Lazzari, M.; Soavi, F.; Mastragostino, M., Safe, high-energy supercapacitors based on solvent-free ionic liquid electrolytes. *J. Pwr. Sources* **2008**, *185*, 1575 1579.
- 2. Newell, R.; Faure-Vincent, J.; Iliev, B.; Schubert, T.; Aradilla, D., A new high performance ionic liquid mixture electrolyte for large temperature range supercapacitor applications (- 70° C to 80° C) operating at 3.5 V cell voltage. *Electrochim. Acta.* **2018**, *267*, 15 19.
- 3. Van Aken, K. L.; Beidaghi, M.; Gogotsi, Y., Formulation of ionic liquid electrolyte to expand the voltage window of supercapacitors. *Angew. Chem.* **2015**, *127*, 4888 4891.
- 4. MacFarlane, D. R.; Tachikawa, N.; Forsyth, M.; Pringle, J. M.; Howlett, P. C.; Elliott, G. D.; Davis, J. H.; WatanabeM.; Simon, P.; Angell, C. A., Energy applications of ionic liquids. *Energ. Env. Sci.* **2014**, *7*, 232 250.
- 5. Sakaebe, H.; Matsumoto, H., N-Methyl-N-propylpiperidinium bis(trifluoromethane sulfonyl)imide (PP13–TFSI)–novel electrolyte base for Li battery. *Electrochem. Commun.* **2003**, *5*, 594 598.
- 6. Ibsen, K. N.; Ma, H.; Banerjee, A.; Tanner, E. E. L.; Nangia, S.; Mitragotri, S., Mechanism of Antibacterial Activity of Cholin-Based Ionic Liquids (CAGE). *ACS Biomater. Sci. Eng.* **2018**, *4*, 2370-2379.
- 7. Musial, M.; Olejniczak, A. B.; Denel-Bobrowska, M.; Zorebski, E.; Dzida, M., In Vitro Anticancer and Antivirus Activities of Cyano- and Bis(Trifluoromethylsulfonyl)imide-Based Ionic Liquids. *ACS Sust. Chem. Eng.* **2021**, *9*, 16459-16465.
- 8. Gehlot, P. S.; Gupta, H.; Rathore, M. S.; Khatri, K.; Kumar, A., Intrinsic MRI contrast from amino acid-based paramagnetic ionic liquids. *Mater. Adv.* **2020**, *1*, 1980-1987.
- 9. Zhang, M.; Li, L.; Wang, M.; Li, T.; Song, K.; Nie, Y.; Ren, B., 3D Printing for Biological Scaffolds using Poly(Ionic Liquid)/Gelatin/Sodium Alginate Ink. *Macromol. Mater. Eng.* **2021**, *306* (7).
- 10. Krishnadoss, V.; Kanjilal, B.; Masoumi, A.; Banerjee, A.; Dehzangi, I.; Pezhouman, A.; Ardehali, R.; Martins-Green, M.; Leijten, J.; Noshadi, I., Programmable bio-ionic liquid functionalized hydrogels for *in situ* 3D bioprinting of electronics at the tissue interface. *Mats Today Adv* **2023**, *17*, 100352-100364.
- 11. Banerjee, A.; Ibsen, K.; Brown, T.; Mitragotri, S., Ionic Liquids for oral insulin delivery. *Proceeding of the National Academy of Sciences* **2018**, *115* (28), 7296-7301.

- 12. Tanner, E. E. L.; Curreri, A. M.; Balkaran, J. P. R.; Selig-Wober, N. C.; Yang, A. B.; Kendig, C.; Fluhr, M. P.; Kim, N.; Mitragotri, S., Design Principles of Ionic Liquids for Transdermal Drug Delivery. *Adv. Mater.* **2019**, *31* (27), 1901103-1901112.
- 13. Rizzo, S.; Arnaboldi, S.; Cirilli, R.; Gennaro, A.; Isse, A. A.; Sannicolò, F.; Mussini, P. R., An "inherently chiral" 1,1′-bibenzimidazolium additive for enantioselective voltammetry in ionic liquid media. *Electrochem. Commun.* **2018**, *89*, 57-61.
- 14. Rizzo, S.; Arnaboldi, S.; Mihali, V.; Cirilli, R.; Forni, A.; Gennaro, A.; Isse, A. A.; Pierini, M.; Mussini, P. R.; Sannicolò, F., "Inherently Chiral" Ionic-Liquid Media: Effective Chiral Electroanalysis on Achiral Electrodes. *Angew. Chem. Int. Ed.* **2017**, *56* (8), 2079-2082.
- 15. Zhao, H.; Afriyie, L. O.; Larm, N. E.; Baker, G. A., Glycol-functionalized ionic liquids for high-temperature enzymatic ring-opening polymerization. *RSC Adv.* **2018**, *8*, 36025 36033.
- 16. Trivedi, S.; Ravula, S.; Baker, G. A.; Pandey, S.; Bright, F. V., Controlling Microarray Feature Spreading and Response Stability on Porous Silicon Platforms by Using Alkene-Terminal Ionic Liquids and UV Hydrosilylation. *Langmuir* **2020**, *36* (19), 5474-5482.
- 17. Ravula, S.; Larm, N. E.; Liu, Y.; Atwood, J. L.; Baker, S. N.; Baker, G. A., Ionothermal synthesis of magnetically-retrievable mesoporous carbons from alkyne-appended ionic liquids and demonstration of their use in selective dye removal. *New J. Chem.* **2018**, *42* (3), 1979-1986.
- 18. Tang, S.; Baker, G. A.; Zhao, H., Ether- and alcohol-functionalized task-specific ionic liquids: attractive properties and applications. *Chem. Soc. Rev.* **2012**, *41* (10), 4030-4066.
- 19. Clark, R.; Nawawi, M. A.; Dobre, A.; Pugh, D.; Liu, Q.; Ivanov, A. P.; White, A. J. P.; Edel, J. B.; Kuimova, M. K.; McIntosh, A. J. S., et al., The effect of structural heterogeneity upon the microviscosity of ionic liquids. *Chem. Sci.* **2020**, *11*, 6121-6133.
- 20. Russina, O.; Triolo, A.; Gontrani, L.; Caminiti, R., Mesoscopic structural heterogeneities in room temperature ionic liquids. *J. Phys. Chem. Lett.* **2012**, *3*, 27-33.
- 21. Gebbie, M. A.; Dobbs, H. A.; Valtiner, M.; Israelachvilli, J. N., Long-range electrostatic screening in ionic liquids. *Proc. Nat. Acad. Sci. USA* **2015**, *112* (24), 7432-7437.
- 22. Gebbie, M. A.; Valtiner, M.; Banquy, X.; Fox, E. T.; Henderson, W. A.; Israelachvilli, J. N., Ionic liquids behave as dilute electrolyte solutions. *Proc. Nat. Acad. Sci. USA* **2013**, *110* (24), 9674-9679.
- 23. MacFarlane, D. R.; Forsyth, M.; Izgorodina, E. I.; Abbott, A. P.; Annat, G.; Fraser, K., On the concept of ionicity in ionic liquids. *Phys. Chem. Chem. Phys.* **2009**, *11*, 4962-4967.
- 24. Nelyubina, Y. V.; Shaplov, A. S.; Lozinskaya, E. I.; Buzin, M. I.; Vygodskii, Y. S., A volume-based approach for predicting thermophysical behavior of ionic liquids and ionic liquid crystals. *J. Am. Chem. Soc.* **2016**, *138*, 10076-10079.

- 25. Binnemans, K., Ionic Liquid Crystals. Chem. Rev. 2005, 105, 4148-4204.
- 26. Hendil-Jakani, H.; Baroni, P.; Noirez, L.; Chancelier, L.; Gebel, G., Highlighting a Solid-Like Behavior in RTILs: Tri-octylmethylammonium Bis(trifluoromethansulfonyl)imide TOMA-TFSI. *J. Phys. Chem. Lett.* **2013**, *4*, 3775-3778.
- 27. Anaredy, R. S.; Shaw, S. K., Long-range ordering of ionic liquid fluid films. *Langmuir* **2016,** *32*, 5147-5154.
- 28. Anaredy, R. S.; Shaw, S. K., Developing distinct chemical environments in ionic liquid films. *J. Phys. Chem. C* **2018**, *122*, 19731-19737.
- 29. Anaredy, R. S.; Shaw, S. K., Directing long-range molecular ordering in ionic liquid films: A tale of two interfaces. *J. Phys. Chem. C* **2019**, *123*, 8975-8982.
- 30. Nishida, J.; Breen, J. P.; Wu, B.; Fayer, M. D., Extraordinary slowing of structural dynamics in thin films of a room temperature ionic liquid. *ACS Cent. Sci.* **2018**, *4*, 1065-1073.
- 31. Shin, J. Y.; Yamada, S. A.; Fayer, M. D., Dynamics of a room temperature ionic liquid in supported ionic liquid membranes vs the bulk liquid: 2D IR and polarized IR pump-probe experiments. *J. Am. Chem. Soc.* **2017**, *139*, 311-323.
- 32. Shin, J. Y.; Yamada, S. A.; Fayer, M. D., Carbon dioxide in a supported ionic liquid membrane: Structural and rotational dynamics measured with 2D IR and pump-probe experiments. *J. Am. Chem. Soc.* **2017**, *139*, 11222-11232.
- 33. Sieling, T.; Brand, I., In Situ spectroelectrochemical investigation of potential-dependent changes in an amphiphilic imidazolium-based ionic liquid film on the Au(111) electrode surface. *ChemElectroChem* **2020**, *7*, 3233-3243.
- 34. Ma, K.; Jarosova, R.; Swain, G. M.; Blanchard, G. J., Charge-Induced Long-Range Order in a Room-Temperature Ionic Liquid. *Langmuir* **2016**, *32* (37), 9507-9512.
- 35. Ma, K.; Jarosova, R.; Swain, G. M.; Blanchard, G. J., Modulation of an induced charge density gradient in the room temperature ionic liquid BMIM⁺BF₄⁻. *J. Phys. Chem. C* **2018**, *122*, 7361-7367.
- 36. Wang, Y.; Jarosova, R.; Swain, G. M.; Blanchard, G. J., Characterizing the magnitude and structure-dependence of free charge density gradients in room-temperature ionic liquids. *Langmuir* **2020**, *36*, 3038-3045.
- 37. Sloutskin, E.; Ocko, B. M.; Tamam, L.; Kuzmenko, I.; Gog, T.; Deutsch, M., Surface layering in ionic liquids: An X-ray reflectivity study. *J. Am. Chem. Soc.* **2005**, *127*, 7796-7804.
- 38. Santos, C. S.; Murthy, S.; Baker, G. A.; Castner, E. W., Communication: X-ray scattering from ionic liquids with pyrrolidinium cations. *J. Chem. Phys.* **2011**, *134*, 121101 (1-4).

- 39. Annapureddy, H. V. R.; Kashyap, H. K.; De Biase, P. M.; Margulis, C. J., What is the origin of the prepeak in the X-ray scattering of imidazolium-based room-temperature ionic liquids? *J. Phys. Chem. B* **2010**, *114*, 16838-16846.
- 40. Imai, Y.; Abe, H.; Yoshimura, Y., X-ray diffraction study of ionic liquid based mixtures. *J. Phys. Chem. B* **2009**, *113*, 2013-2018.
- 41. Dupont, J., On the solid, liquid and solution structural organization in imidazolium ionic liquids. *J. Braz. Chem. Soc.* **2004**, *3*, 341-350.
- 42. Tokuda, H.; Tsuzuki, S.; Susan, M. A. B. H.; Hayamizu, K.; Watanabe, M., How ionic are room temperature ionic liquids? An indicator of the physicochemical properties. *J. Phys. Chem. B* **2006**, *110*, 19593-19600.
- 43. Schreiner, C.; Zugmann, S.; Hartl, R.; Gores, H. J., Fractional Walden rule for ionic liquids: Examples from recent measurements and a critique of the so-called ideal KCl line for the Walden plot. *J. Chem. Eng. Data* **2010**, *55*, 1784-1788.
- 44. Baldelli, S., Interfacial structure of room-temperature ionic liquids at the solid-liquid interface as probed by sum frequency generation spectroscopy. *J. Phys. Chem. Lett.* **2013**, *4*, 244-252.
- 45. Bovio, S.; Podesta, A.; Lenardi, C.; Milani, P., Evidence of extended solidlike layering in [Bmim][NTf2] ionic liquid thin films at room temperature. *J. Phys. Chem. B* **2009**, *113*, 6600-6603.
- 46. Atkin, R.; Borisenko, N.; Druschler, M.; El Abedin, S. Z.; Endres, F.; Hayes, R.; Huber, B.; Roling, B., An in situ STM/AFM and impedance spectroscopy study of the extremely pure 1-butyl-1-methylpyrrolidinium tris(pentafluoroethyl)trifluorophosphate/Au(111) interface: potential dependent solvation layers and the herringbone reconstruction. *Phys. Chem. Chem. Phys.* **2011**, *13*, 6849-6857.
- 47. Rotenberg, B.; Salanne, M., Structural Transition at Ionic Liquid Interfaces. *J. Phys. Chem. Lett.* **2015**, *6* (4978-4985).
- 48. Han, M.; Kim, H.; Leal, C.; Negrito, M.; Batteas, J. D.; Espinosa-Marzal, R. M., Insight into the electric double layer of ionic liquids revealed through its temporal evolution. *Adv. Mater. Interfaces* **2020**, *7*, 2001313 (1-10).
- 49. Wu, B.; Breen, J. P.; Fayer, M. D., Structural dynamics in ionic liquid thin films: The effect of cation chain length. *J. Phys. Chem. C* **2020**, *124*, 4179-4189.
- 50. Wu, B.; Breen, J. P.; Xing, X.; Fayer, M. D., Controlling the dynamics of ionic liquid thin films via multilayer surface functionalization. *J. Am. Chem. Soc.* **2020**, *142*, 9482-9492.

- 51. Thomaz, J. E.; Bailey, H. E.; Fayer, M. D., The influence of mesoscopic confinement on the dynamics of imidazolium-based room temperature ionic liquids in polyether sulfone membranes. *J. Chem. Phys.* **2017**, *147*, 194502 1-11.
- 52. Triolo, A.; Russina, O.; Bleif, H.-J.; DiCola, E., Nanoscale segregation in room temperature ionic liquids. *J. Phys. Chem. B* **2007**, *111*, 4641-4644.
- 53. Wu, F.; Karunaratne, W. V.; Margulis, C. J., Ionic liquid mixture at the vacuum interface and the peaks and antipeaks analysis of X-ray reflectivity. *J. Phys. Chem. C* **2019**, *1233*, 4914-4925.
- 54. Hay, C. E.; Marken, F.; Blanchard, G. J., Detection and Characterization of Liquid|Solid and Liquid|Solid Interfacial Gradients of Water Nano-Droplets in Wet N-Octyl-2-Pyrrolidone. *Langmuir* **2014**, *30*, 9951-9961.
- 55. Chuang, T. J.; Eisenthal, K. B., Theory of fluorescence depolarization by anisotropic rotational diffusion. *J. Chem. Phys.* **1972**, *57* (12), 5094-5097.
- 56. Debye, P., *Polar Molecules* Chemical Catalog Co.: New York 1929; p 84.
- 57. Edward, J. T., Molecular volumes and the Stokes-Einstein equation. *J. Chem. Ed.* **1970**, *47* (4), 261-270.
- 58. Favro, D. L., Theory of the Rotational Brownian Motion of a Free Rigid Body. *Phys. Rev.* **1960,** *119* (1), 53-62.
- 59. Hu, C.-M.; Zwanzig, R., Rotational friction coefficients for spheroids with the slipping boundary condition. *J. Chem. Phys.* **1974**, *60* (11), 4354-4357.
- 60. Perrin, F., Mouvement brownien d'un ellipsoide I. Dispersion diélectrique pour des molécules ellipsoidales. *J. Phys. Radium* **1934,** *5*, 497.
- 61. Tao, T., Time-Dependent Fluorescence Depolarization and Brownian Rotational Diffusion Coefficients of Macromolecules. *Biopol.* **1969**, *8*, 609-632.
- 62. Blanchard, G. J., Picosecond Spectroscopic Measurement of a Solvent Dependent Change of Rotational Diffusion Rotor Shape. *J. Chem. Phys.* **1987**, *87* (12), 6802-6808.
- 63. Blanchard, G. J.; Cihal, C. A., Orientational Relaxation Dynamics of Oxazine 118 and Resorufin in the Butanols Valence-Dependent and State-Dependent Solvation Effects *J. Phys. Chem.* **1988**, *92* (21), 5950-5954.
- 64. Mueller, R.; Kammler, H. K.; Wegner, K.; Pratsinis, S. E., OH surface density of SiO₂ and TiO₂ by thermogravimetric analysis. *Langmuir* **2003**, *19*, 160-165.

- 65. Peiris, T. A. N.; Senthilarasu, S.; Wijayantha, K. G. U., Enhanced performance of flexible-dye-sensitized solar cells: Electrodeposition of Mg(OH)₂ in a nanocrystalline TiO₂ electrode. *J. Phys. Chem. C* **2011**, *116*, 1211-1218.
- 66. Ashida, T.; Miyamura, A.; Oka, N.; Sato, Y.; Yagi, T.; Taketoshi, N.; Baba, T.; Shigesato, Y., Thermal transport properties of polycrystalline tin-doped indium oxide films. *J. Appl. Phys.* **2009**, *105*, 073709-1-4.
- 67. Abb, M.; Albella, P.; Aizpurua, J.; Muskens, O. L., All-optical control of a single plasmonic nanoantenna-ITO hybrid. *Nano Lett.* **2011**, *11* (6), 2457-2463.
- 68. Bohne, D.; Fischer, S.; Obermeier, E., Thermal conductivity, density, viscosity, and Prandtl-numbers of ethylene glycol-water mixtures. *Ber. Bunsenges. Phys. Chem.* **1984**, *88*, 739-744.
- 69. Bazant, M. Z.; Storey, B. D.; Kornyshev, A. A., Double Layer in Ionic Liquids: Overscreening versus Crowding. *Phys. Rev. Lett.* **2011**, *106*.
- 70. Fedorov, M. V.; Kornyshev, A. A., Ionic Liquids at Electrified Interfaces. *Chem. Rev.* **2014**, *114*, 2978-3036.
- 71. Oldham, K. B., Gouy-Chapman-Stern Model of the Double Layer at a (Metal)(Ionic Liquid) Interface. *J. Electroanal. Chem.* **2008**, *613*, 131-138.
- 72. Gebbie, M. A.; Dobbs, H. A.; Valtiner, M.; Israelachvili, J. N., Long-range electrostatic screening in ionic liquids. *Proc. Nat. Acad. Sci. USA* **2015**, *112* (24), 7432-7437.
- 73. Schroder, U.; Wadhawan, J. D.; Compton, R. G.; Marken, F.; Suarez, P. A. Z.; Consorti, C. S.; de Souza, R. F.; Dupont, J., Water-induced ion diffusion: voltammetric studies in 1-methyl-3-[2,6-(S)-dimethylocten-2-yl]imidazolium tetrafluoroborate, 1-butyl-3-methylimidazolium tetrafluoroborate and hexafluorophosphate ionic liquids. *New J. Chem.* **2000**, *24*, 1009-1015.
- 74. Wang, Y.; Jarosova, R.; Swain, G. M.; Blanchard, G. J., Characterizing the magnitude and structure-dependence of free charge density gradients in room temperature ionic liquids. *Langmuir* **2020**, *36*, 3038-3045.
- 75. Jerome, F. S.; Tseng, J. T.; Fan, L. T., Viscosities of aqueous glycol solutions. *J. Chem. Eng. Data* **1968**, *13* (4), 496.
- 76. Sequr, J. B.; Oberstar, H. E., Viscosity of Glycerol and Its Aqueous Solutions. *Ind. Eng. Chem.* **1951**, *43* (9), 2117-2120.
- 77. Baker, S. N.; Baker, G. A.; Munson, C. A.; Chen, F.; Bukowski, E. J.; Cartwright, A. N.; Bright, F. V., Effects of Solubilized Water on the Relaxation Dynamics Surrounding 6-Propionyl-2-(N,N-dimethylamino)naphthalene Dissolved in 1-Butyl-3-methylimidazolium Hexafluorophosphate at 298 K. *Ind. Chem. Eng. Res.* **2003**, *42*, 6457-6463.

- 78. Zhang, X. X.; Liang, M.; Hunger, J.; Buchner, R.; Maroncelli, M., Dielectric Relaxation and Solvation Dynamics in a Prototypical Ionic Liquid + Dipolar Protic Liquid Mixture: 1-Butyl-3-Methylimidazolium Tetrafluoroborate + Water. *J. Phys. Chem. B* **2013**, *117*, 15356-15368.
- 79. Liang, M.; Zhang, X. X.; Kaintz, A.; Ernsting, N. P.; Maroncelli, M., Solvation Dynamics in a Prototypical Ionic Liquid + Dipolar Aprotic Liquid Mixture: 1-Butyl-3-methylimidazolium Tetrafluoroborate + Acetonitrile. *J. Phys. Chem. B* **2014**, *118*, 1340-1352.
- 80. Lopes, J. N. A. C.; Padua, A. A. H., Nanostructural Organization in Ionic Liquids. *J. Phys. Chem. B* **2006**, *110*, 3330-3335.
- 81. Xiao, D.; Rajian, J. R.; Li, S.; Bartsch, R. A.; Quitevis, E. L., Additivity in the Optical Kerr Effect Spectra of Binary Ionic Liquid Mixtures: Implications for Nanostructural Organization. *J. Phys. Chem. B* **2006**, *110* (33), 16174-16178.
- 82. Cosby, T.; Kapoor, U.; Shah, J. K.; Sangoro, J., Mesoscale Organization and Dynamics in Binary Ionic Liquid Mixtures. *Journal of Physical Chemistry Letter* **2019**, (10), 6274-6280.

CHAPTER 2. Ionic Liquids Exhibit the Piezoelectric Effect
Adapted with permission from:
Md. Iqbal Hossain and G. J. Blanchard; Ionic Liquids Exhibit the Piezoelectric Effect. <i>J. Phys. Chem. Lett.</i> 2023 , 14, 2731-2735.

2.1 Introduction

The piezoelectric effect has been known since 1880^1 and it has found wide application in areas ranging from spark sources to nano-actuators and biosensors. The direct piezoelectric effect produces a charge separation in a material upon application of force and this is understood to occur based on the distortion of the material structure on the unit cell or molecular scale. This effect is seen in non-centrosymmetric crystalline materials, such as quartz, LiNbO₃, BaTiO₃ and Pb[Zr_xTi_{1-x}]O₃ ($0 \le x \le 1$) (PZT), and also in some ceramics,² nanomaterials,³ polymers,⁴⁻⁵ composites⁶⁻¹³ and even in non-crystalline materials including DNA,¹⁴⁻¹⁷ viral proteins¹⁸⁻¹⁹ and amino acids.²⁰

Materials that exhibit the direct piezoelectric effect also exhibit the converse piezoelectric effect, where the application of charge to a material causes a bulk physical distortion, and this effect has found use in many applications, especially in nanoactuators and other small-amplitude motion control applications. In all known examples of the direct and converse piezoelectric effect, the material manifesting these effects is a solid. We report for the first time the observation of the direct piezoelectric effect in a neat liquid. The piezoelectric liquids reported here are room temperature ionic liquids (RTILs), a class of compounds that exhibits a range of unusual and useful properties,²¹ and that are generally recyclable.²²⁻²³ Based on the data reported here we can now identify the induced free charge density gradient, ρ_f , reported earlier in ionic liquids²⁴⁻³³ as the converse piezoelectric effect.

2.2 Methods

2.2.1 Materials Used

Room temperature ionic liquids 1-butyl-3-methyl imidazolium bis(trifluoromethylsulfonyl)imide (BMIM⁺TFSI⁻, >99%, <500 ppm H₂O) and 1-hexyl-3-methyl imidazolium bis(trifluoromethylsulfonyl)imide (HMIM⁺TFSI⁻, 98%) were purchased from Sigma-

Aldrich in the purity grade indicated and were then purified prior to use according to a procedure reported previously.^{27,34} Following purification, the water content of the RTILs was measured by Karl Fischer (Mettler-Toledo C10S) titration and found to be less than 50 ppm. Ethylene glycol and sodium chloride (Sigma Aldrich) were used as received.

2.2.2 Measurement of the Direct Piezoelectric Effect in RTILs

The cell used to quantitate the piezoelectric effect in RTILs is schematized in Fig. 2.1. The body of the cell is made of steel, the piston is made of Delrin® and is equipped with a steel center electrode. The Delrin® piston contains an O-ring (Viton) to ensure a tight seal upon contacting the RTIL. The seal is liquid-tight but not air-tight, such that air can escape until the piston contacts the RTIL. The dimensions of the piston are 1.2 cm diameter, and with the O-ring, 1.4 cm in diameter, which is the same as the inside diameter of the cylinder. The bottom of the O-ring is 2.5 mm above the bottom of the piston. For the 200 µL sample size used for all measurements, the thickness of the RTIL confined in the cylinder is 0.64 mm (see calculation in SI). The force-induced charge is measured as an open circuit potential difference between the cell body and the piston center electrode as a function of force applied to the piston. The force applied is measured with a digital force gauge (Vetus 500N). In this configuration the force and potential difference are along the same axis.

2.2.3 Open Circuit Potential Measurements

Open circuit potential measurements were performed using an electrochemical bench (CH Instruments 604B). For these measurements the input impedance is ca. $10^{12} \Omega$ with a small stray capacitance contribution that can be seen in the control (blank) measurements (vide infra).

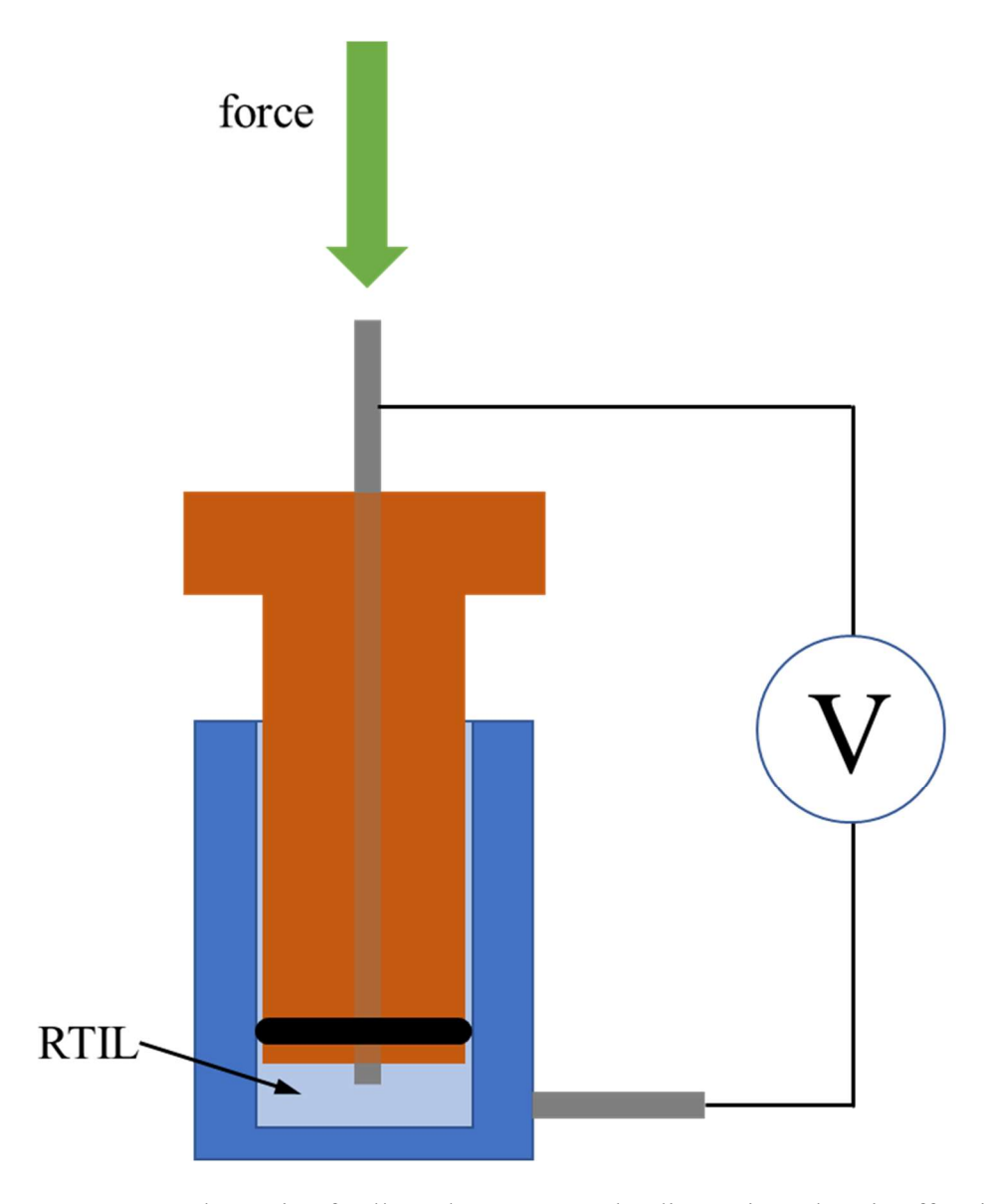


Figure 2.1 Schematic of cell used to measure the direct piezoelectric effect in RTILs. The piston is non-conductive (Delrin®) and contains an electrode along its center axis. The cylinder is made of steel. The system is sealed using an O-ring.

2.3 Results and Discussion

As noted in the Introduction, the piezoelectric effect has been observed in composite materials, some of which contain ionic liquids as a constituent, but in all of those systems, the resulting material exists in the solid state.⁷⁻¹³ The work we report here is the observation of the piezoelectric effect in neat ionic liquids. The notion of the piezoelectric effect in a liquid is a topic that has not received much discussion in the literature, for several reasons. The first is that the signature of the converse piezoelectric effect is a change in the dimension(s) of a material upon the application of a potential across the material, and the definition of a liquid is a material that assumes the shape of its container, making the characterization of such changes challenging. The second reason is that charge separation in liquids is typically characterized as a nominally uniform, diffusionmediated spatial distribution of dissociated ions in bulk media, and the imposition of charge (e.g., an electrode surface) leads to ion organization on the sub-nm length scale but not beyond.³⁵ This behavior is well-characterized in molecular liquids, but our work with RTILs has demonstrated the existence of an induced charge density gradient that persists over multiple tens of microns. It is clear for this reason and others that RTILs cannot be understood in the same conceptual framework as molecular liquids.

We have measured the direct piezoelectric effect in neat RTILs and show the potential vs. force data for BMIM⁺TFSI⁻ in Fig. 2.2 and for HMIM⁺TFSI⁻ in Fig. 2.3. The magnitude of the force impulse applied is indicated on the potential vs. time graphs (Figs. 2.2a and 2.3a). The dependence of open circuit potential on force applied is presented in Figs. 2.2b and 2.3b, revealing a linear dependence over the range studied for both RTILs. The data are reproducible over multiple experiments, and fluctuations in the signal baseline are a consequence of the high input impedance

of the electrochemical bench and electrical connections between the cell and bench. The functional form of the data, *i.e.*, the shape of the potential pulse resulting from the application of force, is

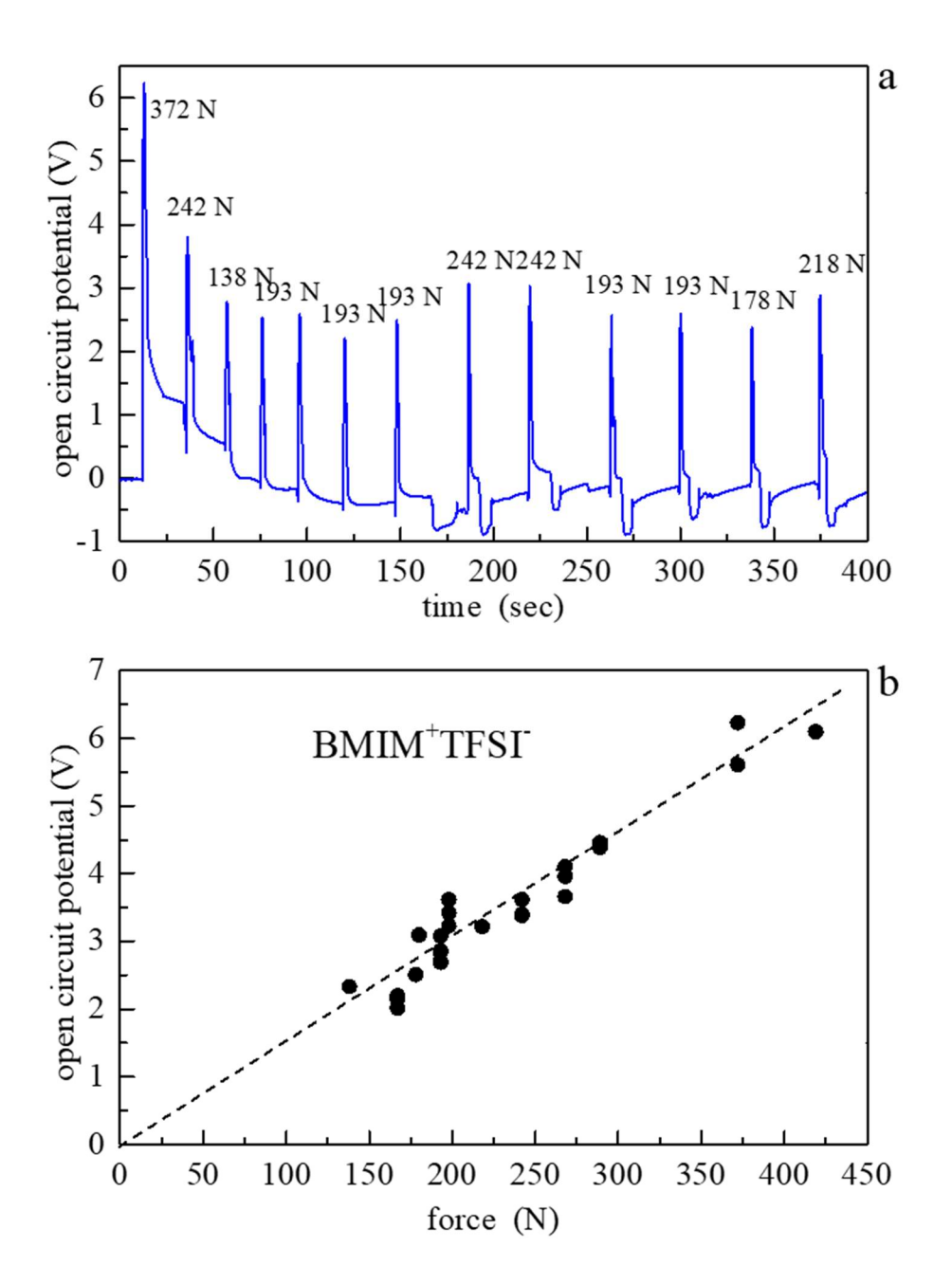


Figure 2.2 (a) Potential measured vs. time raw experimental data for BMIM $^+$ TFSI $^-$. The values indicated above each peak are the force applied. Scan time for the open circuit potential measurement shown was 400 sec. (b) Potential measured vs. force applied for multiple timescans. The slope of the dependence is 16 ± 1 mV/N.

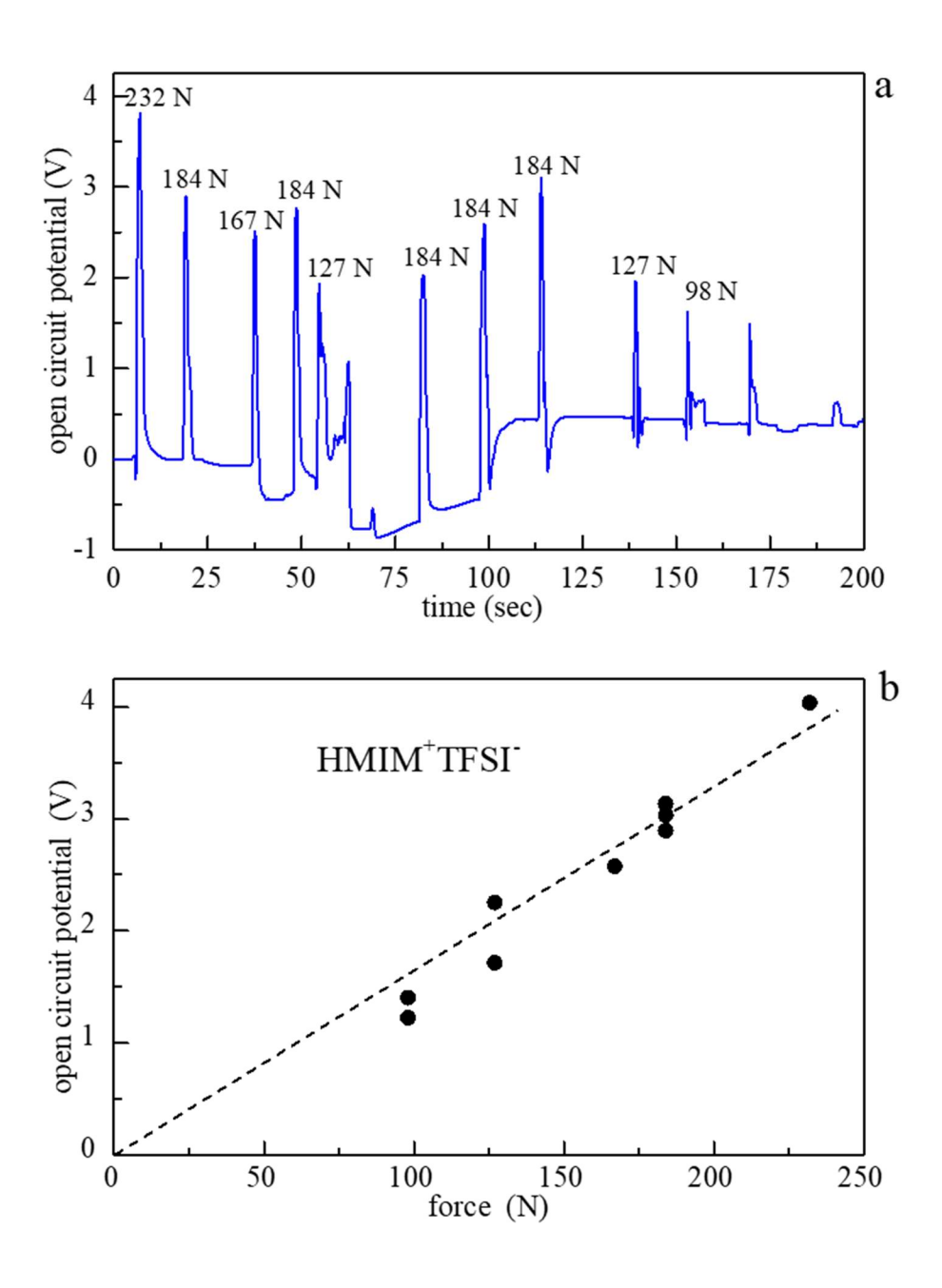


Figure 2.3 (a) Potential measured vs. time raw experimental data for HMIM $^+$ TFSI $^-$. The values indicated above each peak are the force applied. Scan time for the open circuit potential measurement shown was 200 sec. (b) Potential measured vs. force applied. The slope of the dependence is 17 ± 1 mV/N.

determined by the mechanical relaxation of the cylinder/piston apparatus and does not reflect an intrinsic relaxation effect in the RTILs. We show in Fig. 2.4 the control experiments, where the cell is filled with either neat ethylene glycol (red lines) or 1M NaCl in ethylene glycol (black lines), in the absence of force (Fig. 2.4a) and with the application of force (Fig. 2.4b) in the same manner as for the RTILs. The open circuit potential is 350 mV or less in all cases, with a slow build-up over time due to the charging of stray capacitance within the system. In all cases the magnitude of the control experiment data is a factor of *ca*. 20 smaller than the potential maxima shown in Figs. 2.2 and 2.3 for the RTILs, and there is no measurable piezoelectric response for either the neat molecular liquid or a 1M NaCl solution.

The magnitude of the direct piezoelectric effect in the RTILs reported here is 16 ± 1 mV/N for BMIM⁺TFSI⁻ and 17 ± 1 mV/N for HMIM⁺TFSI⁻, as determined from the slope of the best-fit lines shown in Figs 2.2b and 2.3b. Based on the geometry of the cell and the volume of RTIL used (200 μ L), these slopes correspond to piezoelectric constants, d_{33} , of 0.34 ± 0.02 pC/N and 0.36 ± 0.02 pC/N assuming a dielectric constant of $\varepsilon \sim 10$ for both RTILs³⁶ (calculation in SI). It is noteworthy that the magnitude of the values we recover for RTILs are within a factor of ten of quartz (d_{33} = -2.3 pC/N). These data also suggest that the RTIL cation aliphatic chain length do not play a dominant role in determining the piezoelectric response, and more investigation will be required to establish the relationship between RTIL constituent structure and piezoelectric response.

A material that exhibits the direct piezoelectric effect should also exhibit the converse piezoelectric effect, and this phenomenon is manifested as the induced free charge density gradient, ρ_f , that we have reported before.²⁵⁻³³ The quantity ρ_f is a consequence of organization in RTILs that persists over ca. 100 µm when the RTIL is placed in contact with a charged surface. The charge density gradient does not necessarily imply the existence of a spatial variation in

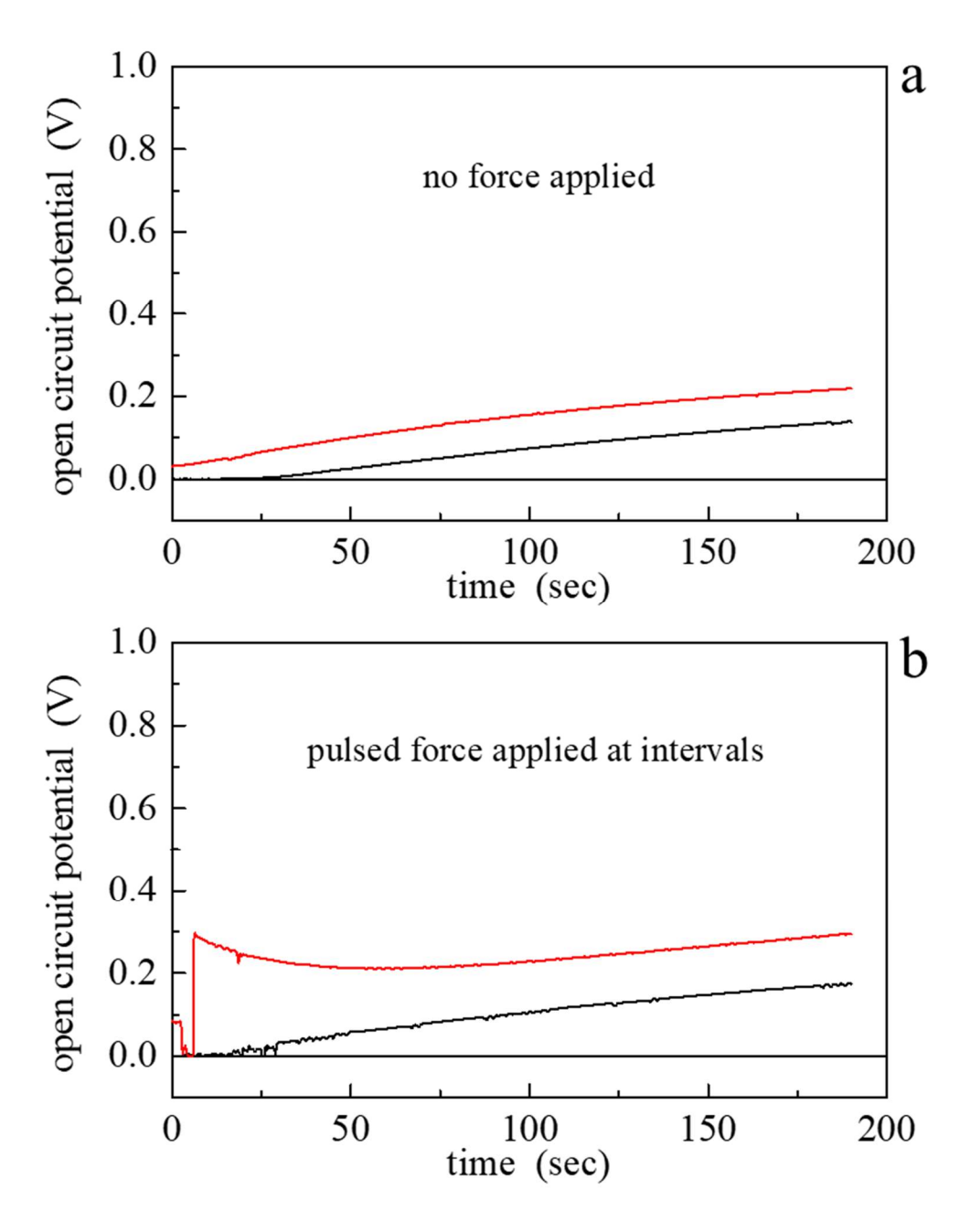


Figure 2.4 (a) Potential measured vs. time raw experimental data for neat ethylene glycol (red line) and 1M NaCl in ethylene glycol (black line) where no pulsed force is applied to the piston of the apparatus. Three scans are shown to indicate run-to-run variations in the baseline, and to show a slow increase in open circuit potential. (b) Potential measured vs. time for neat ethylene glycol (red line) and 1M NaCl in ethylene glycol (black line) where force is applied at regular intervals, analogous to that used for the data shown in Figs. 2 and 3. The slight increase at early time is an electronic artifact and is not correlated to the application of force. For both data sets, the slow baseline drift is due to stray capacitance in the apparatus and detection electronics.

molecular structural organization but recent work has revealed a connection between ρ_f and a spatial variation in molecular organization within these systems,²⁴ and the observation of the direct piezoelectric effect is consistent with induced structural order (*vide infra*). This behavior is not consistent with the known properties of molecular liquids.

The direct and converse piezoelectric effects in RTILs cannot be interpreted solely in the context of known theory for the piezoelectric effect, and traditional materials characterization methods such as resonant ultrasound spectroscopy will not be directly applicable to liquid phase piezoelectrics. These factors underscore the need for the development of a new theoretical construct for the piezoelectric effect in RTILs. The current theory for the converse piezoelectric effect in solids is based on the piezoelectric material being treated as a dielectric, where there is no net free charge density in the bulk material and any charge resides at the interface(s) of the material or at domain boundaries. While we have implicitly assumed a (mostly) dielectric material to explain the free charge density gradient in these materials, it is well known that RTILs dissociate to some extent,³⁷ which gives rise to the presence of a steady state concentration of unassociated ions at any given time. The analogy between piezoelectric solids and liquids may be better approximated by comparison of RTILs to ceramics or micro/nanocrystalline materials where charge can accumulate at grain boundaries. This analogy is consistent with the known nanoscale compositional heterogeneity of RTILs upon dilution, and such organization may exist in some manner in neat RTILs owing to the amphiphilic nature of typical RTIL cations. 24-26

Another issue is that the theory for piezoelectric solids couples Hooke's law with the response of a dielectric material to the presence of an electric field. While Hooke's law applies to the solid and liquid phases, at least under conditions of appropriate confinement and under compressive force (pressure), liquids exhibit very limited compressibility. It is thus likely that the current theory

for solid state piezoelectric materials will require some modification to account for the experimental observations presented here.

The observation of the direct piezoelectric effect in RTILs carries an interesting implication about organization within these materials. Solid phase piezoelectric materials are noncentrosymmetric, and despite some reports of piezoelectric behavior in nominally centrosymmetric media, symmetry breaking has been invoked as a mechanism for the observed behavior.³⁸⁻⁴⁰ Bulk liquids are centrosymmetric and the observation of a surprisingly large direct piezoelectric response in RTILs implies a force-induced macroscopic lifting of a center of inversion in these liquids. Local organization is well-established both experimentally and theoretically in RTILs, 41-53 although the molecular-scale details of that organization are complex. Modeling and scattering studies consistently show organization on the several nm length-scale, ⁵³ and experimental studies have revealed order on length-scales ranging from nm to tens of µm, depending on the means used to probe the organization.^{24-27, 41-45, 49-52} Much work remains to develop a better understanding of organization in RTILs. The data presented in Figs. 2.2 and 2.3 indicate that the bulk center of symmetry in RTILs is broken by the application of force, and the existence of ρ_I in these materials suggests that charge can be used to produce the same structural effect. Clearly further work is required to understand the structural details associated with the direct and converse piezoelectric effects in RTILs.

2.4 Conclusions

We have reported for the first time the direct piezoelectric effect in a bulk liquid phase material, the room temperature ionic liquids BMIM⁺TFSI⁻ and HMIM⁺TFSI⁻. The magnitude of the direct piezoelectric effects in these materials is an order of magnitude smaller than that of quartz, a widely used piezoelectric material. The existence of the direct piezoelectric effect in

RTILs implies organization being induced in these media that lifts the bulk center of symmetry that is characteristic of most liquid phase media, and these results invite the development of a theoretical framework in which to understand these phenomena. The discovery of the piezoelectric effect in a neat liquid opens the door to applications that have previously not been accessible with solid state materials, and RTILs are more readily recyclable and in many instances pose fewer environmental issues than many currently used piezoelectric materials.

REFERENCES

- 1. Curie, J.; Curie, P., Développement par compression de l'électricité polaire dans les cristaux hémièdres à faces inclinées. *Bull Soc. Mineralog. de France* **1880,** *3, 4,* 90-93.
- 2. Hao, J.; Li, W.; Zhai, J.; Chen, H., Progress in high-strain perovskite piezoelectric ceramics. *Mat. Sci. Eng. Reports* **2019**, *135*, 1-57.
- 3. Zhang, Y.; Kim, H.; Wang, Q.; Jo, W.; Kingon, A. I.; Kim, S.-H.; Jeong, C. K., Progress in lead-free piezoelectric nanofiller materials and related composite nanogenerator devices. *Nanoscale Adv.* **2020**, *2*, 3131-3149.
- 4. Maity, K.; Mandal, D., Chapter Seven Piezoelectric polymers and composites for multifunctional materials. In *Advanced Lightweight Multifunctional Materials*, Costa, P.; Costa, C. M.; Lanceros-Mendez, S., Eds. Woodhead Publishing: 2021; pp 239-282.
- 5. Mishra, S.; Unnikrishnan, L.; Nayak, S. K.; Mohanty, S., Advances in piezoelectric polymer composites for energy harvesting applications: A systematic review. *Macromol. Mater. Eng.* **2019**, *304*, 1800463.
- 6. Yamada, T.; Ueda, T.; Kitayama, T., Piezoelectricity of a high-content lead zirconate titanate/polymer composite. *J. Appl. Phys.* **1982**, *53*, 4328-4332.
- 7. Tagantsev, A. K., Piezoelectricity and flexoelectricity in crystalline dielectrics. *Phys. Rev.* B **1986**, *34*, 5883-5889.
- 8. Pugal, D.; Jung, K.; Aabloo, A.; Kim, K. J., Ionic polymer-metal composite mechanoelectrical transduction: review and perspectives. *Polym. Int.* **2010**, *59*, 279-289.
- 9. Tiwari, R.; Garcia, E., The state of understanding of ionic polymer metal composite architecture: a review. *Smart Mater. Struct.* **2011,** *20*, 083001.
- 10. Yudin, P. V.; Tagantsev, A. K., Fundamentals of flexoelectricity in solids. *Nanotech.* **2013**, *24*, 432001.
- 11. Vatani, M.; Vatani, M.; Choi, J. W., Multi-layer stretchable pressure sensors using ionic liquids and carbon nanotubes. *Appl. Phys. Lett.* **2016**, *108*, 061908.
- 12. Feng, C.; Rajapaksha, C. P. H.; Cedillo, J. M.; Piedrahita, C.; Cao, J.; Kaphle, V.; Lussem, B.; Kyu, T.; Jakli, A., Electroresponsive ionic liquid crystal elastomers. *Macromol. Rapid Commun.* **2019**, *40*, 1900299.
- 13. Emon, M. O. F.; Lee, J.; Choi, U. H.; Kim, D. H.; Lee, K. C.; Choi, J. W., Characterization of a soft pressure sensor on the basis of ionic liquid condentration and thickness of the piezoresistive layer. *IEEE Sens. J.* **2019**, *19*, 6076-6084.

- 14. Ando, Y.; Fukada, E., Piezoelectric properties of oriented deoxyribonucleate films. *J. Polym. Sci.: Polym. Phys. Ed.* **1976,** *14*, 63-79.
- 15. Zhang, N.; Shan, J.; Xing, J., Piezoelectric properties of single-strand DNA molecular brush biolayers. *Acta Mech. Sol. Sinica* **2007**, *20*, 206-210.
- 16. Lucarelli, F.; Tombelli, S.; Minunni, M.; Marrazza, G.; Mascini, M., Electrochemical and piezoelectric DNA biosensors for hybridisation detection. *Anal. Chim. Acta* **2008**, *609*, 139-159.
- 17. Fathizadeh, S.; Behnia, S., Control of a DNA based piezoelectric biosensor. *J. Phys. Soc. Japan* **2020**, *89*, 024004.
- 18. Tao, K.; Xue, B.; Li, Q.; Hu, W.; Shimon, L. J. W.; Makam, P.; Si, M.; Yan, X.; Zhang, M.; Cao, Y., et al., Stable and optoelectronic dipeptide assemblies for power harvesting. *Mater. Today* **2019**, *30*, 10-16.
- 19. Lee, B. Y.; Zhang, J.; Zueger, C.; Chung, W.-J.; Yoo, S. Y.; Wang, E.; Meyer, J.; Ramesh, R.; Lee, S.-W., Virus-based piezoelectric energy generation. *Nature Nanotech.* **2012**, *7*, 351-356.
- 20. Guerin, S.; Stapleton, A.; Chovan, D.; Mouras, R.; Gleeson, M.; McKeown, C.; Noor, M. R.; Silien, C.; Rhen, F. M. F.; Kholkin, Andrei L., et al., Control of piezoelectricity in amino acids by supramolecular packing. *Nature Mater.* **2018**, *17*, 180-186.
- 21. Pei, Y.; Zhang, Y.; Ma, J.; Fan, M.; Zhang, S.; Wang, J., Ionic liquids for advanced materials. *Mater. Today Nano* **2022**, *17*, 100159.
- 22. Dinodia, M., Ionic liquids: Environment-friendly greener solvents for organic synthesis. *Curr. Org. Synth.* **2022**, *19*, 543-557.
- 23. de los Ríos, A. P.; Irabien, A.; Hollmann, F.; Fernández, F. J. H., Ionic liquids: Green solvents for chemical processing. *J. Chem.* **2013**, *2013*, 402172.
- 24. Hossain, M. I.; Adhikari, L.; Baker, G. A.; Blanchard, G. J., Relating the induced free charge density gradient in a room temperature ionic liquid to molecular-scale organization. *J. Phys. Chem. B* **2023**, *127*, 1780-1788.
- 25. Hossain, M. I.; Blanchard, G. J., The effect of dilution on induced free charge density gradients in room temperature ionic liquids. *Phys. Chem. Chem. Phys.* **2022**, *24*, 3844-3853.
- 26. Hossain, M. I.; Blanchard, G. J., Dilution-induced changes in room temperature ionic liquids. Persistent compositional heterogeneity and the importance of dipolar interactions. *J. Mol. Liq.* **2022**, *367*, 120447 (1-9).
- 27. Ma, K.; Jarosova, R.; Swain, G. M.; Blanchard, G. J., Charge-induced long-range order in a room-temperature ionic liquid. *Langmuir* **2016**, *32*, 9507-9512.

- 28. Ma, K.; Jarosova, R.; Swain, G. M.; Blanchard, G. J., Modulation of an induced charge density gradient in the room temperature ionic liquid BMIM⁺BF₄⁻. *J. Phys. Chem. C* **2018**, *122*, 7361-7367.
- 29. Wang, Y.; Adhikari, L.; Baker, G. A.; Blanchard, G. J., Cation structure-dependence of the Pockels effect in aprotic ionic liquids. *Phys. Chem. Chem. Phys.* **2022**, *24*, 18067-18072.
- 30. Wang, Y.; Adhikari, L.; Baker, G. A.; Blanchard, G. J., Cation structure-dependence of the induced free charge density gradient in imidazolium and pyrrolidinium ionic liquids. *Phys. Chem. Phys.* **2022**, *24*, 19314-19320.
- 31. Wang, Y.; Jarosova, R.; Swain, G. M.; Blanchard, G. J., Characterizing the magnitude and structure-dependence of free charge density gradients in room temperature ionic liquids. *Langmuir* **2020**, *36*, 1152-1155.
- 32. Wang, Y.; Parvis, F.; Hossain, M. I.; Ma, K.; Jarosova, R.; Swain, G. M.; Blanchard, G. J., Local and long-range organization in room temperature ionic liquids. *Langmuir* **2021**, *37*, 605-615.
- 33. Wang, Y.; Swain, G. M.; Blanchard, G. J., Charge-induced birefringence in a room temperature ionic liquid. *J. Phys. Chem. B* **2021**, *125*, 950-955.
- 34. Jarosova, R.; Swain, G. M., Rapid preparation of room temperature ionic liquids with low water content as characterized by Ta-C:N electrode. *J. Electrochem. Soc.* **2015**, *162*, H507-H511.
- 35. Schmickler, W., Electronic effects in the electric double layer. *Chem. Rev.* **1996,** *96*, 3177-3200.
- 36. Wakai, C.; Oleinikova, A.; Ott, M.; Weingärtner, H., How polar are ionic liquids? Determination of the static dielectric constant of an imidazolium-based ionic liquid by microwave dielectric spectroscopy. *J. Phys. Chem. B* **2005**, *109*, 17028-17030.
- 37. Nordness, O.; Brennecke, J. F., Ion dissociation in ionic liquids and ionic liquid solutions. *Chem. Rev.* **2020**, *120*, 12873-12902.
- 38. Biancoli, A.; Francher, C.; Jones, J.; Damjanovic, D., Breaking of macroscopic centric symmetry in paraelecrtic phases of ferroelectric materials and implications for flexoelectricity. *Nature Mater.* **2015**, *14*, 224-228.
- 39. Hashemizadeh, S.; Biancoli, A.; Damjanovic, D., Symmetry breaking in hexagonal and cubic polymorphs of BaTiO₃. *J. Appl. Phys.* **2016**, *119*, 094105.
- 40. Aktas, O.; Kangama, M.; Linyu, G.; Catalan, G.; Ding, X.; Zunger, A.; Salje, E. K. H., Piezoelectricity in nominally centrosymmetric phases. *Phys. Rev. Res.* **2021**, *3*, 043221.

- 41. Anaredy, R. S.; Shaw, S. K., Long-range ordering of ionic liquid fluid films. *Langmuir* **2016,** *32*, 5147-5154.
- 42. Anaredy, R. S.; Shaw, S. K., Developing distinct chemical environments in ionic liquid films. *J. Phys. Chem. C* **2018**, *122*, 19731-19737.
- 43. Gebbie, M. A.; Dobbs, H. A.; Valtiner, M.; Israelachvili, J. N., Long-range electrostatic screening in ionic liquids. *Proc. Nat. Acad. Sci. USA* **2015**, *112*, 7432-7437.
- 44. Gebbie, M. A.; Smith, A. M.; Dobbs, H. A.; Lee, A. A.; Warr, G. G.; Banquy, X.; Valtiner, M.; Rutland, M. W.; Israelachvili, J. N.; Perkin, S., et al., Long range electrostatic forces in ionic liquids. *ChemComm* **2017**, *53*, 1214-1224.
- 45. Gebbie, M. A.; Valtiner, M.; Banquy, X.; Fox, E. T.; Henderson, W. A.; Israelachvili, J. N., Ionic liquids behave as dilute electrolyte solutions. *Proc. Nat. Acad. Sci. USA* **2013**, *110*, 9674-9679.
- 46. Israelachvili, J. N.; Min, Y.; Akbulut, M.; Alig, A.; Carver, G.; Greene, W.; Kristiansen, K.; Meyer, E.; Pesika, N.; Rosenberg, K., et al., Recent advances in the surface forces apparatus (SFA) technique. *Rep. Prog. Phys.* **2010**, *73*, 036601.
- 47. Lucio, A. J.; Shaw, S. K.; Zhang, J.; Bond, A. M., Large-amplitude Fourier-transformed AC voltammetric study of the capacitive electrochemical behavior of the 1-butyl-3-methylimidazoluim tetrafluoroborate-polycrystalline gold electrode interface. *J. Phys. Chem. C* **2017**, *121*, 12136-12147.
- 48. Nishida, J.; Breen, J. P.; Wu, B.; Fayer, M. D., Extraordinary slowing of structural dynamics in thin films of a room temperature ionic liquid. *ACS Cent. Sci.* **2018**, *4*, 1065-1073.
- 49. Shin, J. Y.; Yamada, S. A.; Fayer, M. D., Dynamics of a room temperature ionic liquid in supported ionic liquid membranes vs. the bulk liquid: 2D IR and polarized IR pump-probe experiments. *J. Am. Chem. Soc.* **2017**, *139*, 311-323.
- 50. Shin, J. Y.; Yamada, S. A.; Fayer, M. D., Carbon dioxide in a supported ionic liquid membrane: structural and rotational dynamics measured with 2D IR and pump-probe experiments. *J. Am. Chem. Soc.* **2017**, *139*, 11222-11232.
- 51. Wu, B.; Breen, J. P.; Fayer, M. D., Structural dynamics in ionic liquid thin films: The effect of cation chain length. *J. Phys. Chem. C* **2020**, *124*, 4179-4189.
- 52. Wu, B.; Breen, J. P.; Xing, X.; Fayer, M. D., Controlling the dynamics of ionic liquid thin films via multilayer surface functionalization. *J. Am. Chem. Soc.* **2020**, *142*, 9482-9492.
- 53. Shimizu, K.; Bernardes, C. E. S.; Canongia Lopes, J. N., Structure and aggregation in the 1-alkyl-3-methylimidazolium bis(trifluoromethylsulfonyl)imide ionic liquid homologous series. *J. Phys. Chem. B* **2014**, *118*, 567-576.

APPENDIX

Calculation of cell volume for piezoelectric measurements.

Conversion of potential vs. force results to d_{33} values.

1. Calculation of cell volume.

Diameter of cylinder = 14 mm

Diameter of piston = 12 mm

Diameter of O-ring = 14 mm

Distance from base of piston to base of O-ring = 2.5 mm

Volume of Ring between cylinder and piston in the region between the bottom of the O-ring and the bottom of the cylinder:

$$V_{ring} = \pi h \left(r_2^2 - r_1^2 \right) = \pi (0.25cm) \left((0.70cm)^2 - (0.60cm)^2 \right) = 0.10_2 cm^3$$

$$V_{IL} = 200 \mu L = 2.00 x 10^{-4} L * 10^{3} cm^{3} / L = 0.20_{0} cm^{3}$$

$$V_{IL} - V_{ring} = 0.20_0 cm^3 - 0.10_2 cm^3 = .09_8 cm^3 \approx 0.10 cm^3$$

$$h_{cylinder} = \frac{\left(V_{IL} - V_{ring}\right)}{\pi r^2} = \frac{0.09_8 cm^3}{\pi (0.70 cm)^2} = 0.06_4 cm$$

Calculation of d_{33} from the slope of the force-dependence of the open circuit potential. When the cell is viewed as a capacitor, V/f = the slope of the line, and $\varepsilon_r \sim 10$ for both RTILs.

$$V = \frac{q}{C} = \frac{d_{33}fx}{C} = \frac{d_{33}fx}{\varepsilon_0 \varepsilon_r A}$$

$$d_{33} = \left(\frac{V}{f}\right) \left(\frac{\varepsilon_0 \varepsilon_r A}{x}\right) = \left((16 \pm 1)x10^{-3} \frac{V}{N}\right) \left(\frac{8.854x10^{-12} \frac{C}{Vm} \cdot 10 \cdot 1.54x10^{-4} m^2}{6.4x10^{-4} m}\right)$$

$$=3.4x10^{-13}\frac{C}{N}=0.34\pm0.02\frac{pC}{N}$$

CHAPTER 3. Structure-Dependence of the Piezoelectric Effect in Ion Mechanistic Insights	ic Liquids.	Possible
Md. Iqbal Hossain, Laxmi Adhikari, Gary A. Baker, Lorenzo Guazzelli, Patri J. Blanchard, Structure-Dependence of the Piezoelectric Effect in Ion Mechanistic Insights. (<i>Manuscript under process</i>)		

3.1 Introduction

The piezoelectric effect is well-known and has been observed only in solids, until recently. We have reported the two imidazolium room temperature ionic liquids (RTILs) exhibit both the direct and converse piezoelectric effect. The discovery of the direct piezoelectric effect in RTILs was based on the observation of induced charge density gradients in RTILs when exposed to charged interfaces, with the gradient persisting on the order of 50 µm into the bulk medium. Among the surprising findings in the study of the induced free charge density gradient in RTILs is that the gradient persists upon dilution of the RTILs with molecular solvents up to concentrations of ca. 30 mol% molecular solvent. These findings suggest that it is not molecular-scale organization, but rather organization within the RTILs on the order of nanometers or longer, that is responsible for the effects we observe.

Organization in RTILs over length scales ranging from hundreds of nm to micrometers has been reported by a number of groups, with the length scale and type of organization depending on the means used to detect the organization. There is a complementary body of information on phase transitions in RTILs, based on temperature and/or pressure and, as with the studies of the liquid phase RTILs, the details of the phase transitions depend on both the means by which the phase transitions are examined and the identities of the RTILs. The results from these bodies of work are, generally, that each RTIL exhibits system-specific behavior, with many RTILs exhibiting a liquid-to-glass phase transition with increasing pressure, with some undergoing a subsequent glass to crystalline phase transition with increasing pressure. Other RTILs do not undergo a glass to crystalline phase transition with increasing pressure, but do exhibit a glass to crystalline phase transition with decreasing pressure.

The vast majority of these studies have used diamond anvil cell (DAC) technology to achieve pressure control, with either Raman scattering or X-ray diffraction (XRD) to characterize the morphology of the RTIL at elevated pressures. Unfortunately, to date, the pressure region that is most accessible with DAC technology is somewhat higher than that where the piezoelectric effect has been observed.

For solid state materials, only those that do not possess a center of inversion have the potential to exhibit a piezoelectric response. While there have been a limited number of reports where materials possessing a nominal center of inversion exhibit the piezoelectric effect, it appears that these materials distort to lift the inversion center, allowing the existence of the piezoelectric effect. Given that the operative model for solid piezoelectric materials has, to this point, provided predictions that are consistent with the experimental data, we assume that the "unit cell" of the structure responsible for the piezoelectric effect in RTILs must not possess a center of inversion. 53-⁵⁴ In analogy to our dilution studies on RTILs, it is likely that the basic relevant structural unit in RTILs is at least of nanometer dimensions; larger than individual RTIL constituent anions and cations. We also expect that any organization on the nanometer scale present in the RTILs, will necessarily depend on the structures of the constituent cations and anions. In an effort to understand the relationship between the direct piezoelectric effect in RTILs and constituent ion structures, we have evaluated the magnitude of the piezoelectric effect for several pyrrolidinium and imidazolium cations paired with tetrafluoroborate and bis(trifluoromethylsulfonyl)imide anions. Our experimental potential vs. applied force data reveal not only an RTIL constituentdependent piezoelectric response, but also a threshold force for the piezoelectric effect that likewise depends on RTIL constituent structures.

3.2 Methods

3.2.1 Materials Used

1-butyl-3-methyl The imidazolium ionic liquids imidazolium bis(trifluoromethylsulfonyl)imide (BMIM⁺TFSI⁻, >99%, <500 ppm H₂O, Sigma-Aldrich) and 1hexyl-3-methyl imidazolium bis(trifluoromethylsulfonyl)imide (HMIM+TFSI-, 98%, Sigma-Aldrich) were purified before use according to a procedure reported elsewhere.^{3, 55} purification, the water content of the RTILs was determined by Karl Fischer (Mettler-Toledo C10S) titration and found to be less than 50 ppm. The pyrrolidinium ionic liquids were synthesized The pyrrolidinium ionic liquids 1-butyl-3-methylpyrrolidinium bis(trifluoromethylsulfonyl)imide (BMPyrr⁺TFSI⁻), 1-hexyl-3-methylpyrrolidinium bis(trifluoromethylsulfonyl)imide (HMPyrr⁺TFSI⁻) 1-octyl-3-methylpyrrolidinium bis(trifluoromethylsulfonyl)imide and (OMPyrr+TFSI-) were synthesized following methods reported earlier, 56-57 with slight modifications.6 1-citronellol-3-methylimidazolium The chiral ionic liquid bis(trifluoromethylsulfonyl)imide (CitMIM⁺TFSI⁻) was synthesized by the Guazzelli group and was sent to the Blanchard labs for evaluation.

3.2.2 Measurement of the Direct Piezoelectric Effect

A schematic of the cell used to quantitate the piezoelectric effect is shown in Fig. 2.1. It is in the form of a cylinder-and-piston configuration, with the cylinder being made of steel, and the piston made of Delrin[®]. The piston contains a steel center steel electrode and has a Viton O-ring mounted near the base to create a liquid-tight seal for the RTIL contained within the cylinder. The O-ring seal is not air-tight, allowing air to escape prior to the piston contacting the RTIL. The piston is 12 mm diameter and cylinder is 14 mm diameter, with the O-ring providing sealed contact between the piston and cylinder. The sample size for all measurements reported here is 200 µL, resulting

in a RTIL thickness of 0.64 mm.¹ Force is applied to the cylinder, producing a potential difference between the piston electrode and cylinder body. The force is measured using a digital force gauge (Vetus 500N). The apparatus is configured such that the force and potential difference are along the same axis, providing data that are related to the piezoelectric coefficient d_{33} .

3.2.3 Open Circuit Potential Measurements

Open circuit potential measurements were made with an electrochemical bench (CH Instruments 604B). The input impedance of the bench for open circuit potential (OCP) measurements is ca. $10^{12} \Omega$. There is characteristically a small component arising from stray capacitance that can be seen in the control measurements.¹

3.3 Results and Discussion

As noted above, we reported recently on the direct piezoelectric effect in two imidazolium ionic liquids. In this work we report on the magnitude of the direct piezoelectric effect in several more RTILs, with imidazolium cations with C₈ alkyl and citronellyl functionalities, pyrrolidinium cations with C₄, C₆, C₈ and C₁₀ alkyl functionalities, and we compare the piezoelectric response of imidazolium RTILs with BF₄⁻ and TFSI⁻ anions. We find that the magnitude of the direct piezoelectric effect does depend on both cation and anion structure, and, significantly, that the potential vs. force relationship for all RTILs is characterized by a structure-dependent force threshold. This latter point likely speaks to the mechanism of the direct piezoelectric response in RTILs. We consider the magnitude of the piezoelectric response and the threshold force separately.

In the initial report, we found that the piezoelectric coefficient, d_{33} , for BMIM⁺TFSI⁻ and HMIM⁺TFSI⁻ were the same to within the experimental uncertainty and were within a factor of ten of d_{33} for quartz. To better understand the dependence of d_{33} on cation aliphatic chain length, we

have measured the relationship between open circuit potential and force applied for BMIM⁺TFSI⁻ (C₄), HMIM⁺TFSI⁻ (C₆) and OMIM⁺TFSI⁻ (C₈) (Figs. 3.1a-c). These data reveal that all three RTILs have the same d_{33} to within the experimental uncertainty (Table 3.1). Significantly, the addition of an unsaturation and a stereocenter to the imidazolium aliphatic chain does have a measurable effect on d_{33} (Fig. 3.1d). Despite the chirality intrinsic to the CitMIM+TFSI- cation, the value of d_{33} is smaller than for the 1-alkyl-3-methylimidazolium RTILs. We will return to a

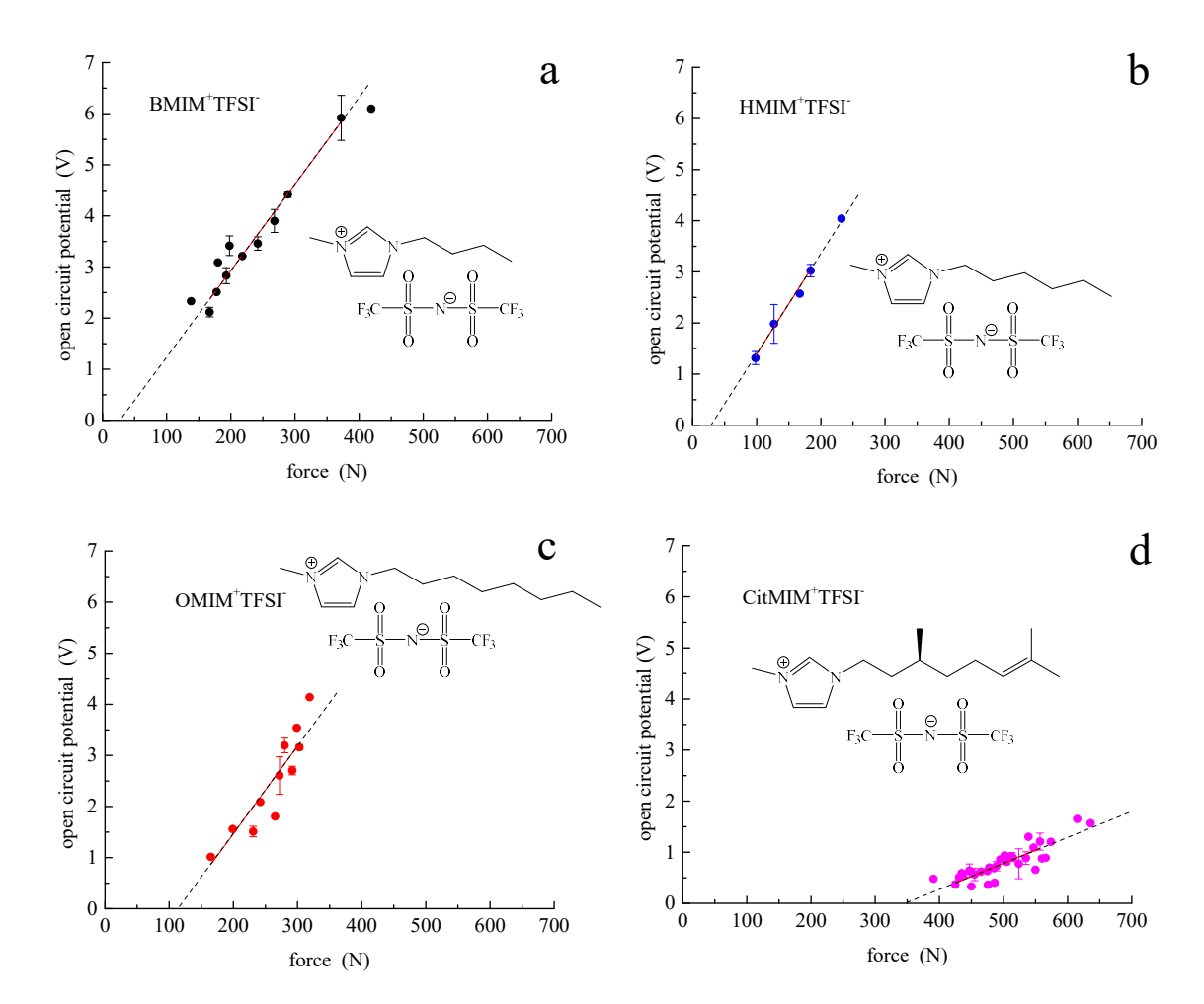


Figure 3.1 Potential (V) vs. force (N) data for (a) BMIM⁺TFSI⁻, (b) HMIM⁺TFSI⁻, (c) OMIM⁺TFSI⁻, and (d) CitMIM⁺TFSI⁻.

discussion of this finding, but it is clear from the data that the organization of CitMIM⁺TFSI⁻ is substantially different than the alkylimidazolium RTILs.

To evaluate the role of the cation polar headgroup, we show in Fig. 3.2 the potential vs. force relationships for 1-alkyl-1-methylpyrrolidone RTILs for BMPyrr $^+$ TFSI $^-$ (C₄), HMPyrr $^+$ TFSI $^-$ (C₆), OMPyrr $^+$ TFSI $^-$ (C₈) and DMPyrr $^+$ TFSI $^-$ (C₁₀). As was the case for the imidazolium cations, the aliphatic chain length does not appear to have an influence on d_{33} for the pyrrolidinium RTILs.

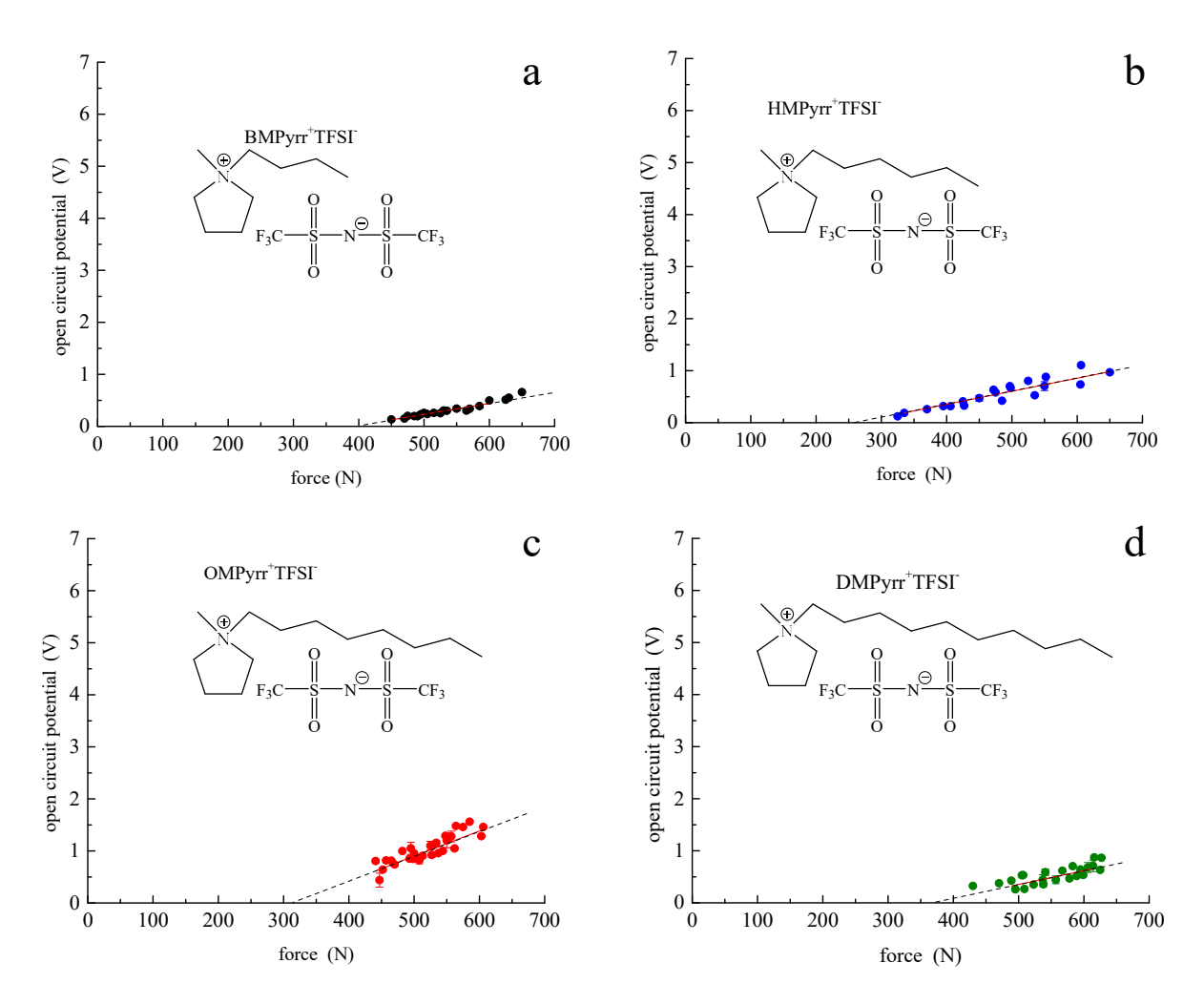
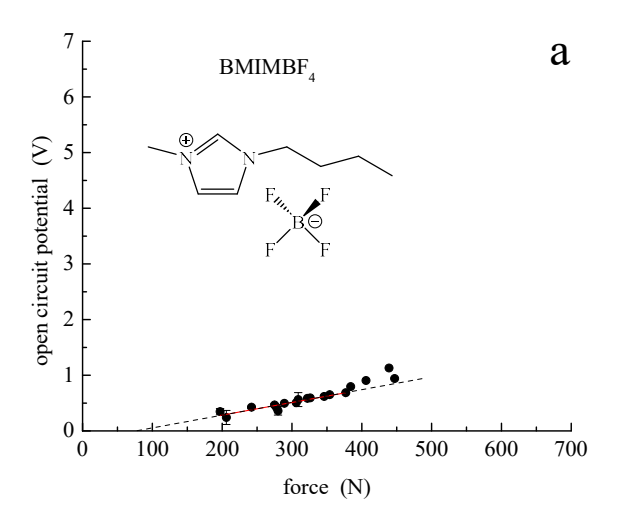


Figure 3.2 Potential (V) vs. force (N) data for (a) BMPyrr⁺TFSI⁻, (b) HMPyrr⁺TFSI⁻, (c) OMPyrr⁺TFSI⁻, and (d) DMPyrr⁺TFSI⁻.

When comparing the results for the imidazolium and pyrrolidinium RTILs, however, the imidazolium RTILs possess a d_{33} value ca. six times larger than the pyrrolidinium RTILs.

The piezoelectric coefficient also depends on RTIL anion identity (Fig. 3.3). Comparing BMIM⁺TFSI⁻ and OMIM⁺TFSI⁻ to BMIM⁺BF₄⁻ and OMIM⁺BF₄⁻, the BF₄⁻ RTILs are characterized



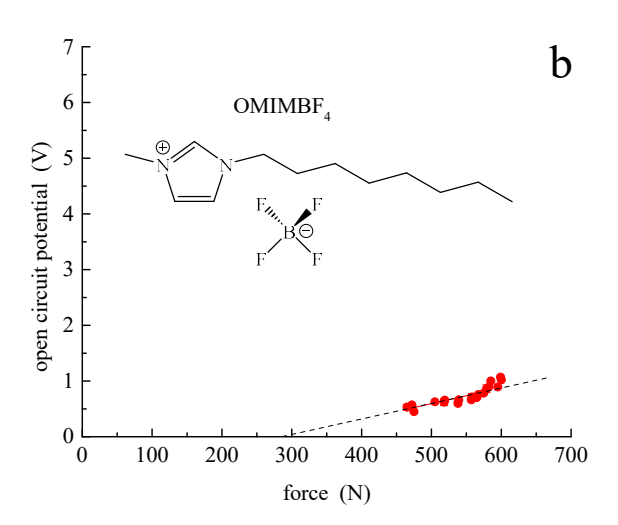


Figure 3.3 Potential (V) vs. force (N) data for (a) BMIM⁺BF₄⁻ and (b) OMIM⁺BF₄⁻.

by d_{33} values a factor of ca. 6 smaller than the TFSI⁻ RTILs. Note the cation aliphatic chain independence for both TFSI⁻ and BF₄⁻ RTILs. The d_{33} values reported for the imidazolium BF₄⁻ RTILs are essentially the same as those for the pyrrolidinium TFSI⁻ RTILs (Table 3.1).

Taken collectively, the d_{33} data for the RTILs examined demonstrate several trends. The first is that the piezoelectric response is nominally independent of cation alkyl chain length, but is does depend on the structure of the aliphatic chain (CitMIM $^+$ TFSI $^-$). This result is somewhat surprising because a requirement for the piezoelectric effect to be operative, at least in a solid, is that there is no center of inversion in the medium. The use of a chiral constituent would ensure the absence of a center of intersion, at least for a solid state material, which may be present upon the application of force (*vide infra*). The piezoelectric response does depend on the identity of the cationic polar headgroup and the anion, although information from these data alone is not sufficient to infer any details about local organization.

With these data in mind, we turn to a discussion of the other important feature in the data shown in Figs. 3.1-3.3. Specifically, regression of the potential vs. force data for each RTIL reveals that there is a threshold force required for the piezoelectric response. This feature was not apparent in our initial report based on its relatively small value for the alkylMIM+TFSI RTILs, but the acquisition of more data and the use of regression analysis shows clearly the existence of a threshold force. The threshold force is seen to depend on RTIL cation and anion structure (Table 3.1). The presence of this feature in the data is important because it provides a means of reconciling the piezoelectric effect in RTILs with the piezoelectric effect in solid state materials.

There is a significant literature on pressure-induced phase transitions in RTILs, with the majority of the data being X-ray diffraction, Raman scattering, or both. 22-24, 26-29, 32-43, 45-52 In that literature, the most commonly observed phase transition is from liquid to glass with increasing pressure, although there is evidence for crystalline phases under certain conditions. The significant limitation of that literature, however, is that the range of pressures studied is substantially higher than we apply to the RTILs to observe a piezoelectric response. Given the experimental geometry

of our piezoelectric measurement system, typical pressure ranges we access are on the order of 0.003 GPa, and the pressure ranges accessed by DAC apparati are typically in the range of 0.4 to 3 GPa. Thus, the structureal features associated with the pressure-induced phase transitions reported for RTILs cannot be used directly to explain the phenomenon we observe. Despite this limitation, we hypothesize that pressure-induced phase transitions in RTILs are a potential explanation for the operation of the piezoelectric effect in this class of materials. The threshold force required to observe the piezoelectric effect exhibits a dependence on both RTIL cation and anion structure, and we would expect any pressure-induced changes in organization to depend sensitively on the structure of the constituents. The most convincing means to verify this hypothesis is through experimental data. At the present time the Xie laboratories at MSU are measuring the pressure-dependent X-ray diffraction data for HMIM+TFSI.

3.4 Conclusions

Our data have demonstrated several important points. First, the piezoelectric effect in ionic liquids is a general effect for this class of materials, and is not restricted to a small subset of structures. This finding is important because it speaks to the utility of these materials for technological applications. Our findings also demonstrate that the magnitude of the piezoelectric response of RTILs does indeed depend on the identities of the cation and anion constituents, thereby providing a route for optimization of the effect. The magnitude of the CitMIM+TFSI-piezoelectric response relative to RMIM+TFSI- RTILs demonstrates that simple chirality of one RTIL constituent is not sufficient to impart organization on the bulk system. In other words, the smallest structural unit required for the piezoelectric material to be operative is larger than either individual ions or ion-paired units. We know that the converse piezoelectric effect in RTILs is associated with a charge displacement gradient, $\nabla \cdot D$, that persists for ca. 50 μ m. The organization

that is important to the direct piezoelectric effect is thus greater than molecular-scale, with an upper-bound determined by the length-scale of $\nabla \cdot D$. Structural organization on the μm length scale is unprecedented in a "normal" liquid phase medium, and would be readily detectible through scattering studies, and there is no experimental evidence in support of such structural order in a bulk RTIL. One way to evaluate the existence and characteristic length scale of organization in a liquid phase medium is through dilution studies, and we consider the results of such studies in the following chapters.

Table 3.1 Fitting results for potential vs. force data for the RTILs reported in this work. N = number of data points, slope = potential/force in units of mV/N. Threshold force (X-int) in N, and d_{33} in units of pC/N.

RTIL	N	Slope (mV/N)	Std. Error	Y-int (mV)	Std. Error	X- int (N)	Std. Error	<i>d</i> ₃₃ (pC/N)	Std. Error
BMIM ⁺ TFSI ⁻	12	16.9	1.7	-457	424	27	25	0.36	0.04
HMIM ⁺ TFSI ⁻	5	19.7	1.2	-574	167	29	9	0.42	0.03
OMIM ⁺ TFSI ⁻	11	17.2	2.5	-1964	641	115	41	0.37	0.05
CitMIM ⁺ TFSI ⁻	31	5.2	0.8	-1807	386	349	75	0.11	0.02
BMIM ⁺ BF ₄ ⁻	18	2.3	0.3	-171	80	75	36	0.05	0.01
OMIM ⁺ BF ₄ -	19	2.8	0.6	-816	325	289	131	0.06	0.01
BMPyrr ⁺ TFSI ⁻	20	2.1	0.2	-824	79	391	47	0.05	0.01
HMPyrr ⁺ TFSI ⁻	20	2.5	0.2	-652	76	260	35	0.05	0.01
OMPyrr ⁺ TFSI ⁻	29	4.8	0.7	-1510	344	313	83	0.10	0.02
DMPyrr ⁺ TFSI ⁻	24	2.7	0.6	-970	334	366	151	0.06	0.01

REFERENCES

- 1. Hossain, M. I.; Blanchard, G. J., Ionic Liquids Exhibit the Piezoelectric Effect. *J. Phys. Chem. Lett.* **2023**, *14*, 2731-2735.
- 2. Hossain, M. I.; Adhikari, L.; Baker, G. A.; Blanchard, G. J., Relating the induced free charge density gradient in a room temperature ionic liquid to molecular-scale organization. *J. Phys. Chem. B* **2023**, *127*, 1780-1788.
- 3. Ma, K.; Jarosova, R.; Swain, G. M.; Blanchard, G. J., Charge-induced long-range order in a room-temperature ionic liquid. *Langmuir* **2016**, *32*, 9507-9512.
- 4. Ma, K.; Jarosova, R.; Swain, G. M.; Blanchard, G. J., Modulation of an induced charge density gradient in the room temperature ionic liquid BMIM⁺BF₄-. *J. Phys. Chem. C* **2018**, *122*, 7361-7367.
- 5. Wang, Y.; Adhikari, L.; Baker, G. A.; Blanchard, G. J., Cation structure-dependence of the Pockels effect in aprotic ionic liquids. *Phys. Chem. Chem. Phys.* **2022**, *24*, 18067-18072.
- 6. Wang, Y.; Adhikari, L.; Baker, G. A.; Blanchard, G. J., Cation structure-dependence of the induced free charge density gradient in imidazolium and pyrrolidinium ionic liquids. *Phys. Chem. Phys.* **2022**, *24*, 19314-19320.
- 7. Wang, Y.; Jarosova, R.; Swain, G. M.; Blanchard, G. J., Characterizing the magnitude and structure-dependence of free charge density gradients in room temperature ionic liquids. *Langmuir* **2020**, *36*, 1152-1155.
- 8. Wang, Y.; Parvis, F.; Hossain, M. I.; Ma, K.; Jarosova, R.; Swain, G. M.; Blanchard, G. J., Local and long-range organization in room temperature ionic liquids. *Langmuir* **2021**, *37*, 605-615.
- 9. Wang, Y.; Swain, G. M.; Blanchard, G. J., Charge-induced birefringence in a room temperature ionic liquid. *J. Phys. Chem. B* **2021**, *125*, 950-955.
- 10. Hossain, M. I.; Blanchard, G. J., The effect of dilution on induced free charge density gradients in room temperature ionic liquids. *Phys. Chem. Chem. Phys.* **2022**, *24*, 3844-3853.
- 11. Hossain, M. I.; Blanchard, G. J., Dilution-induced changes in room temperature ionic liquids. Persistent compositional heterogeneity and the importance of dipolar interactions. *J. Mol. Liq.* **2022**, *367*, 120447 (1-9).
- 12. Anaredy, R. S.; Shaw, S. K., Long-range ordering of ionic liquid fluid films. *Langmuir* **2016**, *32*, 5147-5154.
- 13. Anaredy, R. S.; Shaw, S. K., Developing distinct chemical environments in ionic liquid films. *J. Phys. Chem. C* **2018**, *122*, 19731-19737.

- 14. Gebbie, M. A.; Dobbs, H. A.; Valtiner, M.; Israelachvili, J. N., Long-range electrostatic screening in ionic liquids. *Proc. Nat. Acad. Sci. USA* **2015**, *112*, 7432-7437.
- 15. Gebbie, M. A.; Smith, A. M.; Dobbs, H. A.; Lee, A. A.; Warr, G. G.; Banquy, X.; Valtiner, M.; Rutland, M. W.; Israelachvili, J. N.; Perkin, S., et al., Long range electrostatic forces in ionic liquids. *ChemComm* **2017**, *53*, 1214-1224.
- 16. Gebbie, M. A.; Valtiner, M.; Banquy, X.; Fox, E. T.; Henderson, W. A.; Israelachvili, J. N., Ionic liquids behave as dilute electrolyte solutions. *Proc. Nat. Acad. Sci. USA* **2013**, *110*, 9674-9679.
- 17. Nishida, J.; Breen, J. P.; Wu, B.; Fayer, M. D., Extraordinary slowing of structural dynamics in thin films of a room temperature ionic liquid. *ACS Cent. Sci.* **2018**, *4*, 1065-1073.
- 18. Shin, J. Y.; Yamada, S. A.; Fayer, M. D., Dynamics of a room temperature ionic liquid in supported ionic liquid membranes vs. the bulk liquid: 2D IR and polarized IR pump-probe experiments. *J. Am. Chem. Soc.* **2017**, *139*, 311-323.
- 19. Shin, J. Y.; Yamada, S. A.; Fayer, M. D., Carbon dioxide in a supported ionic liquid membrane: structural and rotational dynamics measured with 2D IR and pump-probe experiments. *J. Am. Chem. Soc.* **2017**, *139*, 11222-11232.
- 20. Wu, B.; Breen, J. P.; Fayer, M. D., Structural dynamics in ionic liquid thin films: The effect of cation chain length. *J. Phys. Chem. C* **2020**, *124*, 4179-4189.
- 21. Wu, B.; Breen, J. P.; Xing, X.; Fayer, M. D., Controlling the dynamics of ionic liquid thin films via multilayer surface functionalization. *J. Am. Chem. Soc.* **2020**, *142*, 9482-9492.
- 22. Tomita, K.; Mizukami, M.; Nakano, S.; Ohta, N.; Yagi, N.; Kurihara, K., X-ray diffraction and resonance shear measurement of nano-confined ionic liquids. *Phys. Chem. Chem. Phys.* **2018**, *20*, 13714-13721.
- 23. Vila, J.; Fernandez-Castro, B.; Rilo, E.; Carrete, J.; Dominguez-Perez, M.; Rodriguez, J. R.; Garcia, M.; Varela, L. M.; Cabeza, O., Liquid-solid-liquid phase transition hysteresis loops in the ionic conductivity of ten imidazolium-based ionic liquids. *Fluid Ph. Eq.* **2012**, *320*, 1-10.
- 24. Saouane, S.; Norman, S. E.; Hardacre, C.; Fabbiani, P. A., Pinning down the solid-state polymorphism of the ionic liquid [bmim][PF₆]. *Chem. Sci.* **2013**, *4*, 1270-1280.
- 25. Carmona Esteva, F. J.; Zhang, Y.; Colon, Y. J.; Maginn, E. J., Molecular dynamics simulation of the influence of external electric fields on the glass transition temperature of the ionic liquid 1-ethyl-3-methylimidazolium bis(trifluoromethylsulfonyl)imide. *J. Phys. Chem. B* **2023**, *127*, 4623-4632.

- 26. Yoshimura, Y.; Takekiyo, T.; Imai, Y.; Abe, H., Pressure-induced spectral changes of room-temperature ionic liquid, N,N-diethyl-N-methyl-N-(2-methoxyethyl)ammonium bis(trifluoromethylsulfonyl)imide, [DEME][TFSI]. *J. Phys. Chem. C* **2012**, *116*, 2097-2101.
- 27. Su, L.; Zhu, X.; Wang, Z.; Cheng, X.; Wang, Y.; Yuan, C.; Chen, Z.; Ma, C.; Li, F.; Zhou, Q., et al., In situ observation of multiple phase transitions in low-melting ionic liquid [BMIM][BF4] under high pressure up to 30 GPa. *J. Phys. Chem. B* **2012**, *116*, 2216-2222.
- 28. Choudhury, A. R.; Winterton, N.; Steiner, A.; Cooper, A. I.; Johnson, K. A., *In situ* crystallization of ionic liquids with melting points below -25°C. *CrystEngComm* **2006**, *8*, 742-745.
- 29. Lima, T. A.; Paschoal, V. H.; Faria, L. F. O.; Riberio, M. C. C.; Ferreira, F. F.; Costa, F. N.; Giles, C., Comparing two tetraalkylammonium ionic liquids. II. Phase transitions. *J. Chem. Phys.* **2016**, *144*, 224505 (1-10).
- 30. Abe, H.; Takekiyo, T.; Hatano, N.; Shigemi, M.; Hamaya, N.; Yoshimura, Y., Pressure-induced frustration-frustration process in 1-butyl-3-methylimidazolium hexafluorophosphate, a room temperature ionic liquid. *J. Phys. Chem. B* **2014**, *118*, 1138-1145.
- 31. Beichel, W.; Yu, Y.; Dlubek, G.; Krause-Rehberg, R.; Pionteck, J.; Pefefferkorn, D.; Bulut, S.; Bejan, D.; Friedrich, C.; Krossing, I., Free volume in ionic liquids: a connection of experimentally accessible observables from PALS and PVT experiments with the molecular structure from XRD data. *Phys. Chem. Chem. Phys.* **2013**, *15*, 8821-8830.
- 32. Li, H.; Zhang, Y.; Zhu, X.; Cheng, X.; Shao, C.; Wu, J.; Li, J.; Ren, Y.; Wang, Z.; Wang, Y., et al., In situ solidification of ionic liquid [EMIM][EtOSO₃] from melt under high pressure. *High. Pr. Res.* **2013**, *33*, 751-759.
- 33. Russina, O.; Fazio, B.; Schmidt, C.; Triolo, A., Structural organization and phase behaviour of 1-butyl-3-methylimidazolium hexafluorophosphate: an high pressure Raman spectroscopy study. *Phys. Chem. Chem. Phys.* **2011**, *13*, 12067-12074.
- 34. Su, L.; Li, M.; Zhu, X.; Wang, Z.; Chen, Z.; Li, F.; Zhou, Q.; Hong, S., In situ crystallization of low-melting ionic liquid [BMIM][PF₆] under high pressure up to 2 GPa. *J. Phys. Chem. B* **2010**, *114*, 5061-5065.
- 35. Yoshimura, Y.; Abe, H.; Takekiyo, T.; Shigemi, M.; Hamaya, N.; Wada, R.; Kato, M., Superpressing of a room temperature ionic liquid, 1-ethyl-3-methylimidazolium tetrafluoroborate. *J. Phys. Chem. B* **2013**, *117*, 12296-12302.
- 36. Su, L.; Li, L.; Hu, Y.; Yuan, C.; Shao, C.; Hong, S., Phase transition of [C_n-mim][PF₆] under high pressure up to 1.0 GPa. *J. Chem. Phys.* **2009**, *130*, 184503 (1-4).
- 37. Faria, L. F. O.; Penna, T. C.; Riberio, M. C. C., Raman spectroscopic study of temperature and pressure effects on the ionic liquid propylammonium nitrate. *J. Phys. Chem. B* **2013**, *117*, 10905-10912.

- 38. Shigemi, M.; Takekiyo, T.; Abe, H.; Hamaya, N.; Yoshimura, Y., Pressure-induced solidification of 1-butyl-3-methylimidazolium tetrafluoroborate. *J. Solution Chem.* **2014**, *43*, 1614-1624.
- 39. Imai, Y.; Takekiyo, T.; Abe, H.; Yoshimura, Y., Pressure- and temperature-induced Raman spectral changes of 1-butyl-3-methylimidazolium tetrafluoroborate. *High. Pr. Res.* **2011**, *31*, 53-57.
- 40. Yoshimura, Y.; Abe, H.; Imai, Y.; Takekiyo, T.; Hamaya, N., Decompression-induced crystal polymorphism in a room-temperature ionic liquid, N,N-diethyl-N-methyl-N-(2-methoxyethyl) ammonium tetrafluoroborate. *J. Phys. Chem. B* **2013**, *117*, 3264-3269.
- 41. Wu, J.; Zhu, X.; Li, H.; Su, L.; Yang, K.; Cheng, X.; Yang, G.; Liu, J., Combined Raman scattering and X-ray diffraction study of phase transition of the ionic liquid [BMIM][TFSI] under high pressure. *J. Solution Chem.* **2015**, *44*, 2106-2116.
- 42. Chen, L.; Li, H.; Zhu, X.; Su, L.; Yang, K.; Yuan, C.; Yang, G.; Li, X., Structural and conformational properties of 1-decyl-3-methylimidazolium tetrafluoroborate under high pressure. *J. Mol. Struct.* **2017**, *1137*, 610-614.
- 43. Takekiyo, T.; Koyama, Y.; Shigemi, M.; Matsuishi, K.; Abe, H.; Hamaya, N.; Yoshimura, Y., Conformational adjustment for high-pressure glass formation of 1-alkyl-3-methylimidazolium tetrafluoroborate. *Phys. Chem. Chem. Phys.* **2017**, *19*, 863-870.
- 44. Paschoal, V. H.; Faria, L. F. O.; Riberio, M. C. C., Vibrational spectroscopy of ionic liquids. *Chem. Rev.* **2017**, *117*, 7053-7112.
- 45. Li, H.; Wang, Z.; Chen, L.; Wu, J.; Huang, H.; Yang, K.; Wang, Y.; Su, L.; Yang, G., Kinetic effect on pressure-induced phase transitions of room temperature ionic liquid, 1-ethyl-2-methylimidazolium trifluoromethanesulfonate. *J. Phys. Chem. B* **2015**, *119*, 14245-14251.
- 46. Yoshimura, Y.; Shigemi, M.; Takaku, M.; Yamamura, M.; Takekiyo, T.; Abe, H.; Hamaya, N.; Wakabayashi, D.; Nishida, K.; Funamori, N., et al., Stability of the liquid state of imidazolium-based ionic liquids under high pressure at room temperature. *J. Phys. Chem. B* **2015**, *119*, 8146-8153.
- 47. Capitani, F.; Fasolato, C.; Mangialardo, S.; Signorelli, S.; Gontrani, L.; Postorino, P., Heterogeneity of propyl-ammonium nitrate solid phases obtained under high pressure. *J. Phys. Chem. Solids* **2015**, *84*, 13-16.
- 48. Russina, O.; Lo Celso, F.; Triolo, A., Pressure-responsive mesoscopic structures in room temperature ionic liquids. *Phys. Chem. Chem. Phys.* **2015**, *17*, 29496-29500.
- 49. Faria, L. F. O.; Nobrega, M. M.; Temperini, M. L. A.; Riberio, M. C. C., Ionic liquids based on the bis(trifluoromethylsulfonyl)imide anion for high-pressure Raman spectroscopy measurements. *J. Raman Spectrosc.* **2013**, *44*, 481-484.

- 50. Capitani, F.; Trequattrini, F.; Palumbo, O.; Paolone, A.; Postorino, P., Phase transitions of PYR₁₄-TFSI as a function of pressure and temperature: the competition between smaller volume and lower energy conformer. *J. Phys. Chem. B* **2016**, *120*, 2921-2928.
- 51. Faria, L. F. O.; Riberio, M. C. C., Phase transitions of triflate-based ionic liquids under high pressure. *J. Phys. Chem. B* **2015**, *119*, 14315-14322.
- 52. Riberio, M. C. C.; Padua, A. A. H.; Costa Gomes, M. F., Glass transition of ionic liquids under high pressure. *J. Chem. Phys.* **2014**, *140*, 244514 (1-6).
- 53. Biancoli, A.; Francher, C.; Jones, J.; Damjanovic, D., Breaking of macroscopic centric symmetry in paraelecrtic phases of ferroelectric materials and implications for flexoelectricity. *Nature Mater.* **2015**, *14*, 224-228.
- 54. Hashemizadeh, S.; Biancoli, A.; Damjanovic, D., Symmetry breaking in hexagonal and cubic polymorphs of BaTiO₃. *J. Appl. Phys.* **2016**, *119*, 094105.
- 55. Jarosova, R.; Swain, G. M., Rapid preparation of room temperature ionic liquids with low water content as characterized by Ta-C:N electrode. *J. Electrochem. Soc.* **2015**, *162*, H507-H511.
- 56. Burrell, A. K.; Del Sesto, R. E.; Baker, S. N.; McCleskey, T. M.; Baker, G. A., The Large Scale Synthesis of Pure Imidazolium and Pyrrolidinium Ionic Liquids. *Green Chem.* **2007**, *9*, 449-454.
- 57. Baker, G. A.; Pandey, S.; Pandey, S.; Baker, S. N., A New Class of Cationic Surfactants Inspired by N-alkyl-N-methyl Pyrrolidinium Ionic Liquids. *Analyst* **2004**, *129*, 890-892.

CHAPTER 4. The Effect of Dilution on Induced Free Charge Density Gradients in Room Temperature Ionic Liquids
Adapted with permission from:
Md. Iqbal Hossain and G. J. Blanchard; The effect of dilution on induced free charge density gradients in room temperature ionic liquids. <i>Phys. Chem. Chem. Phys.</i> , 2022 , 24, 3844 – 3853.

4.1 Introduction

Room temperature ionic liquids (RTILs) have received a great deal of attention because of their utility in a number of applications, ranging from chemical synthesis and catalysis to chemical sensing, supercapacitors, reactive gas storage and transport, and ion propulsion. Among the attractive properties of ionic liquids are their characteristically wide electrochemical window, extremely low vapor pressure and their ability to solubilize both polar and non-polar compounds. Despite the wide use of RTILs, this class of materials remains to be understood fully. A larger goal of our work is to improve our fundamental understanding of the structural and dynamical properties of RTILs.

In a liquid medium, thermal energy gives rise to Brownian motion of the constituent species, and an important question is precisely what the dominant species in a RTIL are. The anion and cation can exist as discrete ionic species or as a paired, dipolar moiety and the equilibrium constant for this process has been the subject of much investigation. Estimates have ranged from very little dissociation to extensive dissociation,⁷⁻⁸ and several recent works have concluded that imidazolium RTILs are *ca.* 60% dissociated at room temperature.⁹⁻¹⁰ Understanding the extent of dissociation is central to evaluating other RTIL properties, such as conductivity and dielectric response.

Recent work from our group and others has pointed to the existence of relatively long-range order in RTILs, but the details of the "order" seen by these groups remains to be connected. The Israelachvilli group reported order on the nanometer length scale based on force measurements and suggested based on that finding that the free ion concentration in RTILs was very low.^{7, 11-13} The Fayer group, in a series of elegant experiments using small molecules as probes, has identified organization with a persistence length on the order of tens to hundreds of nm in RTILs, ¹⁴⁻¹⁹ and

the Shaw group has identified the evolution of structural order on the micrometer length scale in thin RTIL films. $^{20-23}$ Very recently, the Welton group has identified spatial variation in n, the refractive index, over distances of tens to hundreds of nm using Raman scattering. 24 It is clear from all these studies that RTILs exhibit structural order over length scales vastly in excess of what is typical for liquid phase solvents.

In addition to the structural order seen by the Fayer, Shaw and Welton groups, the Blanchard group has identified the existence of an induced free charge density gradient (ρ_l) in RTILs that persists over length scales on the order of 50 µm.²⁵⁻²⁹ The free charge density gradient exists in the form of a gradient in the concentration of discrete ionic species in the RTIL, induced by the presence of a charged surface in contact with the RTIL, and sensed by either rotational diffusion²⁵⁻²⁶ or induced birefringence²⁹ experiments. Not only does the length scale of this gradient differ from the organization seen by others, but the charge density gradient does not necessarily correspond to a structural gradient. It is of fundamental interest to determine how local and longer-range organization in RTILs is related to the induced free charge density gradient. In the work presented here one focus is on the effect of dilution on ρ_f , which is seen to collapse upon the addition of 20 to 30 mol\% of diluent. We also report that, as a result of this finding, we have identified the existence of molecular-scale aggregates in RTIL solutions of acetonitrile (ACN) and methanol, even at high dilution, well beyond the point where ρ_f is no longer seen. These distinct and complementary findings suggest the existence of persistent compositional heterogeneity in diluted RTIL systems. The RTILs we have chosen for this work are BMIM⁺BF₄-, BMIM⁺TFSI⁻ and HMIM+TFSI in order to gauge the importance of cation and anion identity, and for the characterization of ρ_f we have used the cationic chromophore cresyl violet (CV⁺). The structures of these compounds are shown in Fig. 4.1. The data we report for these systems provide insight

into the short-range organization in RTILs and the relationship of this organization to the longerrange charge density gradient.

BMIM+

$$BF_4$$
 F_{F}
 F_{F

Figure 4.1 Structures of the RTIL cations and anions, and the chromophore cresyl violet, used in this work.

4.2 Experimental Section

4.2.1 Chemicals

BMIM⁺BF₄⁻ (\geq 97.0%), BMIM⁺TFSI⁻ (\geq 99%, H₂O <500 ppm) and HMIM⁺TFSI⁻ (\geq 98%, Sigma-Aldrich) were used after purification (*vide infra*). Acetonitrile (anhydrous, 99.8%, ~50 ppm H₂O) and methanol (anhydrous, 99.8%, ~50 ppm H₂O) were purchased from Sigma-Aldrich, dried

over activated 4 Å molecular sieves and stored inside a dry box (glove box). Cresyl Violet perchlorate (Eastman Kodak Co.), ethanol (\geq 99.5%, Sigma-Aldrich), activated charcoal (powder, -100 particle size, Sigma-Aldrich), and isopropyl alcohol (\geq 99.5%, Macron Fine Chemicals) were used without further purification. Water used in these studies was purified with a Milli-Q filtration system (Millipore). ITO coated glass slides (Nanocs Inc., IT10-111-25, 10Ω /sq) and silicone rubber sheet of 1 mm thickness (MSC Direct) were needed to prepare the cell spacer as described below.

4.2.2 Purification of ILs

As-received RTILs BMIM $^+$ BF $_4^-$, BMIM $^+$ TFSI $^-$ and HMIM $^+$ TFSI $^-$ were stored over activated carbon for at least two weeks. After this time, the activated carbon powder has been removed from RTILs using a syringe filter (Durapore membrane, 0.22 μ m sterile filtration, Millex). Next, the RTILs are heated to 85 °C for five hours while purging with ultrapure Argon (99.9995%, Linde). The procedure was performed with the RTILs in a round bottom flask on a N2-purged Schlenk line. The water content in the RTILs was measured Karl Fischer titration (Mettler Toledo C10SD) and found to be \leq 45 ppm). The purified RTILs are then stored in a dry glove box until they are used in experiments.

4.2.3 Preparation of RTIL-Chromophore Solution

Stock solution of chromophore (ca. 5.34 x 10^{-4} M) in ethanol was prepared. The chromophore (final concentration of 5.34 x 10^{-5} M) + RTILs solution was prepared by dispensing $100 \mu L$ of the chromophore stock solution (30 minutes sonication prior to use) using an Eppendorf pipette into a scintillation vial, followed by 3 h at $100 \, ^{\circ}$ C to evaporate the ethanol. The vial was then cooled in a desiccator. An aliquot of 1 mL of purified RTIL was transferred by Eppendorf pipette to the vial. This stock solution was then stirred for at least 12 h before use. All glassware

was stored in an oven at 150 °C for at least 24 h before use to minimize water contamination. All sample preparation procedures were performed in a N₂-purged vinyl dry box (Coy Laboratories, Grass Lake, MI). The water vapor in the box was \leq 5 ppm, as measured with a hygrometer.

4.2.4 Sample Cell Preparation

The sample cell used in this work has been described elsewhere.²⁶ Briefly, ITO coated supports were cleaned by sonication in a detergent solution, then Milli-Q water, and isopropanol for 15 min each. ITO was used because it carries a net positive surface charge.³⁰ No current or voltage was applied to either support in the work we report here.²⁶ After that the supports were washed with ethanol (200 proof, anhydrous) and dried in an oven at 200 °C for 40 mins. After cooling by purging nitrogen, a UV/ozone cleaner was used to clean the supports for 20 min. The cell spacer (1.6 mm) was cut from a silicone rubber sheet, washed by sonication in detergent solution, and in Milli-Q water, and then dried with flowing N₂ for 15 min each.

4.2.5 Fluorescence Anisotropy Decay Measurements

The TCSPC imaging instrument used in this work has been described in detail elsewhere.³¹ The system is the combination of a time correlated single photon counting (TCSPC) laser system coupled with an inverted confocal laser scanning microscope (Nikon Eclipse Ti-U) which provides 1.2 µm depth resolution with a 10X objective (N.A. 0.30). The light source is a synchronously pumped, cavity dumped dye laser (Coherent 701-3) excited by the second harmonic output of a passively mode locked Nd: YVO₄ laser. The output of the dye laser is *ca*. 5 ps pulses at a repetition rate of 4 MHz. The TCSPC electronics (Becker & Hickl SPC-152) are used to acquire polarized emission transients. Time resolution is limited by the avalanche photodiode detectors (ID Quantique) to *ca*. 100 ps. Signal averaging in the plane of detection is performed by acquisition of time-resolved data over a region of the sample at a pre-determined depth using a confocal

scanning head (Beck & Hickl DCS-120). Mechanical control over microscope stage vertical position provides spatial (depth) resolution for the time-resolved anisotropy decay measurements. Primary depth-dependent reorientation data are provided in the Supporting Information. Uncertainties in the primary data are the standard deviations of fitted time constants for 65,536 sets of time-resolved data (256 x 256 array) and uncertainties in derived quantities are propagated from uncertainties in the primary data.

4.2.6 Binary Systems Preparation

Binary RTIL/solvent systems were prepared by mass. We mixed measured masses of each component for a given RTIL/solvent system and from that information calculated the mole fraction volumetrically (v/v)%. To minimize water contamination, all binary systems were prepared in a N₂-purged vinyl dry box (Coy Laboratories, Grass Lake, MI). Sealed samples were maintained in the dry box until measurements were performed.

4.3 Results and Discussion

As indicated in the Introduction, there are two related issues we address in this work. The first is the effect of dilution on the induced free charge density gradient seen in RTILs and the second is the role of compositional (spatial) heterogeneity in RTILs that have been diluted. In particular, we are interested in the characteristic differences in the role of hydrogen bonding in diluted RTIL systems and for that reason we report on the effect of dilution of RTILs with protic (methanol) and aprotic (acetonitrile) solvents. In the discussion that follows, we briefly recap the properties of the induced free charge density gradient seen in RTILs and discuss the manner in which we probe the effects of dilution of RTILs prior to consideration of the specific results.

The Blanchard group has reported on the ability of a charged surface in contact with a RTIL to induce a free charge density gradient, ρ_f . The gradient was initially identified through the

dependence of the rotational diffusion time constant, τ_{OR} , of a charged chromophore in the RTIL on the distance from the charged support. The gradient in the density of charged (dissociated) species in the RTIL produces a corresponding gradient in the amount of free and complexed chromophore, and thus a gradient in the average volume of the reorienting entity. The spatial extent of ρ_f has been shown to be ca. 50 μ m (e⁻¹ depth). The magnitude of the gradient can be inferred from the normalized change in τ_{OR} with distance from the charged surface and it depends on the identity of the RTIL constituent species.²⁷ The quantity ρ_f is related to a gradient in the dielectric response of the RTIL and through control of the surface charge, σ_s , on the RTIL support surface, a gradient in the real part of the RTIL complex refractive index can be characterized.²⁹ Such an induced birefringence is not only important for potential applications, but it also provides a way to characterize ρ_f without the addition of a chromophore to the RTIL. Despite the characterization of ρ_f we have reported to date, a full understanding of the fundamental RTIL properties that support the existence of ρ_f over macroscopic distances remains to be achieved.

Several factors are required to support ρ_f over macroscopic distances, including effective charge screening and limited charge mobility. While the extent of RTIL dissociation is not known with great certainty, a body of work points to these species being ca. 60% dissociated at room temperature. In an effort to understand the relative importance of ionic (charge) mobility in maintaining ρ_f , it is instructive to compare the results for neat RTILs to the known result in the dilute solution limit (the electric double layer) and to characterize the effect of RTIL dilution on the persistence length and magnitude of ρ_f .

It has been reported previously that the interactions between solvents and RTIL constituents differ significantly, *i.e.* RTIL anions and cations experience different interactions with diluting solvents, ^{9,32} and this is not surprising. Further, the role of hydrogen-bonding interactions between

protic solvents and RTIL anions such as BF₄ are thought to facilitate mobility of the anion. ^{9, 32} Based on these findings it is reasonable to expect dilution to exhibit a significant effect on the persistence length and magnitude of ρ_f . To test this hypothesis, we have studied the rotational diffusion dynamics of the cationic chromophore cresyl violet (CV⁺) as a function of distance from a charged support surface and as a function of RTIL and dilution with solvents acetonitrile (polar aprotic solvent) and methanol (polar protic solvent). Our findings demonstrate that ρ_f can withstand significant dilution before ceasing to exist, and that the RTIL/solvent binary systems are not homogeneous, even at comparatively high dilutions. We discuss these findings separately.

The information we acquire is in the form of the dependence of the chromophore rotational diffusion time constant on distance from a charged support surface. The experimental data are polarized time-domain emission decays, taken at polarizations parallel and perpendicular to the excitation polarization, $I_{\parallel}(t)$ and $I_{\perp}(t)$. The difference between these polarized decays, normalized for fluorescence lifetime, is the anisotropy decay function, R(t) (Eq. 4.1),

$$R(t) = \frac{I_{\parallel}(t) - I_{\perp}(t)}{I_{\parallel}(t) + 2I_{\perp}(t)}$$
 [4.1]

The functional form of R(t) provides chemically and physically useful information. For all the measurements we report here, R(t) decays as a single exponential with a time constant τ_{OR} , the orientational relaxation time. The quantity τ_{OR} is related to the viscosity of the medium (η) and the volume of the reorienting entity (V) through the Debye-Stokes-Einstein equation (Eq. 4.2).³³-

$$\tau_{OR} = 6D_{rot}^{-1} = \frac{\eta Vf}{k_B TS} \tag{4.2}$$

Where D_{rot} is the rotational diffusion constant, f is a frictional interaction term and S is a shape factor to account for ellipticity of the rotating entity.³³⁻³⁵ For polar and ionic species f = 1 and S

depends slightly on whether the rotating entity is the free or complexed chromophore and in all cases is close to $1.^{34-35}$ From earlier work we have shown that the depth-dependent change in τ_{OR} is related to the depth-dependent change in the average volume of the reorienting entity, V_{eff} , ²⁵

$$V_{\it eff} = X_{\it dissociated} V_{\it dissociated} + X_{\it associated} V_{\it associated}$$
 [4.3]

The relevant equilibrium is

$$CV^+ + A_{RTIL}^- = (CVA_{RTIL})$$
 [4.4]

With CV^+ being the dissociated chromophore and CVA_{RTIL} being the associated species. The hydrodynamic volumes of CV^+ and A^-_{RTIL} (the RTIL anion) are calculated using the method of Van der Waals increments³⁶ and $X_{dissociated} + X_{associated} = 1$. The variation in V_{eff} with distance from the charged support surface is given by Eq. 4.5,

$$\nabla V_{eff} = \nabla X_{dissociated} V_{dissociated} + \nabla X_{associated} V_{associated}$$
 [4.5]

Which is related to the reorientation time gradient (Eq. 4.6),

$$\nabla \tau_{OR} = \frac{\eta f}{k_{\scriptscriptstyle R} T S} \nabla V_{eff} \tag{4.6}$$

The gradient in V_{eff} is due to the gradient in [A-RTIL] which represents a gradient in the displaced charge (D) in the system (Eq. 4.7),²⁵

$$\nabla \tau_{OR} = k \nabla \cdot D = k \rho_f \tag{4.7}$$

Where k is a proportionality constant, and ρ_f is the free charge density gradient in the RTIL. Because τ_{OR} varies with the identity of the RTIL and the chromophore used, it is important to present data for such measurements in a manner that can be compared across RTILs and in a chromophore-independent manner. We report the normalized gradient in τ_{OR} as²⁷

$$\left(\frac{\Delta \tau_{OR}}{\tau_{OR}}\right)(x) = \frac{\left(\tau_{OR}^{x} - \tau_{OR}^{\infty}\right)}{\tau_{OR}^{\infty}} = \left(\frac{\Delta \tau_{OR}}{\tau_{OR}}\right)(0) \exp(-x/d)$$
[4.8]

Where x is the axis perpendicular to the support surface plane and d is the e⁻¹ persistence length of ρ_f . The quantity τ_{OR}^x is the orientational relaxation time at distance x from the support surface and τ_{OR}^∞ is the orientational relaxation time at distances sufficiently far from the charged support that $\rho_f = 0$. It is the dependence of the quantities $(\Delta \tau_{OR}/\tau_{OR})(0)$ and d on dilution that are of interest. We fit the experimental data using least squares fitting to obtain values of $(\Delta \tau_{OR}/\tau_{OR})(0)$ and d.

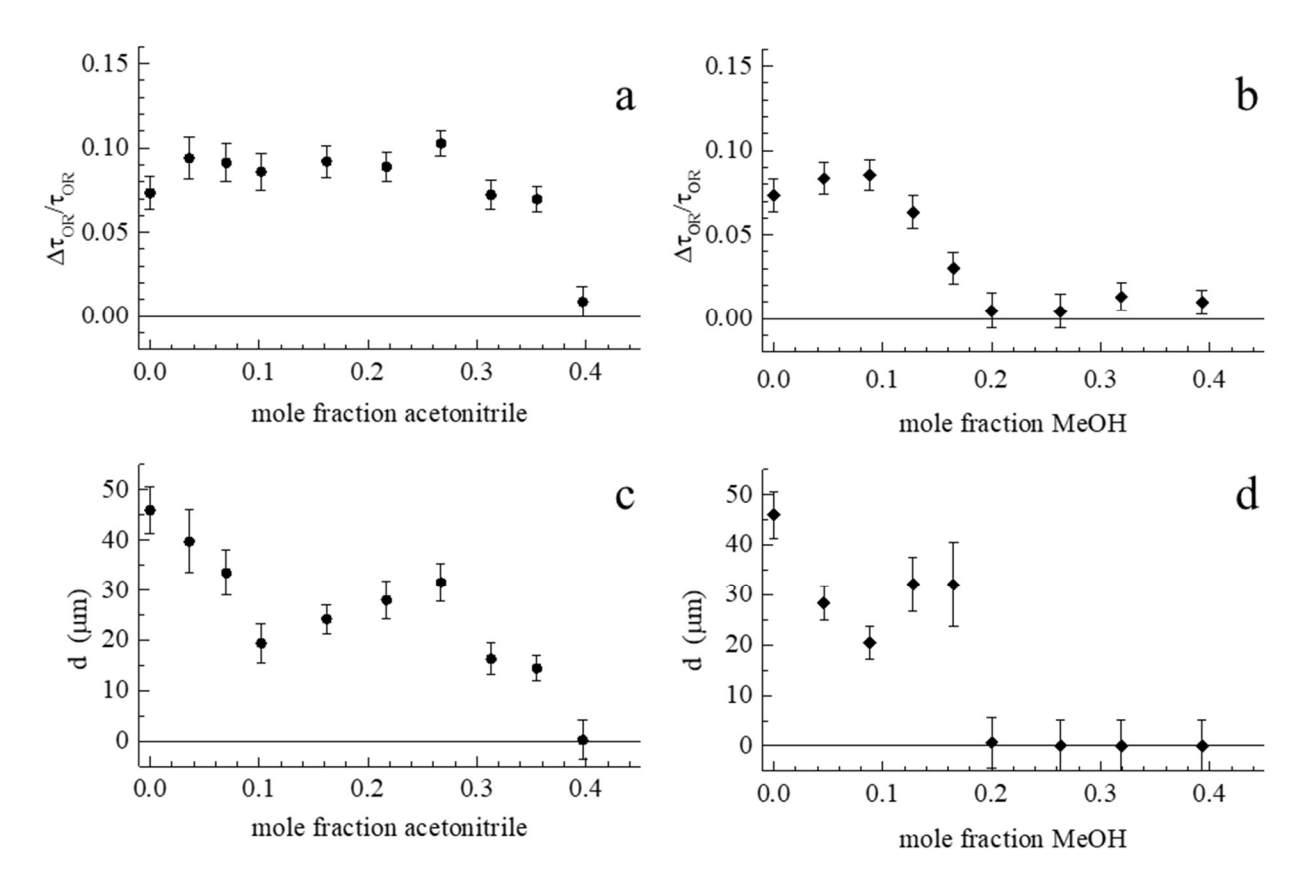


Figure 4.2 Dependence of magnitude of ρ_f , $(\Delta \tau_{or}/\tau_{or})$ (0), (top panels) and persistence length of ρ_f , d, (bottom panels) for BMIM⁺BF₄⁻ on dilution with acetonitrile (left panels) and methanol (right panels). Mole fractions are calculated using the associated RTIL (ion pair) and the molecular solvent.

The quantity $(\Delta \tau_{OR}/\tau_{OR})(0)$ is a gauge of the magnitude of ρ_f and d is a measure of the persistence length of ρ_f , and the dependence of each of these quantities on the amount and identity of diluent added to the RTIL reflects the extent to which these binary systems behave as homogeneous media.

We show the dependence of $(\Delta \tau_{OR}/\tau_{OR})(0)$ (panels a and b) and d (panels c and d) on dilution for the RTILs BMIM⁺BF₄⁻, BMIM⁺TFSI⁻ and HMIM⁺TFSI⁻ with acetonitrile and methanol, in Figs. 4.2-4.4, respectively. These data contain several significant features. The first is that the magnitude of ρ_f depends on the extent of dilution, but this dependence is not a smooth

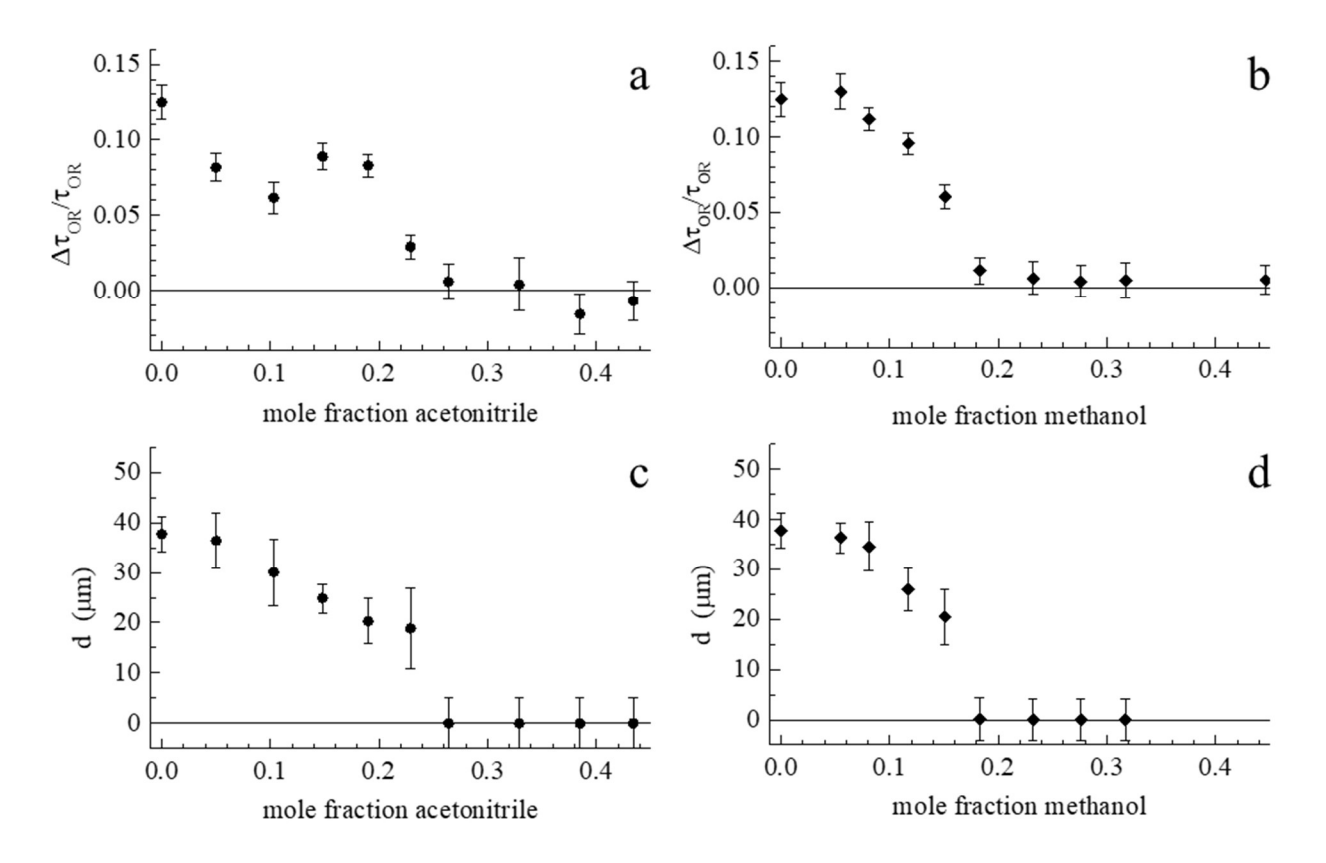


Figure 4.3 Dependence of magnitude of ρ_f , $(\Delta \tau_{or}/\tau_{or})(0)$, (top panels) and persistence length of ρ_f , d, (bottom panels) for BMIM⁺TFSI⁻ on dilution with acetonitrile (left panels) and methanol (right panels). Mole fractions are calculated using the associated RTIL (ion pair) and the molecular solvent.

trend with increasing dilution. Rather, ρ_f remains at a relatively constant level with increasing dilution up to a point and then diminishes to 0 with slight additional dilution. The trend is similar for all the RTILs examined and there is a noticeable difference in the dilution at which ρ_f ceases to persist in acetonitrile and methanol. Both the functional form of the data and the amount of solvent required to cause ρ_f to collapse are consistent with the binary system being spatially

heterogeneous. The basis for this assertion is the known monotonic dependence of RTIL-solvent system viscosity on solvent concentration.³⁷⁻⁴⁰ In a homogeneous system, ion mobility is inversely proportional to viscosity, leading to the prediction that ρ_f should diminish in proportion to the reduction in viscosity, a prediction that is at odds with the functional form of the ρ_f data in Figs. 4.2-4.4. By way of comparison, the viscosities for which ρ_f is seen to vanish is on the order of 20 cP with acetonitrile dilution and 40 cP with methanol dilution for BMIM⁺BF₄⁻. Normal solvents, such as ethylene glycol (15 cP)⁴¹ or even higher viscosity solvents such as glycerol (1400 cP)⁴² do not support free charge density gradients. Ion mobility thus appears not to be the primary factor leading to the loss of ρ_f with dilution.

The dependence of d on dilution is also shown in Figs. 4.2-4.4 (panels c and d), and it does not depend smoothly on dilution. Rather, d is seen to correlate closely with $(\Delta \tau_{OR}/\tau_{OR})(0)$. This information is also consistent with the notion that the RTIL/solvent binary system is not homogeneous, even to significant levels of dilution. The magnitude and spatial extent of ρ_f both appear to change little with dilution until a critical point is reached and the binary RTIL/solvent system will no longer support the charge density gradient. This critical point differs for the two solvents; in acetonitrile, all RTILs exhibit this change in ρ_f and d for X_{ACN} between 0.3 and 0.4, and for X_{MeOH} between 0.2 and 0.25. In addition to the implication that the RTIL/binary solvent system is not uniform, even for relatively high dilution, our findings also suggest that the organization of these binary systems serves to screen ionic charge very effectively.

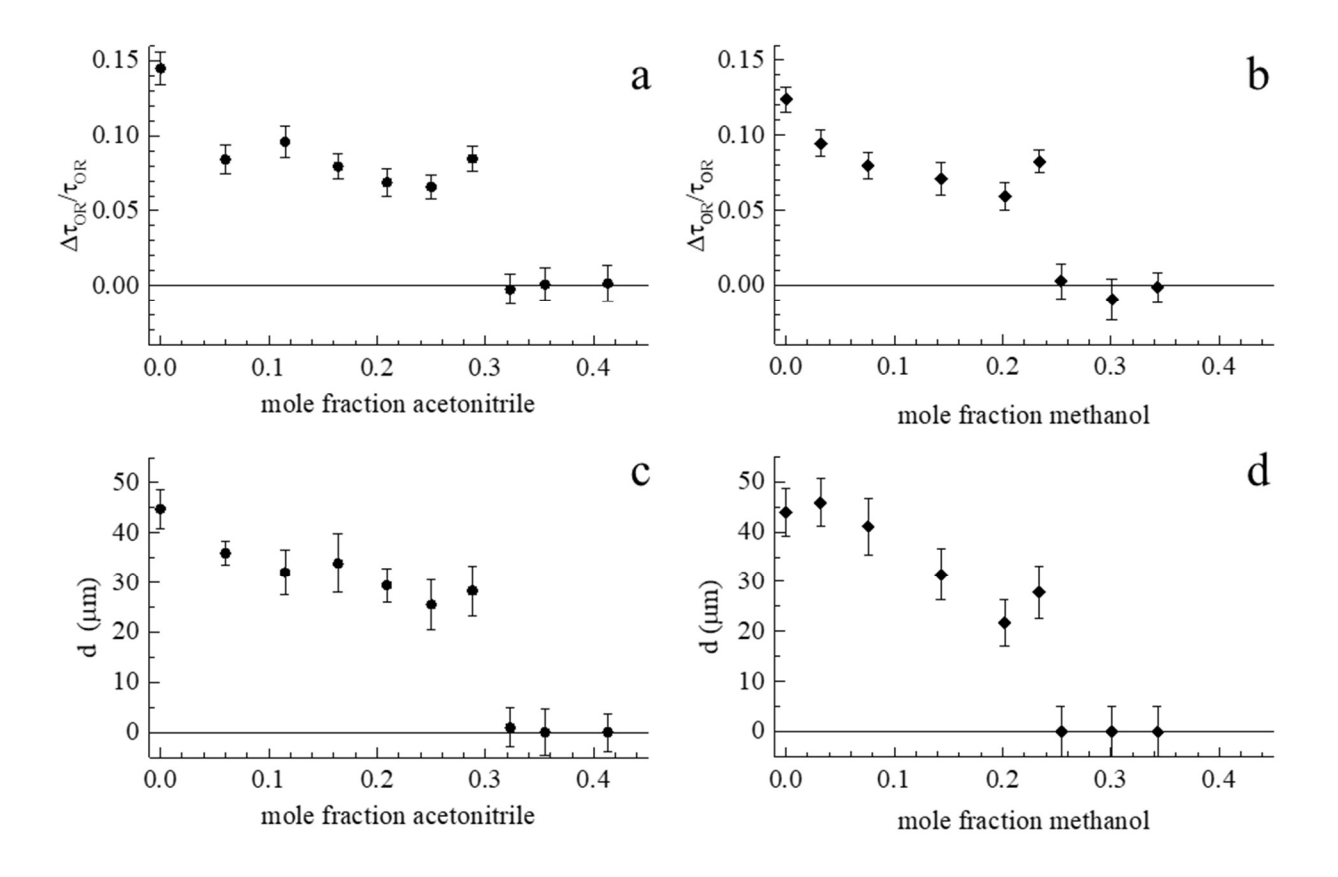


Figure 4.4 Dependence of magnitude of ρ_f , $(\Delta \tau_{or}/\tau_{or})(0)$, (top panels) and persistence length of ρ_f , d, (bottom panels) for HMIM⁺TFSI⁻ on dilution with acetonitrile (left panels) and methanol (right panels). Mole fractions are calculated using the associated RTIL (ion pair) and the molecular solvent.

As noted above, the dependence of bulk viscosity on RTIL/solvent binary system composition has been reported and varies smoothly with extent of dilution. $^{37-40,\,43-46}$ It is important to consider that the measurement of bulk viscosity represents an average of intermolecular interaction energies over poorly-defined macroscopic length scales. Specifically, the viscosity is a measure of the frictional interactions between the species that are present in the liquid and, while it is typically taken as representing intermolecular interactions in liquids, this assumption is not necessarily correct in complex multi-component systems. We have examined the rotational diffusion dynamics of CV^+ in the RTILs shown in Fig. 4.1 at a depth within the sample (> 100 μ m) where ρ_f is seen to have no effect, as a function of dilution with acetonitrile and methanol. The

purpose of this work is to compare the effective viscosity sensed by CV⁺, which is inherently on a molecular length scale, to the known bulk viscosities of the RTILs as a function of dilution.

The Debye-Stokes-Einstein equation (Eq. 4.2) relates the induced orientational anisotropy decay time constant to the thermal energy of the system (k_BT), parameters that relate to the volume and shape of the rotating entity (V and S) and the interactions between the rotating entity and the surrounding medium (η and f). Implicit in this model is that the medium surrounding the rotating entity behaves as a continuum and this approximation is valid when the volume of the rotating species is much larger than the volume of the individual (solvent) molecules surrounding it. $^{33-35}$ Experimentally this approximation is seen to hold reasonably well in polar systems where the reorienting species and the solvent are similar in size. $^{47-48}$ The use of η carries with it the approximation that the intermolecular interactions between solvent molecules are the same as those between the solvent and the rotating entity. This approximation is typically valid and if there is any difference between solvent-solvent and solvent-solute interactions, that difference is constant for all measurements in a given series where solute concentration, for example, is varied.

The relationship between RTIL dilution and bulk viscosity has been reported before for a number of systems, including the ones considered in this work. $^{32, 37, 39-40, 49-51}$ Characteristically, there is a smooth, monotonic dependence of the measured bulk viscosity and amount of diluent added. We can use these data in concert with the hydrodynamic volume of CV^+ (217 Å 3) $^{25, 36}$ to calculate the reorientation time constants as a function of RTIL dilution using Eq. 4.2. For a homogeneous system, where the reorienting entity is the CV^+ chromophore, the experimental dependence of τ_{OR} on solvent dilution should match the predictions of Eq. 2, save perhaps for a small scaling factor, but in any event the functional form of the experimental data and that predicted by Eq. 4.2 should agree. We do not observe this agreement experimentally. We show in

Figs. 4.5 the calculated vs. experimental reorientation times for CV⁺ in the RTILs as a function of dilution with acetonitrile (left) and methanol (right).

The data contained in Figs. 4.5 could be interpreted in several ways. Based on Eq. 4.2, one potential reason for the deviation between experimental and predicted time constants could be that the intermolecular interactions between CV+ and the molecules in its immediate vicinity differ energetically from interactions between two constituent species in the RTIL. Such a difference could also be viewed as a variation in the frictional term, f, with dilution. There is an interesting body of work that shows the nature of solvent-solute coupling can exhibit heterogeneity in complex systems, 52-53 but we believe that such heterogeneity is not dominant in the systems under consideration because the timescale of environmental exchange that would give rise to such an effect would be necessarily much shorter than the measured rotational diffusion times reported here. In other words, any short-term fluctuations in f would be temporally averaged over the timescale relevant for chromophore rotation. Another possible explanation could be in the context of a change in S with dilution, but as noted above, there is insufficient possible variation in the value of S (0.75 < S < 1) to account for these findings.³⁵ For these reasons, we believe the most plausible explanation for these findings is that the volume of the reorienting entity is changing with dilution and, in all cases, the volume of the reorienting entity is larger than the hydrodynamic volume of CV⁺. Indeed, we have found this to be the case in terms of explaining the basis for the observed ρ_f in RTILs and assume changes in the hydrodynamic volume of the reorienting entity accounts for the results we report here.

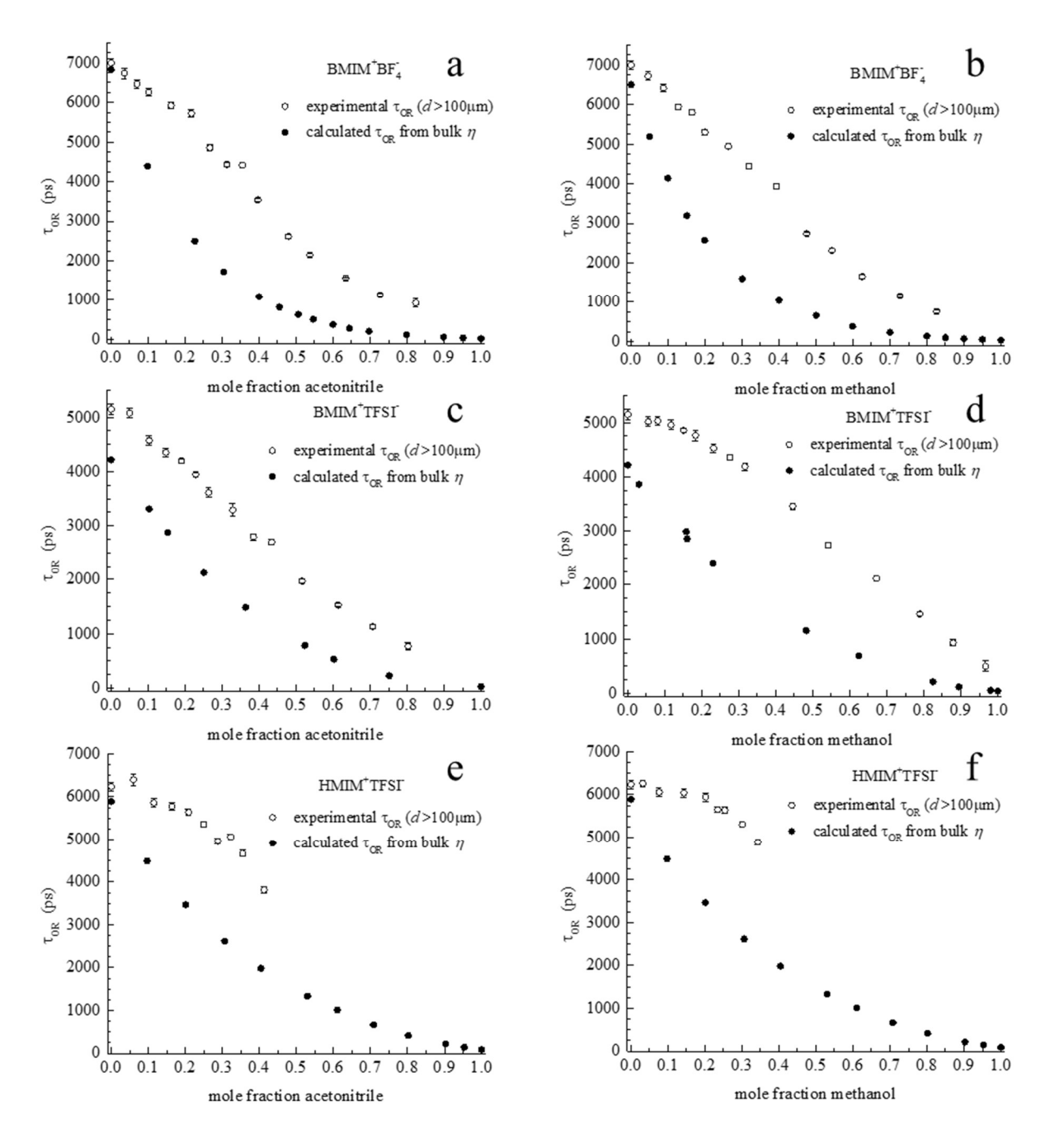


Figure 4.5 Reorientation time constant, τ_{OR}, observed experimentally (open circles) in bulk RTIL as a function of dilution, and calculated using Eq. 4.7 with reported values of the RTIL-solvent bulk viscosity (solid circles) for (a) BMIM⁺BF₄⁻ in acetonitrile, (b) BMIM⁺BF₄⁻ in methanol, (c) BMIM⁺TFSI⁻ in acetonitrile, (d) BMIM⁺TFSI⁻ in methanol, (e) HMIM⁺TFSI⁻ in acetonitrile and (f) HMIM⁺TFSI⁻ in methanol. Mole fractions are calculated using the associated RTIL (ion pair) and the molecular solvent.

It is well established that the rotational diffusion of polar chromophores in polar liquids are consistent with the calculated hydrodynamic volume of the chromophore is in good agreement

with experimental data. 47-48, 54 For reorientation in RTILs, this is not the case, and these data are consistent with the RTIL/solvent system being spatially heterogeneous even under conditions of relatively high dilution. There is literature precedent and support for this assertion^{44, 46, 55-57} and the issue is how to model the reorienting entity. It is possible, in principle, to account for the hydrodynamic volume in excess of that for CV⁺ to be accounted for either as solvent aggregates in the RTIL or RTIL aggregates in the diluent. There is literature precedent for solvent-RTIL interactions that has demonstrated clusters of RTIL ion-pairs in the solvent medium 44-46,55 and we evaluate the data shown in Figs. 5 in that context. The hypothesis is that the CV⁺ chromophore is interacting primarily with the RTIL ion-paired clusters in the binary solvent system and the rotational diffusion time constants reflect the motion of the chromophore-RTIL complex. The hydrodynamic volumes of the RTIL constituents are provided in Table 1. The effective volume of the rotating entity can be used to estimate into the average number of RTIL ion-paired complexes interacting with the chromophore as a function of dilution (Fig. 4.6). In Fig. 4.6 the blue lines indicate the hydrodynamic volumes of the (ion-paired) chromophore plus integer numbers of RTIL ion pairs. There are several significant features contained in these data.

Table 4.1 Hydrodynamic volumes of RTIL cations and anions and CV⁺. Volumes calculated using the method of van der Waals increments (Ref. ³⁶)

Molecule	V (Å ³)
CV ⁺	217
BMIM ⁺	139
HMIM ⁺	173
BF ₄ -	50
TFSI ⁻	169

In considering the data shown in Fig. 6, indicating the effective rotor volume vs. mole fraction of diluent added, it is important to note that the reorientation time constant values do not necessarily need to coincide with the volume of the rotor and an integral number of RTIL ion pairs. Noninteger values of RTIL ion pairs correspond to the average lifetime of the complex being less than the rotational diffusion time constant. The data in Fig. 4.6 show that the number of RTIL ion-pairs complexed to the chromophore appears to increase with increasing solvent dilution. The extent of the effect depends sensitively on the RTIL identity and to a lesser extent on diluent concentration, indicating in all cases an increase in aggregate size with increasing dilution. The dependence on RTIL identity for each diluent shows that aggregation is more pronounced with up to 12 RTIL ion pairs involved in aggregation with the chromophore for BMIM⁺BF₄⁻ in acetonitrile at high dilution, approximately 5 RTIL ion pairs for BMIM⁺TFSI⁻ and something closer to dimer formation at ca. 40% acetonitrile with HMIM+TFSI. We note that for BMIM+TFSI at the same dilution, we observe the same dimer-like formation. Based on these findings, it appears that the RTIL anion and how the diluent interacts with it plays a deterministic role in the aggregate formation we observe, and the RTIL cation is less affected by the type or amount of diluent. The same qualitative trends are seen with methanol as the diluent, allowing no clear distinction between dipolar solvent-RTIL interactions and hydrogen-bonding solvent-RTIL interactions based on these data. While there has been some consideration in the literature for the relative importance of dipolar solvation and hydrogen-bonding interactions in RTIL dilution studies, the data we report here do not show a discernible distinction between these two very distinct molecular interactions. What is clear, however, is that the dilution of the imidazolium RTILs we have studied here leads to the formation of aggregates in the binary system. Dilution does not produce a homogeneous solution, at least to

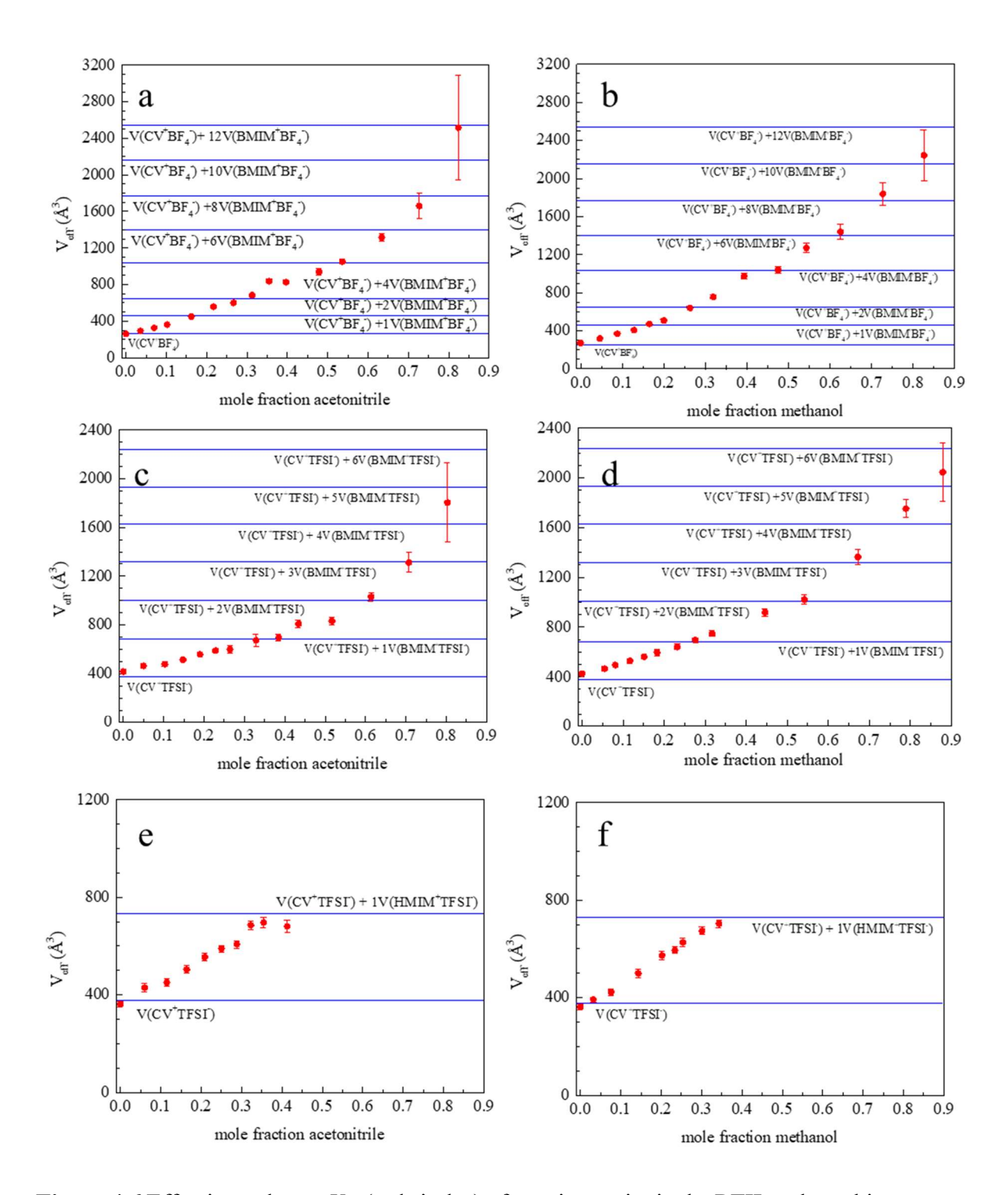


Figure 4.6 Effective volume, V_{eff} (red circles) of rotating entity in the RTIL-solvent binary system as a function of dilution. V_{eff} was determined from the experimental reorientation time constants, τ_{OR} , shown in Figure 4.5. Calculated hydrodynamic volumes of CV⁺-RTIL anion with number of RTIL ion pairs indicated as blue solid lines. (a) BMIM⁺BF₄⁻ in acetonitrile, (b) BMIM⁺BF₄⁻ in methanol, (c) BMIM⁺TFSI⁻ in acetonitrile, (d) BMIM⁺TFSI⁻ in methanol, (e) HMIM⁺TFSI⁻ in acetonitrile and (f) HMIM⁺TFSI⁻ in methanol. Mole fractions are calculated using the associated RTIL (ion pair) and the molecular solvent.

the extent we have diluted the RTILs. We can therefore not make a direct connection to dilute solution limit behavior of aqueous salt solutions for RTILs.

The collapse of the induced free charge density gradient ρ_f with dilution correlates with onset of aggregation between the chromophore and RTIL ion pairs seen in the bulk RTILs. The gradient ρ_f is seen to collapse when dimer-like species are found in the bulk diluted RTILs (*i.e.* $V(CV^+A^-) + 1V(RTIL)$). The structural heterogeneity afforded by the formation of aggregated species may facilitate the mobility of dissociated RTIL ions in the solvent-rich regions of the heterogeneous system, leading to the inability of the system to support ρ_f . Further work is required to understand the relationship between the collapse of ρ_f the formation of dimers and higher multimers in diluted RTIL systems.

4.4 Conclusions

We have examined the dependence of the magnitude and persistence length of ρ_f in three imidazolium RTILs on dilution with polar protic and aprotic solvents methanol and acetonitrile. We find that ρ_f persists in RTILs to varying degrees depending on RTIL and diluent identity, and in all cases the functional form of ρ_f is not a smooth, monotonic diminution with increasing diluent, but rather a stepwise change. This finding is not consistent with dilution producing a homogeneous solution. An examination of changes in the bulk RTIL as a function of dilution using rotational diffusion measurements shows that the rotating entity in bulk RTILs exhibits a larger effective hydrodynamic volume than would be expected based on bulk viscosity data for the diluted RTILs. This excess hydrodynamic volume is understood in the context of aggregation of RTIL ion pairs in the diluted RTIL system. The size of the aggregates is seen to depend on RTIL identity and diluent, and in all cases aggregate size increases with increasing dilution. This finding is consistent with the ρ_f dependence on dilution data. The collapse of ρ_f is seen to correlate with the onset of

RTIL ion pair dimer formation, a condition that may facilitate dissociated RTIL ion mobility in the binary system. Further work on selected solvent systems will likely provide greater insight into the compositional heterogeneity in RTIL-solvent binary systems.

REFERENCES

- 1. Arbizzani, C.; Biso, M.; Cericola, D.; Lazzari, M.; Soavi, F.; Mastragostino, M., Safe, high-energy supercapacitors based on solvent-free ionic liquid electrolytes. *J. Pwr. Sources* **2008**, *185*, 1575 1579.
- 2. MacFarlane, D. R.; Tachikawa, N.; Forsyth, M.; Pringle, J. M.; Howlett, P. C.; Elliott, G. D.; Davis, J. H.; WatanabeM.; Simon, P.; Angell, C. A., Energy applications of ionic liquids. *Energ. Env. Sci.* **2014**, *7*, 232 250.
- 3. Nabity, J. A.; Daily, J. W., Effect of Ionic Liquid Composition on Colloid Thruster Emission and Thrust Performance. *J. Propul. Pwr.* **2017**, *34* (1), 260-266.
- 4. Newell, R.; Faure-Vincent, J.; Iliev, B.; Schubert, T.; Aradilla, D., A new high performance ionic liquid mixture electrolyte for large temperature range supercapacitor applications (- 70° C to 80° C) operating at 3.5 V cell voltage. *Electrochim. Acta.* **2018**, *267*, 15 19.
- 5. Sakaebe, H.; Matsumoto, H., N-Methyl-N-propylpiperidinium bis(trifluoromethane sulfonyl)imide (PP13–TFSI)–novel electrolyte base for Li battery. *Electrochem. Commun.* **2003**, *5*, 594 598.
- 6. Van Aken, K. L.; Beidaghi, M.; Gogotsi, Y., Formulation of ionic liquid electrolyte to expand the voltage window of supercapacitors. *Angew. Chem.* **2015**, *127*, 4888 4891.
- 7. Gebbie, M. A.; Valtiner, M.; Banquy, X.; Fox, E. T.; Henderson, W. A.; Israelachvili, J. N., Ionic liquids behave as dilute electrolyte solutions. *Proc. Nat. Acad. Sci. USA* **2013**, *110*, 9674-9679.
- 8. MacFarlane, D. R.; Forsyth, M.; Izgorodina, E. I.; Abbott, A. P.; Annat, G.; Fraser, K., On the concept of ionicity in ionic liquids. *Phys. Chem. Phys.* **2009**, *11*, 4962-4967.
- 9. Nordness, O.; Brennecke, J. F., Ionic dissociation in ionic liquids and ionic liquid solutions. *Chem. Rev.* **2020**, *120*, 12873-12902.
- 10. Lin, Y.-J.; Hossain, N.; Chen, C.-C., Modeling dissociation of ionic liquids with electrolyte NRTL model. *J. Mol. Liq.* **2021**, *329*, 115524.
- 11. Gebbie, M. A.; Dobbs, H. A.; Valtiner, M.; Israelachvili, J. N., Long-range electrostatic screening in ionic liquids. *Proc. Nat. Acad. Sci. USA* **2015**, *112*, 7432-7437.
- 12. Gebbie, M. A.; Smith, A. M.; Dobbs, H. A.; Lee, A. A.; Warr, G. G.; Banquy, X.; Valtiner, M.; Rutland, M. W.; Israelachvili, J. N.; Perkin, S., et al., Long range electrostatic forces in ionic liquids. *Chem. Commun.* **2017**, *53*, 1214-1224.

- 13. Israelachvili, J. N.; Min, Y.; Akbulut, M.; Alig, A.; Carver, G.; Greene, W.; Kristiansen, K.; Meyer, E.; Pesika, N.; Rosenberg, K., et al., Recent advances in the surface forces apparatus (SFA) technique. *Rep. Prog. Phys.* **2010**, *73*, 036601.
- 14. Nishida, J.; Breen, J. P.; Wu, B.; Fayer, M. D., Extraordinary slowing of structural dynamics in thin films of a room temperature ionic liquid. *ACS Cent. Sci.* **2018**, *4*, 1065-1073.
- 15. Shin, J. Y.; Yamada, S. A.; Fayer, M. D., Dynamics of a room temperature ionic liquid in supported ionic liquid membranes vs the bulk liquid: 2D IR and polarized IR pump-probe experiments. *J. Am. Chem. Soc.* **2017**, *139*, 311-323.
- 16. Shin, J. Y.; Yamada, S. A.; Fayer, M. D., Carbon dioxide in a supported ionic liquid membrane: Structural and rotational dynamics measured with 2D IR and pump-probe experiments. *J. Am. Chem. Soc.* **2017**, *139*, 11222-11232.
- 17. Thomaz, J. E.; Bailey, H. E.; Fayer, M. D., The influence of mesoscopic confinement on the dynamics of imidazolium-based room temperature ionic liquids in polyether sulfone membranes. *J. Chem. Phys.* **2017**, *147*, 194502 1-11.
- 18. Wu, B.; Breen, J. P.; Fayer, M. D., Structural dynamics in ionic liquid thin films: The effect of cation chain length. *J. Phys. Chem. C* **2020**, *124*, 4179-4189.
- 19. Wu, B.; Breen, J. P.; Xing, X.; Fayer, M. D., Controlling the dynamics of ionic liquid thin films via multilayer surface functionalization. *J. Am. Chem. Soc.* **2020**, *142*, 9482-9492.
- 20. Anaredy; S., R.; Shaw, S. K., Developing Distinct Chemical Environments in Ionic Liquid Films. *J. Phys. Chem. C* **2018**, *122*, 19731-19737.
- 21. Anaredy, R. S.; Shaw, S. K., Long-Range Ordering of Ionic Liquid Fluid Films. *Langmuir* **2016**, *32*, 5147-5154.
- 22. Lucio, A. J.; Shaw, S. K.; Zhang, J.; Bond, A. M., Large-Amplitude Fourier-Transformed AC Voltametric Study of the Capacitive Electrochemical Behavior of the 1-Butyl-3-methylimidazolium Tetrafluoroborate—Polycrystalline Gold Electrode Interface. *J. Phys. Chem. C* **2017**, *121*, 12136-12147.
- 23. Anaredy, R. S.; Shaw, S. K., Directing long-range molecular ordering in ionic liquid films: A tale of two interfaces. *J. Phys. Chem. C* **2019**, *123*, 8975-8982.
- 24. Toda, S.; Clark, R.; Welton, T.; Shigeto, S., Observation of the Pockels Effect in Ionic Liquids and Insights into the Length Scale of Potential-Induced Ordering. *Langmuir* **2021**, *37*, 5193-5201.
- 25. Ma, K.; Jarosova, R.; Swain, G. M.; Blanchard, G. J., Charge-Induced Long-Range Order in a Room-Temperature Ionic Liquid. *Langmuir* **2016**, *32*, 9507-9512.

- 26. Ma, K.; Jarosova, R.; Swain, G. M.; Blanchard, G. J., Modulation of an Induced Charge Density Gradient in the Room-Temperature Ionic Liquid BMIM⁺BF₄-. *J. Phys. Chem. C* **2018**, *122*, 7361-7367.
- 27. Wang, Y.; Jarosova, R.; Swain, G. M.; Blanchard, G. J., Characterizing the magnitude and structure-dependence of free charge density gradients in room temperature ionic liquids. *Langmuir* **2020**, *36*, 3038-3045.
- 28. Wang, Y.; Parvis, F.; Hossain, M. I.; Ma, K.; Jarosova, R.; Swain, G. M.; Blanchard, G. J., Local and Long-Range Organization in Room Temperature Ionic Liquids. *Langmuir* **2021**, *37*, 605-615.
- 29. Wang, Y.; Swain, G. M.; Blanchard, G. J., Charge-induced birefringence in a room-temperature ionic liquid. *J. Phys. Chem. B* **2021**, *125*, 950-955.
- 30. Peiris, T. A. N.; Senthilarasu, S.; Wijayantha, K. G. U., Enhanced performance of flexible dye-sensitized solar cells: Electrodeposition of Mg(OH)₂ on a nanocrystalline TiO₂ electrode. *J. Phys. Chem. C* **2011**, *116*, 1211-1218.
- 31. Hay, C. E.; Marken, F.; Blanchard, G. J., Detection and Characterization of Liquid|Solid and Liquid|Solid Interfacial Gradients of Water Nanodroplets in Wet N-Octyl-2-Pyrrolidone. *Langmuir* **2014**, *30*, 9951-9961.
- 32. Li, W.; Zhang, Z.; Han, B.; Hu, S.; Xie, Y.; Yang, G., Effective of water and organic solvents on the ionic dissociation of ionic liquids. *J. Phys. Chem. B* **2007**, *111*, 6452-6456.
- 33. Debye, P., *Polar Molecules* Chemical Catalog Co.: New York 1929; p 84.
- 34. Hu, C.-M.; Zwanzig, R., Rotational friction coefficients for spheroids with the slipping boundary condition. *J. Chem. Phys.* **1974**, *60* (11), 4354-4357.
- 35. Perrin, F., Mouvement brownien d'un ellipsoide I. Dispersion diélectrique pour des molécules ellipsoidales. *J. Phys. Radium* **1934**, *5*, 497.
- 36. Edward, J. T., Molecular volumes and the Stokes-Einstein equation. *J. Chem. Ed.* **1970**, 47, 261-270.
- 37. Herold, E.; Strauch, M.; Michalik, D.; Appelhagen, A.; Ludwig, R., Dynamics of methanol in ionic liquids: Validity of the Stokes-Einstein and Stokes-Einstein-Debye relations. *ChemPhysChem* **2014**, *15*, 3040-3048.
- 38. Schutter, C.; Bothe, A.; Balducci, A., Mixtures of acetonitrile and ethyl isopropyl sulfone as electrolytes for electrochemical double layer capacitors *Electrochim. Acta* **2020**, *331*, 135421.
- 39. Vercher, E.; Llopis, F. J.; Gonzalez-Alfaro, V.; Miguel, P. J.; Orchilles, V.; Martinez-Andreu, A., Volumetric properties, viscosities and refractive indices of binary liquid mixtures of

- tetrafluoroborate-based ionic liquids with methanol at several temperatures. *J. Chem. Thermodyn.* **2015,** *90*, 174-184.
- 40. Wang, J.; Tian, Y.; Zhao, Y.; Zhuo, K., A volumetric and viscosity study for the mixture of 1-n-butyl-3-methylimidazolium tetrafluoroborate ionic liquid with acetonitrile, dichloromethane, 2-butanone and N,N-dimethylformamide. *Green Chem.* **2003**, *5*, 618-622.
- 41. Jerome, F. S.; Tseng, J. T.; Fan, L. T., Viscosities of aqueous glycol solutions. *J. Chem. Eng. Data* **1968**, *13*, 496.
- 42. Segur, J. B.; Oberstar, H. E., Viscosity of glycerol and its aqueous solutions. *Ind. Eng. Chem.* **1951**, *43*, 2117-2120.
- 43. Bester-Rogac, M.; Hunger, J.; Stoppa, A.; Buchner, R., Molar Conductivities and Association Constants of 1-Butyl-3-methylimidazolium Chloride and 1-Buthyl-3-methylimidazolium Tetrafluoroborate in Methanol and DMSO. *J. Chem. Eng. Data* **2010**, *55*, 1799-1803.
- 44. Zheng, Y.-Z.; Zhou, Y.; Deng, G.; Guo, R.; Chen, D.-F., The structure and hydrogen-bond behaviors of binary systems containing ionic liquid 1-butyl-3-methylimidazolium tetrafluoroborate and methanol/ethanol. *Spectrochim. Acta A: Mol. Biomol.Spectr.* **2019**, *223*, 117312.
- 45. Bester-Rogac, M.; Stoppa, A.; Buchner, R., Ion Association of Imidazolium Ionic Liquids in Acetonitrile. *J. Phys. Chem. B* **2014**, *118*, 1426-1435.
- 46. Zheng, Y.-Z.; Want, N.-N.; Luo, J.-J.; Zhou, Y.; Yu, Z.-W., Hydrogen-bonding interactions between BMIMBF₄ and acetonitrile. *Phys. Chem. Chem. Phys.* **2013**, *15*, 18055-18064.
- 47. Blanchard, G. J., A study of the state-dependent reorientation dynamics of oxazine-725 in primary normal aliphatic alcohols. *J. Phys. Chem.* **1988**, *92*, 6303-6307.
- 48. Blanchard, G. J.; Cihal, C. A., Orientational relaxation dynamics of oxazine 118 and resorufin in the butanols. Valence-dependent and state-dependent solvation effects *J. Phys. Chem.* **1988,** *92*, 5950-5954.
- 49. Canongia Lopes, J. N. A.; Costa Gomes, M. F.; Husson, P.; Padua, A. A. H.; Rebelo, L. P. N.; Sarraute, S.; Tariq, M., Polarity, Viscosity, and Ionic Conductivity of Liquid Mixtures Containing [C₄C₁im][NTf₂] and a Molecular Component. *J. Phys. Chem. B* **2011**, *115*, 6088-6099.
- 50. Zhu, A.; Wang, J.; Han, L.; Fan, M., Measurements and correlation of viscosities and conductivities for the mixtures of imidazolium ionic liquids with molecular solutes. *Chem. Eng. J.* **2009,** *147*, 27-35.

- 51. Salinas, R.; Pla-Franco, J.; Lladosa, E.; Monton, J. B., Density, speed of sound, viscosity, and excess properties of binary mixtures formed by ethanol and bis(trifluorosulfonyl)imide-based ionic liquids. *J. Chem. Eng. Data* **2015**, *60*, 525-540.
- 52. Pronk, S.; Lindahl, E.; Kasson, P. M., Dynamic heterogeneity controls diffusion and viscosity near biological interfaces. *Nature Commun.* **2014**, *5* (1), 3034.
- 53. Das, N.; Sen, P., Dynamic heterogeneity and viscosity decoupling: origin and analytical prediction. *Phys. Chem. Chem. Phys.* **2021**, *23* (29), 15749-15757.
- 54. Blanchard, G. J., Counterion-dependent reorientation dynamics of an oxazine in polar protic and aprotic solvents *J. Phys. Chem.* **1991**, *95*, 5293-5299.
- 55. Marekha, B. A.; Kalugin, O. N.; Bria, M.; Buchner, R.; Idrissi, A., Translational Diffusion in Mixtures of Imidazolium ILs with Polar Aprotic Molecular Solvents. *J. Phys. Chem. B* **2014**, *118*, 5509-5517.
- 56. Scharf, N. T.; Stark, A.; Hoffmann, M. M., Ion Pairing and Dynamics of the Ionic Liquid 1-Hexyl-3-methylimidazolium Bis(trifluoromethylsulfonly)imide ([C₆mim][NTf₂]) in the Low Dielectric Solvent Chloroform. *J. Phys. Chem. B* **2012**, *116*, 11488-11497.
- 57. Hu, X.; Lin, Q.; Gao, J.; Wu, Y.; Zhang, Z., Anion-cation and ion-solvent interaction of some typical ionic liquids in solvents with different dielectric constant. *Chem. Phys. Lett.* **2011**, *516*, 35-39.

APPENDIX

$$R(t) = \frac{I_{\parallel}(t) - I_{\perp}(t)}{I_{\parallel}(t) + 2I_{\perp}(t)}$$
 [S1]

$$R(t) = R(0) \exp(-t/\tau_{OR})$$
 [S2]

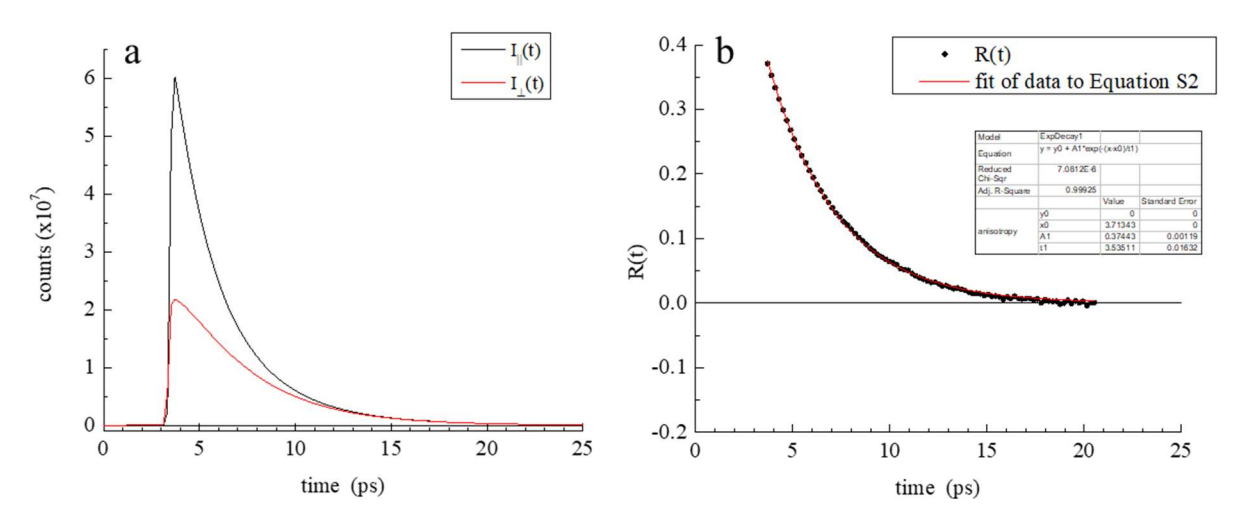


Figure S1 Example of experimental data for CV^+ in BMIM⁺BF₄⁻ (X=0.603) in ACN (X=0.397). (a) show raw experimental $I_{\parallel}(t)$ and $I_{\wedge}(t)$ data. (b) shows R(t) calculated using Eq. S1 and the fit of the function S2 to the experimental data.

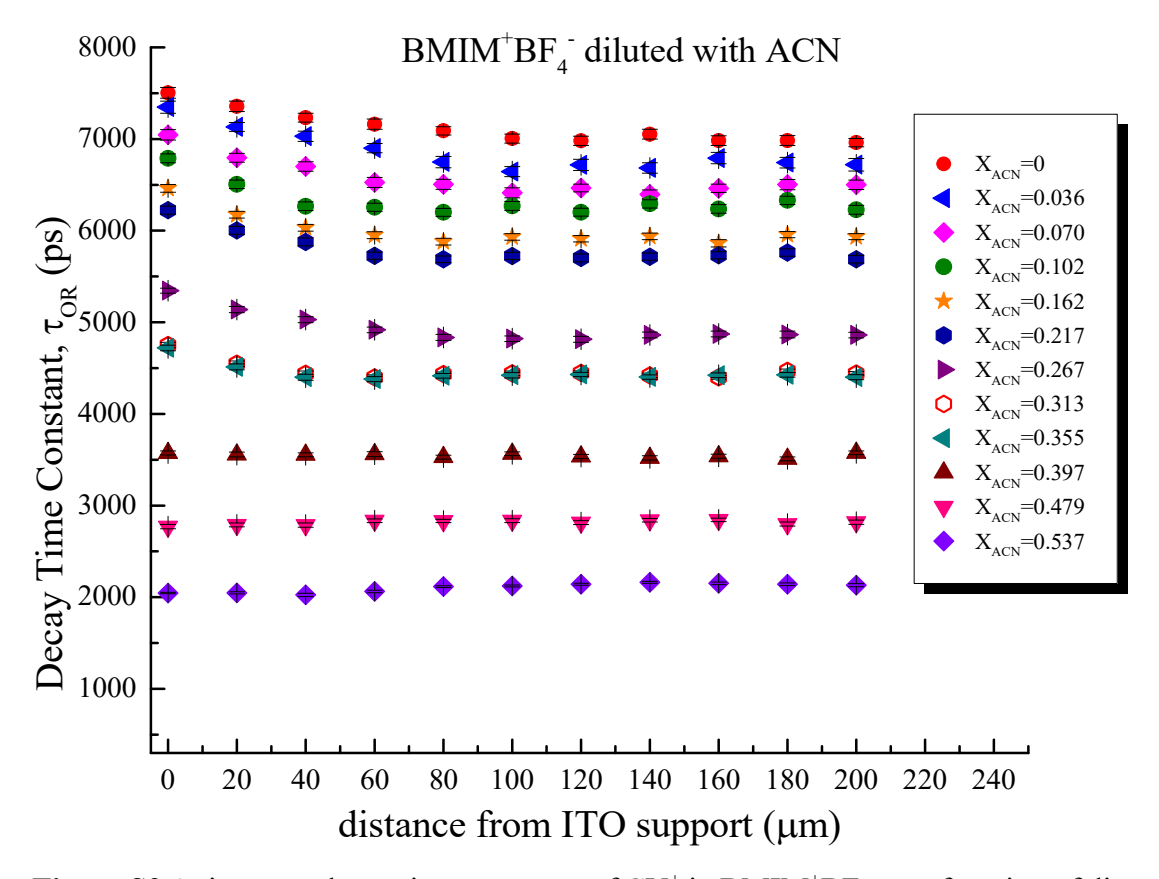


Figure S2 Anisotropy decay time constants of CV^+ in BMIM $^+BF_4^-$ as a function of distance from the ITO support and as a function of dilution with ACN as indicated in the legend. Each time constant is the result of the average of 65,536 (256 x 256 array) $I_{\parallel}(t)$ and $I_{\perp}(t)$ time-resolved data sets. The resulting data are processed according to Eq. 1 and the resulting R(t) function is fitted to a single exponential decay function. The error bars are $\pm 1\sigma$ uncertainties for fits of R(t) to a single exponential decay function. Replicate measurements were performed at least three times.

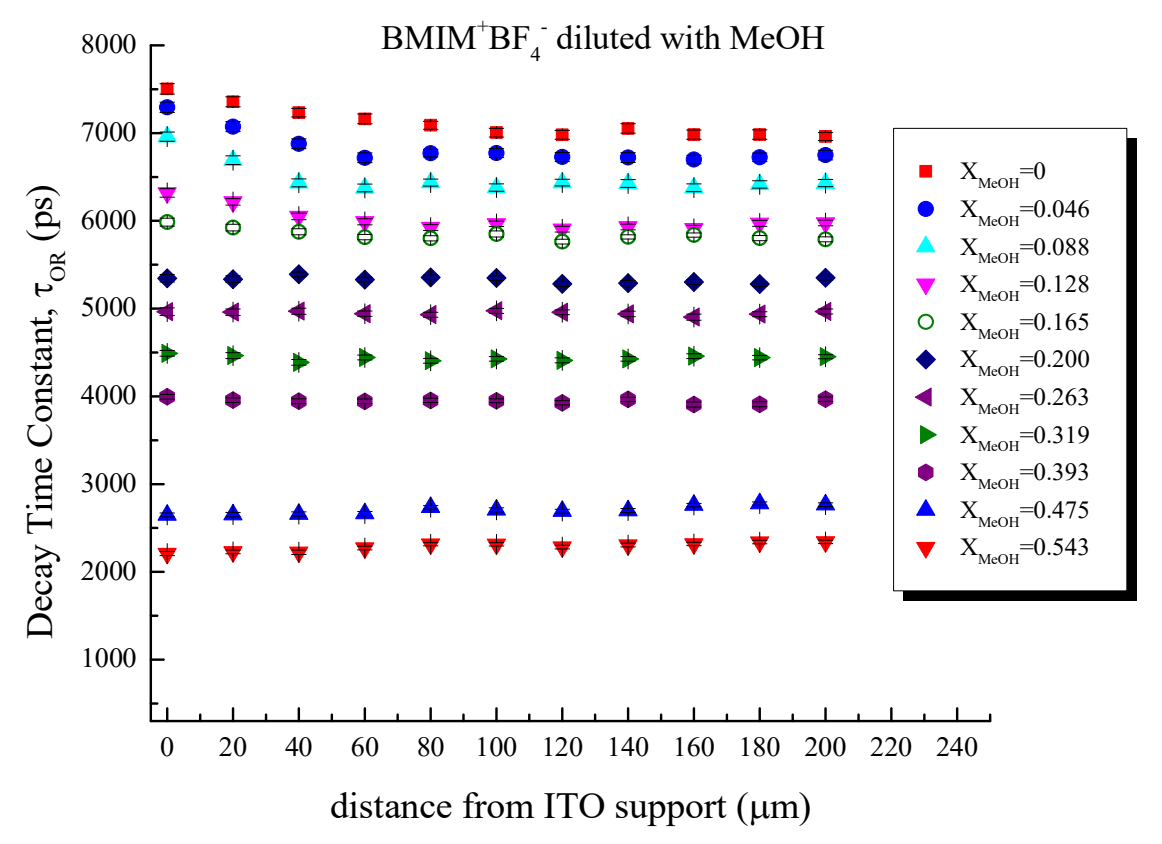


Figure S3 Anisotropy decay time constants of CV^+ in BMIM $^+$ BF $_4^-$ as a function of distance from the ITO support and as a function of dilution with MeOH as indicated in the legend. Each time constant is the result of the average of 65,536 (256 x 256 array) $I_{\parallel}(t)$ and $I_{\perp}(t)$ time-resolved data sets. The resulting data are processed according to Eq. 1 and the resulting R(t) function is fitted to a single exponential decay function. The error bars are $\pm 1\sigma$ uncertainties for fits of R(t) to a single exponential decay function. Replicate measurements were performed at least three times.

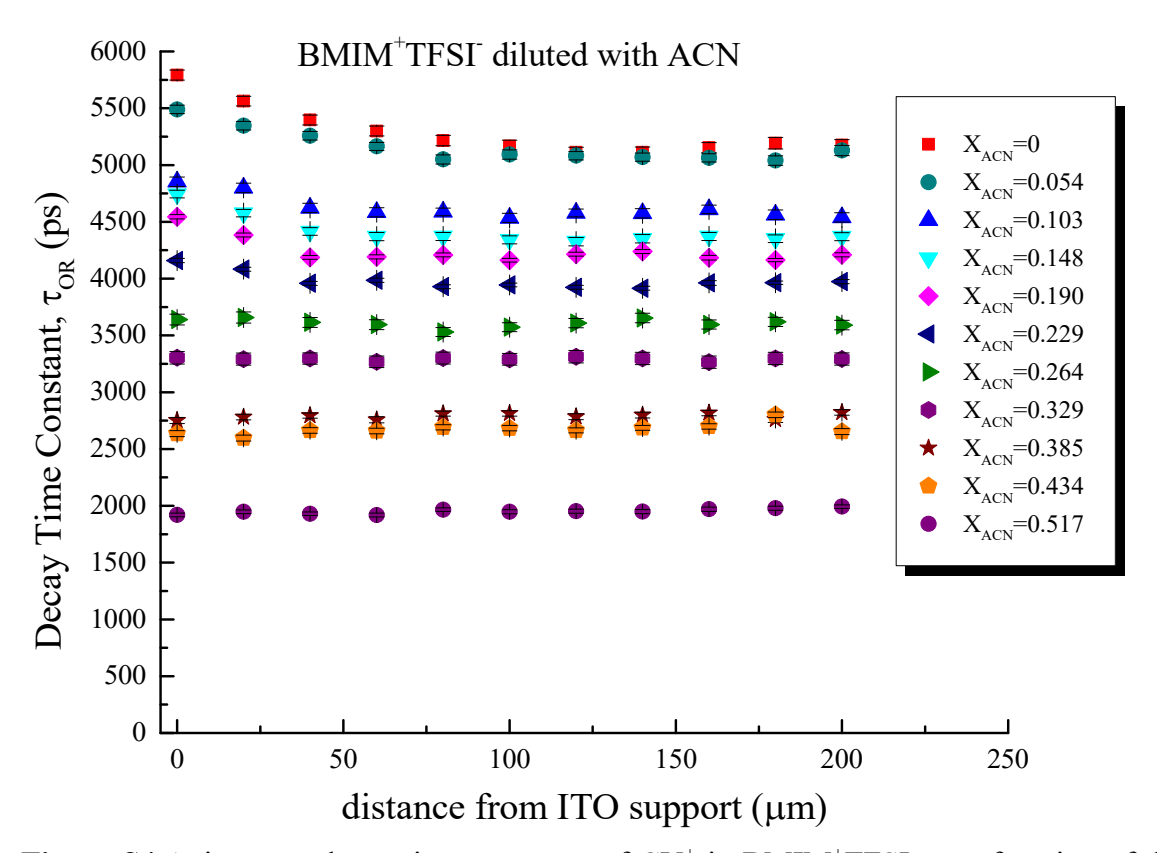


Figure S4 Anisotropy decay time constants of CV^+ in BMIM⁺TFSI⁻ as a function of distance from the ITO support and as a function of dilution with ACN as indicated in the legend. Each time constant is the result of the average of 65,536 (256 x 256 array) $I_{\parallel}(t)$ and $I_{\perp}(t)$ time-resolved data sets. The resulting data are processed according to Eq. 1 and the resulting R(t) function is fitted to a single exponential decay function. The error bars are $\pm 1\sigma$ uncertainties for fits of R(t) to a single exponential decay function. Replicate measurements were performed at least three times.

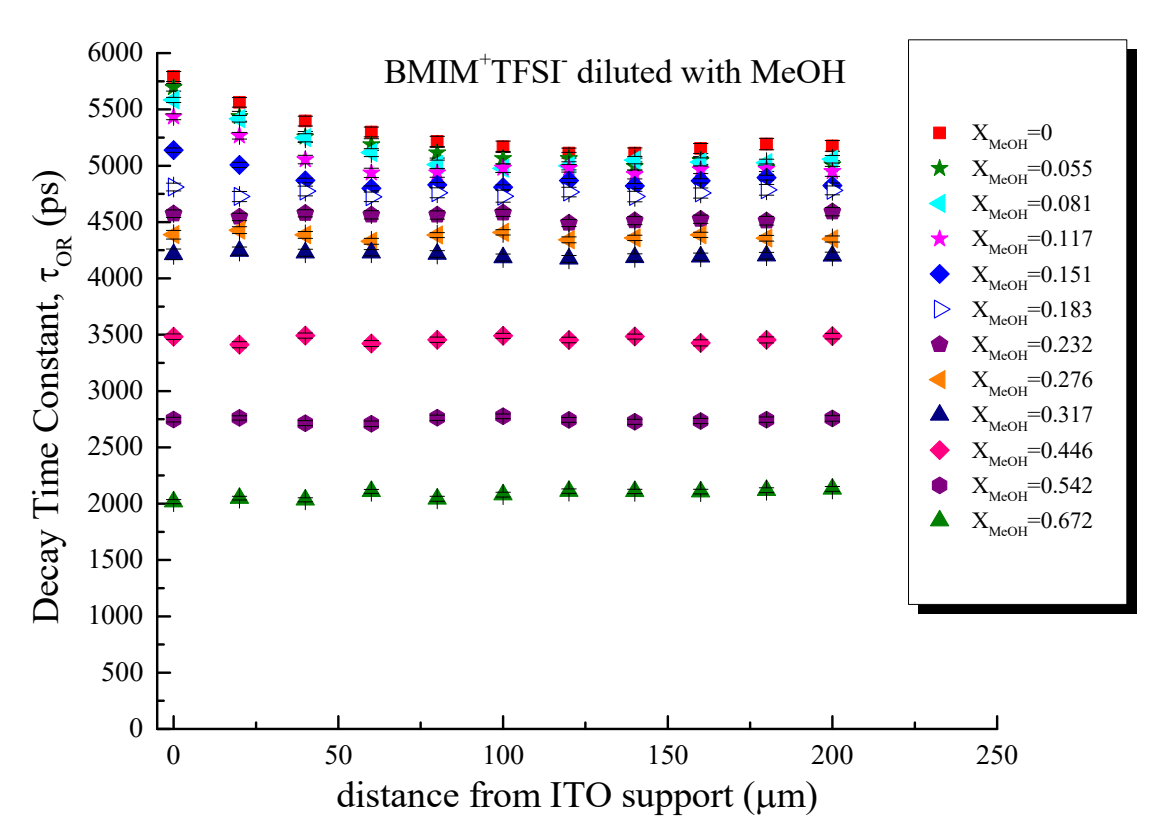


Figure S5 Anisotropy decay time constants of CV^+ in BMIM⁺TFSI⁻ as a function of distance from the ITO support and as a function of dilution with MeOH as indicated in the legend. Each time constant is the result of the average of 65,536 (256 x 256 array) $I_{\parallel}(t)$ and $I_{\perp}(t)$ time-resolved data sets. The resulting data are processed according to Eq. 1 and the resulting R(t) function is fitted to a single exponential decay function. The error bars are $\pm 1\sigma$ uncertainties for fits of R(t) to a single exponential decay function. Replicate measurements were performed at least three times.

HMIM⁺TFSI⁻ diluted with ACN

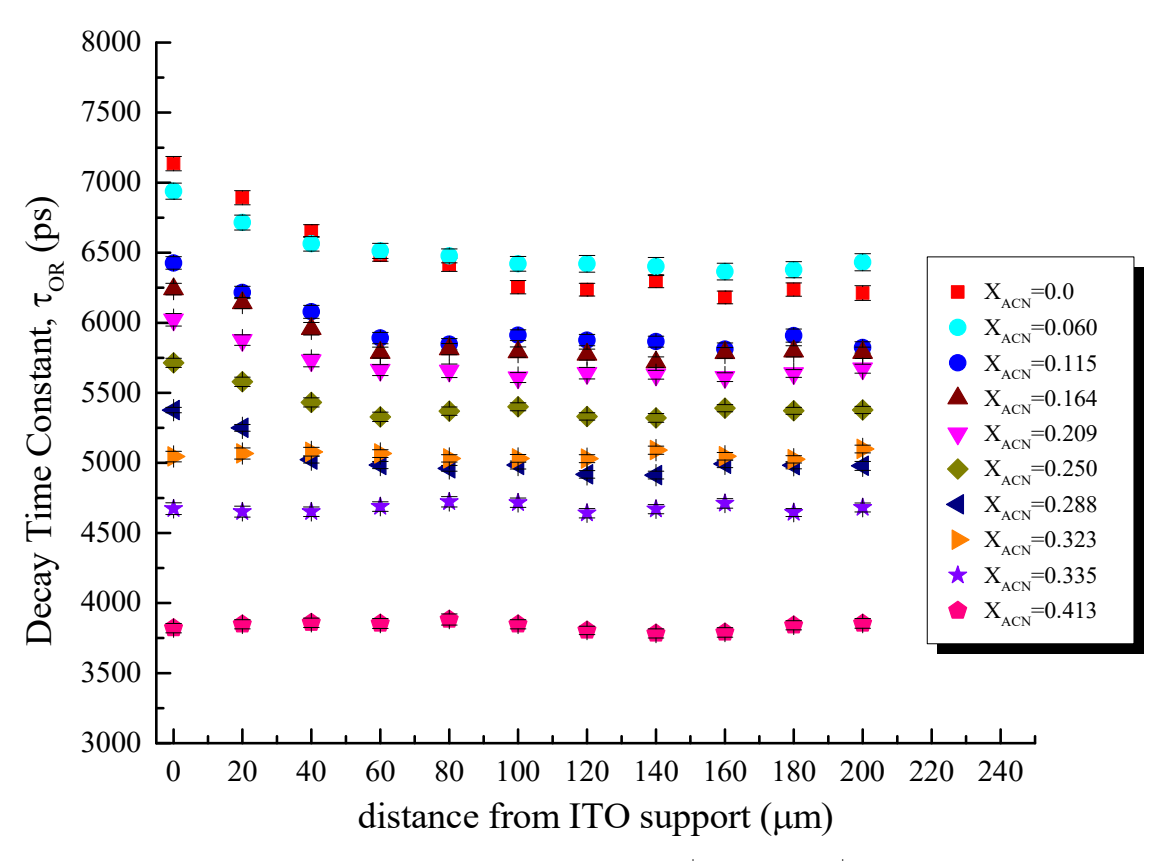


Figure S6 Anisotropy decay time constants of CV^+ in HMIM⁺TFSI⁻ as a function of distance from the ITO support and as a function of dilution with ACN as indicated in the legend. Each time constant is the result of the average of 65,536 (256 x 256 array) $I_{\parallel}(t)$ and $I_{\perp}(t)$ time-resolved data sets. The resulting data are processed according to Eq. 1 and the resulting R(t) function is fitted to a single exponential decay function. The error bars are $\pm 1\sigma$ uncertainties for fits of R(t) to a single exponential decay function. Replicate measurements were performed at least three times.

HMIM⁺TFSI⁻ diluted with MeOH

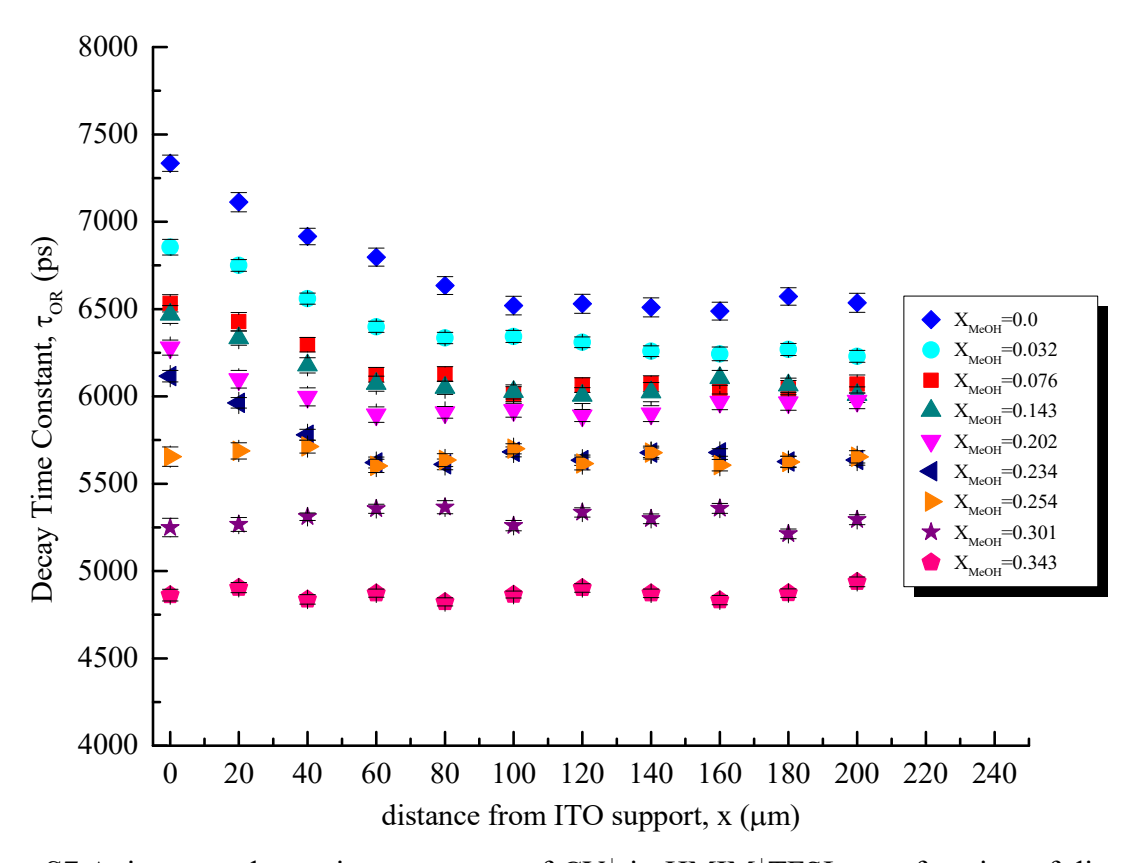


Figure S7 Anisotropy decay time constants of CV^+ in HMIM⁺TFSI⁻ as a function of distance from the ITO support and as a function of dilution with MeOH as indicated in the legend. Each time constant is the result of the average of 65,536 (256 x 256 array) $I_{\parallel}(t)$ and $I_{\perp}(t)$ time-resolved data sets. The resulting data are processed according to Eq. 1 and the resulting R(t) function is fitted to a single exponential decay function. The error bars are $\pm 1\sigma$ uncertainties for fits of R(t) to a single exponential decay function. Replicate measurements were performed at least three times.

CHAPTER 5. Dilution-Induced Changes in Room Temperature Ionic Liquids. Compositional Heterogeneity and the Importance of Dipolar Interactions	Persistent
Adapted with permission from:	
Md. Iqbal Hossain and G. J. Blanchard; Dilution-induced changes in room temper liquids. Persistent compositional heterogeneity and the importance of dipolar interaction of Molecular Liquids 367 (2022) 120447-120455.	

5.1 Introduction

Room temperature ionic liquids (RTILs) are a class of materials that have attracted wide interest because of their physical and chemical properties, including low volatility, wide electrochemical window and ability to dissolve polar as well as nonpolar compounds. These properties have resulted in a variety of applications, ranging from gas sequestration and chemical synthesis to energy storage and ionic propulsion. ¹⁻⁶ Despite the appeal of this class of materials, there remains much to be understood regarding the organization and dynamics of RTILs, and their ability to exhibit and support structural order and charge density gradients over macroscopic distances.

While organization is seen in RTILs, the structural details and length scale of the organization appear to depend on the means used to probe the organization⁷⁻²¹ and the structures of the RTIL cations.²²⁻²⁵ In the work we report here, we are concerned primarily with the effect of dilution on RTILs. There is a substantial body of work that has reported formation of micellar structures in RTILs diluted with water.^{22-23, 26-33} It is thought that the nonpolar functionalities of the amphiphilic RTIL cation associate to minimize interactions with the polar solvent while the ionic headgroups and RTIL counterions are distributed more uniformly, and the presence of such molecular-scale heterogeneity increases with RTIL cation aliphatic chain length.²⁴⁻²⁵ There has also been evidence of compositional non-uniformity in RTILs diluted with non-aqueous solvents,³⁴⁻³⁷ but the reason(s) for the formation of RTIL aggregates in such solvents remains unclear. The formation of compositionally heterogeneous mixtures rather than uniform solutions is an important issue for these systems for reasons of their effect on physical properties. An earlier report by our group focused on methanol and acetonitrile as diluents of several RTILs, and a key implication of that work was that the formation of ion pairs served as a nucleating process in the

formation of nanoscale aggregates.³⁴ Because of the comparatively low viscosity of both solvents, dynamics at high dilution could not be studied with sufficient resolution, and the explicit roles of hydrogen bonding and dipolar interactions between ion pairs were not resolved. In the work we report here, we are interested in further elucidating the molecular-scale processes that are responsible for compositional heterogeneity in RTIL/solvent binary systems. We have chosen dimethyl sulfoxide (DMSO) and propylene carbonate (PC) as solvents because both are polar aprotics and are characterized by comparatively large dielectric constants ($\varepsilon \sim 49$ for DMSO and $\varepsilon \sim 65$ for PC). With this choice of solvents we can evaluate the extent to which dipolar interactions play a role in persistent compositional heterogeneity. We use two RTILs which share a common 1-butyl 3-methyl imidazolium cation (BMIM⁺), with tetrafluoroborate (BF4⁻) and bistriflimide (TFSI⁻) anions. We have made these choices deliberately, to address the questions that remained from the previous report regarding the contribution of hydrogen-bonding to our findings.³⁴ Collectively, these studies are aimed at resolving the role of the RTIL ion structure in mediating ρ_f and persistent organization.

We have probed the properties of BMIM⁺BF4⁻ and BMIM⁺TFSI⁻ diluted with DMSO and PC through the rotational diffusion time constant of the cationic fluorophore cresyl violet (CV⁺) as a function of distance from a charged support surface to understand the dependence of ρ_f magnitude and persistence length on dilution.^{11-12, 17-19, 34} The structures of these compounds are shown in Fig. 5.1. We find that ρ_f does not vary linearly with RTIL dilution. Rather, ρ_f persists up to ca. 20 mol % dilution for BMIM⁺TFSI⁻ and ca. 30 mol % for BMIM⁺BF4⁻ in both DMSO and PC. For greater extents of dilution, ρ_f is not observed. When the same rotational diffusion measurements are performed in the bulk RTIL-solvent binary system, *i.e.*, in regions where ρ_f does not influence CV⁺ reorientation, the dependence of CV⁺ reorientation on dilution is consistent with

the formation of RTIL aggregates, with the characteristic aggregate size depending on the diluent and on the identity of the RTIL anion. These findings underscore the importance of RTIL contact ion pairs in determining the properties of neat and diluted RTILs.³⁴

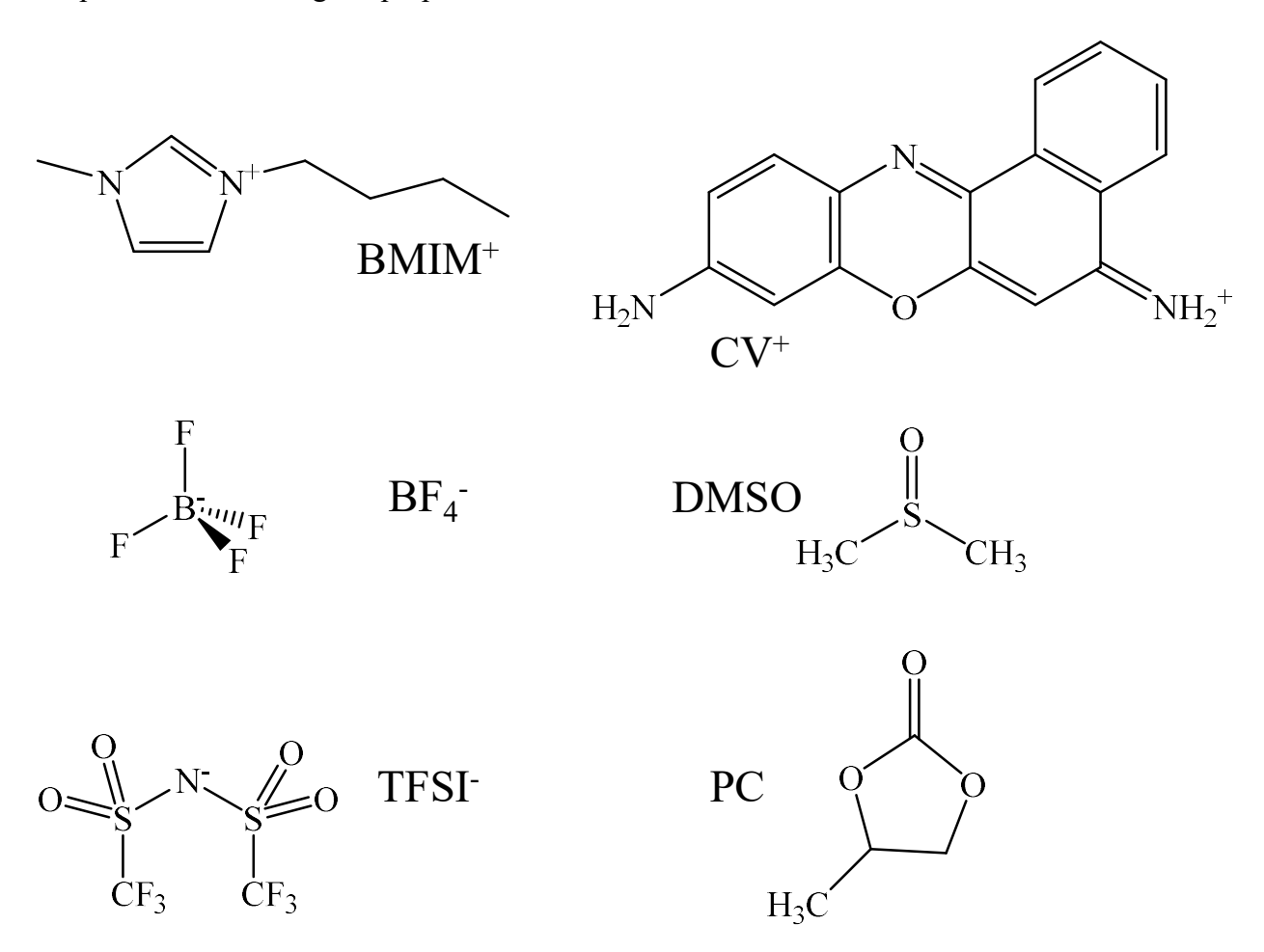


Figure 5.1 Structures of the compounds used in this work. BMIM⁺ = 1-methyl-3-butyl imidazolium, CV^+ = cresyl violet, BF_4^- = tetrafluoroborate, DMSO = dimethyl sulfoxide, TFSI⁻ = bis(trifluoromethane)sulfonamide, and PC = propylene carbonate.

5.2 Experimental Section

5.2.1 Chemicals and Purification

BMIM⁺BF₄⁻ (>97%) and BMIM⁺TFSI⁻ (≥99%, < 500 ppm H₂O) were obtained from Sigma-Aldrich and were purified. RTILs were stored over activated carbon for fourteen days. The activated carbon was removed by syringe filtration (Durapore membrane, 0.22 µm pore diameter, Millex). The RTIL is then heated to 80 °C under reduced pressure for four hours while being purged with Ar. Subsequent Karl Fischer titration (Mettler-Toledo C10SD) yielded < 20 ppm water. Purified samples were stored in a dry glove box until use. Solvents DMSO (anhydrous, 99.9%) and PC (anhydrous, 99.7%) were procured from Sigma-Aldrich and used as received.

5.2.2 Solution Preparation

A stock solution of cresyl violet perchlorate (CV⁺) (Exciton) was made to *ca*. 5.3x10⁻⁴ M in ethanol. A quantity of 100 μL of this stock solution was dispensed into a scintillation vial and evaporated to dryness at 100 °C for three hours, and subsequently cooled to room temperature in a desiccator. The dried chromophore aliquot was taken up in 1 mL of RTIL and the resulting solution was stirred for 12 h prior to use. All glassware used was stored in an oven at 150 °C for at least 24 h and cooled in a desiccator prior to use. All sample preparation was performed in a N₂ purged glove box (Coy Labs, Grass Lake, MI). Binary systems were prepared by mass measurement. Measured masses of RTIL and solvent were used to calculate mole fractions. All binary systems were prepared in a N₂ purged glove bag.

5.2.3 Sample Cell Preparation

The sample cell used here has been described and used elsewhere. ^{12, 34} The cell is fabricated using an indium doped tin oxide (ITO)-coated microscope slide. ITO is known to carry a positive surface charge, and no potential or current was applied across the ITO film in this work. ^{12, 38} The

slides were cleaned ultrasonically in detergent, washed with Milli-Q water and *i*-propanol. The slides were subsequently washed with anhydrous ethanol and dried in an oven at 200 °C for 40 min. Following cooling, the support was cleaned using a UV/ozone cleaner for 20 minutes. The thickness of the cell was determined by a silicone rubber spacer (1.6 mm thick) that was cleaned ultrasonically with detergent solution, rinsed with water and dried with N₂. The cell was covered with a microscope coverslip that was cleaned in the same manner as the support slide.

5.2.4 Spatially Resolved Fluorescence Anisotropy Decay Measurements

The instrument used to acquire time-resolved and spatially-resolved data has been described elsewhere.³⁹ Briefly, a confocal scanning inverted microscope (Nikon Eclipse Ti-U) is used for spatial acquisition. Confocal scanning is performed using a Becker & Hickl DCS-120 instrument. The depth of focus for this instrument is ca. 1.2 µm using a 10X objective (Nikon, N.A. 0.30). Time-resolved data are acquired using two-channel time-correlated single photon electronics (Becker & Hickl SPC- 152) equipped with two avalanche photodiode detectors (ID Quantique). The instrument response function for this system is ca. 100 ps, and the light source is a synchronously pumped cavity dumped dye laser (Coherent 701-3 laser and 7220 cavity dumper). The pump source for the dye laser is a Spectra Physics Vanguard passively mode locked NdYVO₄ laser. The pump laser produces 13 ps pulses at a repetition rate of 80 MHz, with 2.5 W average power at both the second harmonic (532 nm) and third harmonic (355 nm) output wavelengths. The second harmonic output is used to excite the dye laser (Pyrromethene 567, Exciton). Dye laser output is ca. 25 mW at 575 nm, with 5 ps pulses at a repetition rate of 4 MHz. The dye laser output is split, with one half sent to a reference photodiode and the remaining light focused into a fiber optic and directed into the confocal scanning head. Time-resolved polarized fluorescence data are acquired across the sample imaged area (256 x 256 pixels) and data sets for each pixel are processed and the results averaged.

5.2.5 Semi-empirical Calculations

Semi-empirical calculations were performed using Hyperchem 8.0 software. PM-3 parameterization was used for geometry optimization and calculation of molecular properties.

5.3 Results and Discussion

We present our investigation of two RTILs diluted with DMSO and PC. The dilution of RTILs has been studied previously, for both fundamental and applied reasons. From a fundamental perspective, understanding how RTILs interact with diluents can provide insight into the driving forces for long-range organization in these materials. The two RTILs chosen have a common cation (BMIM⁺) and different anions (BF₄⁻ and TFSI⁻), for the purpose of elucidating what role the anion plays in RTIL organization. Specifically, BF₄ is known to participate in hydrogen-bonding but it is not known the extent to which it participates in dipolar processes. The solvents were chosen because they are both polar and aprotic, precluding contributions from hydrogen bonding to our experimental data. For both neat RTILs, ρ_f is known to persist over a distance of ca. 50 μ m, ³⁴ and with a magnitude on the order of ca. 50 μ C/cm³/ μ m. ¹⁷ What remains to be established from first principles is the reason that such a gradient can be supported in a fluid medium. One way to potentially address this issue is to study the behavior of RTILs upon dilution. Specifically, if ρ_f is mediated by ion translational mobility then the magnitude and persistence length should scale with D_T , which is related inversely to the viscosity of the medium through the Stokes-Einstein equation. 40-41 We do not observe a smooth, monotonic diminution of either the persistence length, d, or magnitude of ρ_f (expressed as $(\Delta \tau_{OR}/\tau_{OR})(0)$) with dilution. Rather, there are discontinuous changes in these quantities with increasing dilution, and the point at which the changes occur depends on the identity of the diluent. Dilution beyond the point of ρ_f disappearing yields

anisotropy decay data consistent with aggregates of RTILs persisting. The aggregates are found to increase in size with increasing dilution, with aggregate size depending on both RTIL anion and diluent identities. We consider the dilution-dependence of ρ_f and the existence of RTIL aggregates in the diluents separately, then discuss the implications of these findings on the molecular-scale organization that is characteristic of RTILs.

5.3.1 Gradient Magnitude and Persistence Length as a Function of Dilution

We have demonstrated the existence of an induced free charge density gradient, ρ_f , in RTILs previously. 11-12, 17-19 The charge density gradient can be characterized by either of two means; depth-dependent reorientation dynamics of a charged chromophore, or surface charge-induced birefringence. We have chosen the former method for this work because it is more sensitive to molecular-scale processes and ρ_f persistence length, d, than induced birefringence. We extract the chromophore reorientation data from polarized, time-resolved emission data as a function of position within the RTIL sample. These polarized transients, $I_{\parallel}(t)$ and $I_{\perp}(t)$, are used to produce the induced orientational anisotropy function, R(t),

$$R(t) = \frac{I_{\parallel}(t) - I_{\perp}(t)}{I_{\parallel}(t) + 2I_{\perp}(t)}$$
 [5.1]

The relevant information is contained in the functional form of the decay of R(t). For all the measurements reported here, R(t) decays as a single exponential, and the time constant of the decay, τ_{OR} , is related to the properties of the system through the modified Debye-Stokes-Einstein (DSE) equation, 42-44

$$\tau_{OR} = 6D_{rot}^{-1} = \frac{\eta Vf}{k_{\scriptscriptstyle B}TS}$$
 [5.2]

where D_{rot} is the rotational diffusion constant, η is the bulk viscosity of the medium, V is the

hydrodynamic volume of the rotating entity, 45 f is the frictional boundary condition term for interactions between the rotating entity and it's local environment, 43 k_B is the Boltzmann constant, T is the system temperature, and S is a correction factor to account for the ellipsoidal shape of the rotor. 44 The time constant τ_{OR} is seen to depend on distance from the (charged) RTIL support and this depth-dependence results from the existence of a gradient in the concentration of dissociated RTIL ions. 11 Because the viscosity of RTILs depends on the chemical identities of the (ionic) constituents, comparing results between different RTILs is more facile when the data are presented in normalized form, as $(\Delta \tau_{OR}/\tau_{OR})(x)$ vs. x, where x is the distance from the sample cell support surface and $\Delta \tau_{OR} = \tau_{OR}(x) - \tau_{OR}(\infty)$. As τ_{OR} changes to its bulk value, it is seen empirically to have the form of an exponential decay in (x),

$$\left(\frac{\Delta \tau_{OR}}{\tau_{OR}}\right)(x) = \left(\frac{\Delta \tau_{OR}}{\tau_{OR}}\right)(0) \exp(-x/d)$$
 [3]

We show the dependence of $(\Delta \tau_{OR}/\tau_{OR})(x)$ and d for BMIM⁺BF₄⁻ diluted with PC (Fig. 5.2) and DMSO (Fig. 5.3), and for BMIM⁺TFSI⁻ diluted with PC (Fig. 5.4) and DMSO (Fig. 5.5). These data contain several interesting features. The first is that the magnitude of ρ_f in neat RTILs is the same for both RTILs. This finding is consistent with our previous findings, ^{11-12, 17-19, 34} and suggests a physical rather than chemical basis for the existence of ρ_f . It is important to note, however, that while the magnitude of ρ_f is the same for both neat RTILs, and this quantity is likely determined by the surface charge density carried by the support. Interestingly, while ρ_f is the same, the characteristic persistence length, d, differs significantly for the two RTILs, with BMIM⁺BF₄-being characterized by $d \sim 60 \,\mu\text{m}$ and BMIM⁺TFSI⁻ exhibiting $d \sim 40 \,\mu\text{m}$. This finding implicates the RTIL anion as playing a role in determining d.

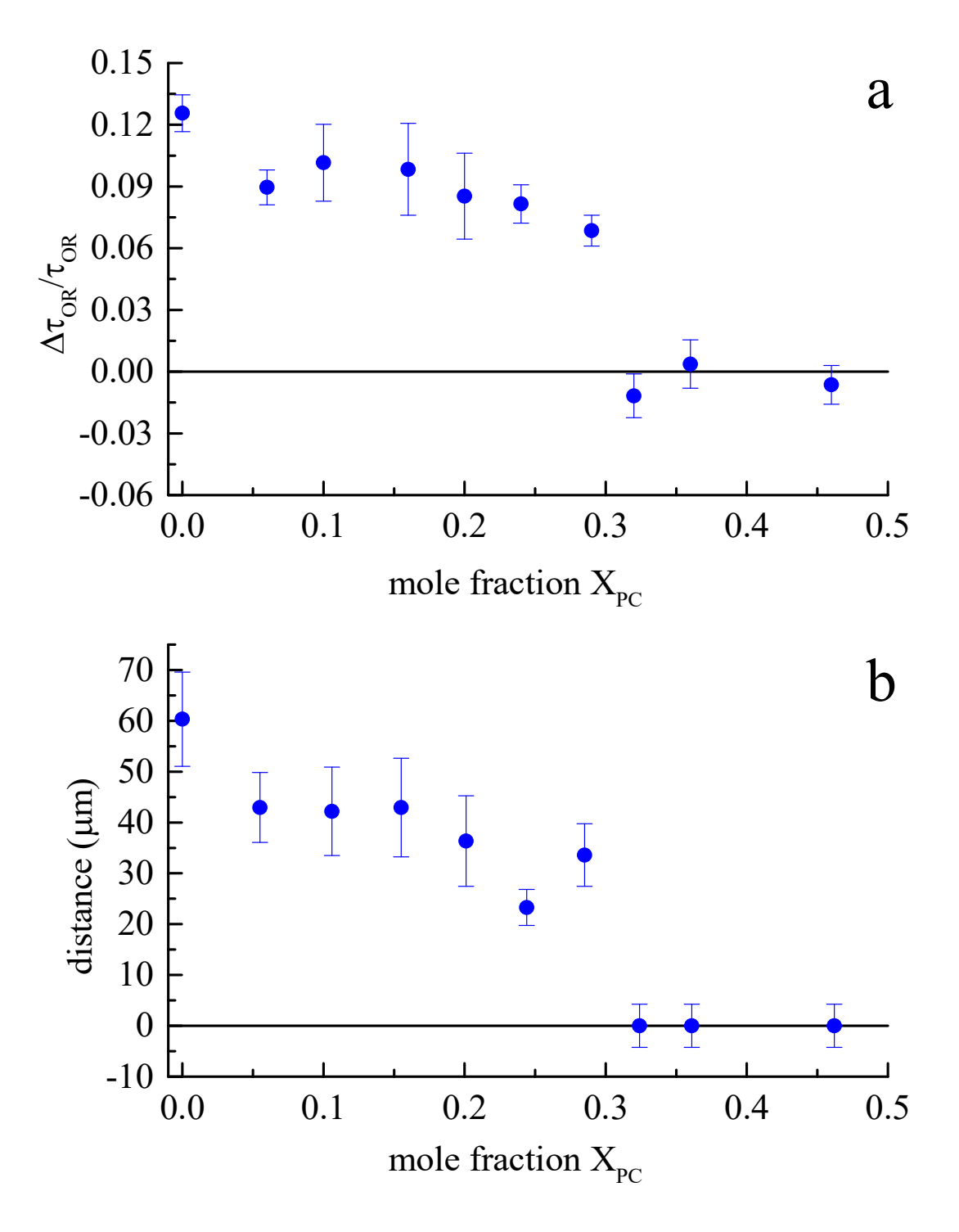


Figure 5.2 (a) Magnitude of ρ_f , expressed as $\Delta \tau_{OR}/\tau_{OR}$ and (b) persistence length of ρ_f , as a function of mole fraction of PC diluent for BMIM⁺BF₄⁻.

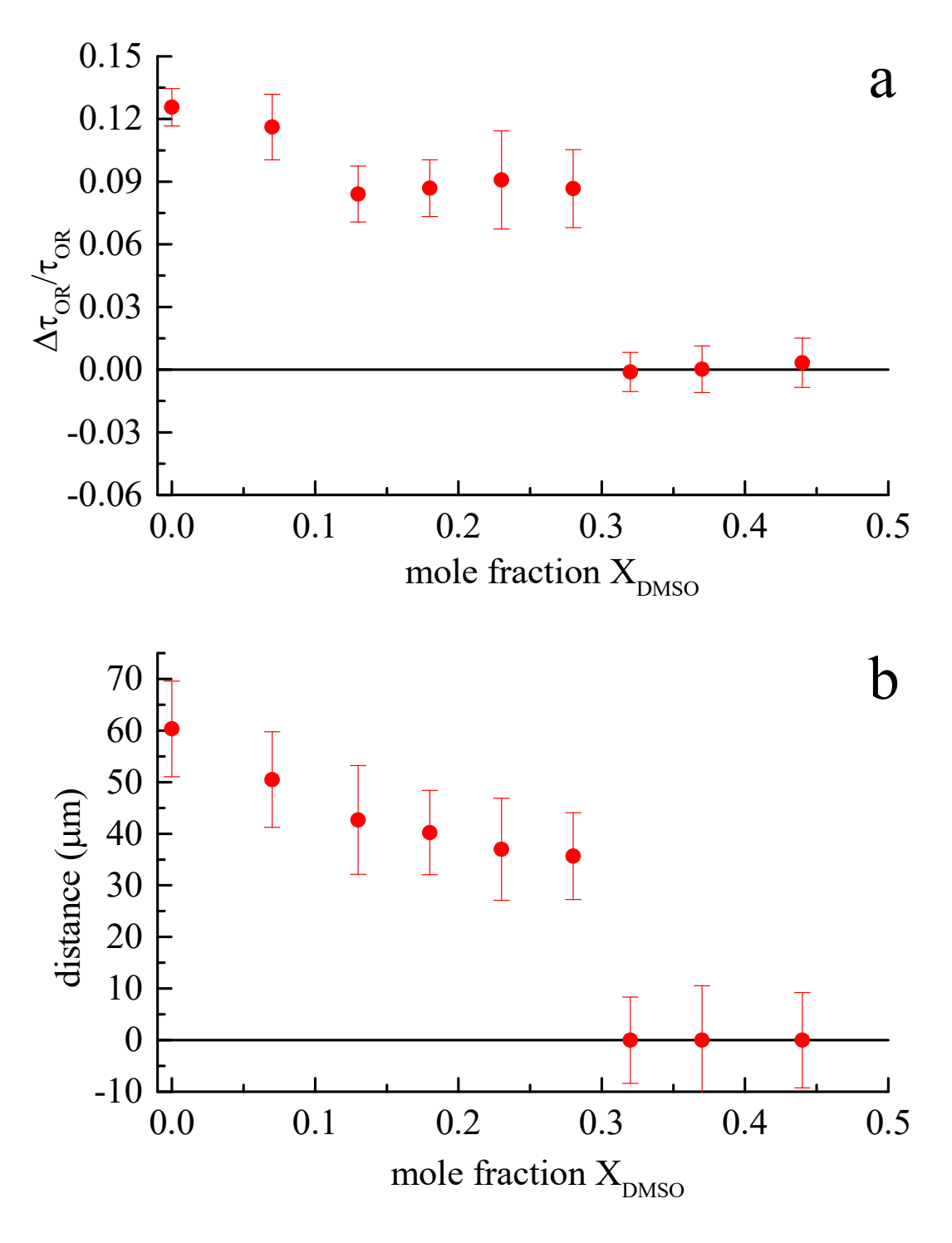


Figure 5.3 (a) Magnitude of ρ_f , expressed as $\Delta \tau_{OR}/\tau_{OR}$ and (b) persistence length of ρ_f , as a function of mole fraction of DMSO diluent for BMIM⁺BF₄⁻.

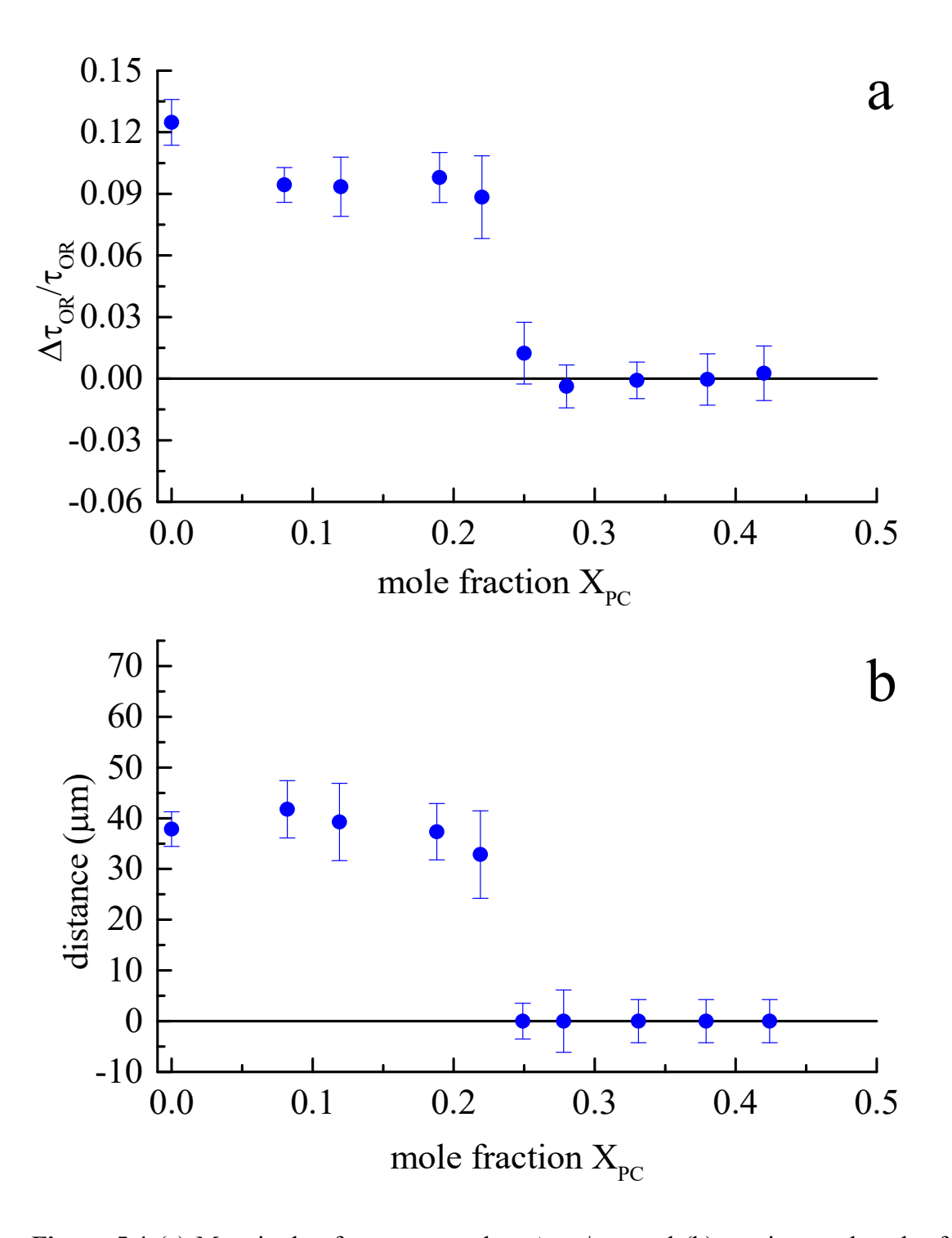


Figure 5.4 (a) Magnitude of ρ_f , expressed as $\Delta \tau_{OR}/\tau_{OR}$ and (b) persistence length of ρ_f , as a function of mole fraction of PC diluent for BMIM⁺TFSI⁻.

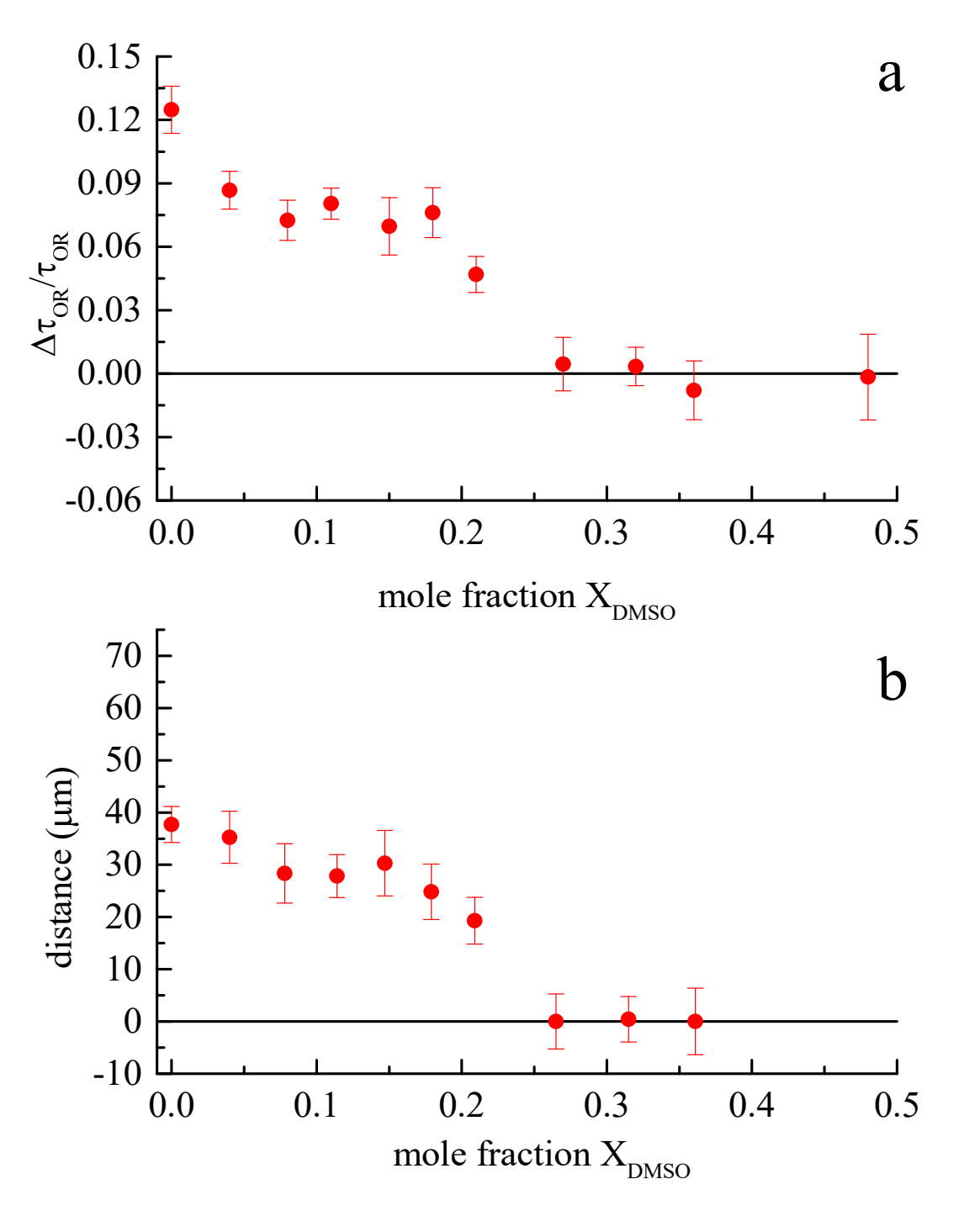


Figure 5.5 (a) Magnitude of ρ_f , expressed as $\Delta \tau_{OR}/\tau_{OR}$ and (b) persistence length of ρ_f , as a function of mole fraction of DMSO diluent for BMIM⁺TFSI⁻.

When the data in Figs. 5.2-5.5 are viewed as a function of dilution, ρ_f is seen to diminish slightly until ca. $X_{diluent} \sim 0.3$ for BMIM⁺BF₄⁻ in both DMSO and PC, and the same behavior is seen until ca. $X_{diluent} \sim 0.2$ for BMIM⁺TFSI⁻ in both solvents. These data suggest again that the RTIL anion plays an important role in supporting ρ_f . The functional form of the data presented in Figs. 5.2-5.5 are not consistent with the formation of homogeneous solutions with the RTILs and the diluents. In a homogeneous solution, ion mobility would be proportional to the bulk viscosity of the solution and the collapse of ρ_f would be a smooth function of dilution. The persistence length would also be expected to diminish rapidly with the addition of diluent and neither of these predictions are consistent with the data. We are thus left to conclude that the RTIL-DMSO and RTIL-PC systems are both spatially heterogeneous and turn to consideration of how to characterize and account for the heterogeneity in these binary systems.

For both neat RTILs, the value of $(\Delta \tau_{OR}/\tau_{OR})(\infty)$ is achieved when the (con)focal plane of the microscope objective is ca. 200 μ m above the charged support surface plane. We can measure τ_{OR} for CV⁺ at a depth of 200 μ m into the RTIL as a function of dilution. The dependence of CV⁺ reorientation on medium viscosity should be predicted by Eq. 5.2 for a homogeneous medium where the bulk viscosity of the binary systems has been reported. We show the comparison between the experimental data (points) and the predictions of Eq. 5.2 (lines) where bulk viscosity was used in the calculations of BMIM⁺BF4⁻ diluted with PC (Fig. 5.6) and DMSO (Fig. 5.7), and for BMIM⁺TFSI⁻ diluted with PC (Fig. 5.8) and DMSO (Fig. 5.9). There is a clear difference between the data and the predictions of Eq. 5.2.

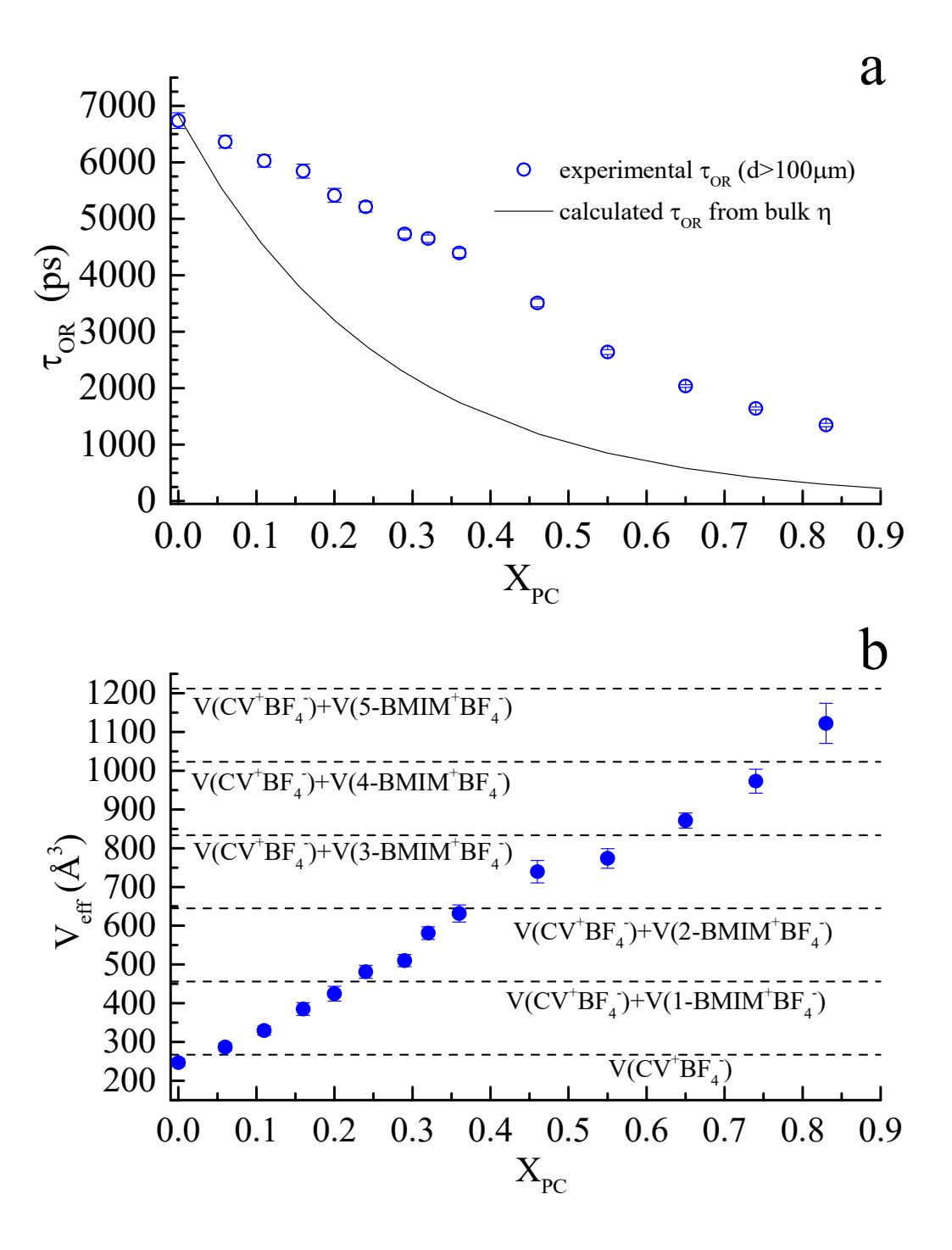


Figure 5.6 (a) Experimental reorientation time constant, τ_{OR} , for CV⁺ in BMIM⁺BF₄⁻ as a function of dilution with PC (open circles). Predicted τ_{OR} values based on Eq. 2 using bulk viscosity data for BMIM⁺BF₄⁻ as a function of dilution with PC (solid line). (b) Effective hydrodynamic volume, V_{eff} , of the reorienting entity as a function of dilution, calculated using Eq. 2 and bulk viscosity data. Dashed lines indicate effective volumes for aggregates with specific numbers of RTIL ion pairs.

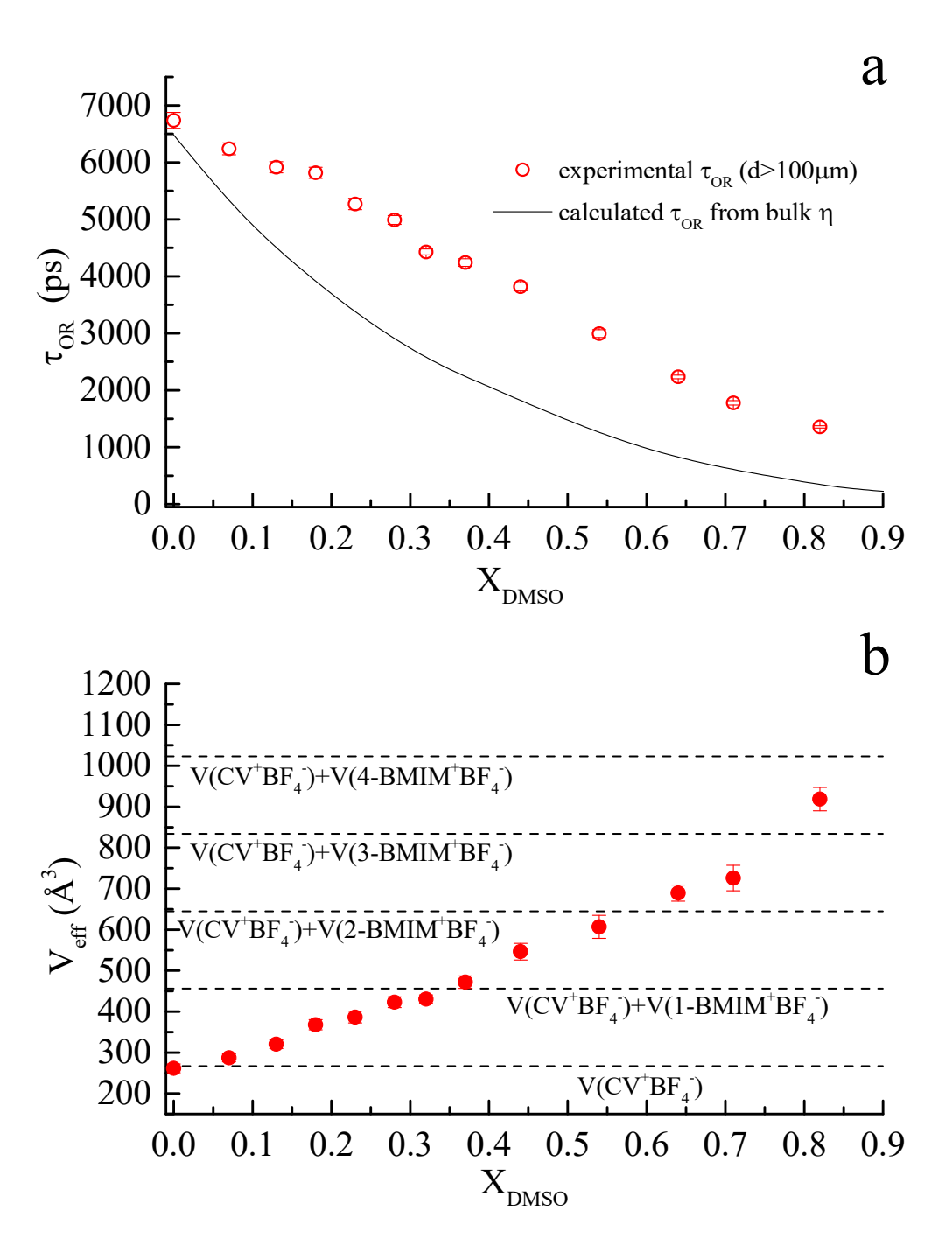


Figure 5.7 (a) Experimental reorientation time constant, τ_{OR} , for CV⁺ in BMIM⁺BF₄⁻ as a function of dilution with DMSO (open circles). Predicted τ_{OR} values based on Eq. 2 using bulk viscosity data for BMIM⁺BF₄⁻ as a function of dilution with DMSO (solid line). (b) Effective hydrodynamic volume, V_{eff} , of the reorienting entity as a function of dilution, calculated using Eq. 2 and bulk viscosity data. Dashed lines indicate effective volumes for aggregates with specific numbers of RTIL ion pairs.

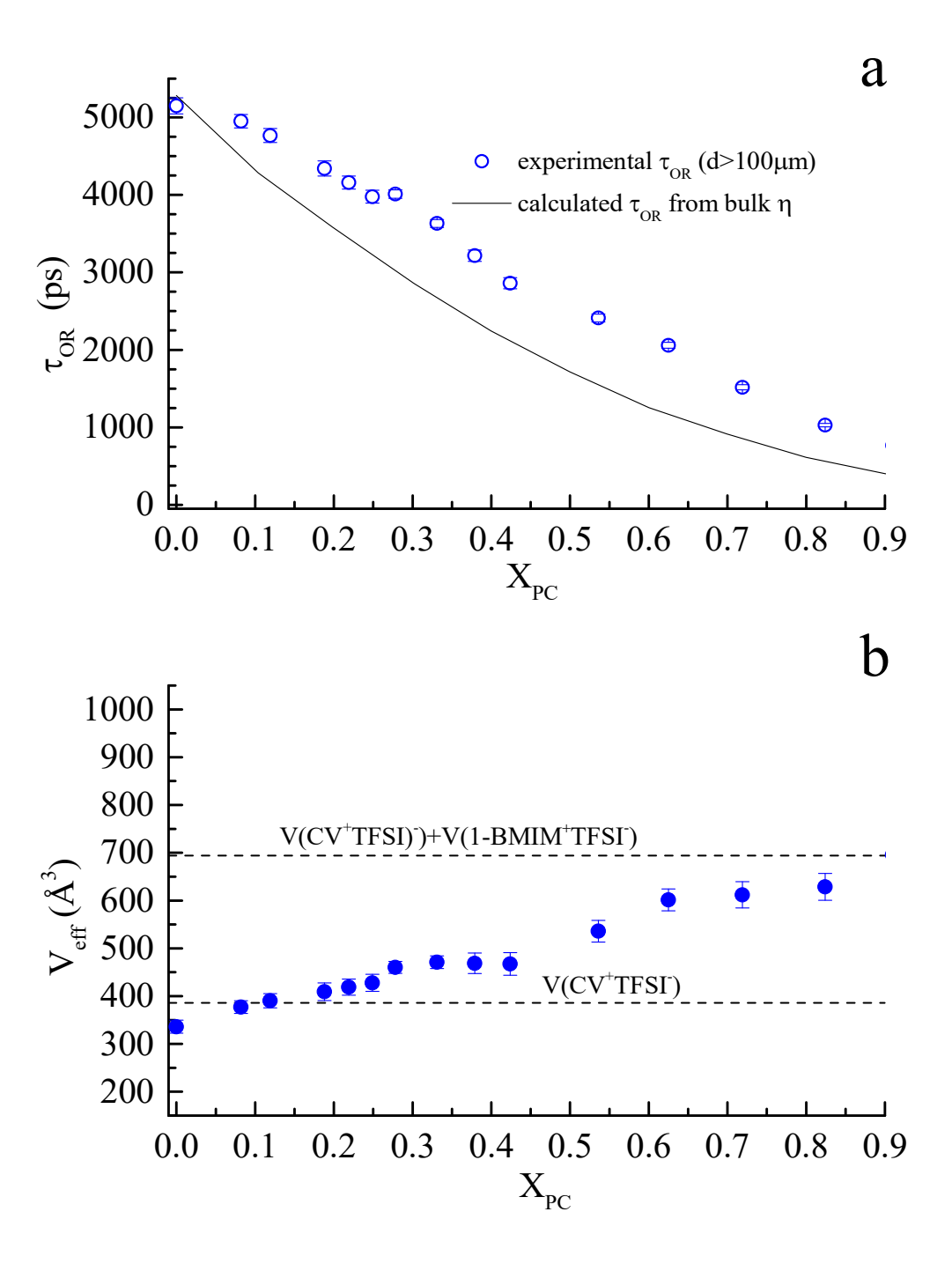


Figure 5.8 (a) Experimental reorientation time constant, τ_{OR} , for CV⁺ in BMIM⁺TFSI⁻ as a function of dilution with PC (open circles). Predicted τ_{OR} values based on Eq. 2 using bulk viscosity data for BMIM⁺TFSI⁻ as a function of dilution with PC (solid line). (b) Effective hydrodynamic volume, V_{eff} , of the reorienting entity as a function of dilution, calculated using Eq. 2 and bulk viscosity data. Dashed lines indicate effective volumes for aggregates with specific numbers of RTIL ion pairs.

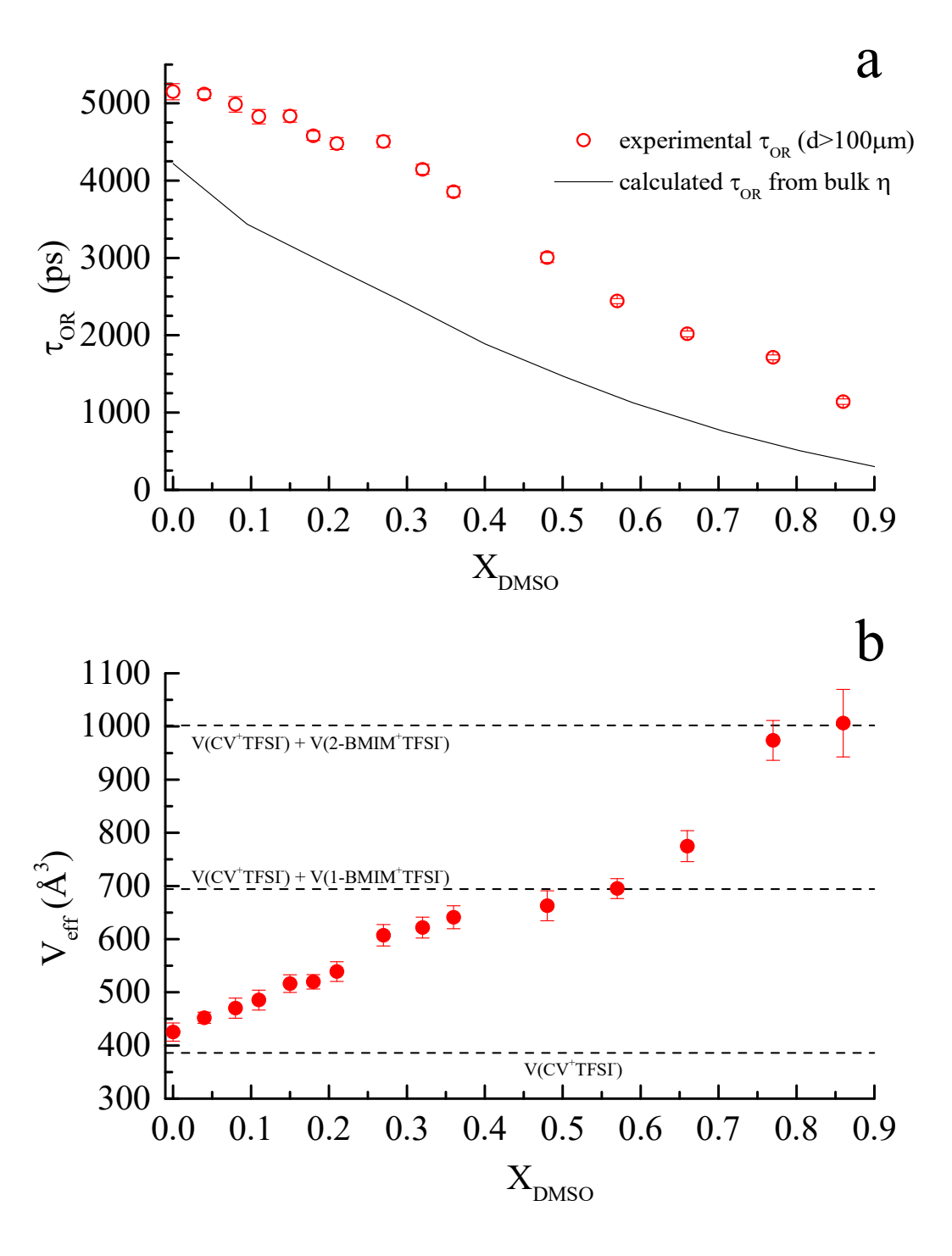


Figure 5.9 (a) Experimental reorientation time constant, τ_{OR} , for CV⁺ in BMIM⁺TFSI⁻ as a function of dilution with DMSO (open circles). Predicted τ_{OR} values based on Eq. 2 using bulk viscosity data for BMIM⁺TFSI⁻ as a function of dilution with DMSO (solid line). (b) Effective hydrodynamic volume, V_{eff} , of the reorienting entity as a function of dilution, calculated using Eq. 2 and bulk viscosity data. Dashed lines indicate effective volumes for aggregates with specific numbers of RTIL ion pairs.

There are several possible explanations for the discrepancy between model and experiment. The numerator in Eq. 5.2 contains three terms, the viscosity of the medium, η , the hydrodynamic volume of the rotating entity, and a frictional term, f, describing the interactions between the rotor and its immediate environment. The viscosity is taken to be the bulk viscosity of the medium, a quantity that is measured macroscopically. Solvent-solvent frictional interactions between like molecules will not be the same as those between solvent and rotor, and the correction for this difference is treated through the term f. For high-friction interactions, the so-called stick limit, f= 1, and changes in this frictional term have been described as the slip limit, where $0 \le f \le 1$, with the value of f depending on the ellipsoidal rotor shape. 43-44 The DSE model assumes the solvent surrounding the rotating moiety is a dielectric continuum, an assumption that is adequate in the limit of the solvent molecules being much smaller than the rotor. 42 This limit does not obtain for the systems under consideration. Gierer and Wirtz have reported a means to account for changes in the frictional term based on the relative sizes of the solvent molecules and the rotating entity, 50 and Prabhu and Dutt have applied this correction to ionic liquid/molecular solvent binary In that work, they also observed a discrepancy between DSE predictions and systems.³⁷ experimental data, but application of the Gierer-Wirtz correction was not sufficient to account for the difference. Attempts to account for the difference between experiment and model for the data shown in Figs. 5.6a-5.9a using this correction were likewise not successful. For the difference between experimental data and the predictions of the modified DSE model based on frictional interactions would require values of f that change with dilution and in all cases, f would have to exceed unity. This is considered to be the "super stick" limit, but there is no widely accepted model to describe such interactions.

Considering that the difference between experiment and model can be accounted for in the

context of the hydrodynamic volume of the rotating entity offers the opportunity to consider molecular association as a contributing factor to the observed dynamics. Treating the data in this context is consistent with the RTIL-solvent binary system exhibiting heterogeneity (*vide supra*).³⁴

We have calculated the hydrodynamic volumes of the species relevant to this work using the method of van der Waals increments (Table 5.1).^{34, 45}

Table 5.1 Hydrodynamic volumes of system constituents

Species	V (Å ³)
BMIM ⁺	139
TFSI ⁻	169
BF ₄	50
CV^+	217
PC	83
DMSO	75

The bulk viscosity for RTIL-solvent binary systems has been reported previously, $^{46-49}$ where the viscosity measurements were made using bulk techniques. From these data we calculate values of τ_{OR} using Eq. 5.2 where the volume of the rotating entity is taken as 217 Å³ (CV⁺). These calculated results are shown as solid lines in Figs. 5.6a-5.9a. The experimental hydrodynamic volume of the reorienting entity is shown as a function of RTIL-solvent composition in Figs. 5.6b-5.9b. There are several noteworthy features contained in these data. The first is that in neat RTILs, the rotational diffusion time constant is consistent with that of CV⁺ associated with the RTIL anion rotating with a stick-limit friction coefficient (f = 1). With the addition of solvent to the RTIL and

the use of bulk viscosity data⁴⁶⁻⁴⁹ in Eq. 5.2, the effective volume (V_{eff}) of the reorienting entity increases, and this trend is seen for all systems examined here. The horizontal dashed lines in Figs. 5.6b-5.9b represent the hydrodynamic volumes of the chromophore-RTIL anion and integer numbers of RTIL ion pairs, as indicated in Eq. 5.3.

$$V_{aggregate} = V_{CV-RTIL\ anion} + nV_{RTIL\ ion\ pair}$$
[5.3]

where $V_{CV-RTIL\ anion}$ is the hydrodynamic volume of CV^+ -BF₄ or CV^+ -TFSI, depending on the RTIL used, $V_{RTIL\ ion\ pair}$ is the volume of BMIM⁺BF₄ or BMIM⁺TFSI and n is number of RTIL ion pairs. Because of the dynamic nature of any liquid phase system, the average lifetime of the aggregate will contribute to the apparent volume, as sensed on the timescale of the anisotropy decay time. It is thus not necessary for n to take on integer values. This finding has precedent and there are several implications of these findings. $^{34,\,51-54}$

The functional form of the V_{eff} data is not consistent with the rotating entity undergoing rotational diffusion in a uniform medium. Rather, these data are consistent with the RTIL-molecular solvent binary system existing as a compositionally heterogeneous medium. Since the RTIL and molecular solvents do not appear to produce phase segregation in any proportion, it is not appropriate to consider this system as a mixture, but the size of the RTIL aggregates observed here suggests that analogy to either a nano-emulsion or a micellar system is apt. While there is precedent for the description of RTIL-water systems in the context of micellar behavior, $^{22,26-33}$ we do not attempt to make that case here. The non-homogeneous nature of the RTIL-molecular solvent binary system is consistent with the functional form of the dilution-dependence of ρ_f and d seen in these systems (Figs. 5.2-5.5). A corollary implication of this persistent heterogeneity is that the means by which ρ_f is supported in RTILs is not mediated by the mobility of individual dissociated ions, at least for modest dilution. This assertion is based on the expectation that, if the RTIL-

molecular solvent system was homogeneous, then dissociation of the RTIL would lead to ions exhibiting translational mobility determined by the viscosity of the medium, ⁴⁰⁻⁴¹ and such a condition would lead at the least to a reduction in the persistence length of ρ_f , if not the magnitude, in a continuous manner that monotonically approaches $\rho_f = 0$ with increasing dilution. The discontinuous nature of this trend (Figs. 5.2-5.5) argues against this prediction.

It is also important to note that there is a qualitative similarity in the functional form of the data for RTIL dilution in DMSO and PC to the analogous data where methanol and acetonitrile are used as diluents.³⁴ This finding is important not only because it points to the generality of this behavior for RTILs, but also because the mobility of ions in methanol and acetonitrile is expected to be substantially higher than in DMSO and PC. Despite the differences in these solvents, the persistence of ρ_f and the characteristic length scale, d, are essentially the same in all solvents, suggesting that the magnitude of ρ_f is determined primarily by the support surface charge density, σ_5 , and the persistence length is best explained either on a physical rather than a chemical basis, or is mediated by the RTIL and the properties of the molecular solvent diluent play a secondary role. Elucidating the primary factors responsible for the magnitude and persistence of d (Eq. 5.3) is a topic that remains under investigation.

Notwithstanding the qualitative similarities discussed above, there is a discernible difference in the extent of aggregation for BMIM⁺BF₄⁻ and BMIM⁺TFSI⁻ in DMSO and PC. Specifically, the aggregation of BMIM⁺BF₄⁻ appears more prominently, *i.e.* is consistent with greater numbers of RTIL ion pairs in the aggregates for a given extent of dilution, than is seen for BMIM⁺TFSI⁻. The clear implication is that the extent of aggregation of RTILs in these and other molecular solvents is determined primarily by RTIL properties. The properties that could be responsible for such difference in behavior must necessarily have to be concerned with strength of

interaction between RTIL ion pairs. While it may be tempting to relate the equilibrium constant for RTIL ion pair dissociation to these differences, we do not attempt to do so. We refrain from this comparison because the accurate determination of Keq for these and other RTILs remains to be achieved, although there are indications that many RTILs exhibit ca. 50% dissociation when not diluted. 56 Unfortunately, there is very little information available on K_{eq} for RTILs when diluted with molecular solvents. RTIL ion pairs can be considered in the context of being a single molecular entity when associated and thus they exhibit a dipole moment that depends on the structure of the ion pair. We understand that there will be a variety of configurations for RTIL ion pairs, but we can estimate the lowest energy conformation with the aid of semi-empirical calculations. We show the results of those calculations for RTIL ion pairs, optimized geometrically at the semi-empirical level in Fig. 5.10. We recognize that these calculations are not quantitatively accurate but, owing to the complexity of the ion paired system in an aggregated format, achieving a quantitative determination of system properties could be challenging. Despite the limitations of computations at this level, the dipole moments for BMIM+TFSI and BMIM+BF4 ion pairs are different by a factor of ca. 2, and that difference is sufficient to account for the greater propensity of BMIM⁺BF₄ ion pairs to aggregate in molecular solvents, presuming dipole-dipole interactions play a significant role in aggregate formation. The similarity of the dipole moments for PC ($\mu =$ 4.9 D) and DMSO ($\mu = 4.1$ D) is consistent with the finding that the extent of aggregation in these systems is determined to a significant extent by the dipole moments of the RTIL ion pairs.⁵⁶ To provide a qualitative estimate of the difference in strength of interaction, the portion of the intermolecular interactions mediated by dipole-dipole interactions is expected to be stronger by a factor of ca. 19 for BMIM⁺BF₄⁻ than for BMIM⁺TFSI based on the relative values of the calculated dipole moments.

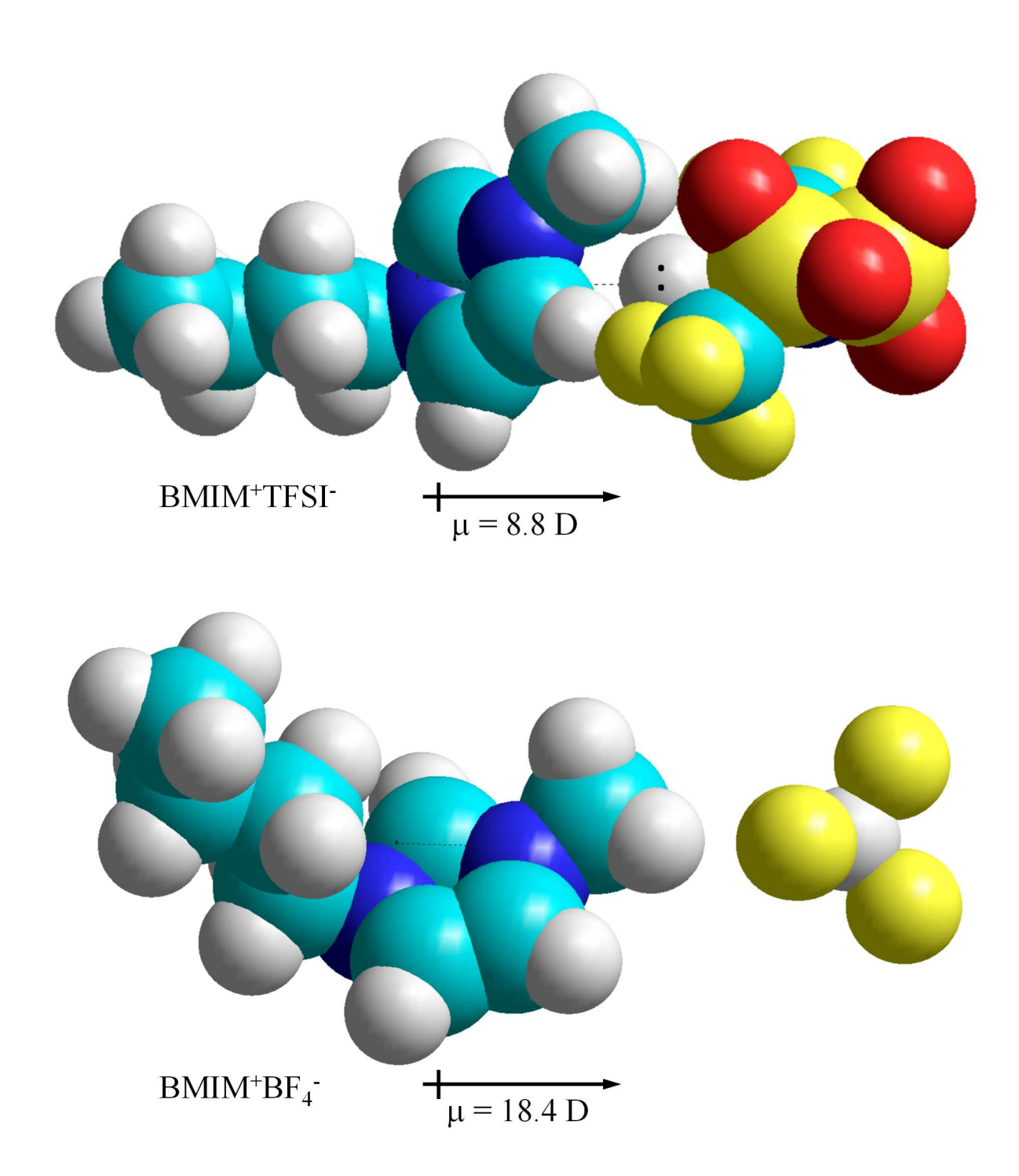


Figure 5.10 (top) BMIM⁺TFSI⁻ ion pair structure calculated at the semi-empirical level with PM3 parameterization. Dipole moment is calculated to be 8.8 D. (bottom) BMIM⁺BF₄⁻ ion pair structure calculated at the semi-empirical level with PM3 parameterization. Dipole moment is calculated to be 18.4 D. (bottom)

5.4 Conclusions

We have reported on the effects of dilution of two imidazolium-based RTILs with two dipolar aprotic solvents, PC and DMSO. Our data on the dependence of the charge-induced free charge density gradient, rf, in these binary systems show that the magnitude and persistence length of ρ_f do not vary in a continuous, monotonic manner with extent of dilution. Rather, there is an abrupt change in the ability of the system to support ρ_f at dilutions of ca. $X_{diluent} = 0.2$ for BMIM⁺TFSI⁻ and ca. $X_{diluent} = 0.3$ for BMIM⁺BF₄⁻. These findings are qualitatively consistent with what has been seen with other solvents.³⁴ and their functional form demonstrates that RTILmolecular solvent binary systems exhibit compositional heterogeneity. Examination of the reorientation dynamics of the probe fluorophore CV⁺ for higher dilutions demonstrates the persistence of compositional heterogeneity, with the size of RTIL aggregates increasing with increasing dilution. Aggregates were seen to be larger for BMIM⁺BF₄⁻ than for BMIM⁺TFSI⁻ in each diluent, consistent with the calculated difference in dipole moment for the RTIL ion pairs. Overall, these findings underscore the importance of dipolar interactions in determining the observed properties of RTILs and suggest that the ability of this class of materials to support a charge density gradient over tens of micrometers is not determined primarily by ion mobility in the binary systems. Further work is underway to elucidate the physical and chemical basis for these materials being able to support ρ_f over macroscopic length scales.

REFERENCES

- 1. Arbizzani, C.; Biso, M.; Cericola, D.; Lazzari, M.; Soavi, F.; Mastragostino, M., Safe, high-energy supercapacitors based on solvent-free ionic liquid electrolytes. *J. Pwr. Sources* **2008**, *185*, 1575 1579.
- 2. MacFarlane, D. R.; Tachikawa, N.; Forsyth, M.; Pringle, J. M.; Howlett, P. C.; Elliott, G. D.; Davis, J. H.; Watanabe, M.; Simon, P.; Angell, C. A., Energy applications of ionic liquids. *Energ. Env. Sci.* **2014**, *7*, 232 250.
- 3. Nabity, J. A.; Daily, J. W., Effect of Ionic Liquid Composition on Colloid Thruster Emission and Thrust Performance. *J. Propul. Pwr.* **2017**, *34* (1), 260-266.
- 4. Newell, R.; Faure-Vincent, J.; Iliev, B.; Schubert, T.; Aradilla, D., A new high performance ionic liquid mixture electrolyte for large temperature range supercapacitor applications (- 70° C to 80° C) operating at 3.5 V cell voltage. *Electrochim. Acta.* **2018**, *267*, 15 19.
- 5. Sakaebe, H.; Matsumoto, H., N-Methyl-N-propylpiperidinium bis(trifluoromethane sulfonyl)imide (PP13–TFSI)–novel electrolyte base for Li battery. *Electrochem. Commun.* **2003**, *5*, 594 598.
- 6. Van Aken, K. L.; Beidaghi, M.; Gogotsi, Y., Formulation of ionic liquid electrolyte to expand the voltage window of supercapacitors. *Angew. Chem.* **2015**, *127*, 4888 4891.
- 7. Anaredy, R. S.; Shaw, S. K., Long-Range Ordering of Ionic Liquid Fluid Films. *Langmuir* **2016**, *32*, 5147-5154.
- 8. Anaredy, R. S.; Shaw, S. K., Developing Distinct Chemical Environments in Ionic Liquid Films. *J. Phys. Chem. C* **2018**, *122*, 19731-19737.
- 9. Anaredy, R. S.; Shaw, S. K., Directing long-range molecular ordering in ionic liquid films: A tale of two interfaces. *J. Phys. Chem. C* **2019**, *123*, 8975-8982.
- 10. Israelachvili, J. N.; Min, Y.; Akbulut, M.; Alig, A.; Carver, G.; Greene, W.; Kristiansen, K.; Meyer, E.; Pesika, N.; Rosenberg, K., et al., Recent advances in the surface forces apparatus (SFA) technique. *Rep. Prog. Phys.* **2010**, *73*, 036601.
- 11. Ma, K.; Jarosova, R.; Swain, G. M.; Blanchard, G. J., Charge-Induced Long-Range Order in a Room-Temperature Ionic Liquid. *Langmuir* **2016**, *32*, 9507-9512.
- 12. Ma, K.; Jarosova, R.; Swain, G. M.; Blanchard, G. J., Modulation of an Induced Charge Density Gradient in the Room-Temperature Ionic Liquid BMIM⁺BF₄-. *J. Phys. Chem. C* **2018**, *122*, 7361-7367.
- 13. Nishida, J.; Breen, J. P.; Wu, B.; Fayer, M. D., Extraordinary slowing of structural dynamics in thin films of a room temperature ionic liquid. *ACS Cent. Sci.* **2018**, *4*, 1065-1073.

- 14. Shin, J. Y.; Yamada, S. A.; Fayer, M. D., Dynamics of a room temperature ionic liquid in supported ionic liquid membranes vs the bulk liquid: 2D IR and polarized IR pump-probe experiments. *J. Am. Chem. Soc.* **2017**, *139*, 311-323.
- 15. Shin, J. Y.; Yamada, S. A.; Fayer, M. D., Carbon dioxide in a supported ionic liquid membrane: Structural and rotational dynamics measured with 2D IR and pump-probe experiments. *J. Am. Chem. Soc.* **2017**, *139*, 11222-11232.
- 16. Thomaz, J. E.; Bailey, H. E.; Fayer, M. D., The influence of mesoscopic confinement on the dynamics of imidazolium-based room temperature ionic liquids in polyether sulfone membranes. *J. Chem. Phys.* **2017**, *147*, 194502.
- 17. Wang, Y.; Jarosova, R.; Swain, G. M.; Blanchard, G. J., Characterizing the magnitude and structure-dependence of free charge density gradients in room temperature ionic liquids. *Langmuir* **2020**, *36*, 3038-3045.
- 18. Wang, Y.; Parvis, F.; Hossain, M. I.; Ma, K.; Jarosova, R.; Swain, G. M.; Blanchard, G. J., Local and Long-Range Organization in Room Temperature Ionic Liquids. *Langmuir* **2021**, *37*, 605-615.
- 19. Wang, Y.; Swain, G. M.; Blanchard, G. J., Charge-induced birefringence in a room-temperature ionic liquid. *J. Phys. Chem. B* **2021**, *125*, 950-955.
- 20. Wu, B.; Breen, J. P.; Fayer, M. D., Structural dynamics in ionic liquid thin films: The effect of cation chain length. *J. Phys. Chem. C* **2020**, *124*, 4179-4189.
- 21. Wu, B.; Breen, J. P.; Xing, X.; Fayer, M. D., Controlling the dynamics of ionic liquid thin films via multilayer surface functionalization. *J. Am. Chem. Soc.* **2020**, *142*, 9482-9492.
- 22. Feng, S.; Voth, G. A., Molecular dynamics simulations of imidasolium-based ionic liquid/water mixtures: Alkyl side chain length and anion effects. *Fluid Phase Eq.* **2010**, *294*, 148-156.
- 23. Jiang, W.; Wang, Y.; Voth, G. A., Molecular Dynamics Simulation of Nanostructural Organization in Ionic Liquid/Water Mixtures. *J. Phys. Chem. B* **2007**, *111*, 4812-4818.
- 24. Wang, Y.; Jiang, W.; Yan, T.; Voth, G. A., Understanding Ionic Liquids through Atomistic and Coarse-Grained Molecular Dynamics Simulations. *Acc. Chem. Res.* **2007**, *40*, 1193-1199.
- 25. Wang, Y.; Voth, G. A., Unique Spatial Heterogeneity in Ionic Liquids. *J. Am. Chem. Soc.* **2005**, *127*, 12192-12193.
- 26. Blesic, M.; Marques, M. H.; Plechkova, N. V.; Seddon, K. R.; Rebelo, L. P. N.; Lopes, A., Self-aggregation of ionic liquids: micelle formation in aqueous solution. *Green Chem.* **2007**, *9*, 481-490.

- 27. Chen, S.; Zhang, S.; Liu, X.; Wang, J.; Wang, J.; Dong, K.; Sun, J.; Xu, B., Ionic liquid clusters: Structure, formation, mechanism, and effect on the behavior of ionic liquids. *Phys. Chem. Phys.* **2014**, *16*, 5893-5906.
- 28. Dong, B.; Li, N.; Zheng, L.; Yu, L.; Inoue, T., Surface Adsorption and Micelle Formation of Surface Active Ionic Liquids in Aqueous Solution. *Langmuir* **2007**, *23*, 4178-4182.
- 29. Inoue, T.; Ebina, H.; Dong, B.; Zhang, L., Electrical conductivity study on micelle formation of long-chain imidazolium ionic liquids in aqueous solution. *J. Coll. Int. Sci.* **2007**, *314*, 236-241.
- 30. Miskolczy, Z.; Sebok-Nagy, K.; Biczok, L.; Gokturk, S., Aggregation and micelle formation of ionic liquids in aqueous solution. *Chem. Phys. Lett.* **2004**, *400*, 296-300.
- 31. Singh, T.; Kumar, A., Aggregation Behavior of Ionic Liquids in Aqueous Solutions: Effect of Alkyl Chain Length, Cations, and Anions. *J. Phys. Chem. B* **2007**, *111*, 7843-7851.
- 32. Sirieix-Plenet, J.; Gaillon, L.; Letellier, P., Behaviour of a binary solvent mixture constituted by an amphiphilic ionic liquid, 1-decyl-3-methylimidazolium bromide and water. Potentiometric and conductometric studies. *Talanta* **2004**, *63*, 979-986.
- 33. Zhang, L.; Xu, Z.; Wang, Y.; Li, H., Prediction of the Solvation and Structural Properties of Ionic Liquids in Water by Two-Dimensional Correlation Spectroscopy. *J. Phys. Chem. B* **2008**, *112*, 6411-6419.
- 34. Hossain, M. I.; Blanchard, G. J., The effect of dilution on induced free charge density gradients in room temperature ionic liquids. *Phys. Chem. Chem. Phys.* **2022**, *24*, 3844-3853
- 35. Marekha, B. A.; Kalugin, O. N.; Bria, M.; Buchner, R.; Idrissi, A., Translational Diffusion in Mixtures of Imidazolium ILs with Polar Aprotic Molecular Solvents. *J. Phys. Chem. B* **2014**, *118*, 5509-5517.
- 36. Prabhu, S. R.; Dutt, G. B., Rotational diffusion of organic solutes in 1-methyl-3-octylimidazolium tetrafluoroborate-diethylene glycol mixtures: Influence of organic solvent on the organized structure of the ionic liquid. *J. Phys. Chem. B* **2014**, *118*, 5562-5569.
- 37. Prabhu, S. R.; Dutt, G. B., Effect of low viscous nondipolar solvent on the rotational diffusion of structurally similar nondipolar solutes in an ionic liquid. *J. Phys. Chem. B* **2015**, *119*, 2019-2025.
- 38. Peiris, T. A. N.; Senthilarasu, S.; Wijayantha, K. G. U., Enhanced performance of flexible dye-sensitized solar cells: Electrodeposition of Mg(OH)₂ on a nanocrystalline TiO₂ electrode. *J. Phys. Chem. C* **2011**, *116*, 1211-1218.

- 39. Hay, C. E.; Marken, F.; Blanchard, G. J., Detection and Characterization of Liquid|Solid and Liquid|Liquid|Solid Interfacial Gradients of Water Nanodroplets in Wet N-Octyl-2-Pyrrolidone. *Langmuir* **2014**, *30*, 9951-9961.
- 40. Einstein, A., Uber die von der molekularkinetischen Theorie der Warme geforderteBewegung von in ruhenden Flussigkeiten suspendierten Teilchen. *Ann. der Phys.* **1905**, 322, 549-560.
- 41. Sutherland, W., A dynamical theory of diffusion for non-electrolytes and the molecular mass of albumin. *Philos. Mag.* **1905**, *9*, 781-785.
- 42. Debye, P., *Polar Molecules* Chemical Catalog Co.: New York 1929; p 84.
- 43. Hu, C.-M.; Zwanzig, R., Rotational friction coefficients for spheroids with the slipping boundary condition. *J. Chem. Phys.* **1974**, *60* (11), 4354-4357.
- 44. Perrin, F., Mouvement brownien d'un ellipsoide I. Dispersion diélectrique pour des molécules ellipsoidales. *J. Phys. Radium* **1934,** *5*, 497.
- 45. Edward, J. T., Molecular volumes and the Stokes-Einstein equation. *J. Chem. Ed.* **1970**, 47, 261-270.
- 46. Ciocirlan, O.; Croitoru, O.; Iulian, O., Densities and viscosities for binary mixtures of 1-butyl-3-methylimidazolium Tetrafluoroborate Ionic Liquid with molecular solvents. *J. Chem. Eng. Data* **2011**, *56*, 1526-1534.
- 47. Stoppa, A.; Hunger, J.; Buchner, R., Conductivities of Binary Mixtures of Ionic Liquids with Polar Solvents. *J. Chem. Eng. Data* **2009**, *54*, 472-479.
- 48. Vranes, M.; Zec, N.; Tot, A.; Papovic, S.; Dozic, S.; Gadzric, S., Density, electrical conductivity, viscosity and excess properties od 1-butyl-3-methylimidazolium bis(trifluoromethylsulfonyl)imide + propylene carbonate binary mixtures. *J. Chem. Thermo.* **2014**, *68*, 98-108.
- 49. Yasmeen, S.; Riyazuddeen; Anwar, N., Interaction of 1-butyl-2-methylimidazolium bis(trifluoromethylsulfonyl)-imide with methanol/dimethyl sulfoxide at (298.15, 303.15, 308.15, 313.15, 318.15 and 323.15) K: Measurements and correlations of thermophysical properties. *J. Mol. Liq.* **2016**, *221*, 1207-1217.
- 50. Gierer, A.; Wirtz, K., Molekulare Theorie der Mikroreibung. Z. Naturforsch. A 1953, 8, 532-538.
- 51. Blanchard, G. J., A study of the state-dependent reorientation dynamics of oxazine-725 in primary normal aliphatic alcohols. *J. Phys. Chem.* **1988**, *92*, 6303-6307.

- 52. Blanchard, G. J., The State Dependent Reorientation of Methylene Blue: The Role of Dipolar Solvent-Solute Interactions. *J. Phys. Chem.* **1989**, *93*, 4315-4319.
- 53. Blanchard, G. J., Counterion-dependent reorientation dynamics of an oxazine in polar protic and aprotic solvents *J. Phys. Chem.* **1991**, *95*, 5293-5299.
- 54. De, C. K.; Ghosh, A.; Mandal, P. K., Hydrophobicity-Dependent Heterogeneous Nanoaggregates and Fluorescence Dynamics in Room Temperature Ionic Liquids. *J. Phys. Chem. B* **2022**, *126*, 1551-1557.
- 55. Nordness, O.; Brennecke, J. F., Ionic dissociation in ionic liquids and ionic liquid solutions. *Chem. Rev.* **2020**, *120*, 12873-12902.
- 56. Rajbangshi, J.; Biswas, R., Heterogeneous dynamics in [BMIM][PF₆] + Cosolvent binary Mixtures: Does It depend upon cosolvent Polarity? *J. Mol. Liq.* **2021**, *341*, 117342.

CHAPTER 6. Relating the Induced Free Charge Density Gradient in a Room Temperature Ionic Liquid to Molecular-Scale Organization
Adapted with permission form:
Md. Iqbal Hossain, Laxmi Adhikari, Gary A. Baker and G. J. Blanchard; Relating the Induced Free Charge Density Gradient in a Room Temperature Ionic Liquid to Molecular-Scale Organization. J. Phys. Chem. B 2023, 127, 8, 1780-1788.

6.1 Introduction

Ionic liquids have proven to be remarkably versatile materials, finding application in areas ranging from supercapacitor electrolytes¹⁻² to organic synthesis,³⁻⁵ carbon capture⁶⁻¹² and ion propulsion. ¹³⁻¹⁴ Despite the broad utility of these materials, much remains to be understood about their properties from a fundamental perspective. For example, there has remained significant uncertainty over the extent to which RTILs dissociate until recently,¹⁵ and the relative importance of association and dissociation vs. ion translational mobility in mediating conductivity remains an open question. In addition, ionic liquids have been shown to exhibit a free charge density gradient, ρ_5 with a spatial extent of ca. 50 μ m, induced by placing the RTIL in contact with a charged surface, ¹⁶⁻²¹ and this gradient persists upon dilution. ²²⁻²³ In addition to the potential practical implications of these unusual RTIL properties for optical, electronic and other applications, neither of these findings are consistent with the behavior of molecular liquids and understanding them from a fundamental perspective requires further investigation.

The existence of order in RTILs is well-established, although the details of the reported order have, to this point, been dependent on the means by which the order was observed. The Fayer group has reported organization over a length scale of hundreds of nm using vibrational molecular probes, $^{24-28}$ and organization on the μ m length scale has been seen by the Shaw group in thin RTIL films. $^{29-30}$ There is also a significant body of x-ray $^{31-36}$ and neutron $^{37-41}$ scattering data pointing to single nm-scale order in RTILs, and these findings are supported by modeling studies. $^{42-50}$ Because of the extensive body of information on organization in RTILs and the existence of ρ_T in these materials, we are interested in better understanding the relationship between this phenomenon and molecular- and longer-scale organization in these systems.

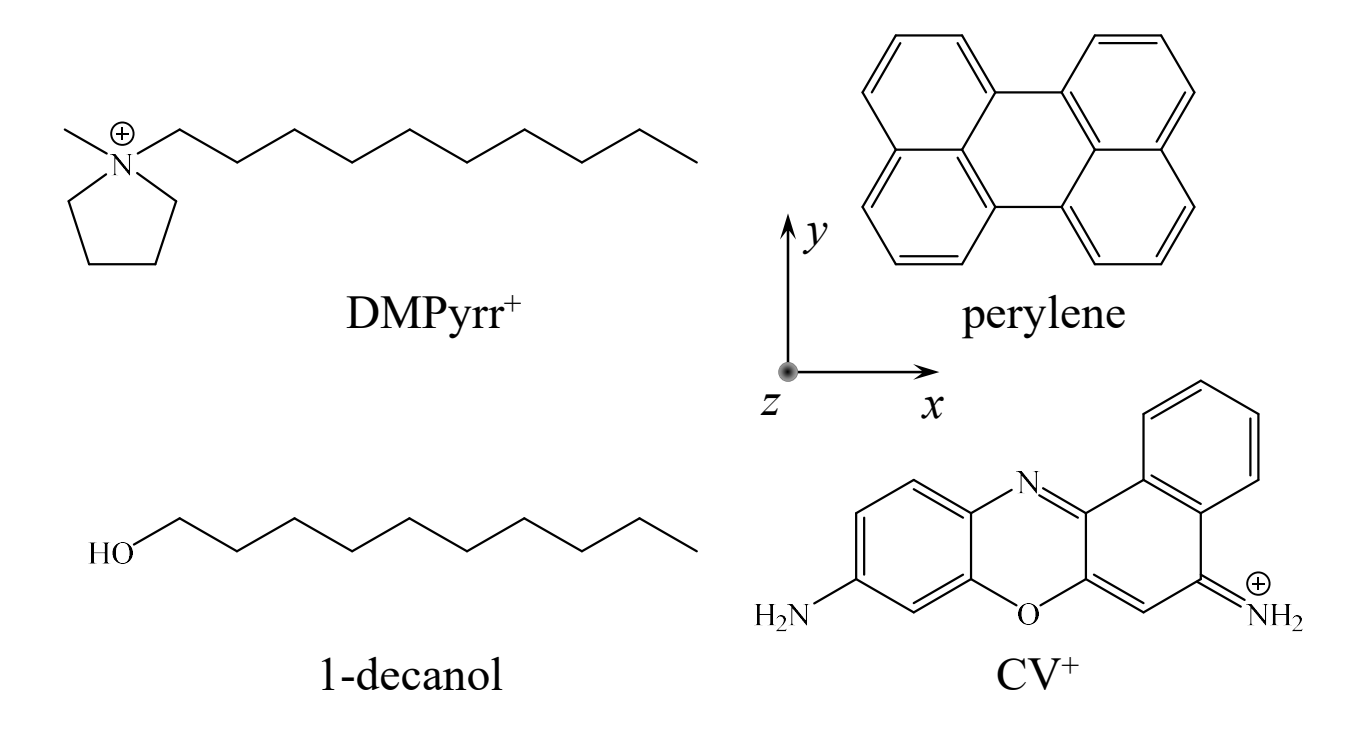


Figure 6.1 Structures of the solvent components and molecular probes used in this work. Top left: RTIL cation DMPyrr⁺ (the TFSI⁻ anion is not shown), bottom left: 1-decanol, top right: perylene, bottom right: cresyl violet (counter anion not shown). The Cartesian axes shown approximate those used for interpretation of the fluorescence depolarization data. The $S_1 \leftarrow S_0$ transition dipole moment defines the *x*-axis for each chromophore.

Our prior work has shown that the primary structural influence on the properties of RTILs is the aliphatic chain length of the RTIL cation. When RTILs are mixed with water, micellar structures have been reported^{42, 51-54} and non-micellar but aggregated RTIL structures have been seen for mixing with other molecular solvents, and the characteristic size of these aggregates is on the order of 1 nm diameter. 22-23 We have undertaken the current study to evaluate RTIL aggregation and its effect on the ability to support ρ_f under the condition that the RTIL cation and the molecular solvent have the same aliphatic chain length. We have chosen the 1-decyl-1-methylpyrrolidinium RTIL cation and 1-decanol as the molecular solvent (Figure 6.1). The motivation for using these species is to examine nanoscale order in a binary system where the aliphatic character is prominent and both constituents have the same aliphatic chain length. The underlying assumption is that a ten-carbon-long aliphatic chain is sufficient to provide reasonable spatial separation between polar domains. The expectation is that order within such a microheterogeneous system will be amenable to spectroscopic interrogation. We have used two fluorophores in this work, the cationic probe cresyl violet (CV⁺) and the non-polar probe perylene (Figure 6.1). We have characterized the fluorescence depolarization dynamics of these chromophores as a function of composition of the DMPyrr⁺TFSI⁻-1-decanol binary system. Our data show that the two chromophores sense the polar/ionic and aliphatic regions of the binary system selectively, and that molecular-scale order is seen in each region. For all system compositions, perylene is seen to reorient as an oblate rotor. For system compositions of 1-decanol mole fraction $X_{decanol} \le 0.75$, CV^+ reorients as an oblate rotor. This behavior allows for the determination of the Cartesian components of the rotational diffusion constant, providing information relevant to the organization of the immediate environments of the probes. Composition-dependent changes in organization differ for the polar

and nonpolar regions and, for the first time, we are able to relate molecular length-scale organization to the induced free charge density gradient ρ_f in an RTIL.

6.2 Experimental Section

6.2.1 Materials Used

The ionic liquid 1-decyl-1-methylpyrrolidinium bis(trifluoromethanesulfonyl) imide (DMPyrr+TFSI-) was prepared using methods described elsewhere. ^{18, 55-56} Karl Fischer titration of the prepared RTILs determined the water content to be 50 ppm or less. The solvent 1-decanol was purchased from Sigma-Aldrich in the highest purity grade available and used as received. Perylene was purchased from Sigma-Aldrich and used as received. Cresyl violet perchlorate was purchased from Exciton and used without further purification.

6.2.2 Preparation of Solutions

Stock solutions of chromophores ($ca. 5 \times 10^{-4} \,\mathrm{M}$) in ethanol (cresyl violet) and in hexane (perylene) were prepared. Aliquots of the chromophore solutions were heated in an oven at 100 °C for ~2-3 h to evaporate solvents (i.e., ethanol or hexane). The final concentrations of chromophores in all the mixtures were $ca. 5 \times 10^{-5} \,\mathrm{M}$ for CV⁺ and $5 \times 10^{-6} \,\mathrm{M}$ for perylene. The solutions were then stirred for at least 24 h before use. All glassware used was maintained at 150 °C for at least 24 h before use to minimize water contamination. Binary RTIL/solvent systems were prepared by weight. We mixed carefully measured masses of each component for a given system and calculated the mole fraction volumetrically from that information. To minimize water contamination, all binary systems were prepared in a N2-purged flexible vinyl glove box (Coy Laboratory Products Inc., Grass Lake, MI). Sealed samples were maintained in the glove box until measurements were performed. The sample cell consisted of a microscope slide coated with ITO, a $ca. 1 \,\mathrm{mm}$ spacer (rubber), and a microscope coverslip.

6.2.3 Rotational Diffusion Measurement

The instrument used to measure the rotational diffusion dynamics of CV⁺ and perylene in the systems studied here has been reported in detail elsewhere. 16,57 Briefly, a confocal scanning timecorrelated single photon counting (TCSPC) imaging instrument was used to acquire the data. The chromophores were excited using the output of a synchronously pumped, cavity-dumped dye laser (Coherent 701-3). The source laser that pumps the dye laser is a passively mode-locked diodepumped Nd:YVO₄ laser (Spectra Physics Vanguard) that produces 2.5 W average power at 532 nm and 355 nm. Pulses are 13 ps fwhm with an 80 MHz repetition rate. The dye laser output is 5 ps pulses at a 4 MHz repetition rate, at 575 nm (Pyrromethene 567, Exciton, Lockbourne, OH) for CV⁺ excitation or 435 nm (Stilbene 430, Exciton) for perylene excitation. Excitation power at the sample is <1 mW average for all measurements. The confocal scanning head (B&H DCS-120) is mounted on a Nikon Eclipse Ti-U inverted microscope. Emission was filtered through color filters and was collected at polarizations parallel and perpendicular to the excitation polarization using two avalanche photodiodes (ID-Quantique ID100) and processed using TCSPC detection electronics (B&H SPC-152). The instrument response function for this system is <100 ps. A Nikon 10× objective was used for data acquisition with B&H software. Uncertainties in the polarized emission and reorientation data are the standard deviations of time constants fitted for 65,536 sets of time-resolved polarized emission data (256 x 256 array). Uncertainties in quantities derived from the anisotropy decay data are propagated from the experimental data.

6.2.4 Steady State Spectroscopy

Absorbance measurements were performed using a Cary 4000 UV-visible spectrometer. All data were acquired with 1 nm spectral resolution. Emission data were acquired using a Jobin-

Yvon Fluorolog 3 spectrometer, with excitation and emission monochromators set to 1 nm resolution for all measurements.

6.3 Results and Discussion

Among the properties of RTILs that has seen application is the ability of these materials to dissolve both polar and nonpolar compounds. As noted above, there is a substantial body of literature that points to nanoscale heterogeneity in RTILs and in RTIL-molecular solvent binary systems. Indeed, the spatially heterogeneous nature of these binary systems is retained even for comparatively high levels of molecular solvents. In the work we consider below, we have deliberately matched the ten-carbon-backbone length of the DMPyrr⁺ aliphatic chain with that of the molecular solvent. The goal was to choose constituents likely to exhibit local organization in the binary solvent systems. We chose polar (ionic) and nonpolar probes in an attempt to evaluate these regions selectively. Before we consider the rotational diffusion data in detail, we first consider the absorption and emission spectra of the two molecular probes in DMPyrr⁺TFSI⁻ and 1-decanol (Figure 6.2).

The absorption and emission spectra of perylene in DMPyrr⁺TFSI⁻ and 1-decanol are shown in Figure 6.2a. These data show that perylene experiences essentially the same chemical environment in the RTIL and the molecular solvent, and we assert that in both cases the chromophore resides in non-polar, aliphatic-rich regions. In support of this claim, the band positions and vibronic structure are the same as those reported for perylene in alkanes.⁵⁸ The

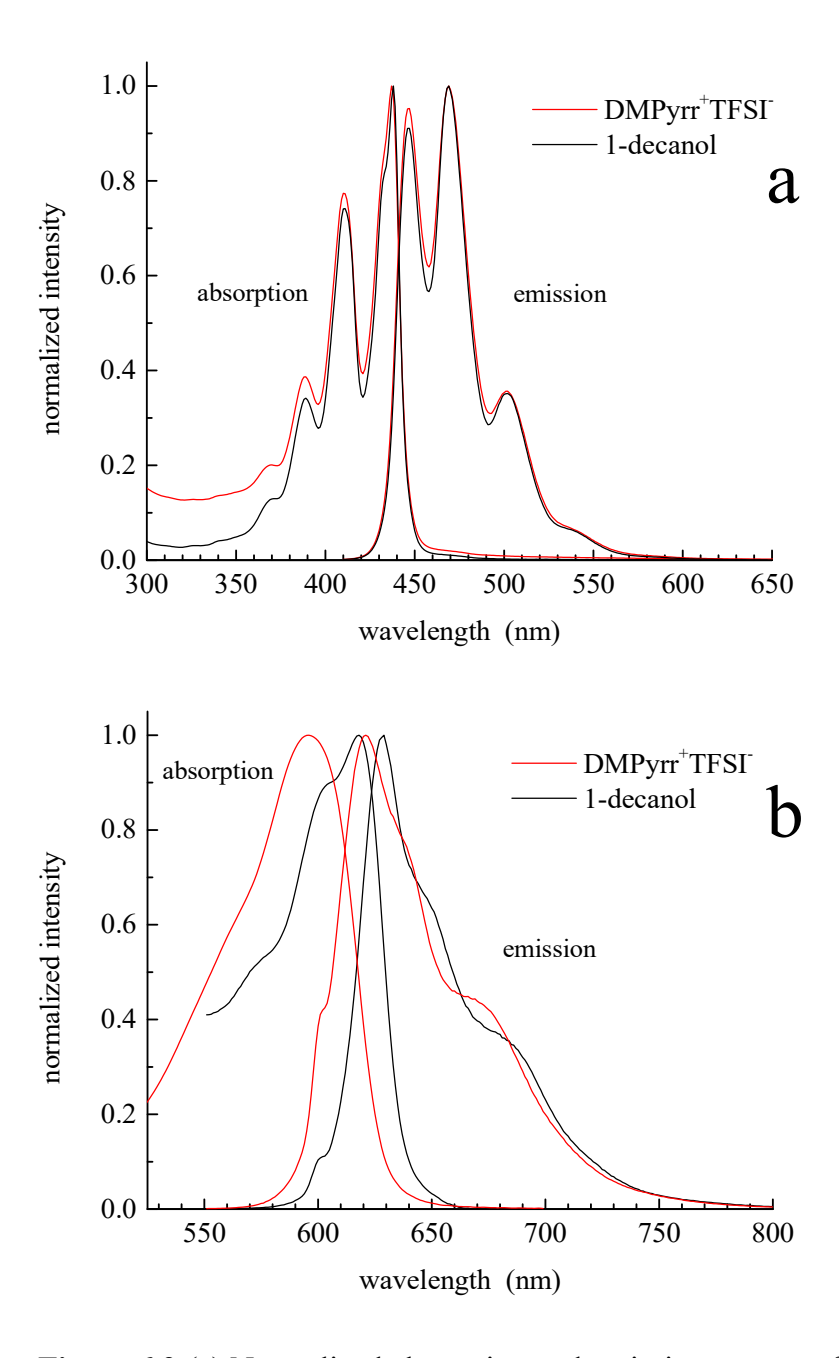


Figure 6.2 (a) Normalized absorption and emission spectra of perylene in DMPyrr⁺TFSI⁻ (red) and 1-decanol (black). (b) Normalized absorption and emission spectra of CV⁺ in DMPyrr⁺TFSI⁻ (red) and 1-decanol (black).

absorption and emission spectra of CV⁺ in DMPyrr⁺TFSI⁻ and 1-decanol are shown in Figure 6.2b. These data reveal that the environment CV⁺ experiences in DMPyrr⁺TFSI⁻ is similar to that which it experiences in polar solvents such as short-chain alcohols. The absorption and emission data for CV⁺ in 1-decanol exhibit a significant shift compared to those seen in the RTIL. The absorption and emission spectra in 1-decanol are both red-shifted relative to those seen in DMPyrr+TFSI-, and they exhibit more partially resolved spectral features. The Stokes shift also appears to be smaller in 1-decanol than it is in DMPyrr⁺TFSI⁻, although this is a qualitative comparison because of the possibly different relative contributions of the vibronic bands associated with low frequency vibrations. These data, in conjunction with the limited solubility of CV⁺ in 1-decanol, suggest that the ground electronic state, S₀, of CV⁺ is de-stabilized more than the first excited singlet state, S₁, in this solvent. Semi-empirical calculations (not shown) indicate that the permanent dipole moments for the CV^+ S₀ and S₁ states are similar in magnitude (ca. 4 D vs. 5 D) and orientation. We take these data to indicate that CV⁺ partitions selectively into a polar or ionic environment if one is available whereas perylene partitions selectively into nonpolar environment(s). We thus expect that the reorientation data for these two chromophores will be different because they reside in environments of different polarity, and comparison of the two datasets will provide insight into composition-dependent organizational changes in the different regions of the binary systems. With this information in mind, we now turn to a discussion of the rotational diffusion data and its interpretation.

Time-resolved polarized fluorescence intensity decay data ($I_{\parallel}(t)$ and $I_{\perp}(t)$) were acquired using the system described above. From the raw experimental data, the anisotropy decay function is generated according to Eq. 6.1,

$$R(t) = \frac{I_{\parallel}(t) - I_{\perp}(t)}{I_{\parallel}(t) + 2I_{\perp}(t)}$$
 [6.1]

The information of interest, the rotational diffusion constant D_{ROT} , and it's Cartesian components, is contained in the functional form of the R(t) decay, and the relationship between these quantities has been described in detail by Chuang and Eisenthal.⁵⁹ The anisotropy decay function can contain up to five exponential decays. Appropriate assignment of the Cartesian axes for the reorienting chromophore (*i.e.*, the transition dipole moment for the $S_1 \leftarrow S_0$ transition defines the *x*-axis and the *z*-axis is perpendicular to the chromophore π -system plane) affords substantial simplification. Under these conditions and with the absorbing and emitting transition dipole moments parallel to one another, one obtains either a one-component or a two-component exponential decay of R(t), depending on the unique axis. Expressed in terms of the Cartesian components of the rotational diffusion constant, D_{ROT} , a prolate rotor is defined as $D_x \neq D_y = D_z$ and an oblate rotor is defined as $D_z \neq D_z = D_z$.

Prolate rotor:
$$R(t) = 0.4 \exp(-6D_z t)$$
 [6.2]

Oblate rotor:
$$R(t) = 0.1 \exp(-(2D_x + 4D_z)t) + 0.3 \exp(-6D_x t)$$
 [6.3]

We consider next the experimental reorientation data for perylene and CV⁺, and then compare the results to evaluate the implications of our data on organization within the DMPyrr⁺TFSI⁻-1-decanol system.

6.3.1 Perylene Reorientation

Perylene can reorient as either a prolate rotor or an oblate rotor, depending on its immediate environment.⁵⁸ Perylene exhibits a two-component anisotropy decay (oblate rotor, Eq. 6.3) in neat DMPyrr⁺TFSI⁻, neat 1-decanol, and all of the binary systems reported here. Because of this, we can extract both D_z and D_x ($\approx D_y$) from the experimental data, providing significant insight into the local organization within these binary DMPyrr⁺TFSI⁻-1-decanol solvent systems. We note that perylene is not sensitive to ρ_f in these binary systems because it is not charged, and any depth-

dependent organization within this system that would be imposed by $\rho_f(vide\ infra)$ is not observed experimentally in the nonpolar regions where perylene is located. We show in Figure 3 the dependence of D_z , D_x and the ratio D_z/D_x on binary system composition. There are several interesting features contained in these data. In Figures 3a and 3b, we report D_z and D_x for perylene as a function of the mole fraction of 1-decanol in the DMPyrr⁺TFSI⁻1-decanol binary system. Both D_z and D_x exhibit a modest dependence on system composition up to $X_{decanol} \approx 0.4$. Above $X_{decanol} = 0.4$, D_z exhibits a discontinuous decrease while D_x achieves a plateau value. There is thus a decrease in the rotational freedom about the perylene z-axis and no x-axis dependence on binary system composition. This is seen clearly in the ratio of D_z/D_x as a function of composition in Figure 3c. It is significant to note that, while the local environment appears to become more isotropic with increasing addition of 1-decanol, based on the ratio D_z/D_x , examination of D_z and $D_{\rm x}$ independently show that the freedom of rotation about z actually decreases with increasing X_{decanol} and rotation about x becomes independent of system composition above $X_{\text{decanol}} \approx 0.4$. We are not aware of any data on the viscosity (η) of this binary system as a function of composition but η for neat DMPyrr⁺TFSI⁻ is reportedly 150 cP⁶⁰ and η for neat 1-decanol is ~12 cP. If this binary system behaves in a manner consistent with other RTIL-molecular liquid binary systems, the bulk viscosity should vary smoothly with composition between the limits of $X_{solvent} = 0$ and $X_{\text{solvent}} = 1$.

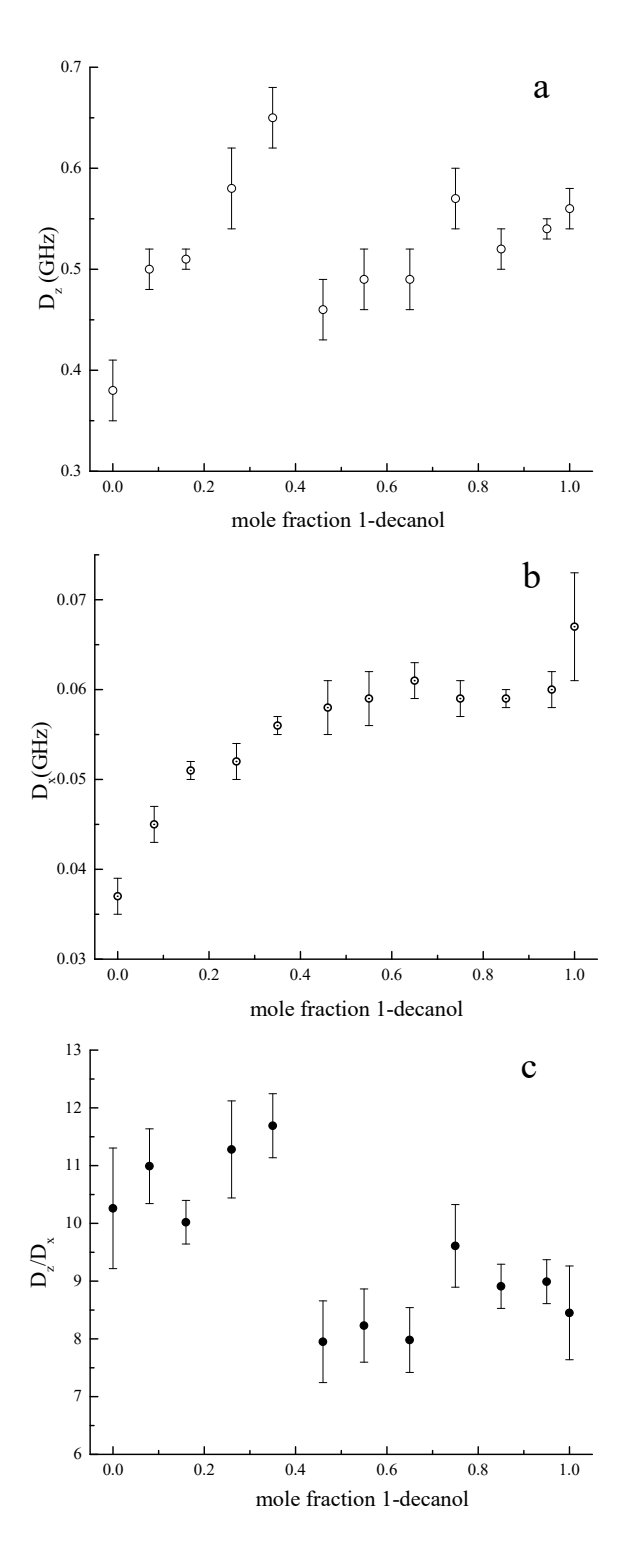


Figure 6.3 (a) The z-Cartesian component of the rotational diffusion constant, D_z , for perylene in the binary DMPyrr⁺TFSI⁻-1-decanol binary system, (b) the x-Cartesian component, D_x , for the same system, and (c) the ratio D_z/D_x .

If that is the case, then the data shown in Figure 3 are inconsistent with the modified Debye-Stokes-Einstein model, ⁶¹⁻⁶³ which predicts:

$$D_{ROT} = \frac{1}{3} \left(D_x + D_y + D_z \right) = \frac{k_B T S}{6 \eta V f}$$
 [4]

As noted above, D_{ROT} is the rotational diffusion constant, k_B is the Boltzmann constant, T is the absolute temperature, η is the bulk viscosity of the medium, V is the hydrodynamic volume of the rotating species, ^{64}S is a shape factor to account for the ellipsoidal shape of the rotating molecule, 63 and f is the solvent-solute frictional boundary condition. 62 Our experimental findings suggest that the binary system exists as a non-homogeneous mixture of domains and that the perylene chromophore is sequestered within one of the domains, presumably a non-polar one. While there is a change in the nature of the nonpolar domain for $X_{decanol} \ge 0.4$, the change is stepwise (discontinuous) in nature and does not depend smoothly on the composition of the mixture.

6.3.2 Cresyl violet Reorientation

Cresyl violet is found to reorient as an oblate rotor for $X_{decanol} \le 0.75$ and as a prolate rotor for higher values of $X_{decanol}$ (Figure 6.4). Cresyl violet is typically seen to reorient as a prolate rotor in molecular solvents, although oblate rotor behavior has been reported for reorientation in a mesophase of 1-dodecanol.⁶⁵ The reorientation of CV^+ as an oblate rotor up to high values of $X_{decanol}$ in this binary system indicates confinement within a relatively structured environment. We note that ρ_T is seen to contribute to CV^+ reorientation dynamics (Figure 6.5) in the DMPyrr⁺TFSI⁻1-decanol binary system up to $X_{decanol} \approx 0.75$. We will return to a discussion of the information contained in the depth-dependent reorientation behavior of CV^+ after considering its reorientation

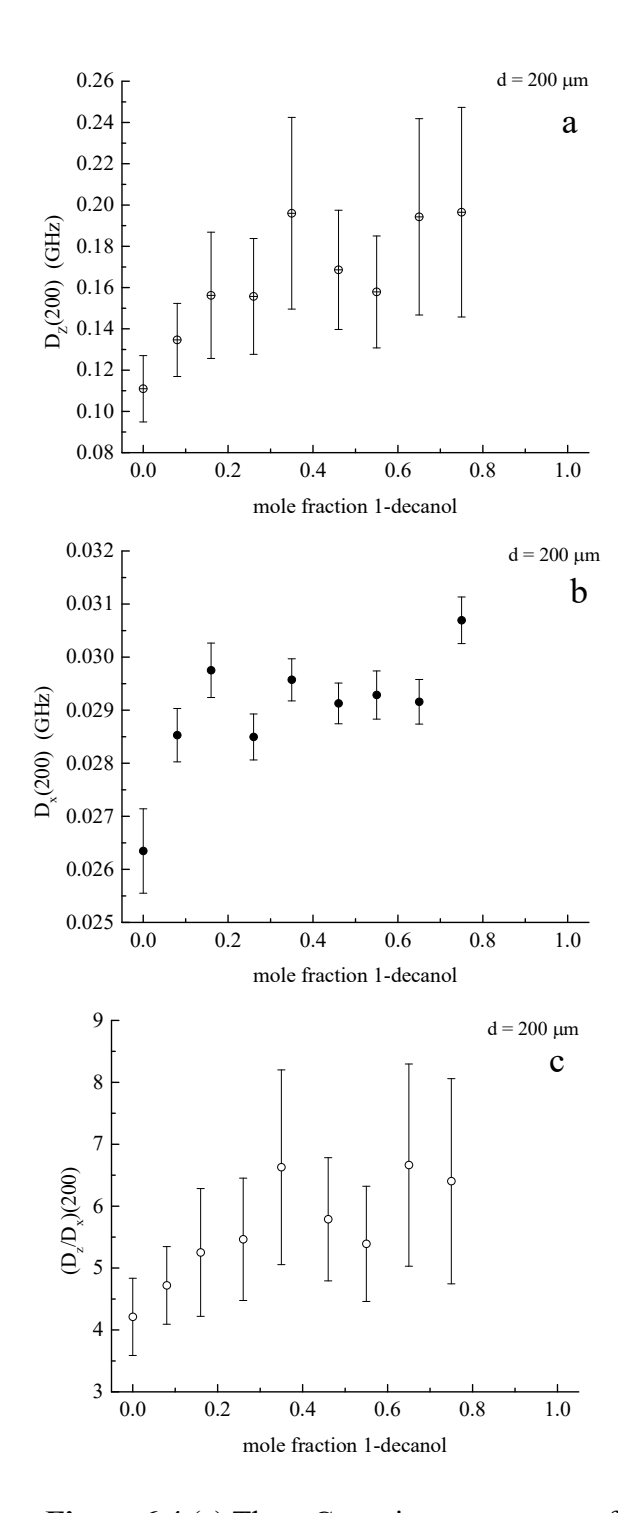


Figure 6.4 (a) The *z*-Cartesian component of the rotational diffusion constant, D_z , for CV⁺ in the binary DMPyrr⁺TFSI⁻-1-decanol binary system, (b) the *x*-Cartesian component, D_x , for the same system, and (c) the ratio D_z/D_x . For $X_{decanol} > 0.75$, CV⁺ exhibits a single-exponential anisotropy decay (not shown).

dynamics in the bulk binary system (*i.e.*, for measurements \sim 200 μ m distant from the charged support surface – ITO in this work).

The rotational diffusion data for CV^+ are summarized in Figures 6.4a and 6.4b for D_z and D_x , respectively. While both components of D_{ROT} are seen to increase with increasing $X_{decanol}$, the increases are modest and are relatively continuous functions of $X_{decanol}$ to within the experimental uncertainty. In contrast to the analogous data for perylene presented earlier (Figure 3a and 3b), there is no discontinuous change in either component of D_{ROT} with changes in $X_{decanol}$ for the molecular probe CV^+ . There is, however, a significant plateau region for both D_z and D_x such that the ratio D_z/D_x (Figure 6.4c) is independent of $X_{decanol}$ from ~0.3 to 0.75. While it may be tempting to perceive a trend in D_z/D_x , the uncertainties in these values do not allow such a conclusion with any level of certainty. Interestingly, the same viscosity-independence is seen for CV^+ , suggesting that this chromophore is also confined within a nanoscale domain in the binary system. We believe that for $X_{decanol}$ ~0.8 and above, the observation of prolate rotor behavior reflects the disruption of a local environment dominated by the RTIL polar head group and counter ion.

In addition to the composition-dependent rotor shape of CV^+ , the induced free charge density gradient, ρ_f , seen in RTILs is also seen in the depth-dependence of the reorientation dynamics for this chromophore. This is an expected result, however, the fact that CV^+ reorients as an oblate rotor in this binary system allows the extraction of more detailed information regarding the chromophore local environment than we have been able to obtain in previous studies where single-exponential decays in R(t) were observed. We present in Fig. 6.5 the depth-dependent change in D_x and D_z for CV^+ , expressed as $\Delta D_i/D_i$ (i=x,z) as a function of binary system composition from $X_{decanol} = 0$ to $X_{decanol} = 0.75$. These data reveal the effect of ρ_f on the effective rotor shape and several notable features emerge from these experiments.

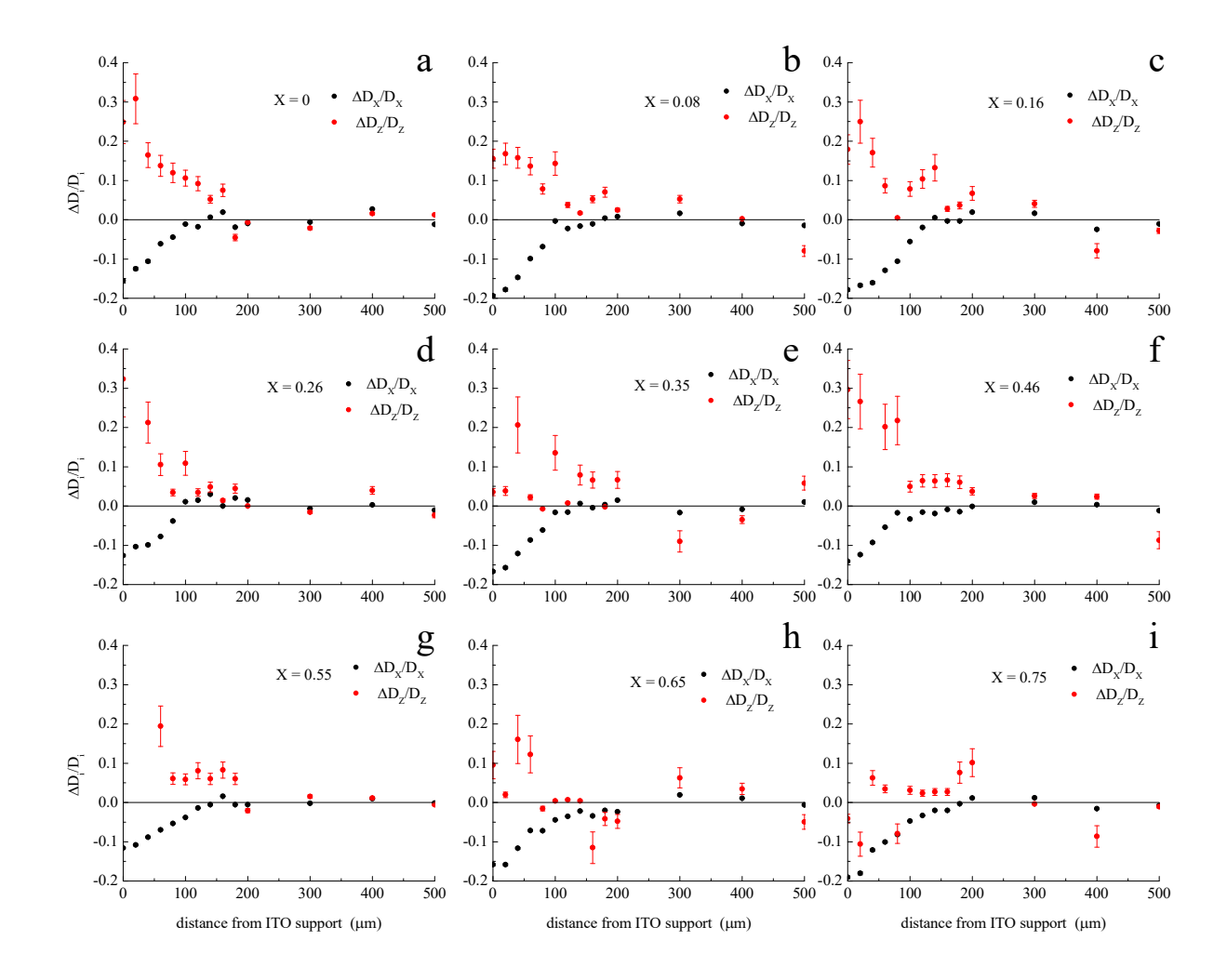


Figure 6.5 Normalized depth-dependent variation in D_z and D_x for CV^+ as a function of DMPyrr⁺TFSI⁻-1-decanol binary system composition. (a) $X_{decanol} = 0$, (b) $X_{decanol} = 0.08$, (c) $X_{decanol} = 0.16$, (d) $X_{decanol} = 0.26$, (e) $X_{decanol} = 0.35$, (f) $X_{decanol} = 0.46$, (g) $X_{decanol} = 0.55$, (h) $X_{decanol} = 0.65$ and (i) $X_{decanol} = 0.75$.

The most prominent feature is that D_x is small near the charged support surface and becomes larger with increasing distance. In contrast, D_z reveals fast reorientation near the charged support surface which slows with increasing distance. In other words, rotational motion about x becomes less hindered with distance from the charged support while rotational motion about z becomes more hindered. While this change does not provide detailed structural information, a change consistent with these data would be an environment proceeding from lamellar organization to one more spherically symmetric. The existence of lamellar or quasi-lamellar organization has been seen before for RTILs near surfaces, 66-67 but in those instances, there was no organization that existed over length scales comparable to that reported for ρ_f , and any connection between those bodies of work and our observations remains to be made. There may be shorter-range organization in RTILs that is consistent quasi-lamellar organization. We show in Figure 5.6 the ratio D_z/D_x for CV^+ in neat DMPyrr⁺TFSI⁻ as a function of distance from the charged support surface. These data clearly show that the CV⁺ local environment becomes more isotropic with the decay of ρ_f . Together, the results shown in Figures 5.5 and 5.6 provide the first direct connection between ρ_f and the molecular organization of the medium. This is an important connection to make because it provides a greater understanding of the factors required to support a macroscopic charge density gradient in a fluid medium.

The data in Figure 6.5 show that ρ_f persists with the addition of 1-decanol up to $X_{decanol}$ = 0.75, a value remarkably higher than that seen in other RTIL-molecular solvent binary systems.²²⁻
²³ The gradient appears to be essentially independent of $X_{decanol}$ for x-axis rotation while ρ_f is seen to influence z-axis rotation more significantly. This is an indication that the overall CV^+ environment depends on $X_{decanol}$ in an anisotropic manner. The extent to which this composition-dependent variation in the local (polar) environment can be inferred for other systems is not clear

because for most other RTIL-molecular solvent binary systems a single exponential decay of R(t) is seen for charged chromophores, precluding the ability to compare reorientation rates about the different Cartesian axes.

The data we have reported for the reorientation dynamics of perylene and CV^+ in the same binary systems provide two perspectives on the complex environments formed. Of particular note is that the discontinuity in D_z for the perylene local environment at $X_{decanol} \sim 0.4$ (Figure 6.3a) has no corresponding change in the local environment of CV^+ and, conversely, the prominent change in CV^+ local environment for $X_{decanol} > 0.75$ is not seen in the reorientation dynamics of perylene. The polar and non-polar environments are necessarily coupled but not to a sufficient extent that the different regions within this binary system have a direct influence on one another. This is not a surprising result because the dominant (van der Waals) forces determining organization in the nonpolar regions are of different magnitude than the (dipolar and ionic) forces that mediate organization in polar regions. It appears that any organizational changes with dilution appear primarily in the nonpolar region(s) of the binary system.

The characteristic persistence length of ρ_f (*i.e.*, the depth at which the decay of ρ_f is e⁻¹ of its magnitude at the RTIL-support interface) in the DMPyrr⁺TFSI⁻–1-decanol system is the same to within the experimental uncertainty as that seen in other RTILs, a finding that suggests a physical rather than chemical structure limitation on the spatial extent of this phenomenon. Despite the RTIL-independence of the persistence length of ρ_f , the DMPyrr⁺TFSI⁻–1-decanol binary system supports ρ_f to much higher concentrations of molecular solvent component than is seen in other binary systems.²²⁻²³ It is tempting to ascribe this finding to the structural similarity in terms of aliphatic chain length (C₁₀) for the RTIL and molecular solvent. The longer aliphatic chain lengths

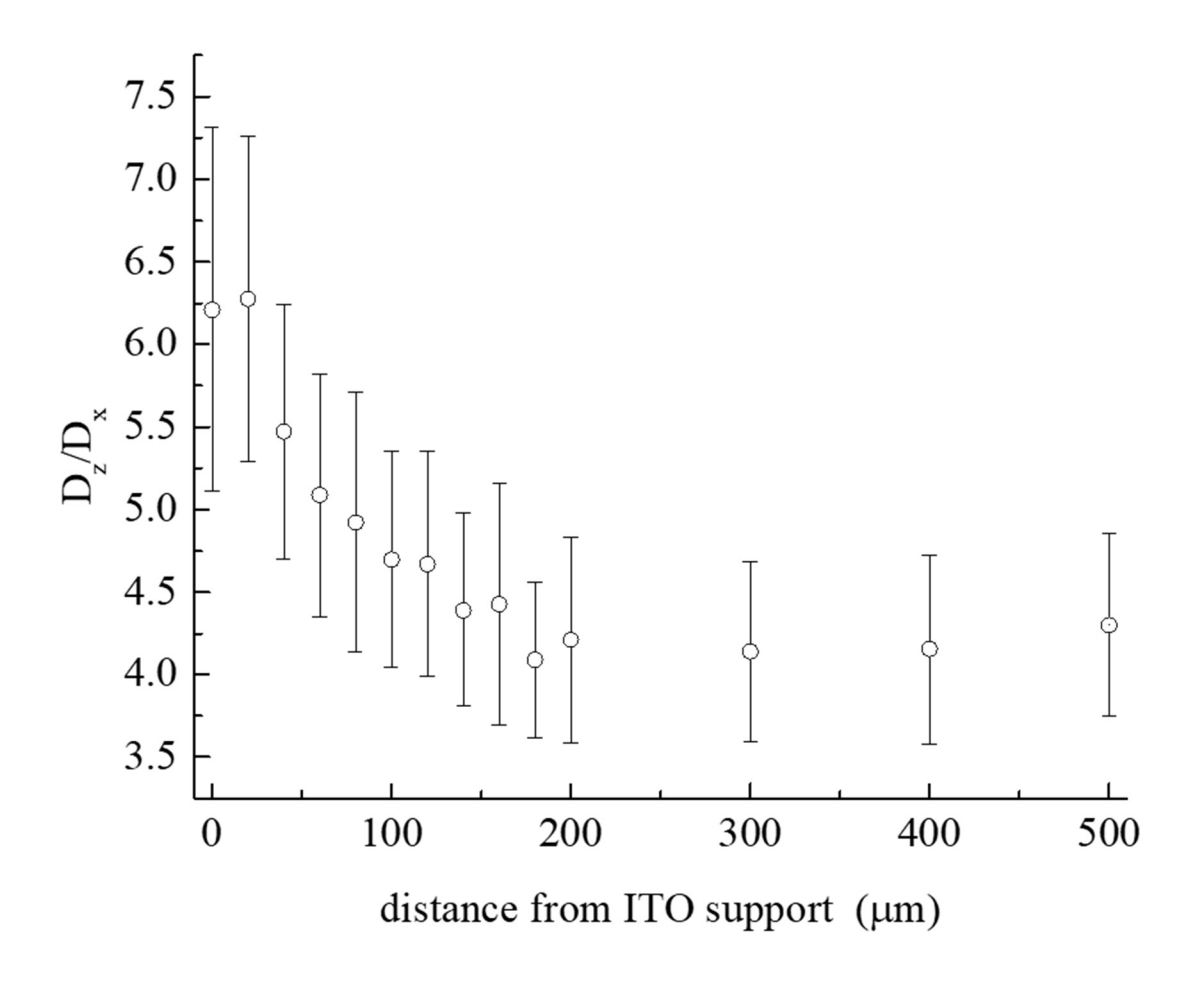


Figure 6.6 Ratio of D_z/D_x as a function of distance from the ITO support for CV^+ in neat DMPyrr⁺TFSI⁻.

likely support local structures in these binary systems where the polar/charged regions are more segregated than in analogous systems with less aliphatic character.

It is also important to consider that this binary system behaves anomalously in terms of the experimental viscosity-dependence, from the perspective of both chromophores. We show in Figure 6.7 the expected dependence of bulk viscosity on system composition. We are not aware of any experimental data on the DMPyrr+TFSI-1-decanol system, but the compositiondependence of viscosity has been reported for several other RTIL-molecular solvent systems. In all cases there is a smooth, continuous dependence of bulk viscosity on the extent of RTIL dilution. Because of the bulk nature of typical viscosity measurements and molecular-scale viscosity sensed by rotational diffusion measurements, the two quantities may not correspond. We have modeled the expected bulk viscosity behavior (Figure 6.7 line) based on the functional form of the dependence seen in other systems, and compare it to the viscosity sensed by perylene and CV⁺ through the reorientation measurements. Both chromophores exhibit essentially viscosityindependent dynamics up to $X_{decanol} \approx 0.75$. The nanoscale dimensions of the compositional heterogeneity seen in RTIL-molecular solvent binary systems, and the confinement of the chromophores within different nanoscale domains, provide an explanation for the discrepancy between the two measurements. The local environment of perylene appears to be characterized by a viscosity of 10-15 cP, with even the reorientation time in neat DMPyrr⁺TFSI being in the same range. These values assume stick limit behavior, which is open to question, but in any event, the local environment of perylene appears to be dominated by a local medium of aliphatic character. CV^+ senses an environment of apparently higher viscosity, in the 30-40 cP range up to $X_{decanol}$ = 0.75. For higher values of $X_{decanol}$, the apparent viscosities are different due primarily to the change of rotor shape and consequent loss of information. The fact that the apparent viscosities are different

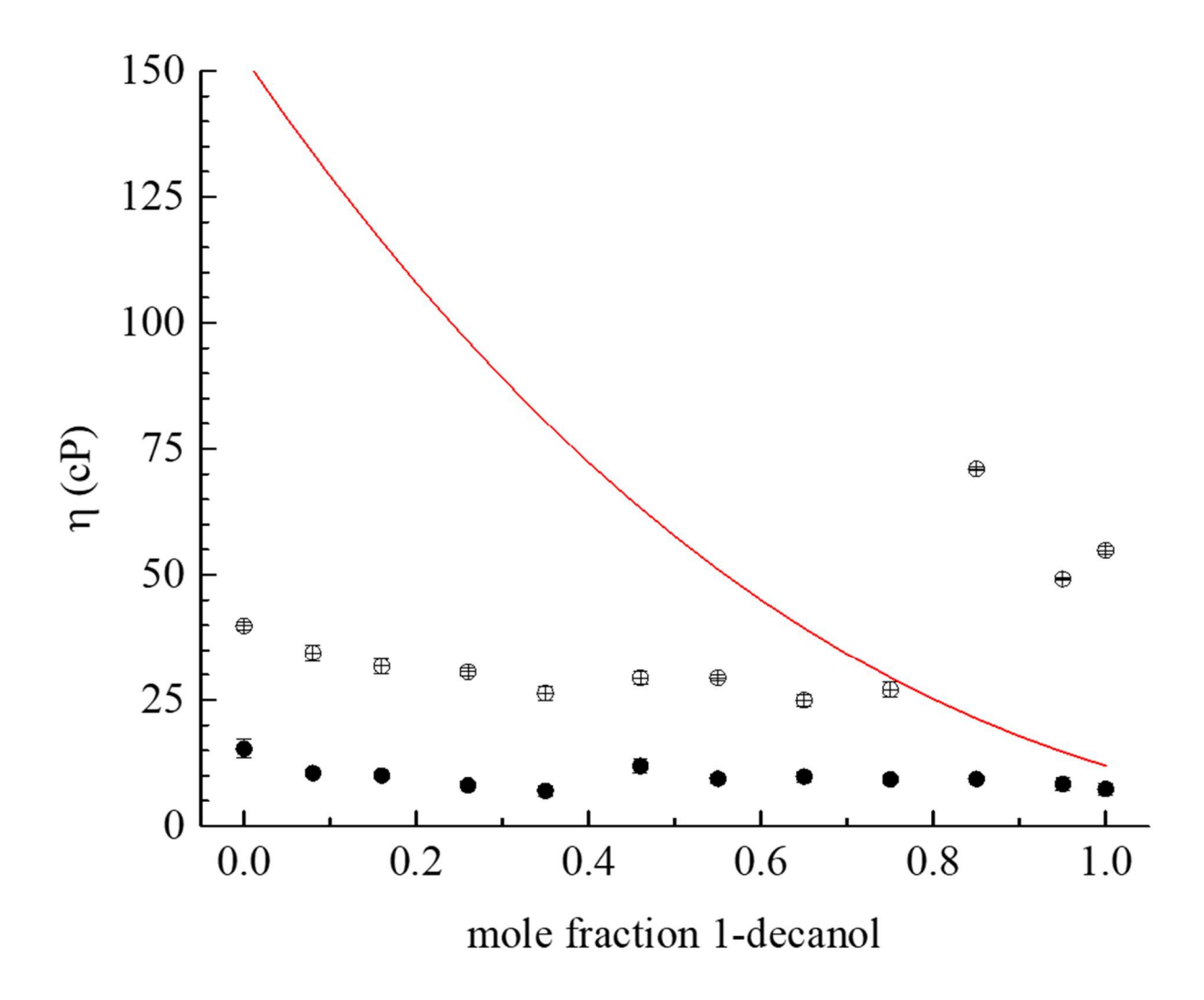


Figure 6.7 Viscosity determined from rotational diffusion data as a function of DMPyrr⁺TFSI⁻1-decanol binary system composition for perylene (solid black circles) and CV⁺ (open circles). Calculated bulk viscosity for the binary system is shown as a red line.

is not surprising for reasons of structural/compositional differences of the local environments, but also because of the likely difference in frictional boundary conditions for the two chromophores. Regardless, the compositional independence of the effective viscosities points to both chromophores being sequestered within different domains within the binary solvent system. The apparent decoupling of viscosity from diffusion has been seen before, for both RTIL and deep eutectic solvent (DES) systems. In those works, this decoupling was interpreted as evidence for heterogeneity within the media, and our findings are consistent with that explanation. 68-74 In other words, the viscosity sensed by reorientation measurements is that of the environment in the immediate proximity of the chromophore, while bulk viscosity is reflective of interactions between larger assemblies (e.g., aggregates) in which the chromophores are confined.

6.4 Conclusions

We have examined the DMPyrr⁺TFSI⁻-1-decanol binary system using two fluorescent probes. The nonpolar probe, perylene, sequesters in the nonpolar region(s) of the binary system and the polar probe, CV^+ , is localized in the polar/ionic region(s) of the system. Both chromophores are seen to exhibit a two-component exponential decay of their anisotropy decay function, allowing for the extraction of two Cartesian components of the rotational diffusion constant, D_{ROT} . The dependence of the rotational diffusion constant components on the composition of the binary system reveals that there are distinct, composition-dependent changes in the local environments of the chromophores, but these changes do not occur at the same 1-decanol concentrations. The rotational diffusion data for CV^+ also contain information on the induced free charge density gradient we have reported previously for RTILs. The persistence length of ρ_T is the same for DMPyrr⁺TFSI⁻ as for other reported RTILs, but the rotational diffusion data demonstrate for the first time a relationship between molecular-scale organization and ρ_T . We

also observe that the diffusion constant components are essentially decoupled from the bulk viscosity of the binary system, a phenomenon reported previously that is taken as an indication of microheterogeneity within the RTIL medium. This is consistent with our findings and the data point collectively to the important role that nonpolar aliphatic domains can play in determining the bulk properties of RTIL systems.

REFERENCES

- 1. Arbizzani, C.; Biso, M.; Cericola, D.; Lazzari, M.; Soavi, F.; Mastragostino, M., Safe, High-Energy Supercapacitors Based on Solvent-Free Ionic Liquid Electrolytes. *J. Pwr. Sources* **2008**, *185* (2), 1575-1579.
- 2. Balducci, A.; Dugas, R.; Taberna, P. L.; Simon, P.; Plée, D.; Mastragostino, M.; Passerini, S., High Temperature Carbon–Carbon Supercapacitor Using Ionic Liquid as Electrolyte. *J. Pwr. Sources* **2007**, *165* (2), 922-927.
- 3. Sharifi, A.; Barazandeh, M.; Abaee, M. S.; Mirzaei, M., [OMIM][BF₄], a Green and Recyclable Ionic Liquid Medium for the One-Pot Chemoselective Synthesis of Benzoxazinones. *Tet. Lett.* **2010**, *51*, 1852-1855.
- 4. Shen, Z.-L.; Ji, S.-J.; Loh, T.-P., Ionic liquid [OMIM][PF₆] as an Efficient and Recyclable Reaction Media for the Cyanosilylation of Aldehydes without Lewis Acid or any Special Activation. *Tet. Lett.* **2005**, *46*, 3137-3139.
- 5. Yadav, J. S.; Reddy, B. V. S.; Premalatha, K., 1-Butyl-3-Methylimidazolium Tetrafluoroborate ([BMIM]BF₄) Ionic Liquid :A Novel and Recyclable Reaction Medium for the Synthesis of *vic*-Diamines. *Adv. Synth. Catal.* **2003**, *345*, 948-952.
- 6. Bates, E. A.; Mayton, R. D.; Ntai, I.; Davis, J. H., CO₂ Capture by a Task-Specific Ionic Liquid. *J. Am. Chem. Soc.* **2002**, *124*, 926-927.
- 7. Chai, S. Y. W.; Ngu, L. H.; How, B. S., Review of carbon capture absorbents for CO₂ utilization. *Grnhse. Gas.: Sci. Tech.* **2022**, *12* (3), 394-427.
- 8. Chaudhary, A.; Bhaskarwar, A. N., Effect of physical properties of synthesized protic ionic liquid on carbon dioxide absorption rate. *Env. Sci. Poll. Res.* **2023**, *30*, 8429-8447.
- 9. Perumal, M.; Jayaraman, D., Amine-Ionic Liquid Blends in CO₂ Capture Process for Sustainable Energy and Environment. *Energ. Env.* **2022**, *0*, 1-16.
- 10. Ramdin, M.; de Loos, T. W.; Vlugt, T. J. H., State-of-the-Art of CO₂ Capture with Ionic Liquids. *Ind. Eng. Chem. Res.* **2012**, *51*, 8149-8177.
- 11. Zhang, X. X.; Zhang, X. X.; Dong, H.; Zhao, Z.; Zhang, S.; Huang, Y., Carbon Capture with Ionic Liquids: Overview and Progress. *Energy Environ. Sci.* **2012**, *5*, 6668-6681.
- 12. Zunita, M.; Hastuti, R.; Alamsyah, A.; Khoiruddin, K.; Wenten, I. G., Ionic Liquid Membrane for Carbon Capture and Separation. *Sep. Purif. Rev.* **2022**, *51* (2), 261-280.
- 13. Donius, B. R.; Rovey, J. L., Ionic Liquid Dual-Mode Spacecraft Propulsion Assessment. J. Spacecr. Rock. 2011, 48 (1), 110-123.

- 14. Prince, B. D.; Fritz, B. A.; Chiu, Y.-H., Ionic Liquids in Electrospray Propulsion Systems. In *Ionic Liquids: Science and Applications*, American Chemical Society: 2012; Vol. 1117, pp 27-49.
- 15. Nordness, O.; Brennecke, J. F., Ion Dissociation in Ionic Liquids and Ionic Liquid Solutions. *Chem. Rev.* **2020**, *120*, 12873-12902.
- 16. Ma, K.; Jarosova, R.; Swain, G. M.; Blanchard, G. J., Charge-Induced Long-Range Order in a Room-Temperature Ionic Liquid. *Langmuir* **2016**, *32* (37), 9507-9512.
- 17. Ma, K.; Jarosova, R.; Swain, G. M.; Blanchard, G. J., Modulation of an Induced Charge Density Gradient in the Room Temperature Ionic Liquid BMIM⁺BF₄-. *J. Phys. Chem. C* **2018**, *122*, 7361-7367.
- 18. Wang, Y.; Adhikari, L.; Baker, G. A.; Blanchard, G. J., Cation Structure-Dependence of the Induced Free Charge Density Gradient in Imidazolium and Pyrrolidinium Ionic Liquids. *Phys. Chem. Chem. Phys.* **2022**, *24*, 19314-19320.
- 19. Wang, Y.; Adhikari, L.; Baker, G. A.; Blanchard, G. J., Structure-Dependence of the Pockels Effect in Aprotic Ionic Liquids. *Phys. Chem. Chem. Phys.* **2022**, *24*, 18067-18072.
- 20. Wang, Y.; Jarosova, R.; Swain, G. M.; Blanchard, G. J., Characterizing the Magnitude and Structure-Dependence of Free Charge Density Gradients in Room Temperature Ionic Liquids. *Langmuir* **2020**, *36*, 3038-3045.
- 21. Wang, Y.; Swain, G. M.; Blanchard, G. J., Charge-induced Birefringence in a Room Temperature Ionic Liquid. *J. Phys. Chem. B* **2021**, *125*, 950-955.
- 22. Hossain, M. I.; Blanchard, G. J., The Effect of Dilution on Induced Free Charge Density Gradients in Room Temperature Ionic Liquids. *Phys. Chem. Chem. Phys.* **2022**, *24*, 3844-3853.
- 23. Hossain, M. I.; Blanchard, G. J., Dilution-Induced Changes in Room Temperature Ionic Liquids. Persistent Compositional Heterogeneity and the Importance of Dipolar Interactions. *J. Mol. Liq.* **2022**, *367*, 120447.
- 24. Nishida, J.; Breen, J. P.; Wu, B.; Fayer, M. D., Extraordinary Slowing of Structural Dynamics in Thin Films of a Room Temperature Ionic Liquid. *ACS Cent. Sci.* **2018**, *4*, 1065-1073.
- 25. Shin, J. Y.; Yamada, S. A.; Fayer, M. D., Dynamics of a Room Temperature Ionic Liquid in Supported Ionic Liquid Membranes vs. the Bulk Liquid: 2D IR and Polarized IR Pump-Probe Experiments. *J. Am. Chem. Soc.* **2017**, *139*, 311-323.
- 26. Shin, J. Y.; Yamada, S. A.; Fayer, M. D., Carbon Dioxide in a Supported Ionic Liquid Membrane: Structural and Rotational Dynamics Measured with 2D IR and Pump-Probe Experiments. *J. Am. Chem. Soc.* **2017**, *139*, 11222-11232.

- 27. Wu, B.; Breen, J. P.; Fayer, M. D., Structural Dynamics in Ionic Liquid Thin Films: The Effect of Cation Chain Length. *J. Phys. Chem. C* **2020**, *124*, 4179-4189.
- 28. Wu, B.; Breen, J. P.; Xing, X.; Fayer, M. D., Controlling the Dynamics of Ionic Liquid Thin Films via Multilayer Surface Functionalization. *J. Am. Chem. Soc.* **2020**, *142*, 9482-9492.
- 29. Anaredy, R. S.; Shaw, S. K., Long-Range Ordering of Ionic Liquid Fluid Films. *Langmuir* **2016,** *32*, 5147-5154.
- 30. Anaredy, R. S.; Shaw, S. K., Developing Distinct Chemical Environments in Ionic Liquid Films. *J. Phys. Chem. C* **2018**, *122*, 19731-19737.
- 31. Kashyap, H. K.; Santos, C. S.; Annapureddy, H. V. R.; Murthy, N. S.; Margulis, C. J.; Castner, E. W. J., Temperature-dependent structure of ionic liquids: X-ray scattering and simulations. *Faraday Disc. Chem. Soc.* **2012**, *154*, 133-143.
- 32. Pott, T.; Meleard, O., New insight into the nanostructure of ionic liquids: a small angle x-ray scattering (SAXS) study on liquid tri-alkyl-methyl-ammonium bis(trifluoromethanesulfonyl)amides and their mixtures. *Phys. Chem. Chem. Phys.* **2009**, *11*, 5469-5475.
- 33. Santos, C. S.; Murthy, N. S.; Baker, G. A.; Castner, E. W., Communication: X-ray scattering from ionic liquids with pyrrolidinium cations. *J. Chem. Phys.* **2011**, *134* (12), 121101.
- 34. Carmichael, A. J.; Hardacre, C.; Holbrey, J. D.; Nieuwenhuyzen, M.; Seddon, K. R., Molecular layering and local order in thin films of 1-alkyl-3-methylimidazolium ionic liquids using X-ray reflectivity. *Mol. Phys.* **2001**, *99* (10), 795-800.
- 35. Sloutskin, E.; Ocko, B. M.; Tamam, L.; Kuzmenko, I.; Gog, T.; Deutsch, M., Surface Layering in Ionic Liquids: An X-ray Reflectivity Study. *J. Am. Chem. Soc.* **2005**, *127* (21), 7796-7804.
- 36. Harris, M. A.; Kinsey, T.; VWagle, D. V.; Baker, G. A.; Sangoro, J., Evidence of a liquid-liquid transition in a glass-forming ionic liquid. *Proc. Nat. Acad. Sci. USA* **2021**, *118* (e2020878228), 1-6.
- 37. Cabry, C. P.; D'Andrea, L.; Shimizu, K.; Grillo, I.; Li, P.; Rogers, S.; Bruce, D. W.; Canongia-Lopes, J. N.; Slattery, J. M., Exploring the bulk-phase structure of ionic liquid mixtures using small-angle neutron scattering. *Faraday Disc. Chem. Soc.* **2018**, *206*, 265-289.
- 38. Triolo, A.; Russina, O.; Arrighi, V.; Juranyi, F.; Janssen, S.; Gordon, C. M., Quasielastic neutron scattering characterization of the relaxation processes in a room temperature ionic liquid. *J. Chem. Phys.* **2003**, *119* (16), 8549-8557.

- 39. Almásy, L.; Turmine, M.; Perera, A., Structure of Aqueous Solutions of Ionic Liquid 1-Butyl-3-methylimidazolium Tetrafluoroborate by Small-Angle Neutron Scattering. *J. Phys. Chem. B* **2008**, *112* (8), 2382-2387.
- 40. Kofu, M.; Tyagi, M.; Inamura, Y.; Miyazaki, K.; Yamamuro, O., Quasielastic neutron scattering studies on glass-forming ionic liquids with imidazolium cations. *J. Chem. Phys.* **2015**, *143* (23), 234502.
- 41. Nemoto, F.; Kofu, M.; Nagao, M.; Ohishi, K.; Takata, S.-i.; Suzuki, J.-i.; Yamada, T.; Shibata, K.; Ueki, T.; Kitazawa, Y., et al., Neutron scattering studies on short- and long-range layer structures and related dynamics in imidazolium-based ionic liquids. *J. Chem. Phys.* **2018**, *149* (5), 054502.
- 42. Feng, S.; Voth, G. A., Molecular dynamics simulations of imidazolium-based ionic liquid/water mixtures: Alkyl side chain length and anion effects. *Fl. Ph. Equilib.* **2010**, *294*, 148-156.
- 43. Bhargava, B. L.; Klein, M. L., Molecular Dynamics Studies of Cation Aggregation in the Room Temperature Ionic Liquid [C10mim][Br] in Aqueous Solution. *J. Phys. Chem. A* **2009**, *113*, 1898-1904.
- 44. Canongia-Lopes, J. N.; Padua, A. A. H., Nanostructural Organization in Ionic Liquids. *J. Phys. Chem. B* **2006**, *110*, 3330-3335.
- 45. Cosby, T.; Kapoor, U.; Shah, J. K.; Sangoro, J., Mesoscale Organization and Dynamics in a Binary Ionic Liquid. *J. Phys. Chem. Lett.* **2019**, *10*, 6274-6280.
- 46. Hayes, R.; Warr, G. G.; Atkin, R., Structure and Nanostructure in Ionic Liquids. *Chem. Rev.* **2015**, *115*, 6357-6426.
- 47. Kapoor, U.; Shah, J. K., Globular, Sponge-like to Layer-like Morphological Transition in 1-n-Alkyl-3-methylimidazolium Octylsulfate Ionic Liquid Homologous Series. *J. Phys. Chem. B* **2018**, *122*, 213-228.
- 48. Russina, O.; Lo Celso, F.; Plechkova, N.; Jafta, C. J.; Appetecchi, G. B.; Triolo, A., Mesoscopic organization in ionic liquids. *Top. Curr. Chem.* **2017**, *375*, 58.
- 49. Shimizu, K.; Bernardes, C. E. S.; Canongia-Lopes, J. N., STructure and Aggregation in the 1-Alkyl-3-Methylimidazolium Ris(trifluoromethylsulfonyl)imide Ionic Liquid Homologous Series. *J. Phys. Chem. B* **2014**, *118*, 567-576.
- 50. Triolo, A.; Russina, O.; Bleif, H.-J.; Di Cola, E., Nanoscale Segregation in Room Temperature Ionic Liquids. *J. Phys. Chem. B* **2007**, *111*, 4641-4644.

- 51. Blesic, M.; Margques, M. H.; Plechkova, N. V.; Seddon, K. R.; Rebelo, L. P. N.; Lopes, A., Self-aggregation of ionic liquids: micelle formation in aqueous solution. *Green Chem.* **2007**, *9*, 481-490.
- 52. Miskolczy, Z.; Sebok-Nagy, K.; Biczok, L.; Gokturk, S., Aggregation and micelle formation of ionic liquids in aqueous solution. *Chem. Phys. Lett.* **2004**, *400*, 296-300.
- 53. Singh, T.; Kumar, A., Aggregation Behavior of Ionic Liquids in Aqueous Solutions: Effect of Alkyl Chain Length, Cations and Anions. *J. Phys. Chem. B* **2007**, *111*, 7843-7851.
- 54. Dong, B.; Li, N.; Zheng, L.; Yu, L.; Inoue, T., Surface Adsorption and Micelle Formation of Surface Active Ionic Liquids in Aqueous Solution. *Langmuir* **2007**, *23*, 4178-4182.
- 55. Baker, G. A.; Pandey, S.; Pandey, S.; Baker, S. N., A New Class of Cationic Surfactants Inspired by N-alkyl-N-methyl Pyrrolidinium Ionic Liquids. *Analyst* **2004**, *129*, 890-892.
- 56. Burrell, A. K.; Del Sesto, R. E.; Baker, S. N.; McCleskey, T. M.; Baker, G. A., The Large Scale Synthesis of Pure Imidazolium and Pyrrolidinium Ionic Liquids. *Green Chem.* **2007**, *9*, 449-454.
- 57. Hay, C. E.; Marken, F.; Blanchard, G. J., Detection and Characterization of Liquid|Solid and Liquid|Solid Interfacial Gradients of Water Nano-Droplets in Wet N-Octyl-2-Pyrrolidone. *Langmuir* **2014**, *30*, 9951-9961.
- 58. Jiang, Y.; Blanchard, G. J., Rotational Diffusion Dynamics of Perylene in n-Alkanes. Observation of a Solvent Length-Dependent Change of Boundary Condition. *J. Phys. Chem.* **1994**, 98, 6436-6440.
- 59. Chuang, T. J.; Eisenthal, K. B., Theory of Fluorescence Depolarization by Anisotropic Rotational Diffusion. *J. Chem. Phys.* **1972**, *57*, 5094-5097.
- 60. Jin, H.; O'Hare, B.; Dong, J.; Arzhantsev, S.; Baker, G. A.; Wishart, J. F.; Benesi, A. J.; Maroncelli, M., Physical Properties of Ionic Liquids Consisting of the 1-Butyl-3-Methylimidazolium Cation with Various Anions and the Bis(trifluoromethylsulfonyl)imide Anion with Various Cations. *J. Phys. Chem. B* **2008**, *112* (1), 81-92.
- 61. Debye, P., *Polar Molecules* Chemical Catalog Co.: New York 1929; p 84.
- 62. Hu, C.-M.; Zwanzig, R., Rotational friction coefficients for spheroids with the slipping boundary condition. *J. Chem. Phys.* **1974**, *60* (11), 4354-4357.
- 63. Perrin, F., Mouvement brownien d'un ellipsoide I. Dispersion diélectrique pour des molécules ellipsoidales. *J. Phys. Radium* **1934**, *5*, 497.
- 64. Edward, J. T., Molecular volumes and the Stokes-Einstein equation. *J. Chem. Ed.* **1970**, 47, 261-270.

- 65. Blanchard, G. J., Picosecond spectroscopic measurement of a solvent dependent change of rotational diffusion rotor shape. *J. Chem. Phys.* **1987**, *87*, 6802-6808.
- 66. Gebbie, M. A.; Smith, A. M.; Dobbs, H. A.; Lee, A. A.; Warr, G. G.; Banquy, X.; Valtiner, M.; Rutland, M. W.; Israelachvilli, J. N.; Perkin, S., et al., Long range electrostatic forces in ionic liquids. *Chem. Comm.* **2017**, *53*, 1214-1224.
- 67. Sheehan, A.; Jurado, L. A.; Ramakrishna, S. N.; Arcifa, A.; Rossi, A.; Spencer, N. D.; Espinoza-Marzal, R. M., Layering of ionic liquids on rough surfaces. *Nanoscale* **2016**, *8*, 4094-4106.
- 68. Das, S. K.; Majhi, D.; Sahu, P. K.; Sarkar, M., Linking Diffusion-Viscosity Decoupling and Jump Dynamics in a Hydroxyl-Functionalized Ionic Liquid: Realization of Microheterogeneous Nature of the Medium. *ChemPhysChem* **2017**, *18*, 198-207.
- 69. Das, S. K.; Sahu, P. K.; Sarkar, M., Diffusion-Viscosity Decoupling in Solute Rotation and Solvent Relaxation of Coumarin 153 in Ionic Liquids Containing Fluoroalkylphosphate (FAP) Anion: A Thermophysical and Phtotphysical Study. *J. Phys. Chem. B* **2013**, *117*, 636-647.
- 70. Subba, N.; Polok, K.; Piatkowski, P.; Ratajska-Gadomska, B.; Biswas, R.; Gadomski, W.; Sen, P., Temperature-Dependent Ultrafast Solvation Response and Solute Diffusion in Acetamide-Urea Deep Eutectic Solvent. *J. Phys. Chem. B* **2019**, *123*, 9212-9221.
- 71. Subba, N.; Tarif, E.; Sen, P.; Biswas, R., Subpicosecond Solvation Response and Partial Viscosity Decoupling of Solute Diffusion in Ionic Acetamide Deep Eutectic Solvents: Fluorescence Up-Conversion and Fluorescence Correlation Spectroscopic Measurements. *J. Phys. Chem. B* **2020**, *124*, 1995-2005.
- 72. Tarif, E.; Mondal, J.; Biswas, R., Interaction and Dynamics in a Fully Biodegradable Glucose-Containing Naturally Abundant Deep Eutectic Solvent: Temperature-Dependent Time-Resolved Fluorescence Measurements. *J. Phys. Chem. B* **2019**, *123*, 9378-9387.
- 73. Barik, S.; Chakraborty, M.; Sarkar, M., How Does Addition of Lithium Salt Influence the Structure and Dynamics of Choline Chloride-Based Deep Eutectic Solvents? *J. Phys. Chem. B* **2020**, *124*, 2864-2878.
- 74. Guo, J.; Baker, G. A.; Hillesheim, P. C.; Dai, S.; Shaw, R. W.; Mahurin, S. M., Fluorescence correlation spectroscopy evidence for structural heterogeneity in ionic liquids. *Phys. Chem. Chem. Phys.* **2011**, *13*, 12395-12398.

CHAPTER 7. Conclusions And Future Directions

7.1 Conclusions

Room temperature ionic liquids (RTILs) exhibit unique physical and chemical properties which originate from their complex molecular organization and thus, are not directly comparable to conventional molecular liquids. Consequently, it is instructive to develop an alternative theoretical framework to treat this very useful class of materials. In this dissertation, our main objectives were to establish analogy between RTILs and piezoelectric materials, and to understand the length scale of organization relevant to the piezoelectric behavior of these materials. By open circuit potential (OCP) measurements under varying pulsed pressure, we successfully demonstrated the direct piezoelectric effect in RTILs. Furthermore, we investigated the structuredependent nature of this effect in RTILs. The structure dependence of RTILs suggests that the piezoelectric effect in RTILs is not determined solely by molecular-scale structure, but rather by organization occurring on the nanometer scale or larger within the RTILs themselves.² Interestingly, the induced free charge density gradient, ρ_f , persists up to 30 mol% dilution of RTILs with molecular solvents.^{3, 4} RTILs form nanometer aggregates on dilution and the size of the aggregates increases with increasing dilution. A key challenge in this dissertation was to establish a connection between free charge density gradients, ρ_f , and molecular-scale organization in the RTILs. Using long alkyl chain (C₁₀) RTILs, we demonstrated for the first-time a correlation between ρ_f and structural organization.⁵

In this dissertation, we have introduced a liquid piezoelectric material and tried to unravel the molecular-level mechanism of this unusual behavior. The potential applications of such a material in various technological fields are substantial. However, there is still much ground to cover to fully grasp the physics and chemistry of the piezoelectric effect in RTILs, and to harness their maximum potential. In the following discussion are few suggested areas to characterize RTILs and compare

their piezoelectric properties with those of well-established solid state piezoelectric materials.

7.2 Future Directions

7.2.1 Atomic Force Microscopy (AFM) Measurements

We have successfully demonstrated the direct piezoelectric effect in RTILs by measuring open circuit potential (OCP) as a function of applied pressure. The piezoelectric effect is described through the relationship between the application of a stress to a material and the resulting charge displacement, D (Eq. 7.1),⁶

where ε is the dielectric constant of the material, E is the applied electric field, δ is the matrix describing the piezoelectric response, with δ^t being the transpose, relating the application of an electric field E to the induced strain, S, *i.e.*, the converse piezoelectric effect. T is the stress applied, which produces a strain, S, with s, the compliance, characterizing the proportionality between stress and strain.

It is not possible to measure the converse piezoelectric effect in RTILs in the liquid phases by traditional methods. This is because the converse piezoelectric effect involves measurement of dimensional change as a function of applied potential and liquids inherently take the shape of their container. Therefore, freezing of RTILs will produce materials with a measurable converse piezoelectric response when a potential is applied across the material. Measuring the (converse) piezoelectric effect quantitatively in solids can be done with atomic force microscopy (AFM), a technique capable of measuring extremely small dimensional changes in (solid) materials resulting from an applied potential difference across the material. The literature provides ample evidence of making mono-, bilayers of RTILs using techniques such as Langmuir-Blodgett and Langmuir-Schaefer techniques (Figure 7.1) 7-11.

Once the mono- or bilayer are formed, they can be transferred onto a charged surface (ITO),

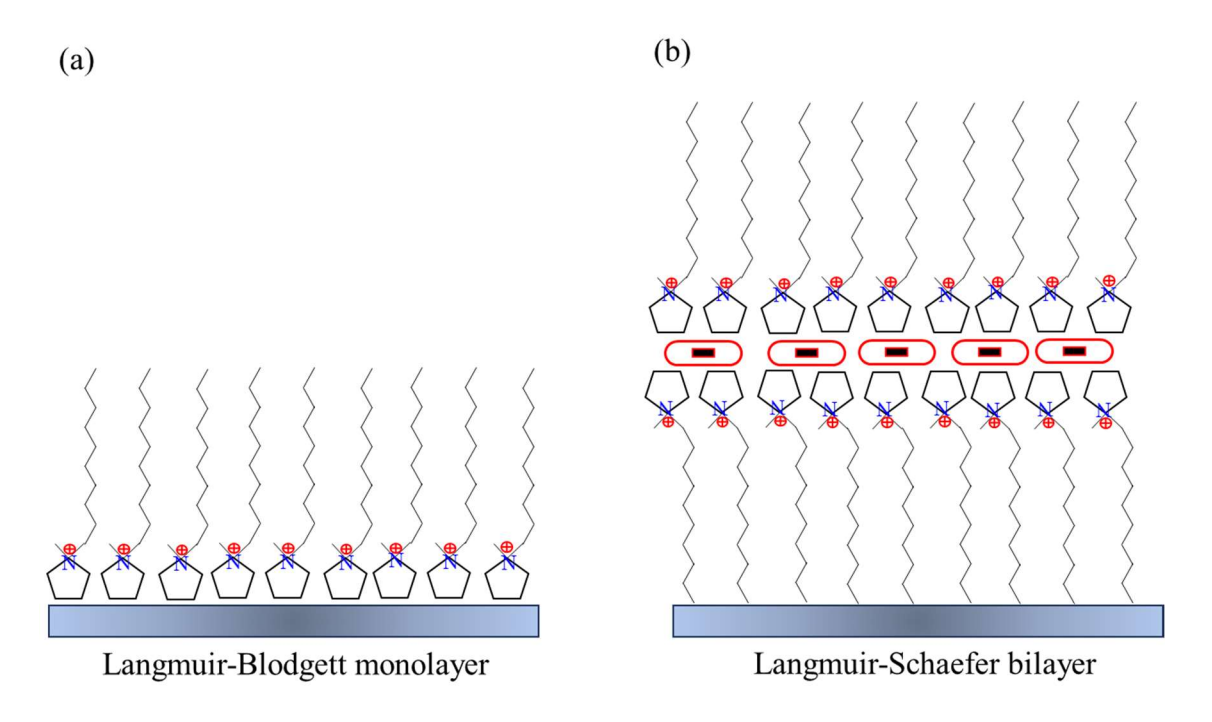


Figure 7.1 Monolayer (a) and bilayer (b) of pyrrolidinium-based ionic liquids.

inducing the free charge density gradient (ρ_f). By controlling the temperature and freezing the sample, we can convert the RTIL into solid mono/bilayers. Subsequently, we can perform AFM measurements using AFM as a function of potential difference between the support surface and the AFM tip. This approach serves two purposes: first, it enables measurement of the converse piezoelectric effect directly, and second, it allows evaluation of the piezoelectric (converse) effect as a function of film thickness. The AFM measurements will determine the magnitude of d_{33} , the piezoelectric coefficient in RTILs for interfaces of molecular dimension.

7.2.2 Non-linear Optical Measurements

RTILs exhibit an induced birefringence due to $\rho_f^{-12, 13}$ which is a manifestation of the converse piezoelectric effect. Our demonstration of the direct piezoelectric effect in RTILs allows

determination of d_{33} , but for liquids, other piezoelectric coefficients cannot be evaluated because

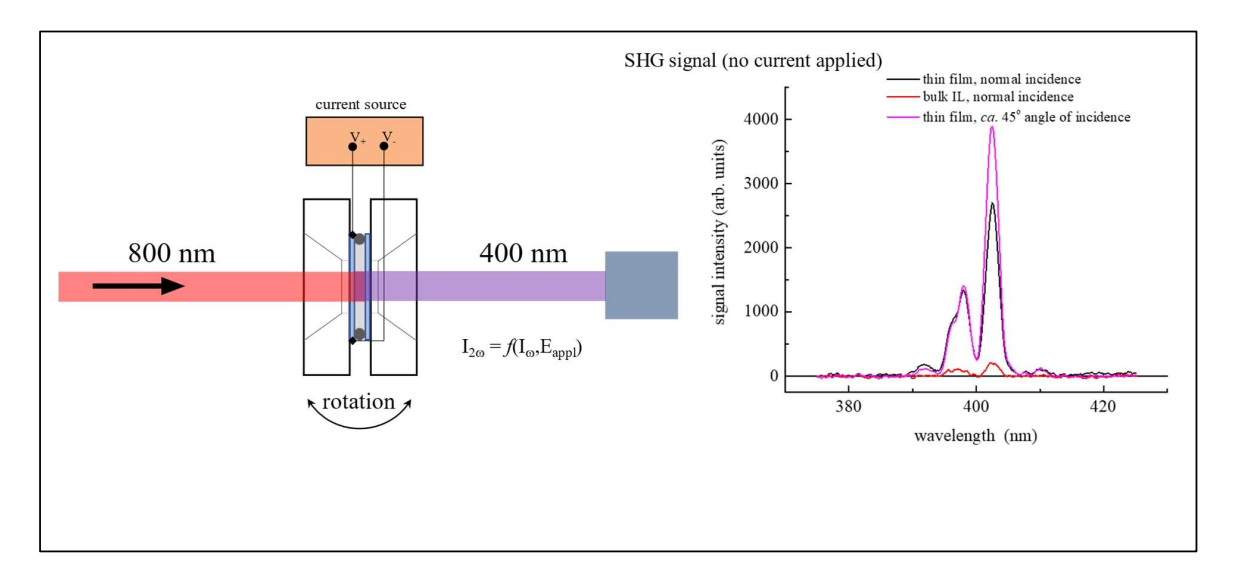


Figure 7.2 Left: Schematic of RTIL SHG measurement. Amplified Ti:Sapphire laser light source, 50 fs, 1 μJ pulses at 800 nm. Right: SHG signal from BMIM⁺TFSI⁻ in 1 mm cuvette. Red = bulk RTIL, normal incidence; black = thin film RTIL, normal incidence, magenta = thin film RTIL, ca. 45° angle of incidence.

of the characteristically small values of Young's modulus and the shear modulus in the liquid phase. Quantitating the direct piezoelectric effect in the solid form of the RTIL at a temperature below its melting point will allow evaluation of piezoelectric coefficients other than d_{33} (e.g., d_{31}), as well as allowing the comparison of d_{33} in the (nominal) liquid and solid phases of the same materials. The key to more detailed evaluation of the piezoelectric effect in RTILs is the identification and use of measurements that can be used for both the solid and liquid phases of RTILs. Optical second harmonic generation (SHG) can be used for this purpose.

The piezoelectric effect and optical second harmonic generation are described by the same third rank tensor d_{ijk} .¹⁴ The quantities δ and δ^t (Eq. 7.1) are the piezoelectric strain tensor and its transpose, respectively. These are third rank tensors, and they are related to the $\chi^{(2)}$ tensor through the relationship $\chi^{(2)} = 2\delta$.¹⁵ Hence, there exists a direct correlation between the piezoelectric response and second order nonlinear optical effects. It is known that RTILs exhibit a usefully large

second order nonlinear optical response at the air-RTIL interface, ¹⁶ and we have demonstrated it experimentally (Fig. 7.2). Measuring the magnitude and polarization-dependence of the second order nonlinear optical response of RTILs at temperatures below and above the RTIL melting point will provide a direct comparison of the magnitude of the piezoelectric effect in the solid and liquid states.

SHG will be observed most easily in an interfacial reflection mode, where the surface order and inherent absence of a center of symmetry of the RTIL-air interface will produce a second order response, as reported by the Shaw group. We hypothesize that the surface charge applied to the interface will modify RTIL organization and the reflected SHG will depend on both the RTIL support surface charge and polarization of the incident electric field.

Comparison to the second order nonlinear optical response of the same solid RTILs will determine the correspondence between RTIL piezoelectric effect in the solid and liquid states. With the calibration of the relationship between the piezoelectric and optical measurements established for solid phase RTIL(s), the optical measurements will be made on RTILs to gauge the change in magnitude of $\Box f$ across the phase transition and its temperature-dependence. This information will provide a convenient means of evaluating the magnitude of piezoelectric phenomena in RTILs in the future.

7.2.3 Piezoelectric Effect under Nano-confinements

Dilution studies of ILs have provided a great deal of molecular-scale insight into the competition between IL associated ions and solvent-ion interactions. In Chapters 4 and 5, we have reported on the interactions of a series of imidazolium based ILs with molecular solvents methanol, acetonitrile, propylene carbonate and DMSO. It has emerged that ILs diluted with other molecular solvents produce compositionally heterogeneous systems, with the size of the nanometer-scale IL

aggregates depending on the identities of both the IL and the molecular fluid diluent.^{3, 4} We thus have control over average IL ion pair aggregate size, and that control yields nanoscale aggregates in the size scale centered around 1 nm in diameter.

As described in Chapter 2, the piezoelectric behavior of ILs is novel and among the many opportunities that stem from this discovery, one that is of foundational importance to the future use of these materials is understanding the relationship between IL dimension and the magnitude of the piezoelectric response. The point is to determine the relationship between nanoscale IL aggregate dimensions and piezoelectric response. To accomplish this task, we will use molecular fluid diluents that are capable of undergoing polymerization. Once the IL nanoscale aggregates are formed in the molecular fluid, the polymerization of the diluent matrix will transform the binary mixture into a solid composite material. A few polymers exhibit the piezoelectric effect, PVDF being the most widely used example, 17-19 but most do not. Moreover, polymers have been used before in the formation of nanocomposite piezoelectric materials, but in those systems, inorganic nanoparticles were used as the piezoelectric material. After the formation of solid composite material with RTILs and polymer, their piezoelectric effect can be measured with all the traditional methods and can be compared with the effect as a function of domain size.

REFERENCES

- 1. Hossain, M. I.; Blanchard, G. J. Ionic Liquids Exhibit the Piezoelectric Effect. *J. Phys. Chem. Lett.* **2023**, *14* (11), 2731-2735.
- 2. Hossain, M. I.; Adhikari, L.; Baker, G. A.; Guazzelli, L.; Mussini, P.; Blanchard, G. J. Structure-Dependence of the Piezoelectric Effect in Ionic Liquids. Possible Mechanistic Insights. (Under Process) 2023.
- 3. Hossain, M. I.; Blanchard, G. J. The Effect of Dilution on Induced Free Charge Density Gradients in Room Temperature Ionic Liquids. *Phys. Chem. Chem. Phys.* **2022**, *24*, 3844-3853.
- 4. Hossain, M. I.; Blanchard, G. J. Dilution-Induced Changes in Room Temperature Ionic Liquids. Persistent Compositional Heterogeneity and the Importance of Dipolar Interactions. *J. Mol. Liq.* **2022**, *367*, 120447.
- 5. Hossain, M. I.; Blanchard, G. J. Relating the Induced Free Charge Density Gradient in a Room-Temperature Ionic Liquid to Molecular-Scale Organization. *J. Phys. Chem. B* **2023**, *127* (8), 1780-1788.
- 6. Curie, J.; Curie, P. Développment par compression de l'électricité polaire dans les cristaux hémièdres à faces inclinées. *Min é rol. France* **1880**, *3*, 90-93.
- 7. Mitra, S.; Das, R.; Singh, A.; Mukhpadhyay, M. K.; Roy, G.; Ghosh, S. K. Surface Activities of a Lipid Analogue Room-Temperature Ionic Liquid and Its Effects on Phospholipid Membrane. *Langmuir* **2020**, *36*, 328-339.
- 8. Lu, Y.; Wang, Y.; Huo, F.; Ma, M.; Ding, W.-L.; He, H.; Zhang, S. Ultralow Friction and High Robustness of Monolayer Ionic Liquids. *ACS Nano* **2022**, *16* (10), 16471-16480.
- 9. Sieling, T.; Christoffers, J.; Brand, I. Langmuir-Blodgett Monolayers of Partially Fluorinated Ionic Liquids as Tow-Dimensional, More Sustainable Functional Materials and Coatings. *ACS Sustainable Chem. Eng.* **2019**, *7*, 11593-11603.
- 10. Smith, A. M.; Lovelock, K. R. J.; Gosvami, N. N.; Licence, P.; Dolan, A.; Welton, T.; Perkin, S. Monolayer to Bilayer Structural Transition in Confined Pyrrolidinium-Based Ionic Liquids. *J. Phys. Chem. Lett.* **2013**, *4*, 378-382.
- 11. Smith, A. M.; Lovelock, K. R.; Perkin, S. Monolayer and bilayer structures in ionic liquids and their mixtures confined to nano-films. *Faraday Discuss.* **2013**, *167*, 279-292.
- 12. Wang, Y.; Swain, G. M.; Blanchard, G. J. Charge-Induced Birefringence in a Room-Temperature Ionic Liquid. *J. Phys. Chem. B* **2021**, *125*, 950-955.

- 13. Toda, S.; Clark, R.; Welton, T.; Shigeto, S. Observation of the Pockels Effect in Ionic Liquids and Insights into the Length Scale of Potential-Induced Ordering. *Langmuir* **2021**, *37*, 5193-5201.
- 14. Ok, K.-M.; Chi, E.-O.; Halasyamani, P. S. Bulk Characterization Methods for Non-Centrosymmetric Materials: Ssecon-Harmonic Generation Piezoelectricity, Pyroelectricity and Ferroelectricity; *Chem. Soc. Rev.* **2006**, *35*, 710-717.
- 15. Miller, R. C. Optical Second Harmonic Generation in Piezoelectric Crystals. *Appl. Phys. Lett.* **1964**, *5*, 17-19.
- 16. Anaredy; S., R.; Shaw, S. K. Long-Range Ordering of Ionic Liquid Fluid Films. *Langmuir* **2016**, *32* (20), 5147-5154.
- 17. Mishra, S.; Unnikrishnan, L.; Nayak, S. K.; Mohanty, S. Advances in Piezoelectric Polymer Composites for Energy Harvesting Applications: A Systematic Review. *Marcomol. Mat. Eng.* **2018**, *1800463*, 1-25.
- 18. Maity, K.; Mandal, D. *In Advanced Lightweight Multifunctional Materials*.; Woodhead Publishing, 2021.
- 19. Ramadan, K. S.; Sameoto, D.; Evoy, S. A review of piezoelectric polymers as functional materials for electromechanical transducers. *Smart Materials and Structures* **2014**, *23*, 033001.